DETERMINATION OF CORRELATES OF PROTECTION AGAINST TUBERCULOSIS IN NONHUMAN PRIMATE MODELS

by

Robert Mauro DiFazio

B.S. (High Distinction) in Letters and Sciences (Chemistry/Molecular and Cellular Biology)

University of Illinois at Urbana-Champaign, 2010

Submitted to the Graduate Faculty of

the School of Medicine in partial fulfillment

of the requirements for the degree of

Doctor of Philosophy

University of Pittsburgh

2016

UNIVERSITY OF PITTSBURGH

SCHOOL OF MEDICINE

This dissertation was presented

by

Robert Mauro DiFazio

It was defended on

2 December 2016

and approved by

Karen A. Norris, PhD, Department of Infectious Diseases

Simon M. Barratt-Boyes, BVSc, PhD, Department of Infectious Disease and Microbiology

Penelope A. Morel, MD, Department of Immunology

Carolyn J. Anderson, PhD, Department of Radiology

Dissertation Advisor: JoAnne L. Flynn, PhD, Department of Microbiology and Molecular Genetics

DETERMINATION OF CORRELATES OF PROTECTION AGAINST TUBERCULOSIS IN NONHUMAN PRIMATE MODELS

Robert Mauro DiFazio, B.S.

University of Pittsburgh, 2016

Tuberculosis (TB) is one of the greatest global health challenges society faces. BCG, the only licensed vaccine for TB, has profoundly variable efficacy and does not prevent the spread of TB. Due to the lack of an effective vaccine, there are no correlates of protection to use in vaccine development. The goal of this dissertation was to develop new tools for pre-clinical and clinical trials of TB vaccines, including new outcome measures and predictive markers of efficacy. Development of these tools will expedite down-selection of vaccinate candidates, reducing their ultimate cost and hastening the reduction and eventual elimination of this disease. BCG afforded the best levels of protection in the rhesus macaque model of TB, which closely resembled TB disease in human infants. Boosting BCG by protein antigens or adenoviral vectored antigens did not improve, and in some cases worsened, outcome. A T cell signature in the lung-draining lymph nodes (LN) at necropsy, early gamma interferon (IFN-γ) ELISPOT and early PET-CT markers correlated with improved outcome in this model. We further characterized the protection afforded by an experimental boost to BCG, H56, which has been shown to prevent reactivation TB in cynomolgus macaques. BCG/H56 prevented establishment of disease in lung-draining LN. BCG/H56 also mitigated lung inflammation, which reduced apparent risk of reactivation TB by PET-CT. Early control of disease in the lung-draining LN, as well as a T cell signature, was associated with reduced risk of reactivation TB. Both studies provided evidence that PET-CT markers correlate with outcome. We thus built a holistic outcome score based

strictly on quantifiable outcomes: gross pathology and bacterial burden determined at necropsy, and constructed models that robustly predict this outcome score early using early PET-CT markers. Altogether, these studies highlight the importance of the lung-draining LN as a site of bacterial persistence and the ability of PET-CT to assess disease and predict vaccine efficacy. Further work will build upon these studies to determine the best site of vaccination to prevent disease, and develop a blood signature correlate for use in clinical trials.

TABLE OF CONTENTS

LIST OF TABLES

LIST OF FIGURES

PREFACE

I would like to dedicate this dissertation to my parents, Barbara and Mauro DiFazio. Reaching this point would have been impossible without their love and support throughout this process.

Thank you first to the members of my dissertation committee (Karen Norris, Simon Barratt-Boyes, Penelope Morel, and Carolyn Anderson) for their advice and guidance. A huge thank you goes out to the collaborators I had on my various projects, including Statens Seruminstitut in Copenhagen, Denmark (Peter Andersen, Else Marie Agger, and Thomas Linderstrøm), the University of Michigan School of Medicine (Denise Kirschner, Jennifer Linderman, Simeone Marino, Elsje Pienaar, and Hayley Warsinske), and the Vaccine Research Center of the National Institute for Allergy and Infectious Disease (Robert Seder, Mario Roederer, and Patricia Darrah). I was very lucky as a graduate student to have access to plentiful funding, and thank the National Institutes of Health (T32 AI60525 and R01 HL110811), the AERAS Global TB Vaccine Foundation, and the Bill and Melinda Gates Foundation for financial support.

The members of our TB consortium at the University of Pittsburgh regularly acknowledge how fortunate we are to have such a fantastic collection of people as comrades-in-arms against TB. We do incredibly challenging work that frequently requires the help of all members of this group. I will begin by thanking the technical staff for assistance with tissue and

blood processing, running assays, and general help over the years (Amy Fraser, Tara Kane, Mark Rodgers, Carolyn Bigbee, Chelsea Chedrick, Cassy Updike, and Cathy Cochran). Nonhuman primates are especially difficult to manage and require expert care, so a big thank you to our veterinary technicians (Jaime Tomko, Melanie O'Malley, Dan Fillmore, Jim Frye, Jim Johnson) and veterinarians (Edwin Klein and Chris Janssen). For their constant support and help with a variety of issues, scientific or otherwise, I'd like to thank the current and former students and postdocs (Hannah Gideon, Collin Diedrich, Yao Phuah, Alex White, Nicole Grant, MacKenzie Bryant). Of special note in this group are the students who shared my bay (Anthony Cadena, Eileen Wong, Sharie Ganchua) for keeping the atmosphere fun to aid in surviving the intense proximity afforded by a poorly designed work environment. Thank you to the other principal investigators of our TB group (Josh Mattila, Chuck Scanga, and Ling Lin) for their generous advice and mentorship during this gauntlet. A huge thank you to Pauline Maiello, statistician extraordinaire, for the massive amounts of support and instilling in me a new-found love for data science. Last and most of all, I am profoundly grateful to JoAnne Flynn for unparalleled mentorship, for constantly pushing me to raise the bar, and for being someone to whom I proudly look up to as a scientific role model.

1.0 INTRODUCTION TO TUBERCULOSIS VACCINOLOGY

1.1 A BRIEF HISTORY OF THE WORLD'S MOST DEADLY MICROBE

Tuberculosis (TB) is one of the greatest infectious challenges that humanity faces. Over the last two centuries alone, TB has claimed the lives of over one billion people. In 2015, there were 10.4 million new cases of TB and 1.8 million deaths, which is almost 5,000 deaths every day [7]. TB is a disease of poverty [8], and disproportionately affects the world's poorest nations [7]. A plethora of evidence suggests that TB has been inflicting human morbidity and mortality for thousands of years. Skeletal remains from over 9,000 years ago bear signs of TB, as do mummified remains from Ancient Egypt [9]. Hammurabi's Code, created by the Babylonian emperor of the same name, has the first written suggestions of TB or TB-like disease [9]. The first thorough description of TB was provided to us by Hippocrates around 400 BC [10], in which he describes 'phthisis,' or a generalized wasting disease characterized by fever, coughing, and night sweats. He posited at the time that phthisis was hereditary from the observation that the disease moved from a disease case to other household contacts. Since TB almost always led to death, he strongly advised his colleagues from visiting patients exhibiting disease so that they might protect their reputations. The infectious nature of TB was first hypothesized by Fracastoro in the 16th century [11]. In his posthumously published work, *De Contagione*, he suggested that some diseases including TB were transmitted by 'fomes,' or tinder in Latin. Although he was

correct about TB's contagious nature, this was not proven for another 300 years. TB can inhabit and cause disease in any physiological compartment [12], so for most of history TB was thought to be multiple diseases. Sylvius, observing pathological similarities between these manifestations, first proposed that they were all the same disease: phthisis [13]. For the next two centuries, until the 19th century, TB was therefore studied as a unified disease. However, during this period, the cause of TB was still unknown, and was thought to be anything from bad air, to an imbalance of humors, to vampirism [14, 15]. This all changed in 1865, when Jean Villemin definitively demonstrated the infectious nature of TB [16]. In this landmark study, he took portions of TB lesions from humans and cattle and inoculated them in rabbits and guinea pigs, which subsequently developed TB. The most significant study came 18 years later when Robert Koch presented his groundbreaking lecture, vaguely titled "The Etiology of Tuberculosis" [17]. Not only did Koch show that this newly identified aerobic bacterium, *Mycobacterium tuberculosis* (Mtb), was specifically the causative agent of TB, but he also ushered in a revolution in microbiology. Infectious disease could have specific agents that cause them, and therefore for the first time be targeted and eliminated.

1.2 CLINICAL EPIDEMOLOGY AND TRANSMISSION OF MTB

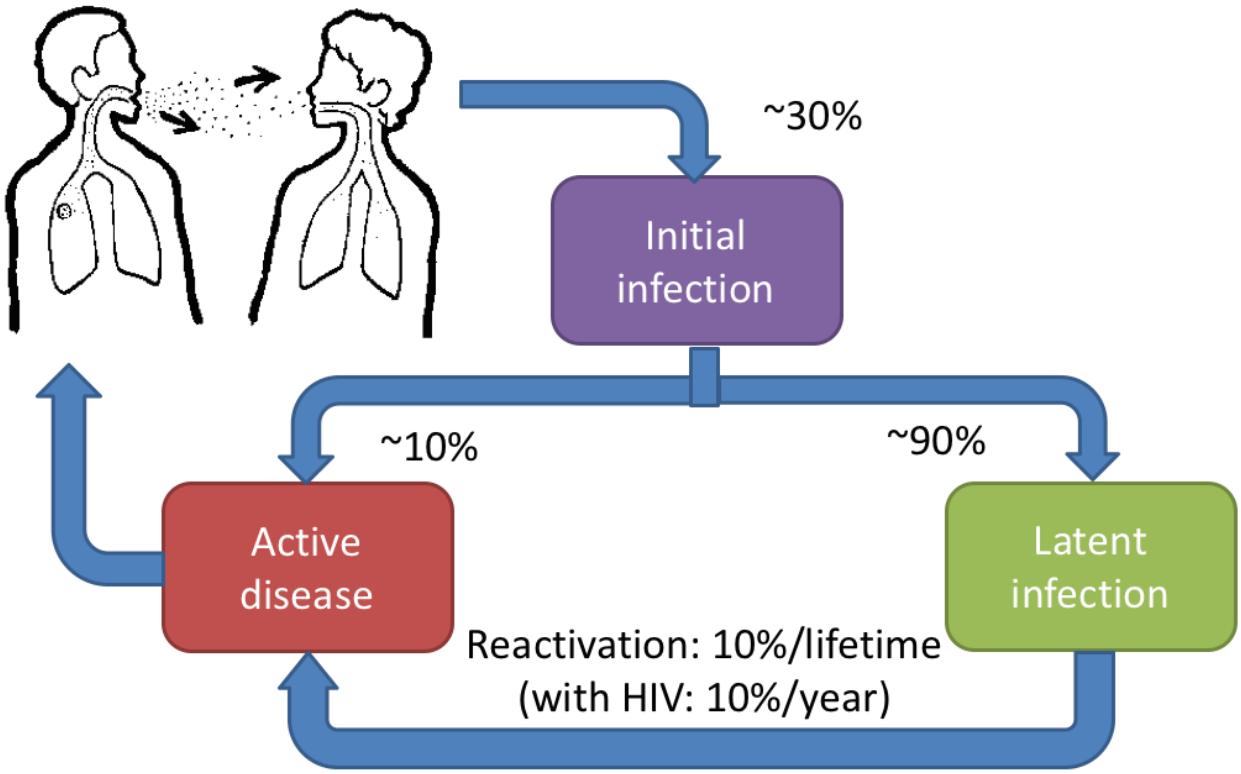

Figure 1: The infectious cycle of tuberculosis (TB). Infectious aerosolized droplets are expelled from humans with active disease (top left). Almost a third of people exposed to these droplets form an infection (purple), 10% of whom have primary contagious disease (red) and 90% of whom control the infection and are latent (green).

There are classically two clinical manifestations of TB—active and latent (Fig. 1)—although it is now understood that a spectrum of disease exists. TB was demonstrated by Jean Villemin to be infectious in nature [16], and the identification of Mtb only further cemented this fact [17]. However, the aerosol component of transmission was not thoroughly elucidated until the late 1950s. At the TB ward of Johns Hopkins University, a "penthouse" was constructed in which air in the ward was fed into this chamber which contained a multitude of guinea pigs [18]. This pilot study demonstrated that the air in the chamber was just as infectious as in the ward. A two-

chamber experiment was then performed in which one chamber contained the air unfettered but the other was exposed to ultraviolet radiation [19]. The first tank of air led to TB in guinea pigs, whereas the sterilized air did not, demonstrating that Mtb is transmitted by aerosol. Typically, humans with active (but not latent) TB will eject Mtb in aerosol droplets by coughing, sneezing, and spitting. In a unique case study, Mtb was also shown to be transmitted in a mini-outbreak of a choir by singing [20].

Approximately 30% of humans exposed to aerosol droplets containing Mtb develop an infection (Fig. 1), as determined in household contact studies [21, 22]. The primary method of diagnosing Mtb infection is the tuberculin skin test (TST) [23]. Unfortunately, vaccination with BCG can confound the results of this test, but Mtb-specific tests using peripheral blood overcome this issue [23]. Chest x-ray (CXR) has also been shown to be a highly effective diagnostic tool for identifying infection. Early TB and latent TB infection (LTBI) can be diagnosed using CXR [24]. A new skin test has been developed using Mtb-specific antigens that is 99.3% specific for infection in BCG vaccinated people [25]. However, one of the antigens in this skin test is present in a few of the novel TB vaccines in the pipeline, which will likely lead to cross reactivity between the new skin test and new vaccines. To overcome this, other biochemical markers of infection are under investigation. IP-10 is a promising new marker, as leukocytes from infected patients stimulated with Mtb-specific antigens produces more IP-10 than healthy controls [26]. The African giant pouched rat can specifically detect Mtb versus similar bacteria using its olfactory sense with 94% accuracy, and can distinguish between sputum naturally inhabited by Mtb and “fake” sputum spiked with Mtb [27]. These data suggest that Mtb-specific volatile compounds are present in the sputum that can be further developed as a diagnostic.

The field of TB is littered with odd and fascinating studies, like the study detailing the outbreak in the choir [20]. Another such study was a retrospective contact study in a US Navy vessel, in which 66 sailors were discovered *post hoc* to be confined in close quarters with 7 fellow seamen with active TB [28]. Thirteen of the sailors (19.8%) remained TST negative after six months of exposure to the active TB cases. In a high TB endemic setting, about 50% of contacts were TST negative [29]. These data suggest the ability of the innate immune system to control Mtb infection. Two genetic loci in a genome-wide linkage study have been associated with TST reactivity in similar studies, hinting that innate control of Mtb could also be genetic [30]. Greater bacterial burden in expelled aerosol droplets and proximity to and exposure time with the contact case additionally correlate with risk of developing infection [31].

Another fascinating historical study was conducted in the Faroe Islands [32]. In some cases, less than a day of exposure to an active case of TB led to TST conversion and primary TB. Nearly all persons infected in this large longitudinal study reported for TST conversion had an "initial fever" and elevated erythrocyte sedimentation rate (ESR), and 63% of persons not selected ended up with "initial fever", suggesting an inflammatory response that occurs regardless of disease outcome [33]. The risk of developing active disease after Mtb infection is greatest in the first 1-2 years following infection and declines exponentially afterwards, with about 10% of humans infected developing active disease [34]. The risk of primary disease is also age dependent, from 4% (ages 0-10), to 9% (10-20), and 14% (30+) [35].

Diagnosis of active disease is based on clinical presentation of signs and symptoms, and/or isolation of Mtb from a patient [23]. Detection of Mtb in the sputum is relatively fast but suffers from a lack of sensitivity, in some instances as low as 32% [36]. Culture of Mtb from a patient sample is the gold standard for diagnosis, but typically takes six weeks to do with the

exception of some systems, e.g. BACTEC, which take about two weeks but are not available in all areas [37]. These data, together with the fact that 90% of infected people do not present clinically, paint a sorry picture, especially considering that these are the current endpoints for clinical trials [38]. Serum-based biomarkers have been developed that appear to distinguish pulmonary TB from other diseases [39], and distinguish between different manifestations of TB [40]. A meta-analysis in 2009 of 254 studies of serological markers of active TB determined that to that date they all suffered from low sensitivity and specificity [41]. What has been achieved by the field since then? A breakthrough transcriptomic study identified a blood signature that could distinguish between active TB and LTBI with 95% sensitivity and 83% specificity [42]. This signature correlated with extent of radiographic pulmonary disease and diminished during chemotherapy, and was observed in geographically distinct cohorts and separate studies [43, 44]. Other transcriptional signatures have also been identified that distinguish between disease states [45]. One only requires three genes, was validated in eight independent data sets from children and adults, diminished with chemotherapy, and was not confounded by HIV status, Mtb resistance to antibiotics, or prior vaccination with BCG [46]. In addition to transcriptional signatures, other putative disease-predictive signatures have been identified using cell phenotypes or functionality [47-51], proteomics [52], and metabolomics [53].

As previously mentioned, active TB is the transmissible form of disease, but clinically latent infection (LTBI) is the more prevalent manifestation (90% of infections; Fig. 1)[23]. The pool of humans with LTBI is staggering, being approximately 2.3 billion people, or 1/3 of the world's population [7]. Persons with LTBI have their infection under control, but have a 10% per lifetime risk of later developing active TB disease [23, 54]. This increases to 10% per year with certain co-morbidities like HIV or diabetes. These and other data therefore suggest that TB does

not have a binary set of outcomes (active or latent) but a spectrum of outcomes, ranging from total control of infection to fulminant disease [55, 56].

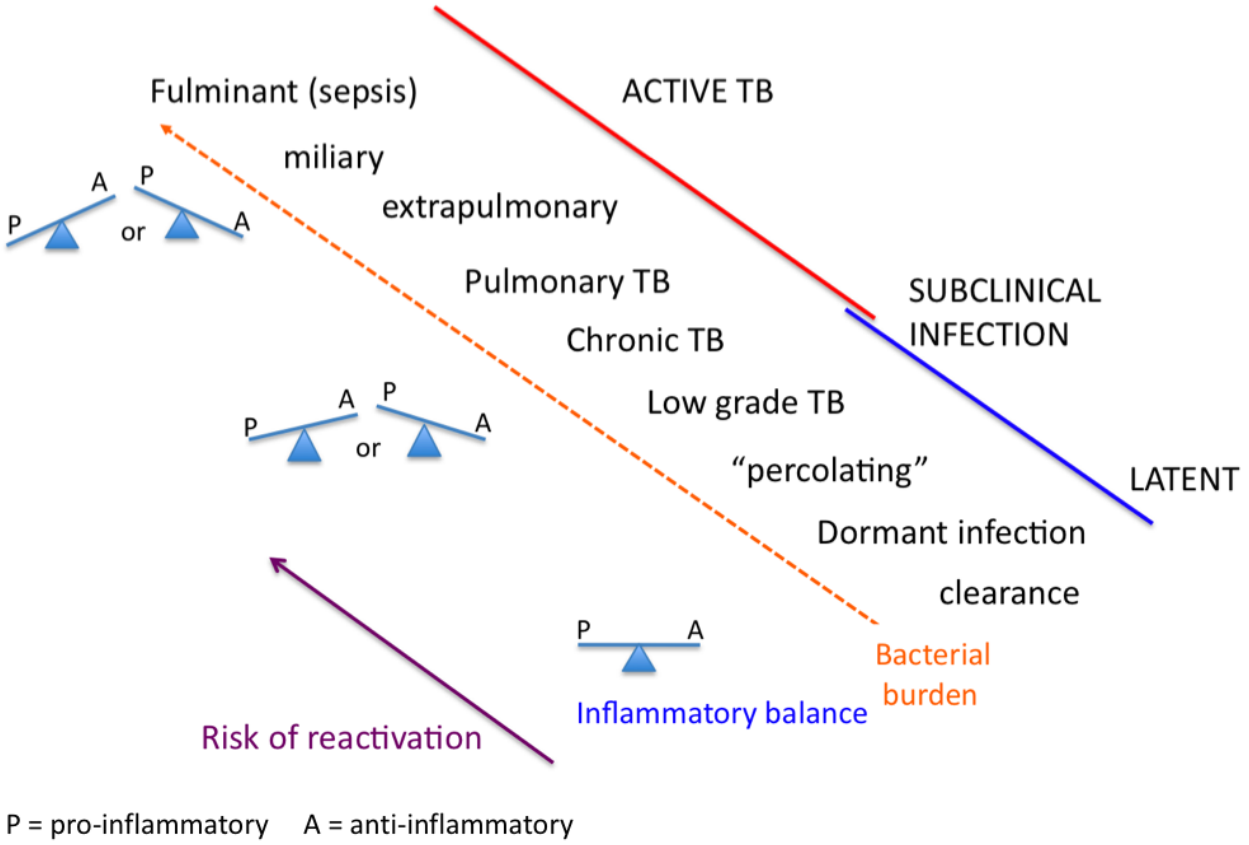

Figure 2: The spectrum of TB. While classically thought of as a binary, TB outcomes are more accurately fit to a spectrum, from complete control of infection to fulminant disease. The control of TB depends on a balance of pro- and anti-inflammatory factors which are discussed in chapter 1.7 in great detail. Figure adopted from [56]. Copyright 2010. The American Association of Immunologists, Inc.

We have provided evidence demonstrating reactivation of a subset of LTBI macaques after CD4 or TNF depletion [57, 58], demonstrating differential risk of reactivation. In the transcriptional study that identified signatures of active TB and LTBI, 10-20% of LTBI patients had a blood signature like patients with active TB [42]. In this study and the naval vessel study, not all

sputum positive patients had clinical TB [28, 42]. These data together provide compelling evidence of subclinical disease and heterogeneity of TB.

1.3 MOLECULAR PATHOGENESIS OF MTB

The pathological hallmark of TB is the granuloma [59, 60]. Typically, in humans, the major site of pathology in the lungs is termed a Ghon focus [61]. This consists of a lesion (granuloma) usually near the subpleural surface or lobar fissures between the upper middle lobe or the lower upper lobe, and an associated lung-draining lymph node (LN) with a granuloma [62]. TB lesions can form cavities observable on CXR. It is thought that this is the primary mechanism of transmission, since 98% of patients with cavities by CXR have Mtb present in their sputum [63]. A wide phenotypic variety of granulomas can be found within a single host. This was noted both in humans [64], and by our laboratory in nonhuman primates [65].

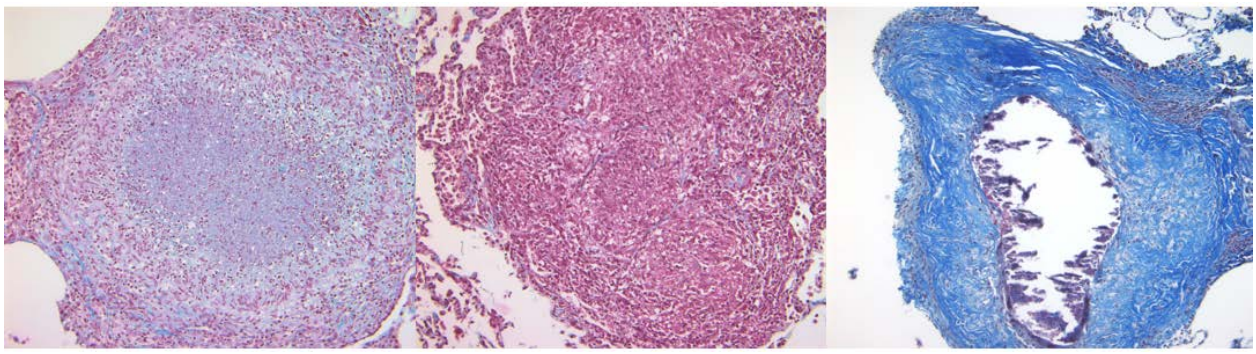

Figure 3: Histomicrographic examples of TB granulomas. The granuloma on the left is a caseous, or necrotizing, granuloma. The central lesion is a non-necrotizing granuloma. The granuloma on the right is a fibrocalcific granuloma. Magnification at 200x. Masson's trichrome stain.

Granulomas form when Mtb bacilli are inhaled and begin to interact with the lung environment. Much of what we know about the early events are derived from mouse studies, and timing and events may be different in humans. Nonetheless, the mouse system provides easier opportunities for assessing very early events in infection. Alveolar macrophages are thought to be the first cell infected. However, two weeks after Mtb challenge in mice, dendritic cells, alveolar macrophages, and neutrophils are all equally infected by Mtb [66]. By three weeks post-infection (p.i.), $CD11b^{hi}CD11c^{hi}$ dendritic cells were the most commonly infected cell type, with residential interstitial macrophages in second place. Mtb has myriad means of hiding in these phagocytic cells, which shall be discussed later in the section. These infected cells begin to respond by producing TNF, which induces ICAM-1 and initiates granuloma formation [67]. Mycobacterial lipids on their own have been demonstrated to be sufficient for granuloma formation [68]. The macrophages that are present in the granuloma range from classically activated macrophages surrounding the necrotic center of the structure, with alternatively activated macrophages near the periphery [69]. Infected monocytes/macrophages are not responsible for directly priming T cells [70]. Rather, the monocytes must differentiate into dendritic cells and transport the bacteria to LN and cooperate there to prime CD4 T cells. These infected dendritic cells then traffic to lung-draining LN carrying Mtb with them. Surface proteins on Mtb can bind DC-SIGN to induce IL-10, which suppresses activation and delays effector cell formation [71]. It also leads to a rapid expansion of T regulatory cells, which also delays priming of CD4 and CD8 T cells and their arrival in the lung [72]. Mtb downregulates maturation markers while inside dendritic cells, even in the presence of stimulatory factors like tumor necrosis factor (TNF), IL-1, and PGE2 [73]. The protein Rv1860, produced by Mtb, leads to loss of dendritic cell functions like cytokine secretion and T cell activation, which ultimately leads to

defective downstream T cell responses to Mtb [74]. By this point in the infection, Mtb has already disseminated from the lung before responses in the LN can be sent back to the lung [75]. Activated T cells are first observed in the LN between 8-10 days p.i., but another 12-14 days pass until these T cells arrive in the lung [76]. Their arrival then coincides with inhibition of growth of Mtb in the lung. By this point, Mtb bacilli have expanded about 40,000 fold before these effector cells appear [70]. After the lymphocytes seem to control Mtb infection, secondary lymphoid-like structures appear peripherally on the lung granulomas as observed in human and nonhuman primate samples [77, 78]. CCL19 and CCL21, which are characteristic chemokines of secondary lymphoid organs, are expressed in granulomas, and deficiency of CCR7 (a receptor for both chemokines) leads to poor granuloma maintenance [79]. Neutrophils may also be infected with Mtb, and granzyme B-producing neutrophils correlate with bacterial burden [80]. Infected neutrophils can carry bacteria to airways during late stage inflammation without cavitation in humans and nonhuman primates [81]. There is strong evidence that inflammatory signaling in human granulomas is spatially organized [82]. Granulomas have been found to be hypoxic in their core (in the region of necrosis, or caseation), which could be a mechanism of persistence for the bacillus [83]. A connection has been demonstrated between the hypoxic response of Mtb and lipid metabolism that may account for bacterial survival in these conditions [84]. Mtb DNA is very stable in lung granulomas and can be measured to determine total counts of live and dead organisms [85, 86]. Mycobacterial DNA in LTBI humans can be detected in the lungs, liver, spleen, and kidneys at autopsy [87]. In fact, in that study, none of the LTBI patients (who died of non-TB causes) had Mtb DNA exclusively in the lungs.

How do macrophages control Mtb, and conversely how are these phagocytic cells subverted by infection? The main mechanism of killing, at least in the murine macrophage, is

through reactive nitrogen intermediates produced by activated macrophages [88]. Interferon gamma (IFN-γ) and TNF can activate macrophages in this fashion, and both molecules together result in a more bactericidal macrophage. Uptake of bacteria by opsonophagocytosis via Fc receptor leads to respiratory burst enabling killing [89]. Should the macrophage fail to kill Mtb, apoptosis may also be utilized as a defense mechanism [90]. Engulfment of apoptotic bodies that contain Mtb allows for greater cross presentation of antigens [91]. Induction of antibacterial effectors induced by both innate and adaptive signals requires the induction of autophagy in macrophages [92]. The atg5 gene is essential for this to occur, but other genes and conventional autophagy pathways are not [93]. On the other side of the coin, Mtb has evolved very many means of thwarting these host defense mechanisms. Uptake by most macrophage receptors, including mannose receptor and complement receptor 3, prevents activation of macrophages and leads to cholesterol-dependent prevention of phagosome-lysosome fusion [94]. Roles for toll-like receptors (TLR) 2, 4, and 9 have been identified for macrophage control by Mtb [95]. Prolonged TLR2 signaling induced by Mtb lipoproteins (LpqH, LpRG, and LpRA) inhibits expression of MHC II in macrophages. TLR2 may be one of the many pathways exploited by Mtb to inhibit MHC I cross presentation to CD8 T cells as well. Mtb has been shown to use a specific type of lipid (phthiocerol dimycocerosate; PDIM) to mask pathogen associated molecular patterns (PAMPs) on its surface [96]. Inhibition of these PDIM lipids leads to TLR-dependent recruitment of macrophages that can kill Mtb. EsxH, part of the ESX-1 type VII secretion system, targets ESCRT and by doing so can block phagosome-lysosome fusion [97]. Mtb may also inhibit apoptosis, which is host beneficial [98]. It achieves this specifically through the bacterial gene nuoG [99]. Inhibition of macrophage apoptosis leads to reduced control of Mtb [100]. Instead, Mtb much prefers to induce necrosis as an additional virulence mechanism [101].

Mtb-driven macrophage necrosis requires ESX-1 and specifically ESAT-6 [102], a secreted protein discussed in detail later. Rv3167c in Mtb negatively regulates phagolysosomal escape and host cell necrosis [103]. Mtb also utilizes antigen export in macrophage vesicles to divert antigens from MHC II [104]. Blocking this export improves CD4 T cell activation.

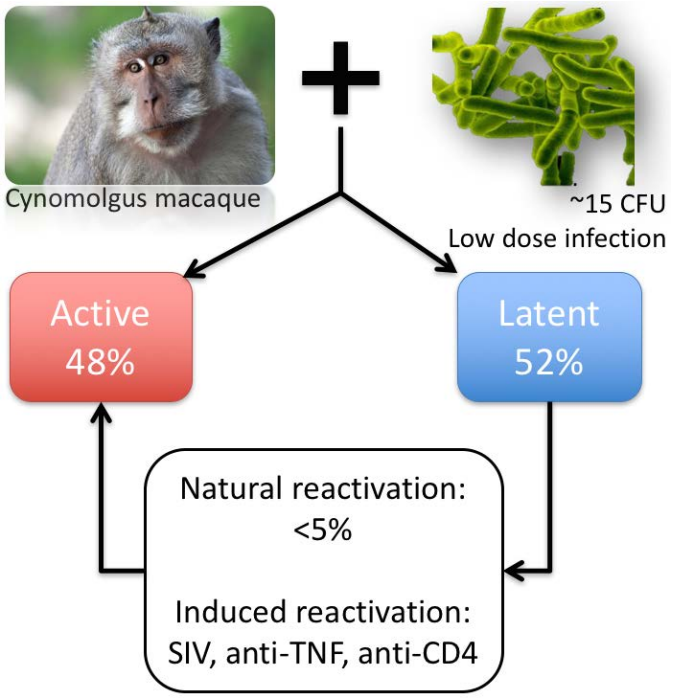

Figure 4: Our nonhuman primate model of TB. Cynomolgus macaques are infected with a low dose (~15 CFU) of Erdman strain Mtb. Half of the macaques will present with active TB and half will have LTBI. The LTBI pool of macaques can naturally reactivate but we can also induce reactivation using SIV, anti-TNF, and anti-CD4 treatments.

1.4 NONHUMAN PRIMATES: A HUMAN-LIKE MODEL OF TB

Many animal models are used in TB research, including mice, zebra fish, cattle, rabbits, guinea pigs, and nonhuman primates [105, 106]. Mice and nonhuman primates are the two more useful models, as the other models suffer from a lack of resources available for immunologic probing. Mice have their shortcomings too, as their pathology is not like humans, and they do not have LTBI. Thus, the nonhuman primate model is best for capturing the full spectrum of TB, in that it

is human-like but also is tractable to experimentation in ways that humans infected with Mtb are not [107]. Nonhuman primate models were first explored in rhesus macaques (*Macaca mulatta*) in the 1970s [108, 109]. However, the cynomolgus macaque (*Macaca fascicularis*) was the first to demonstrate evidence of LTBI after low dose Mtb infection [110]. Our laboratory further characterized this model and have since developed it extensively.

We demonstrated that cynomolgus macaques instilled with low dose Erdman strain Mtb via bronchoscope develop TB very similarly to humans [111]. 50-60% of macaques had active, progressive disease using clinical signs like gastric aspirates [112] and ESR [113], as well as CXR. The other macaques had no signs of disease in the 15-20 months of the study. There is evidence for LTBI in rhesus macaques using H37Rv delivered at a low dose [114]. We have observed formation of a Ghon complex around 5 weeks p.i. [115]. Priming of the T cells response was slow in this study and seen only after 4 weeks p.i. Early necropsy of rhesus macaques infected with H37Rv via aerosol demonstrates that Mtb reaches the hilar LN around 3 weeks p.i. Route of challenge in rhesus influences distribution of disease but not the overall outcome of the challenge [116]. We have used the cynomolgus macaque model to demonstrate that most granulomas form from a single bacterium, and have recapitulated the heterogeneity of lesions seen in humans [86]. Medical imaging has been used in nonhuman primates for tracking disease using a variety of modalities [117, 118]. We use positron emission tomography and computed tomography (PET-CT), which combines a functional map (PET) of the thoracic cavity, depending on the PET probe used, with a spatial map (CT) [2]. PET-CT for TB will be discussed in length towards the end of this introduction. Comparative genomic studies have been performed for rhesus and cynomolgus macaques and found that, while abundant heterogeneity exists in each population, there is a high degree of similarity in both species to human genes

[119]. Every cynomolgus macaque in one study responded to Mtb epitopes defined in rhesus macaques and humans [120].

1.5 THE RISE AND FALL OF BACILLE CALMETTE-GUERIN

By the turn of the 20th century, 1 in 7 deaths was due to TB (1 in 4 deaths in children) [7]. The identification of Mtb as the causative agent of TB was a turning point for both the TB field and microbiology in general [17]. Inspired by the work of Pasteur, thoughts began to turn to attenuation for vaccination. In 1902, Edmond Nocard isolated a strain of bacterium from bovine mastitis. This bacterium, called 'lait Nocard,' was sent to Albert Calmette and his assistant Camille Guerin in 1908. After 230 serial passages, this bacterium (now known as *Mycobacterium bovis*) was no longer pathogenic in laboratory animals, and was (apparently) ready for trials in humans as BCG [121]. BCG was first tested in infants born from tuberculous mothers, and was shown to protect them from disease and to be safe generally [122]. Adoption was slow, and was not helped by the "Lübeck catastrophe," in which 252 vaccinated infants were administered BCG accidentally laced with virulent Mtb [123]. Although 67 (27%) of the infants died, 68% of those who developed disease exhibited spontaneous resolution, demonstrating remarkable resistance to Mtb. Encouragingly, BCG showed efficacy in Europe. As BCG was shipped worldwide, though, other nations were reluctant still to embrace the vaccine. A large study in the Southern United States had shown little to no efficacy of BCG [124]. These data, along with a decline in TB incidence due to economic development, contributed to the decision to not deploy BCG in the United States, the main strategy of which was to instead identify LTBI patients and give them chemotherapy once available in the 1950s. This was interestingly still

contrary to evidence of efficacy in other parts of the world, like a study showing 77% efficacy of preventing disease in the United Kingdom [125], another showing efficacy for more than sixty years in Native Americans [126], and a very recent study demonstrating efficacy in a Norwegian cohort [127]. However, a massive vaccine efficacy study of BCG in Chingleput, India, using two versions of BCG showed zero protection [128], thus establishing that BCG has a wide range of efficacy depending on where it is administered. BCG demonstrated 64% efficacy against disease in Indian children in the United Kingdom, suggesting that variability in efficacy is not due to host genetics [129]. Sensitization with soil nontuberculous mycobacteria (NTM) abrogates BCG replication and immunity, suggesting that this could be the root of the problem in variable efficacy [130]. BCG vaccines in Malawi produce less IFN-γ than British vaccines, with the authors suggesting that NTM again are the likely cause of this variation [131]. Overall, a meta-analysis demonstrated that while BCG does protect infants from the worst manifestations of TB disease, e.g. spinal or meningeal TB, it does not prevent infection and provides about 50% protection against later TB [132]. Genomic comparisons between BCG and Mtb have identified many regions of difference (RD)—deletions in genes during passage to produce BCG—between them [133]. BCG induces CD8 T cells in newborns that produce IFN-γ in response to Mtb [134]. CD4 T cells are produced in greater quantities, and typically have an effector T cell phenotype [135]. BCG exhibits a lack of long-lived central memory T cells, which may be why it fails to protect later in life [136, 137]. This was mirrored by the Norwegian BCG efficacy study that had shown waning of BCG efficacy over time [127]. Re-vaccination with BCG was pursued as a method of boosting immunity, but had no strong results [138]. Interestingly, BCG re-vaccination efficacy was geographically dependent (19% in Salvador to 1% in Manaus), with a negative

correlation between efficacy and areas with high NTM, consistent with the hypothesis that NTM abrogate BCG-induced immunity.

1.6 THE MENGAGERIE OF MTB ANTIGENS

There are approximately 4000 genes in Mtb, and therefore myriad proteins which could be recognized by T cells. Many different immunodominant and subdominant antigens produced by Mtb have been identified, and more continue to be found. One of the earliest was the Ag85 complex, consisting of Ag85A-C, which has a role in cell wall biogenesis and fibronectin binding [139]. These proteins are cross reactive with NTM and are also produced by BCG [51]. Expression of Ag85B in BCG correlates with macrophage uptake, but Ag85B deficient BCG has the same efficacy as wild type BCG in mice [140]. However, BCG overexpressing Ag85 was shown in mice and guinea pigs to be superior to BCG in protection against TB, determined by a reduction in bacterial burden or increased survival [141]. ESAT-6 was first identified as a small, immunogenic protein from the culture filtrate of Mtb [142], and is arguably the most significant virulence factor that Mtb secretes. ESAT-6 stimulated IFN-γ correlates strongly with pathology in cattle after BCG vaccination [143]. ESAT-6 specific antibodies are some of the first detected during infection and increase with severity of infection [144]. ESAT-6 binds directly to TLR2 via six C-terminal residues, and prevents cellular activation [145]. ESAT-6 can form pores and cause cytolysis of epithelial cells [146]. ESAT-6 can directly inhibit IFN-γ, TNF, and IL-17 production by CD4 T cells, reduce CD25 and CD69 expression, and block proliferation [147]. ESAT-6 has been shown to also be an adhesin which binds to laminin, and is essential for dissemination of the bacterium within the host [148]. ESAT-6 permeabilizes the membrane of

the phagosomal compartment, allowing the contents of that compartment to mix with the cytosol [102]. This activates the NLRP3 inflammasome and drives type I IFN [149], which is detrimental to immunity against Mtb [150]. ESAT-6 uses its C-terminal region to accomplish this [151]. Mtb can do this and nonpathogenic mycobacteria cannot, and can be made to pathogenic by adding ESX-1 and ESAT-6. Recombinant BCG expressing ESAT-6, while more able to reduce bacterial burden after challenge, is also more virulent in mice [152], highlighting the potential pathogenicity of ESAT-6. CFP-10 is another small, immunodominant Mtb antigen found just upstream of ESAT-6 [153]. Both ESAT-6 and CFP-10 are contained in RD1, a genetic region deleted in BCG versus Mtb [154]. Both proteins are secreted as a 1:1 homodimer by ESX-1, a type VII secretion system [155]. Many of the RD1 genes work together to export ESAT-6/CFP-10 [156]. Infection of mice with Mtb lacking ESX-1 leads to poor granuloma formation [157], suggesting the role of this system in pathogenesis. Interestingly, while ESAT-6 alone inhibits IFN-γ production by CD4 T cells, ESAT-6/CFP-10 homodimers do not [147].

TB10.4 is also essential for virulence and is in the subfamily of ESAT-6 like proteins [130, 158]. Over 70% of BCG vaccinees respond to this protein [130, 159]. Similar proteins to this that are immunodominant and recognized by BCG include Mtb32a and Mtb39a [160]. In LTBI patients, dominant CD4 targets are all contained in three antigenic islands [161]. This suggests that vaccination with only one or some of the antigens contained within will be ineffective. The myriad immunodominant antigens should be exciting for those wishing to developing vaccines. However, in a study that compared 21 strains of Mtb, most of the 491 confirmed human CD4 and CD8 T cell epitopes are hyperconserved, i.e. conserved as well as housekeeping genes [162]. These data suggest that it is beneficial to Mtb for the host to mount a strong T cell response. Considering that one of those hyperconserved genes is ESAT-6, and that

ESAT-6 is critical for granuloma formation (at least in mice) [157], this also suggests that granuloma formation is beneficial as well. Protection of mice from Mtb challenge does not correlate with immunodominance by IFN-γ ELISPOT, suggesting that alternative antigens should be considered as well. Mice vaccinated with cryptic epitopes of ESAT-6 versus dominant ones show reduced bacterial burden [163]. Subdominant antigens in Mtb have indeed been identified. One such protein is Rv2660c, originally found to be expressed by Mtb under conditions of nutrient starvation and hypoxia [164]. CD4 T cells from LTBI patients respond to Rv2660c more than T cells from patients with active disease [165]. A report suggests that Rv2660c RNA may not be translated [166], but the translated protein has also been observed in BCG using mass spectrometry [167].

1.7 CELLULAR IMMUNITY TO MTB

What is known about protection from Mtb? There is a rich store of data from the last thirty years investing cellular mechanisms of immunity in murine, nonhuman primate, and human systems (Rev. in [168, 169]). CD4 T cells producing Th1 associated cytokines like IFN-γ and TNF take a central position in this canon, but other cell types and molecules have been shown to be just as, and potentially more, important. The strongest evidence that CD4 T cells are critical to immunity is that HIV infection greatly increases the risk of reactivation TB in humans with LTBI [170, 171]. We have recapitulated these results in macaques, demonstrating that infecting LBTI macaques with SIV leads to 100% reactivation which correlates with early T cell depletion [172]. Interestingly, CD4 depletion by antibody only reactivates half of LBTI macaques suggesting both a spectrum of risk and that SIV is not simply depleting CD4 T cells in these

animals [58]. ESAT-6 specific CD4 T cells adoptively transferred to mice before Mtb challenge produce high levels of Th1 cytokines, but no protection is seen until 7 days p.i., highlighting the immense ability of Mtb to hide inside phagocytic cells [173]. CD4 T cells expand rapidly upon arrival at the granuloma to help contain Mtb [174], and may have assistance from memory lymphocytes residing in the tissue [167]. Direct recognition of macrophages by CD4 T cells is required for control of Mtb [175]. A CXCR3+ parenchymal CD4 T cell population has been identified that correlates strongly with protection against Mtb [176]. These cells produce less IFN-γ than their counterparts in circulation, and migrate rapidly to the lung parenchyma upon adoptive transfer. PBMCs from patients with active disease stimulated with Mtb produce more Th2 cytokines, while PBMCs from healthy controls produce more Th1 in response to Mtb, suggesting that Th2 is detrimental [177]. Mice that receive Th1 polarized cells mounted epitope specific protective responses, while mice that receive Th2 cells have lung fibrosis and more severe disease [178]. IL-4 has been implicated in TB disease in mice [179], but IL-4 mRNA is not observed in human granulomas [180]. Recent evidence hints that IL-4 may be present only within the context of helminthic co-infections [181]. The critical role of IFN-γ was demonstrated in KO mice, which markedly increased their susceptibility to Mtb challenge [182, 183]. IL-12 from dendritic cells acts directly on CD4 to prime for IFN-γ production [184], and IL-12 deficient mice were more susceptible than wild type mice [185]. Treating mice with exogenous IL-12 increases their survival and diminishes bacterial burden [186]. This does not occur in IFN-γ KO mice, demonstrating that IL-12 is offering protection through IFN-γ. A case study of a baby with IFN-γ receptor deficiency who developed fatal BCG-induced disease complements the murine data [187]. Indeed, humans deficient in IL-12 receptor beta-1 chain have increased risk of TB disease [188], and a small deletion hotspot in human IFNGR1 is associated with dominant

susceptibility to mycobacterial infection [189]. Additional murine evidence depicts the essential role for IFN-γ produced by CD4 and its role in the CD8 response [190]. TNF also has a major role to play in cellular immunity, as in its absence a delay in the recruitment and activation of mononuclear cells occurs and leads to fatal BCG infection [191] or Mtb infection in mice [192]. The principal finding in humans is that anti-TNF therapy greatly increases the risk of reactivation TB in patients with LTBI [193]. We have also demonstrated that anti-TNF reactivates 50-75% of LTBI macaques [57]. IFN-γ dependent phagosome maturation in human macrophages is inhibited by TNF blockers [194]. Removing TNF may disturb the integrity of the granuloma in mice [195], likely through a reduction in inflammatory chemokines [196], although overt granuloma structural changes were not seen in macaques [57]. TNF blockade also interferes with the function of effector memory CD8 T cells by inducing their death through complement [197]. The expansion of γδ T cells is also stunted by anti-TNF [198].

Clearly IFN-γ and TNF produced by CD4 T cells have important roles to play in TB. Is that the whole picture, though? IFN-γ levels in PBMCs and bronchoalveolar lavage (BAL) cells frequently correlate with poor outcomes [143, 199, 200]. IFN-γ accounts for only 30% of Mtb control observed in the murine lung, but about 80% of the control in the spleen [201]. Increasing IFN-γ in this model induces lethal pathology the lungs but increases protection in the spleen, suggesting that IFN-γ might control Mtb well in extrapulmonary sites but is not sufficient to do so in the lung, and is pathogenic in large quantities. CD4 T cells have been shown to protect mice independently of IFN-γ [202]. Antigen specific CD4 T cells that cannot produce IFN-γ nor TNF also can still protect mice from Mtb challenge [203, 204]. CD4 T cell independent protection can even be seen in a study where vaccination of CD4 KO mice still induces protection [205]. In contrast to these studies, transfer of IFN-γ deficient CD4 T cells to CD4

deficient mice was less protective than transfer of wild-type T cells [190]. Thus, IFN-γ and TNF, even CD4 T cells, are not the whole picture.

What other putative cell types are associated with cellular immunity to Mtb? CD8 T cells have been shown to be important for protection against Mtb [206]. CD8 T cells can produce granulysin which kills Mtb directly [207]. Mice deficient in β2-microglobulin or MHC class I (and therefore CD8 T cells) were more susceptible than wild type mice [206]. Depletion of CD8 in the chronic stage of Mtb infection in mice leads to increased bacterial burden, suggesting that CD8 are important for long term control [208]. Depletion in rhesus macaques challenged with a high dose of Mtb ablates the partial protection conferred by BCG in that model [209]. Unpublished studies from our own lab demonstrate that depletion of CD8 T cells prior to low dose infection of cynomolgus macaques leads to increased bacterial burden, while depletion during LTBI only reactivates a subset of animals. However, the role of CD8 T cells is still controversial as demonstrated in two vaccine studies in mice where elicitation of CD8 was either not protective [210] or was compensated for when absent [211].

Regulatory T cells (T_{reg}) have been implicated in TB pathogenesis, as depletion of these cells leads to a 10-fold reduction in Mtb in mice [212]. Contrary to those data, ICAM KO mice have fewer T_{reg} cells due to aberrant signaling of transforming growth factor β (TGF-β) through SMAD3 [213], and these mice are more susceptible to Mtb challenge. In nonhuman primates, the frequency of T_{reg} cells in PBMC decreases with Mtb challenge and increases in the airways [214]. LTBI macaques had higher T_{reg} frequencies in PBMCs pre-challenge, while macaques with active TB had increased T_{reg} cells in PBMC during challenge. It is likely that Tregs are important for controlling pathology, but also may impair clearance of the bacilli, and need more intensive study. The role of other so-called nonconventional T cells is just beginning to gain

appreciation. γδ T cells can lyse macrophages containing Mtb and are an early source of IFN-γ [215]. IL-17 production is dominated by γδ T cells [216], and these cells have shown the ability to generate recall responses following BCG and Mtb challenge in macaques [217]. Natural killer T cells (NKT) are present in humans with active TB in smaller numbers than in LTBI [218]. NKT may recognize glycolipids on BCG which can augment its efficacy [219]. Mucosa-associated invariant T cells (MAIT) recognize Mtb antigens in patients with active TB [220]. CD1-restricted T cells, which recognize mycobacterial lipids, bind monomycolate and C32-phosphomycoketide and are detected in PBMC of infected humans [221]. These T cells can produce IFN-γ and TNF, but do not vary in frequency between disease status and do not correlate with T cell responses to proteins [222]. MAIT cells are more prevalent in airways than in PBMC, and may play an early role in priming the immune response for pathogen elimination [223].

There is an underappreciated role for B cells in Mtb infection, which is not surprising since Mtb is typically an intracellular pathogen. There is some evidence that monoclonal antibodies against cell wall components of Mtb are protective [224]. The Mtb proteins ESAT-6, α-crystallin, and MSTA-10 are broadly recognized by antibodies from sera of macaques [225]. There is an early, transient antibody signature in LTBI macaques that stably increases in active TB and reactivation disease [226]. In humans, antibody levels increase with bacillary burden [226], but attempts to use antibody responses as biomarkers of disease have not yet been successful given the heterogeneity in responses in humans and macaques. B cells present primarily in clusters around the periphery of the granuloma and have germinal center-like properties [78]. B cells can regulate neutrophilia during Mtb infection and BCG vaccination by modulating the IL-17 response [227]. B cells readily produce pro- and anti-inflammatory cytokines, including IL-1β, IL-10, IL-17, IL-21, and TNF [228]. Stimulation of B cells from

human patients with LTBI via TLR-4 and 9 produces the greatest quantity of cytokine, and plasma cells (CD138+CD27-) from these individuals typically produce the most cytokines upon stimulation. Antibodies can be differentially glycosylated during post-translation modifications, and antibodies between active TB and LTBI have been recently found to have distinguishing patterns of glycosylation [229]. Antibodies from LTBI patients in this study had enhanced Fc effector profiles and were more effective at promoting intracellular killing of Mtb in macrophages.

There are plenty of other cytokines and signaling entities that have been implicated to have a role in Mtb infection. IL-17 has been implicated in immunity to Mtb, especially when driven by IL-23 [230]. As previously mentioned, γδ T cells dominate production of IL-17 and can even generate recall to Mtb following BCG vaccination [216, 217]. IL-17 can recruit Th1 cells, which are linked to BCG-induced protection in mice [231]. IL-17 boosted by BCG correlates to protection in cattle [232]. In one study, BCG-associated protection was IFN-γ independent but IL-17 dependent, mediated by CXCL13 induction to facilitate the localization of CXCR5+ T cells made in lymphoid structures near granulomas [233]. However, while potentially beneficial, IL-17 has also been linked to increased pathology and bacterial burden in the spleen, and may contribute to dissemination [234]. PBMCs from humans with active TB also express more IL-17 than LTBI patients [48]. IL-10 is another cytokine implicated in TB, with IL-10 mRNA detected in high levels in human TB lesions being mainly produced by macrophages [180]. Mtb is able to inhibit TNF-dependent apoptosis by inducing IL-10 dependent secretion of soluble TNF receptor 2 from macrophages [235]. Mtb antigens can stimulate IL-10 production through TGF-β signaling [236]. Autocrine IL-10 production in macrophages induces an alternatively activated state that suppresses anti-Mtb effector

mechanisms without compromising T cell immunity [237]. IL-10 KO mice also have reduced bacterial burden in the lungs after challenge, preceded by an accelerated IFN-γ response in the lung via influx of CD4 T cells [234]. While IL-10 seems to contribute to Mtb pathogenesis, depletion of IL-10 185 days p.i. in mice leads to Mtb regrowth, essentially due to unchecked Th1-sponsored inflammation [238]. We have also shown that IL-17 and IL-10, when balanced, are the strongest correlate of sterilization within individual macaque lung granulomas [239]. Computational modeling supports this hypothesis [240]. Another immunoregulatory molecule, TGF-β, is produced in greater quantities from PBMC of active TB patients compared to LTBI, and can be localized in lung lesions [241, 242]. Mtb antigens can stimulate the production of TGF-β and IL-10 through TGF-β [241, 243]. BCG modified to express a peptide that blocks TGF-β confers additional protection in mice [244]. Mtb can directly stimulate monocytes to active TGF-β [245], and blocking TGF-β using siRNA improves TB disease in mice [246]. Nematode co-infection induces TGF-β which dampens the IFN-γ response, increasing the susceptibility of mice to Mtb challenge [247]. Not all immunoregulatory molecules are bad, though, as PD-1 KO mice are very susceptible to Mtb challenge, due to CD4-driven host inflammation and tissue destruction that does not reduce bacterial burden [248]. Type I interferon (IFN), while important for clearance of viruses, has been solidly demonstrated to be pathogenic in the context of Mtb infection. An association of bacterial hypervirulence with enhanced production of type I IFN has been demonstrated in the murine model, through suppression of Th1 [249]. In both murine and human cells, type I IFN is preferentially induced by Mtb in an ESX-1 dependent mechanism [250]. In a murine study utilizing intranasal instillation of poly(I:C), adjuvant driven type I IFN exacerbates TB disease [251]. A type I IFN gene signature was identified in patients with active TB in Indonesia where monocytes were

identified as the primary producers of this molecule [44]. The balance of type I and II IFN production determines the outcome of another mycobacterial disease—leprosy [252]. Induction of type I IFN leads to suppression of IL-1 and is detrimental for TB immunity [150]. IL-1 and PGE2 inhibit macrophage necrotic cell death [253]. Depletion of IL-1 promotes detrimental TB outcomes, whereas overproduction of IL-1 is beneficial [254]. IL-1 induces PGE2, which enhances the antimicrobial activity of macrophages and inhibits production of type I IFN [255].

1.8 THE NEED FOR REAL CORRELATES OF PROTECTION

There are currently no correlates of protection against TB. The main reason for this is that randomized, controlled clinical trials of effective vaccines are required to identify correlates [256], and there are no effective vaccines against TB. Instead, those in the TB field have sought to identify correlates of risk of active disease or LBTI. However, this is extremely misleading. LTBI is not protection, as those individuals still have a risk of developing active disease [23, 54]. In order to actually identify correlates, we will have to improve upon nature and confer something more potent that natural immunity against this disease. It is still worth an exploration of what is associated with disease or latency. One of the primary outcome measures in pre-clinical and clinical trials of novel TB vaccines is the stimulation of IFN-γ, although this has never been shown to correlate with protection against Mtb infection [257, 258]. In fact, many studies suggest that IFN-γ correlates with active disease in human PBMCs [199], with pathology in cattle after BCG vaccination [143], and is higher in BAL cells from patients with active TB and drops after TB chemotherapy [200]. Protection against TB in mice conferred by BCG boosted by H1, a vaccine containing Ag85B and ESAT-6, does not correlate with IFN-γ

production in PBMCs [259]. Multifunctional T cells have been shown to correlate with protection in other infectious diseases where cellular immunity is important [260]. However, multifunctional Th1 cells in blood correlate with active TB in children [261], with active TB in adults [262], and with bacterial burden in macaques [263]. CD4 T cell production of IFN-γ, IFN-γ/TNF/IL-2, and CD8 T cell production of IFN-γ do not correlate with risk of TB disease after BCG vaccination during the first two years of life [264]. A reduction in central memory CD4 T cells and increase in IL-17 were associated with active TB in adults [48]. AERAS 402, an experimental viral based vaccine, elicits robust cellular immune responses in macaques but these responses do not correlate with protection [265]. Transcriptional signatures are being investigated, but may be different between adults and children [266]. One study found 13 molecules associated with protection in mice against TB shared between five experimental vaccines [267]. Another two studies found signatures including activated CD4 T cells associated with increased risk of TB disease [268, 269].

1.9 NOVEL VACCINES FOR TB

An effective vaccine for TB could target the disease at multiple stages. Therapeutic vaccines would act as host-directed therapy to ameliorate active disease. Post-exposure vaccination would target patients with LTBI and works to prevent active (transmissible) disease. The gold standard of TB vaccination would be a pre-exposure vaccine, one that prevents initial infection. However, since no correlates of protection to TB exist, a pre-exposure vaccination is a high bar to reach. A post-exposure vaccine would still be desirable since by preventing active disease, the

transmissible form of the disease is blocked, thereby halting transmission of Mtb. Currently, vaccines that target all three of these stages are in clinical development.

Table 1: Vaccines utilized in this dissertation.

Name	Type	Antigens	Delivery	Refs.
BCG	Live attenuated	M. bovis (many)	intradermal	[132, 257, 270]
M72	Protein subunit Live attenuated	Mtb32a (Rv1196) Mtb39a (Rv0125)	intramuscular aerosol	[271-273]
H56	Protein subunit	ESAT-6 (Rv3875) Ag85B (Rv1886c) Rv2660c	intramuscular	[274-277]
EB	Live attenuated	ESAT-6 (Rv3875) Ag85B (Rv1886c)	intramuscular aerosol	Experimental but similar to H1
4ag	Live attenuated	ESAT-6 (Rv3875) Rv1733 Rv2626 RpfD	intramuscular aerosol	Experimental

The two main strategies in the vaccine field for TB are to replace BCG, or boost and/or broaden the immune response to BCG later in life. The majority of vaccines seeking to replace BCG are recombinant strains of BCG adjusted to be more immunogenic. These include strains of BCG that overexpress antigens (rBCG30, which overexpresses Ag85B [141, 278]), strains that express pore-forming toxins to allow escape to the cytosol for cross presentation of antigens (VPM1002 [279-281]), or strains that do both (AERAS 401 [282] and AERAS 422 [283], which was discontinued due to safety concerns [284]). Another approach has been to attenuate Mtb itself, by removing phoP and fadD26, which are major regulators of pathogenicity [285-288]. An attenuated Mtb strain lacking sigH has also been developed and shown efficacy in rhesus macaques [289]. There is a significant issue with this approach to new vaccines for TB. Since there can be no real replacement trial due to the partial efficacy of BCG, any vaccine must be given on top of BCG anyway, at least in most countries in the world. Thus boosting and/or broadening the immune response to BCG with heterologous vaccination is the more desirable strategy [290].

The vaccine furthest along the path towards deployment in people is MVA85A, which contains Ag85A encoded in modified vaccinia Ankara. MVA85A was shown to be safe and immunogenic in adults [291], in adolescents and children [292], in BCG-vaccinated infants [293], and in HIV infected adults with active TB [294]. However, this vaccine completely failed to protect infants from either Mtb infection or TB disease [295], nor was it effective in HIV+ adults [296]. While this highlights the ability for clinical trials for novel TB vaccines to be effectively run [38], this failure should not have been surprising due to lack of efficacy in pre-clinical models [286, 297]. This heterologous boost is now being tested through a new route of administration [298, 299]. Nevertheless, actual efficacy is not being assessed in pre-clinical

models, only peripheral immunogenicity. This approach is likely to fail as well, as peripheral recall responses have repeatedly been shown to not correlate with efficacy [264, 265, 295]. AERAS 402 is another viral vector heterologous boost that has been demonstrated to be safe and immunogenic in humans [300]. This vaccine did not increase protection in macaques delivered intramuscularly, despite generating potent immune responses to vaccine antigens [265]. This vaccine as well is now being investigated by different delivery routes [222, 301]. ID93 was developed as a heterologous protein fusion boost targeted against multidrug resistant Mtb and has been tested in mice and macaques [302, 303]. Administration of this vaccine during TB chemotherapy in mice and macaques has shown to improve clearance of Mtb over chemotherapy alone [303]. M72 is a fusion protein boost containing Mtb32a (Rv0125) and Mtb39a (Rv1196), two immunodominant Mtb proteins. This vaccine has been tested in mice [304, 305], guinea pigs [271], rabbits [306], macaques [273], and humans [272, 307-310]. H1 is another fusion protein vaccine, consisting of Ag85B and ESAT-6. This vaccine has also been tested in a variety of pre-clinical models [311-313]. This vaccine induces long-lived central memory CD4 T cells that correlate with protection in mice, produce memory-associated cytokines (TNF, IL-2, or both), and have strong proliferative potential even after one year [314, 315]. The maintenance of memory is associated with Mtb control in this model, and these vaccine-specific cells can mobilize quickly from the LN to the lung [136, 316]. H1 has been shown to be safe and immunogenic in humans [317, 318]. H56, similar to H1 but includes Rv2660c, was developed as a multistage vaccine to engender protection against both primary TB and reactivation [274]. H56 protects nonhuman primates from experimental reactivation with anti-TNF [275], induces a population of lung-homing CD4 T cells in mice [277], and is safe and immunogenic in human adults [276]. H4 and H28 are similar vaccines but utilize TB10.4 instead of ESAT-6 to avoid

confounding ESAT-6 based diagnostics. These vaccines have also been shown to be safe and immunogenic [315, 319]. However, ESAT-6 is responsible for most of the protection conferred in these vaccines, suggesting that vaccines moving forward need to contain that protein [320].

1.10 FAILURE TO LAUNCH: THE NEED FOR NEW APPROACHES

The fact that we now have 14 vaccines in clinical trials (for safety, immunogenicity, and protection) represents an enormous advance towards eradication of TB. However, significant roadblocks exist between where we are and the implementation of an efficacious TB vaccine. Three main problems are: 1) intramuscular boosting of BCG, and even intradermal administration of BCG, may not be the most effective routes of vaccination; 2) the vast majority of the vaccines in clinical trials have yet to demonstrate greater efficacy than BCG in pre-clinical models; and 3) the current endpoints for clinical trials are ineffectual and increase the length and cost of the trials.

Evidence both old and new points to routes other than intradermal for BCG and intramuscular for heterologous boosting [321]. Old data in rhesus macaques vaccinated with intravenous BCG (1 mg) show significant resistance to Mtb challenge, with 57% of animals have no evidence of TB pathology 12 weeks p.i. and the rest exhibiting minimal disease [108]. Vaccination of rhesus macaques with aerosol BCG is not associated with adverse effects and protects the animals almost as well as intravenous BCG [109]. Intravenous BCG induces potent systemic and lung-resident CD4, CD8, and γδ T cell responses while aerosol BCG only induces those responses in the lung [322]. That being said, pulmonary administration of BCG induces higher frequencies of mucosal antibodies and γδ T cells in the lung compared to intravenous

BCG, which induces stronger peripheral responses [322]. Pulmonary "challenge" in TST+ humans with purified Mtb proteins leads to rapid expansion of T cells 48 hours later, suggesting that prior priming in the lung generates a memory pool capable of rapid response [323]. Intravenous Mtb challenge of mice leads to earlier production of Th1 in the lung [324]. Simultaneous intravenous/aerosol Mtb challenge in this model demonstrates early protection conferred by intravenous challenge to the lung challenge, suggesting that intravenous vaccination is a tractable strategy for control of Mtb, although perhaps difficult to implement on a wide scale, particularly in infants. LTBI patients have a 79% lower risk of developing active TB after reinfection versus uninfected individuals, hinting that prior Mtb infection in the lung generates local immunity to subsequent infection [325]. As previously mentioned, interference of NTM in BCG vaccination is seen as the major reason for lack of BCG efficacy [130, 131, 138]. Oral tolerance to NTM has been shown in a new study to interfere with intradermal BCG, but not BCG delivered by aerosol [326].

Table 2: Adjuvants utilized in this dissertation

Name	Components	Immunity	Refs
IC-31®	antibacterial 11-mer peptide ($KLKL_5KLK$) CpG motif (ODN1a)	Th1/Th2	[327]
CAF01	cationic liposome (DDA) glycolipid immunomodulator (TDB)	Th1/Th17	[318, 328, 329]
AS01E	cationic liposome (DDA) glycolipid immunomodulator (TDB)	Th1	[330]
Ad5	replication-deficient human adenovirus 5	Th1	[331-333]

In addition to new routes of vaccination, dosing and adjuvants are also important to investigate. Repeated immunization has been shown to induce entry of immune cells into non-lymphoid tissues [334]. Different adjuvants given with ID93 in mice produce different efficacy against Mtb challenge [335]. Different vectors or formulations of the same antigen direct the specificity of the adaptive response to target more or less protective epitopes [336]. For example, Ag85A delivered in Ad5 produces an IL-12 polarized response, while delivery in VSV induces more type I IFN [337]. Deliver of ID93 in two different TLR-4 agonists give slightly more protection against Mtb challenge in mice than having only one [338].

New endpoints for pre-clinical and clinical trials will more effectively identify promising vaccine candidates reducing time and cost. As mentioned previously, PET-CT is an incredibly powerful tool to probe disease progression and efficacy of interventions in our human-like macaque model of TB [2]. High resolution CT is better than CXR at predicting active TB with a sensitivity of 96% versus 48% [339]. However, much of the strength of the modality comes from PET and the use of FDG as a probe, which incorporates into metabolically active cells. In the context of TB, FDG avidity in granulomas is likely conferred by macrophages, neutrophils, and activated lymphocytes [340]. Two different patterns of TB have been identified using PET: a pulmonary type more localized to the lung; and a lymphatic pattern associated with more intense systemic infection [341]. An increase in standard uptake values (SUV) of FDG in the thoracic LN occurs in household contacts who later have LTBI [342]. The maximal SUV in the lung can distinguish between active TB and old TB with 100% sensitivity and specificity using double phase PET imaging over 60 minutes [343]. Another case series has also suggested a role for PET to distinguish between active TB and LTBI [344]. In our cynomolgus macaque model, an early increase in the number of new lung granulomas and SUV predict development of active TB

[345]. LTBI human subjects with higher maximal SUV are at a higher risk of reactivation TB [346], and we have demonstrated the ability to assess risk of reactivation in macaques using PET [5]. PET can also be used to predict progression of HIV associated TB disease in humans [347]. In addition to probing disease, PET-CT has been used to investigate the efficacy of TB chemotherapy. The maximal SUV in LN and number of FDG-avid LN are higher in drug non-responders [348, 349]. We have shown in cynomolgus macaques that PET-CT can evaluate drug efficacy [2, 350]. This technology was used to evaluate a new application of an antibiotic for multidrug resistant Mtb in humans [351], and the PET-CT data from that study matched our nonhuman primate data from a similar study [350]. Therefore, PET-CT is a robust means to assess TB interventions, and represents a potent and novel method to evaluate vaccine efficacy.

2.0 STATEMENT OF THE PROBLEM

The World Health Organization estimates that there were 10.4 million new cases of TB in 2015 and 1.8 million deaths, or almost 5,000 deaths every day, due to lack of an effective vaccine. This disease disproportionately affects the world's poorest nations and will cost them $1-3 trillion over the next decade. Many infants worldwide are vaccinated with BCG, but the vaccine has variable efficacy and does not protect against pulmonary infection, which is the most common form of TB. The immune responses necessary to protect against infection or disease are unknown, hindering the development of new vaccines. Many novel vaccine candidates are in development, but clinical trials are lengthy and expensive. There are no validated biomarkers for protection against active disease; clinical signs and symptoms are used as an endpoint measure instead, but can take months or years to appear.

In this series of studies, we utilized both human-like (nonhuman primate, NHP) models of disease and novel vaccines to determine mechanisms of successful vaccine-induced immunity. Studying human TB is very challenging due to an inability to manipulate the system, accurately determine time, dose or strain of infection, and sample physiologic compartments besides blood. An animal model can overcome these obstacles. However, the most common model (murine) does not faithfully reflect disease progression or pathology observed in human TB. To meet this need, we have used one NHP model of disease (cynomolgus macaque), which presents with infection outcomes like humans—including latent infection—and the full spectrum of human

granulomas and pathology, as well as an NHP model that is more susceptible to active tuberculosis (rhesus macaque). The close similarity of disease to humans makes these models more translatable to human clinical studies than other models, while still being more tractable than studying actual humans. We utilized live serial PET-CT imaging, which allows us to track pathology and compare number and size of lesions, along with uptake of ^{18}F-fluorodeoxyglucose—interpreted as a general marker of inflammation. Using this advanced model system coupled with PET-CT, we have addressed the need for correlates of protection in the following aims:

2.1 AIM 1: DETERMINE ABILITY OF PRIME-BOOST VACCINATION TO PROTECT AGAINST TUBERCULOSIS

HYPOTHESIS: Prime-boost vaccination provides superior protection against tuberculosis compared to boost alone.

Rhesus macaques were either unvaccinated, vaccinated with BCG, or primed with BCG and boosted with one of six vaccines. Outcomes were compared between these cohorts to evaluate the efficacy of prime-boost vaccination. Macaques were then partitioned by outcome to identify early markers predictive of outcome, and T cell signatures in lung-draining lymph nodes associated with improved outcome.

2.2 AIM 2: CHARACTERIZE PROTECTION AGAINST REACTIVATION ENGENDERED BY VACCINATION

HYPOTHESIS: Early events in lung granulomas and lymph nodes are associated with low apparent risk of reactivation disease.

Cynomolgus macaques were either unvaccinated, vaccinated with BCG, or primed with BCG and boosted with H56:CAF01, previously shown to protect LTBI macaques from anti-TNF induced reactivation. Macaques were necropsied at six months post-Mtb challenge, and phenotypes associated with protection were characterized. This study was then repeated but macaques were necropsied at six weeks post-Mtb challenge. Outcomes at necropsy and immunological signatures in primary tissues were then identified that correspond to protection against reactivation.

2.3 AIM 3: IDENTIFY PREDICTIVE MARKERS OF VACCINE EFFICACY

HYPOTHESIS: PET-CT predicts vaccine efficacy early post-Mtb infection.

Control macaques from a variety of past studies were utilized to develop a holistic outcome score. Macaques from AIM 1 and AIM 2 were then fit to this score. PET-CT and peripheral blood markers were then identified that correlated with outcome.

3.0 MODULATION OF INFLAMMATORY RESPONSE ASSOCIATED WITH IMPROVED OUTCOME IN THE RHESUS MACAQUE MODEL OF TUBERCULOSIS

Data from this chapter will be incorporated with additional data from collaborators at the NIH NIAID Vaccine Research Center and subsequently published as a co-first author manuscript.

3.1 ABSTRACT

Tuberculosis (TB) is a major global health crisis. Vaccination with BCG fails to protect against pulmonary TB, the transmissible form of the disease, highlighting a desperate need for a new vaccine. The goal of this study was to evaluate prime-boost vaccination as a tractable strategy for combatting TB. BCG significantly reduces burden of TB in the lungs of rhesus macaques experimentally infected with *Mycobacterium tuberculosis*, the causative agent of TB. Recombinant human adenovirus 5 given after BCG greatly undermines the protection conferred by BCG. Macaques with lower lung inflammation assessed by PET-CT have better outcomes at the conclusion of the study. Lung-draining lymph nodes, but not lung granulomas, exhibited different frequencies of cytokine-producing T cells between better and worse outcomes. This study demonstrates the success of PET-CT as a predictive tool and presents a need to continue investigating routes of vaccination and types of regimens.

3.2 INTRODUCTION

An estimated one billion people have succumbed to tuberculosis (TB) over the past two centuries [7]. Bacille Calmette-Guérin (BCG) was developed between 1908 and 1921 to curb the mortality inflicted by this disease [122, 352]. The deployment of this vaccine and industrialization of the western world greatly reduced the incidence of TB in the developed world [132, 353], but it still greatly impacts much of the rest of the world [7]. 100 million doses of this vaccine are given annually, protecting infants from the worst manifestations of TB but not protecting adolescents and adults from pulmonary infection and disease [7, 132]. A modern study of BCG efficacy in Norway demonstrates 60% efficacy at preventing TB disease for the first two decades of life declining to 40% in the second two decades [127]. Interestingly, in a study in human infants, BCG generates both high and low inflammatory responses, and neither correlate with risk for Mtb infection [264]. The primary new strategies that seek to bolster the waning immunity conferred by BCG are the replacement of BCG with a new live attenuated vaccine and boosting and/or broadening of the initial response to BCG [354]. Since BCG does confer partial efficacy to infants [132], any clinical trial cannot exclude BCG, which makes the replacement of BCG unlikely. Therefore, much of the attention of global health agencies is on this prime-boost strategy.

Thirteen vaccine candidates are in clinical trials [355], and many more are in pre-clinical trials [356], all employing a variety of antigens and delivery systems. The lack of both an effective vaccine and complete natural clearance of *Mycobacterium tuberculosis* (Mtb; the causative agent) means that there are no correlates of protection against infection. Th1 and Th17 type immunity have been shown in animal models and humans to a lesser extent to be important for control of Mtb (Rev. in [169]). Vaccination with BCG has been shown in humans to promote

Th1 cellular immunity [137]. Two subunit vaccines developed to boost and broaden the immune response to BCG are M72 and H56, both in human clinical trials [355]. M72 is composed of two proteins, Mtb32a and Mtb39a, and has been shown to enhance Th1 immunity in murine [305], guinea pig [271], rabbit [306], and cynomolgus macaques [273] as Mtb72F delivered in a variety of systems. This vaccine shows similar immunogenicity in humans as M72 delivered in AS01E [330], an adjuvant that elicits Th1 immunity through TLR4 [357]. H56 is composed of three proteins, ESAT-6/Ag85B/Rv2660c, and has been demonstrated to provide protection from Mtb infection pre- and post-Mtb exposure in the murine model [274], and protects cynomolgus macaques from anti-TNF induced reactivation [275]. H56 delivered in CAF01, a liposomal adjuvant designed to elicit Th1 and Th17 immunity [328], is thought to mediate protection through long-lived central memory CD4 T cells [315, 316] and by generating CD4 T cells that express lung homing markers and efficiently migrate to that site [277]. However, eliciting these responses in T cells in the blood through vaccination has yet to pan out to successful prophylaxis. To wit, the first novel human TB vaccine elicited strong recall responses in the blood and yet exhibited no efficacy in preventing Mtb infection in the lung [295]. Additionally, studies in human infants show that BCG elicits multifunctional CD4 T cells that are not associated with protection against active TB disease [264]. Our laboratory and others have demonstrated that T cell responses in the blood do not match those seen in the lung [239, 263], suggesting that a blood signature, unless correlated with outcome, is a poor measure in and of itself. This highlights the need for new outcome measures and tools to assess vaccine efficacy in pre-clinical models to downselect promising candidates to advance into humans.

The goal of this study was to evaluate prime-boost vaccination as a tractable strategy in combatting TB. We sought to compare two routes of booster vaccination: subunit vaccination in

adjuvants delivered intramuscularly; and antigens encoded in non-replicative adenovirus vectors delivered intramuscularly and by aerosol. This is the first nonhuman primate study to directly compare intramuscular vaccination to intramuscular and aerosol vaccination, or to compare the same vaccine as a protein fusion or in a viral vector. This allowed us to compare both the ability of these systems to enhance the efficacy of BCG and to directly compare the routes of vaccination and antigens delivered. We also demonstrate the use of PET-CT as a powerful tool to assess outcome early after Mtb challenge, and highlight the role of the lung-draining lymph nodes (LN) as critical sites of immunity against TB.

3.3 RESULTS

3.3.1 Humane endpoint as an outcome measure

Table 3: Cohorts in study and vaccination schedules. This table describes the eight separate groups in this the study, along with number of macaques in each group (n), their prime vaccination, boosts including antigen and vehicle, and an abbreviated schedule with route information (see materials and methods for more detail concerning boosts, dosing, route, and the schedule). i.d.=intradermal. i.m.=intramuscular. aero=aerosol.

Group	n	Prime	Boosts	Boost schedule
1	12	PBS	---	---
2	8	BCG (i.d.)	---	---
3	8	BCG (i.d.)	M72:AS01E	Weeks 16 and 20 (i.m.)
4	6	BCG (i.d.)	H56:CAF01	Weeks 20 and 25 (i.m.)
5	7	BCG (i.d.)	Ad5(empty)	Week 25 (i.m. and aero)
6	8	BCG (i.d.)	Ad5(M72)	Week 20 (i.m. and aero)
7	8	BCG (i.d.)	Ad5(EB)	Week 20 (i.m. and aero)
8	7	BCG (i.d.)	Ad5(4ag)	Week 25 (i.m. and aero)

Sixty-four rhesus macaques were utilized for this study (Table 3): unvaccinated controls (Control, n=12); macaques vaccinated with BCG Danish only delivered i.d. (BCG, n=8); macaques vaccinated with BCG boosted by protein subunit vaccines (H56 in adjuvant CAF01, n=6; M72 in adjuvant AS01E, n=8) delivered twice i.m.; macaques vaccinated with BCG boosted by a non-replicative human adenovirus 5 (Ad5) vector containing no antigen delivered

once i.m. and by aerosol as a control (BCG-Ad5(empty), n=7); and macaques vaccinated with BCG boosted by Ad5 containing three antigen sets (ESAT-6/Rv1733/Rv2626/RpfD, n=7; ESAT-6/Ag85B, n=8; M72, n=8) delivered once i.m. and aerosol. During vaccination, our collaborators at the NIAID Vaccine Research Center (VRC) collected immunologic data including bronchoalveolar lavage (BAL) cell responses to vaccine antigens, as well as responses from peripheral blood mononuclear cells (PBMCs). The rhesus macaques were transferred to us and then at 30 weeks post-BCG vaccination challenged with via bronchoscope with low-dose (8-16 CFU) Mtb Erdman strain.

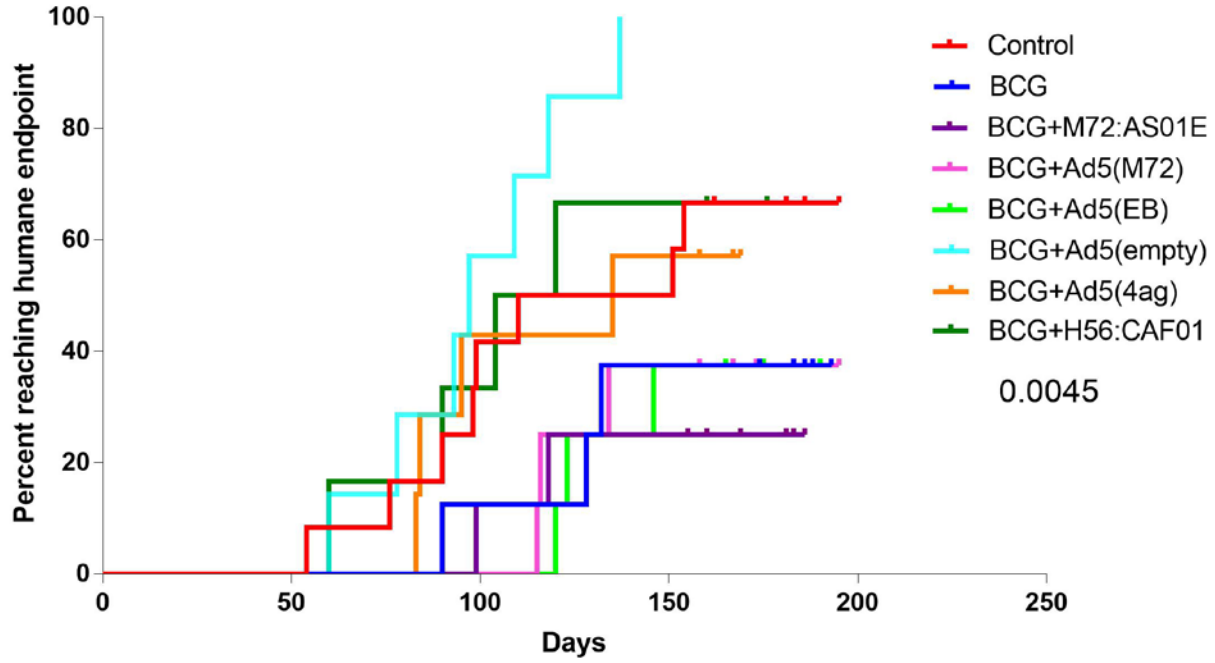

Figure 5: A comparison of the percent of macaques in each group that reached humane endpoint before the conclusion of the study. Reaching human endpoint was determined by clinical criteria described in the materials and methods. Difference between the groups was assessed using the Mantel-Cox test with p value directly reported.

The pre-determined endpoint of the study was 6 months post-infection, at which time animals were necropsied. Any animals reaching humane endpoints were necropsied earlier using

defined clinical criteria (see Materials and Methods). We observed significant differences in the numbers of macaques in each group who reached humane endpoint before the conclusion of the study (p=0.0045; Fig. 5). Two thirds (66.67%) of the control animals reached humane endpoint before the conclusion of the study. Vaccination with BCG improved general welfare of the macaques, with only about a third (37.5%) reaching humane endpoint before 6 months. Boosting BCG had variable impact upon this outcome measure, from 25% (BCG+M72:AS01E) to 66.67% (BCG+H56:CAF01) reaching humane endpoint before 6 months. Boosting BCG with empty Ad5 greatly increased the macaques' susceptibility to Mtb, as none of the animals reached the end of the study.

3.3.2 BCG confers protection against TB disease

We first assessed the ability of BCG to protect rhesus macaques using our outcome measures:

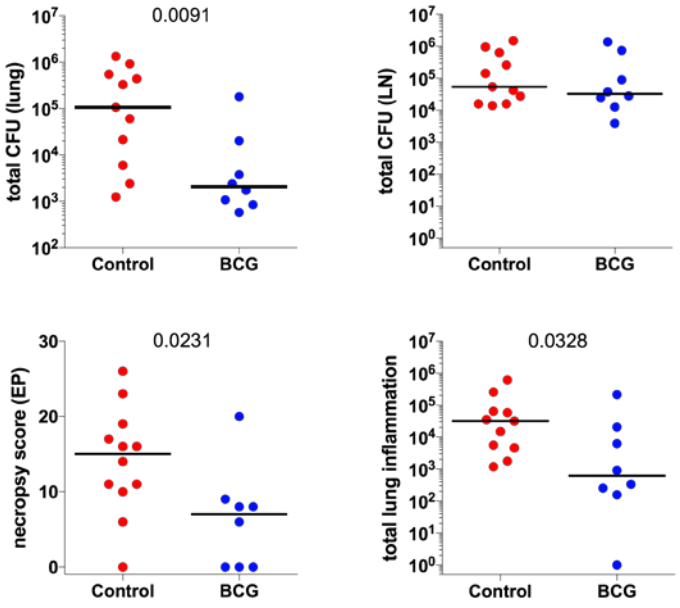

Figure 6: A comparison of control macaques to BCG vaccinated macaques. Each dot represents one animal and bars represent medians. Comparisons were done using the Mann-Whitney test with p values reported.

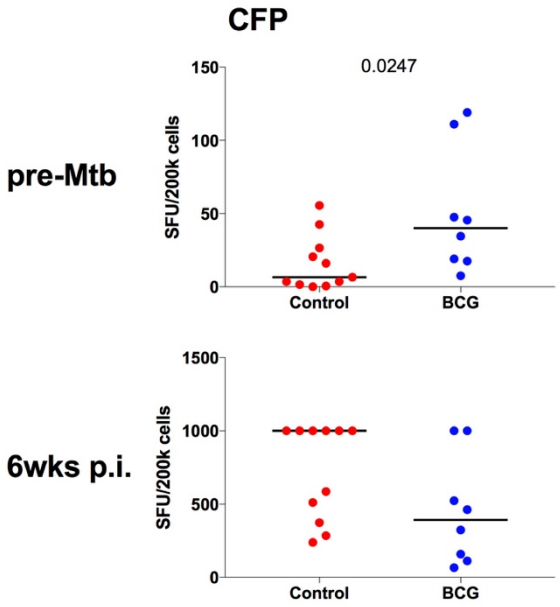

Figure 7: Antigen-specific IFN-γ responses to CFP (pan-mycobacterial stimulation) before challenge or six weeks post-challenge between control macaques to BCG vaccinated macaques. Each dot represents one animal and bars represent medians. Comparisons between the groups were done using the Mann-Whitney test with p value reported. SFU=spot forming units.

i.e. total bacterial burden in the lung and lymph nodes (LN), extrapulmonary pathology observed grossly, and total lung inflammation assessed by PET, where total lung inflammation is the sum of all image voxels of FDG-avid lung pathology. Previously published data have shown variable effects of BCG on protection in macaques, although several of these studies used high dose Mtb challenge [286, 358]. We show that BCG does induce some level of protection against disease progression following low dose challenge (Fig. 6). Compared to unvaccinated animals, there was a significant reduction in total CFU in the lungs (nearly 100-fold, p=0.0091), but not in the thoracic lymph nodes. We also observed a significant reduction in extrapulmonary involvement (p=0.0231), and in lung inflammation (p=0.0328). This protection was associated with significant increase of IFN-γ ELISPOT responses to culture filtrate protein (CFP, pan-mycobacterial) before challenge, and a trend towards lower responses after challenge (Fig. 7).

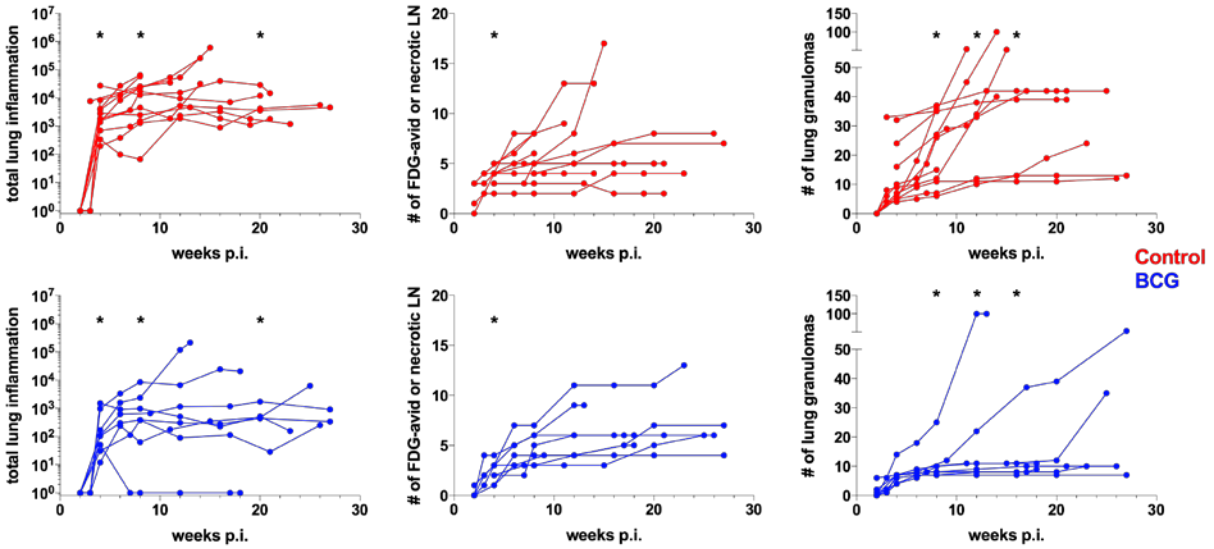

Figure 8: PET-CT markers from challenge until necropsy between control macaques to BCG vaccinated macaques. Each line represents one animal. Comparisons of markers between groups was done using the Mann-Whitney test (* indicates significant difference) with p values reported in the text. ***Left*** Time points with significant difference were 4, 8, and 20 weeks p.i. ***Center*** Time point with significant difference was 4 weeks p.i. ***Right*** Time points with significant difference were 8, 12, and 16 weeks p.i.

BCG was not effective at preventing establishment of infection, as determined by similar numbers of lung granulomas in unvaccinated and BCG vaccinated animals at 4 weeks post-infection (Fig. 8). However, BCG vaccinated macaques have fewer lung granulomas than controls at 8 weeks (p=0.0306), 12 weeks (p=0.0301), and 16 weeks (p=0.0477) after Mtb challenge. BCG vaccinated macaques also have less total lung inflammation p.i. at 4 weeks (p=0.0026), 8 weeks (p=0.0099), and 20 weeks (p=0.0304). At 4 weeks p.i., we observed fewer involved LN by PET (p=0.0089). Thus, BCG is at least partially effective in this model system.

3.3.3 Protein fusions do not improve BCG-induced protection

We next sought to assess the impact of boosting BCG with protein fusions containing Mtb and/or BCG antigens on outcomes in specific compartments of the rhesus macaques. Neither M72 or H56 protein fusions in adjuvants was effective at boosting BCG-induced protection using these outcome measures (Fig. 9). Surprisingly, a trend towards increased lung bacterial burden with protein boost was observed (top left). There was no effect on LN bacterial burden or lung inflammation, but there was a trend towards decreased extrapulmonary pathology with M72/AS01E boost (bottom left).

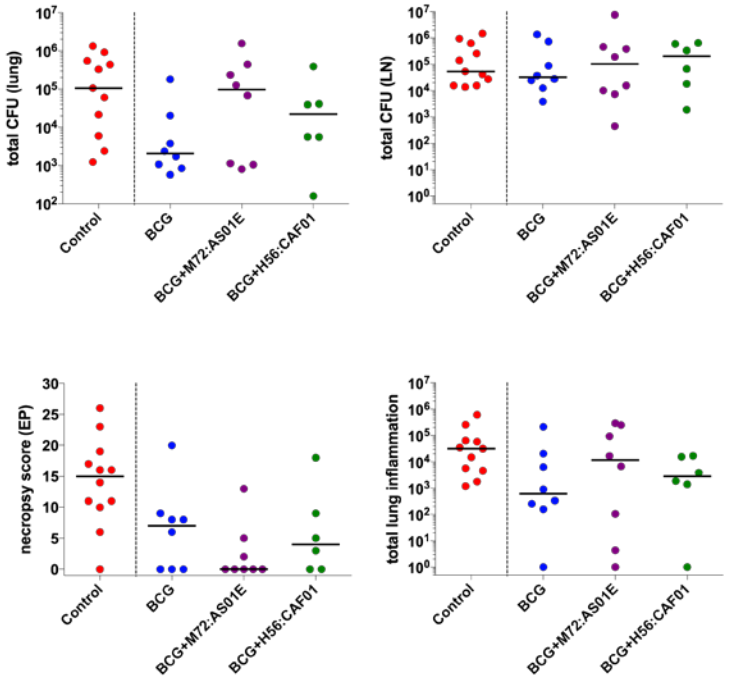

Figure 9: A comparison of BCG vaccinated animals to animals vaccinated with BCG and protein subunit vaccines delivered in adjuvant. Each dot represents one animal, and bars represent medians. Comparisons were done using Dunn's multiple comparisons. None of the comparisons were statistically significant. The values for the controls are shown for comparison but were not included in the statistical analysis.

There was no difference in early IFN-γ ELISPOT responses between any of the cohorts (Fig. 10). There was additionally no difference in amounts of inflammation in the lung by PET between the groups (Fig. 11).

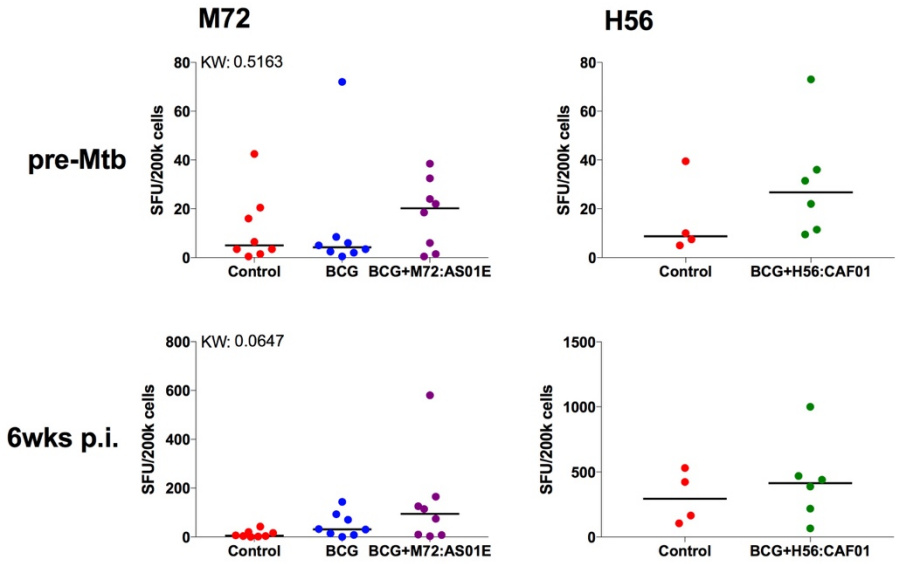

Figure 10: Antigen-specific IFN-γ responses to vaccine antigen peptide pools (indicated above) before challenge or six weeks post-challenge between BCG vaccinated macaques and BCG and protein subunit vaccines delivered in adjuvant. Each dot represents one animal and bars represent medians. Comparisons between the groups were done using the Kruskal-Wallis test (KW, left) or the Mann-Whitney test (right). None of the comparisons were statistically significant. SFU=spot forming units.

An increased number of lung granulomas was observed at 4 and 8 weeks p.i. in the BCG+H56:CAF01 group versus the BCG+M72:AS01E group (p=0.0125 and p=0.0078 respectively), and versus BCG alone at 4 weeks p.i. (p=0.0263). BCG+M72:AS01E vaccinated macaques had fewer inflamed or necrotic LN by PET than BCG vaccinees at 8 weeks p.i. (p=0.0302). Thus, these two different protein fusions were ineffective at boosting BCG-induced protection in this model.

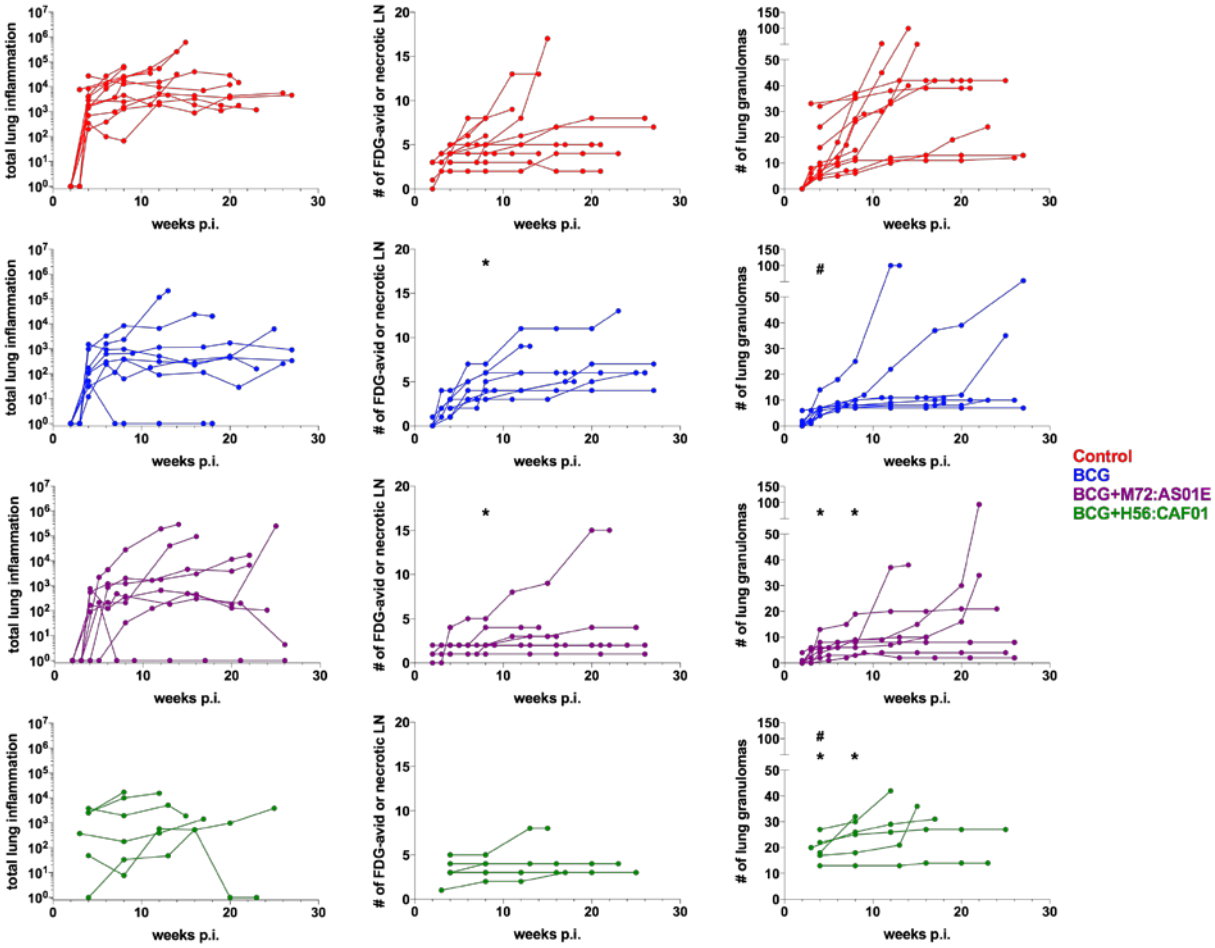

Figure 11: PET-CT markers from challenge until necropsy between BCG vaccinated macaques and BCG and protein subunit vaccines delivered in adjuvant. Each line represents one animal. Comparisons of markers between groups was done using Dunn's multiple comparisons test (* and # indicate significant difference) with p values reported in the text**.** ***Center*** Time point with significant difference was 8 weeks p.i. ***Right*** Time points with significant difference were 4 and 8 weeks p.i.

3.3.4 Adenoviral vectors do not improve protection conferred by BCG

Next, we assessed the ability of a viral vector to boost BCG-induced protection. As a control, we administered empty Ad5 to BCG-vaccinated animals. Surprisingly, this empty viral vector significantly increased the bacterial burden in the lung (p=0.0072) and the total lung inflammation by PET (bottom right, p=0.0554), compared to BCG alone. While not statistically significant, boosting with Ad5 containing antigens seemed to partially rescue the increase in lung bacterial burden and total lung inflammation. We also observed a trend towards addition protection over BCG alone against extrapulmonary pathology, particularly in the Ad5-

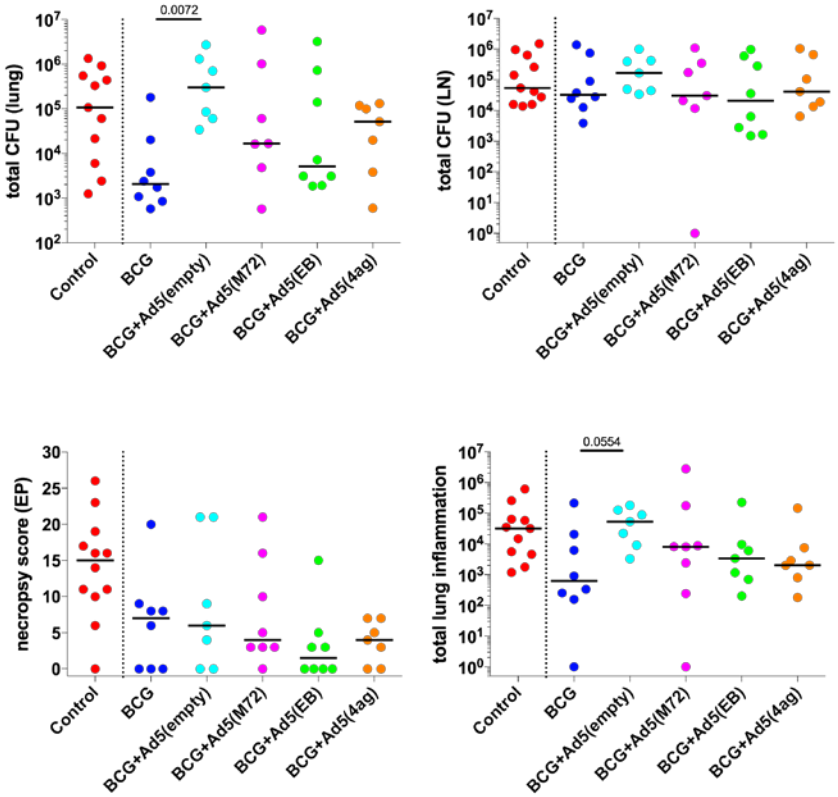

Figure 12: A comparison of BCG vaccinated animals to animals vaccinated with BCG and antigens delivered in Ad5. Each dot represents one animal, and bars represent medians. Comparisons were done using Dunn's multiple comparisons and p values are directly reported. The values for the controls are shown for comparison but were not included in the statistical analysis.

Ag85B/ESAT6 group (bottom left). There was no effect on lymph node bacterial burden. Our collaborators at the VRC have shown that Ad5-containing Mtb antigens delivered i.m. and by aerosol leads to high levels of Mtb-specific CD4 and CD8 T cells in the lungs (Fig. 13). Although some macaques have as many as 20% of memory CD4 and 50% of memory CD8 responding to vaccine antigens, none of the animals have improved outcomes, suggesting that even strong recall in the BAL is not sufficient for vaccine-induced protection. Recall responses to various vaccine antigens were observed by IFN-γ ELISPOT with some significant differences

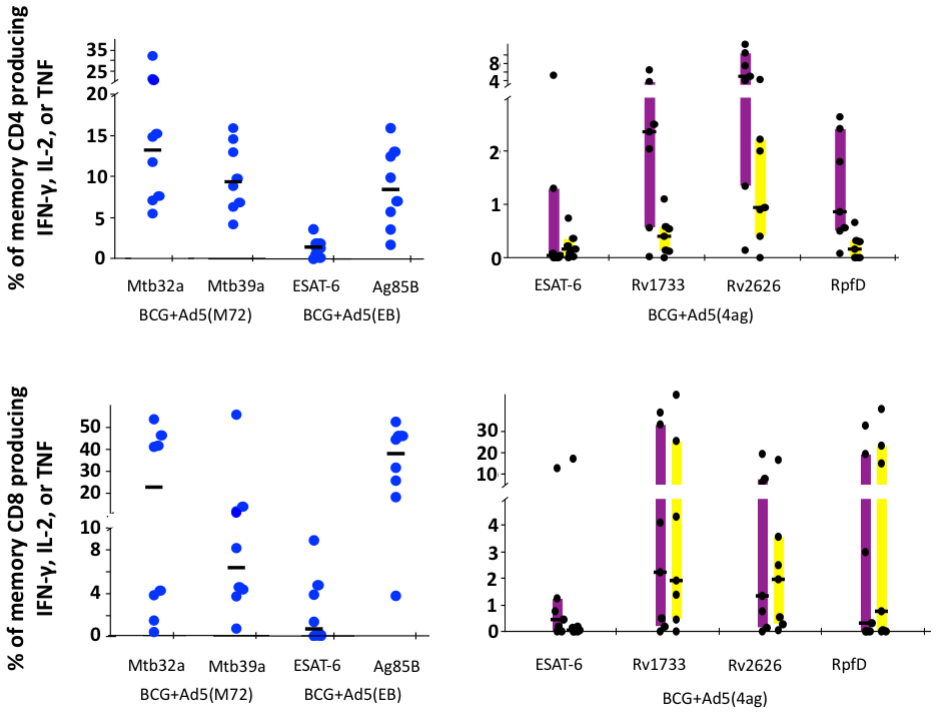

Figure 13: Frequency of memory T cells in BAL fluid that produce cytokines in response to vaccine-specific antigen peptide pools in macaques receiving an Ad5 boost by aerosol. Top panels are CD4 T cells and bottom panels are CD8 T cells. Responses to vaccine antigens are split by each antigen, e.g. M72 by its two antigens Mtb32a and Mtb39a, indicated underneath and grouped by vaccine regimen. Each dot represents one animal and bars represent medians. Data collected by our collaborators at the NIAID VRC.

between cohorts (Fig. 14). There was no difference during challenge between the vaccine regimens for most of the PET-CT markers (Fig. 15). Macaques vaccinated with BCG+Ad5(empty) had significantly more granulomas than BCG (p=0.0183), BCG+Ad5(EB) (p=0.0047), and BCG+Ad5(M72) (p=0.0027) at 4 weeks p.i., and those same groups at 8 weeks p.i. (p=0.0384, p=0.0072, and p=0.0026 respectively). Thus, the delivery of antigens via the Ad5 viral vector, even when up to 4 antigens were incorporated into the viral vector, was ineffective at boosting BCG-induced protection, and in fact was detrimental in several compartments.

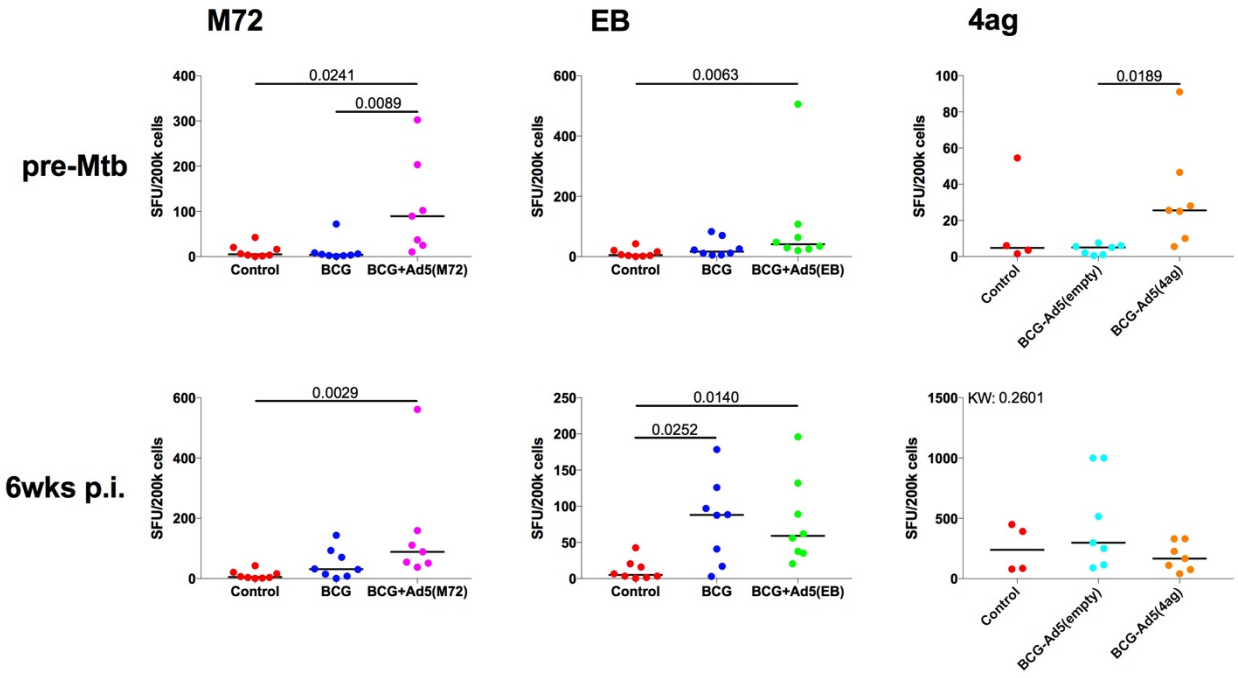

Figure 14: Antigen-specific IFN-γ responses to vaccine antigen peptide pools (indicated above) before challenge or six weeks post-challenge between BCG vaccinated macaques and BCG and antigens delivered in Ad5. Each dot represents one animal and bars represent medians. Comparisons between the groups were done using the Kruskal-Wallis test (KW) and Dunn's multiple comparisons with p values reported. SFU=spot forming units.

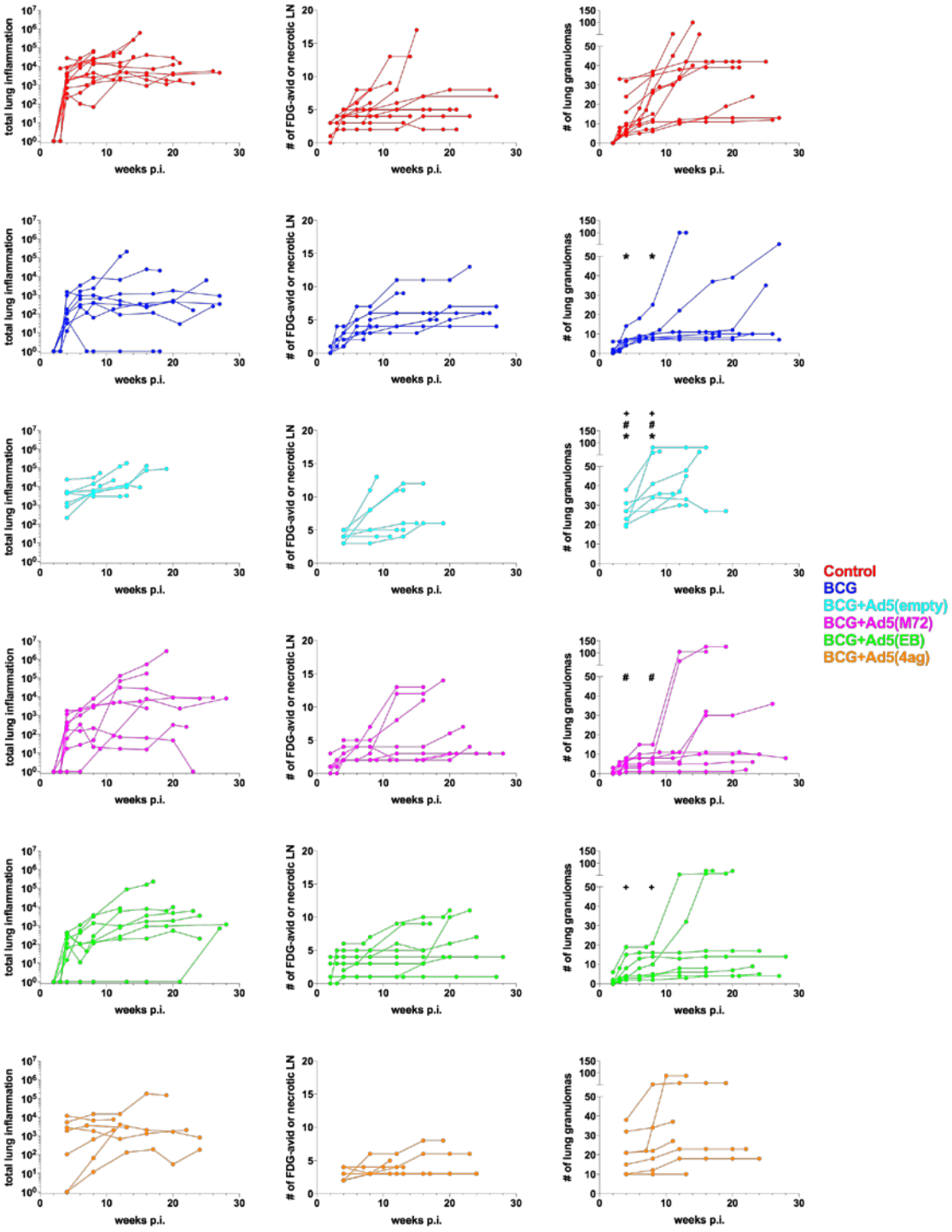

Figure 15: PET-CT markers from challenge until necropsy between BCG vaccinated macaques and BCG and antigens delivered in Ad5. Each line represents one animal. Comparisons of markers between groups was done using Dunn's multiple comparisons (* # + indicate significant difference) with p values reported in the text. ***Right*** Time points with significant difference were 4 and 8 weeks p.i.

3.3.5 Direct comparison of protein vs viral vectored vaccines

This study provided the opportunity to compare the ability of protein vs viral vector boost using the same antigens, namely M72. Direct comparison of M72 protein to adenoviral vector, as boosts to BCG showed no differences, with the exception of a trend hinting that delivery of protein in adjuvant by i.m. gave slightly better protection against extrapulmonary pathology (Fig. 16, bottom left, p=0.0928). There was no difference between these routes of administration in

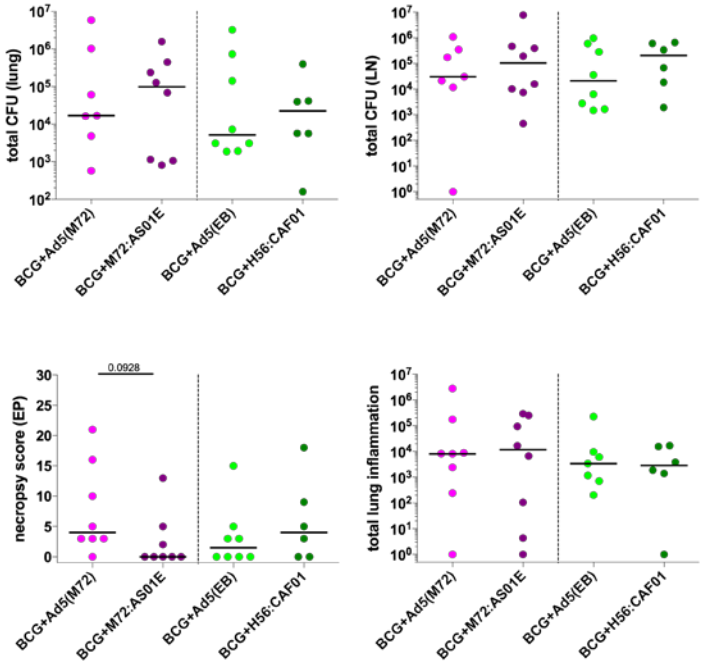

Figure 16: A comparison of BCG and protein subunit vaccines delivered in adjuvant with BCG and antigens delivered in Ad5. Each dot represents one animal, and bars represent medians. Comparisons were done using the Mann-Whitney test and p value was directly reported.

PET-CT markers during challenge as well (Fig. 17). We also compared the protein H56 in adjuvant to Ad5-EB; these share two antigens (Ag85B and ESAT6), but H56 also contains the protein Rv2660c [274]. No difference was observed between the protein and adenoviral vaccine

here either, in any of our outcome measures at necropsy. BCG+Ad5(EB) vaccinated macaques had fewer lung granulomas at 4 weeks p.i. (p=0.0188) and 8 weeks p.i. (p=0.0097) than BCG+H56:CAF01 vaccinees. Thus, we did not find major differences between protein or adenoviral-vectored vaccines as boosts to BCG in this model, with neither type of vaccine improving upon BCG vaccination.

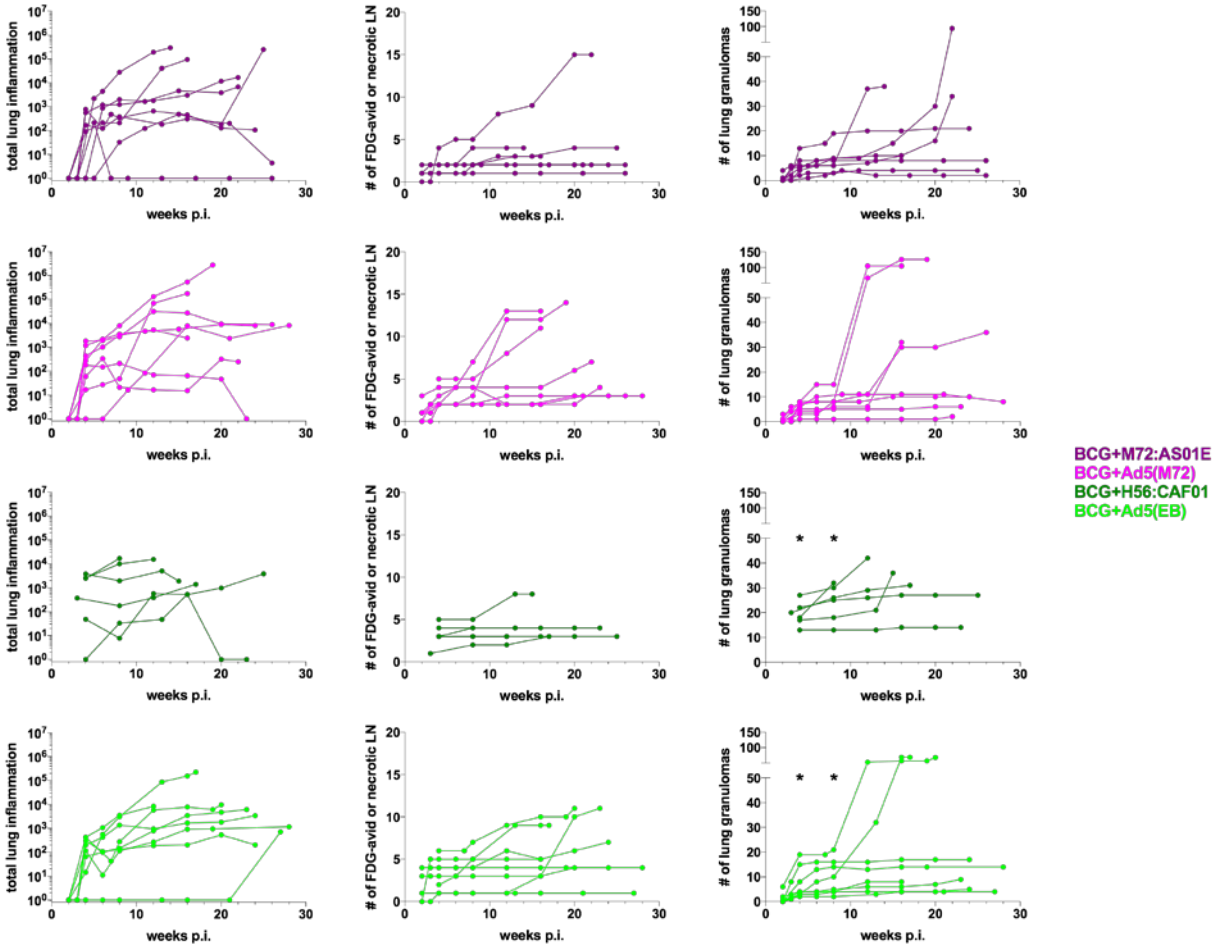

Figure 17: PET-CT markers from challenge until necropsy between BCG and protein subunit vaccines delivered in adjuvant with BCG and antigens delivered in Ad5. Each line represents one animal. Comparisons of markers between groups was done using the Mann-Whitney test (* indicates significant difference) with p values reported in the text to specifically compare the two regimens with M72, and to compare the regimens with H56 and EB. ***Right*** Time points with significant difference were 4 and 8 weeks p.i.

3.3.6 Stratifying outcome of macaques based on quantifiable measures

The data we have presented thus far, while not showing an appreciable improvement in outcome using any of the prime-boost strategies, demonstrate a wide spectrum of outcomes within each cohort, with some macaques doing very well and others doing quite poorly (Fig. 18).

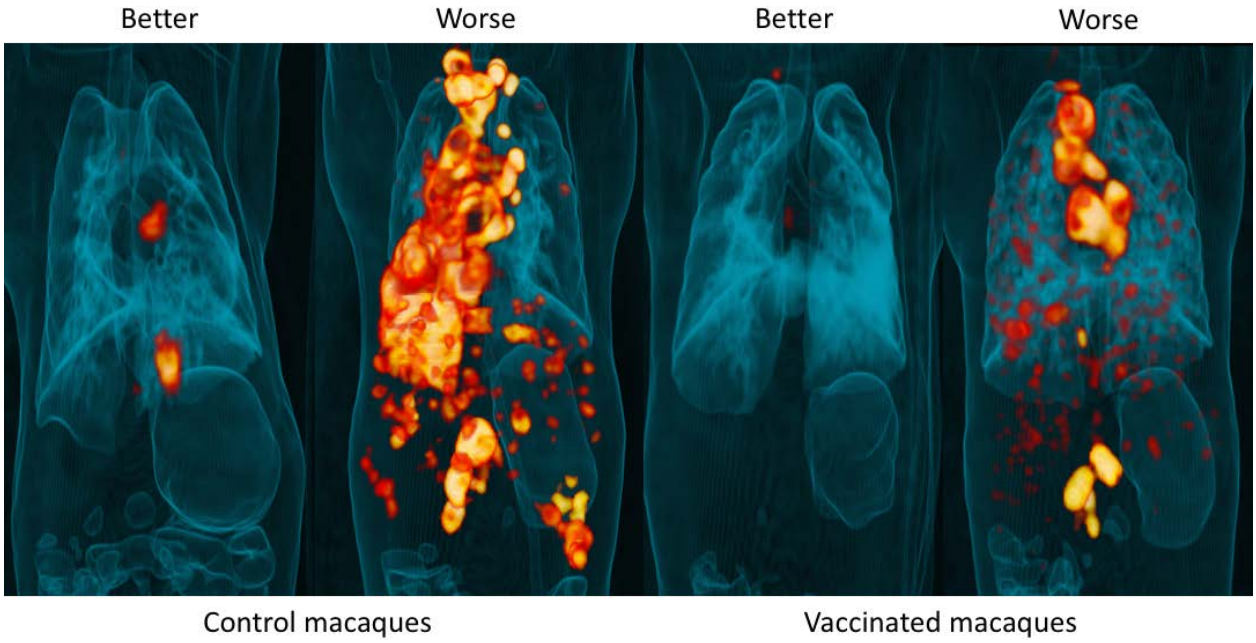

Figure 18: Radiologic examples of spectrum of TB disease in rhesus macaques. Representative PET-CT scans from 1-3 days prior to necropsy. The left two panels are examples of rhesus macaques with better and worse outcomes from the control cohort, and the right two panels are examples of macaques with better and worse outcomes from among the vaccinated cohorts.

Instead of using vaccination as a proxy for improved outcome, a cluster analysis could be used to separate the macaques in this study into groups based upon similarity of overall outcome. Then correlates of improved outcome, and immune responses at necropsy associated with better outcomes, could be identified regardless of vaccine regimen. A cluster analysis groups data points (in this case macaques) together into clusters based upon parameters (here, outcomes at

necropsy) so that members of one group are more similar than those of other groups. *K*-means clustering [3] uses the variability in parameters (outcomes at necropsy) to plot data points (macaques) on a subspace and then identifies the most likely way to generate *k* clusters based on those points. Using gross pathology and bacterial burden at necropsy with *k*=3, *k*-means clustering was utilized to identify three groups separated by their variability in outcomes at necropsy (Fig. 19, top). How exactly, though, are these three groups separated by variability in

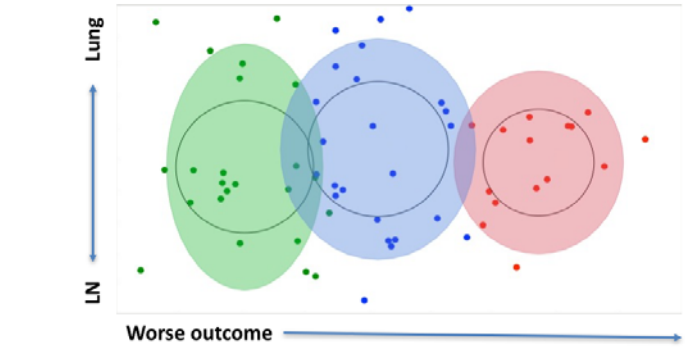

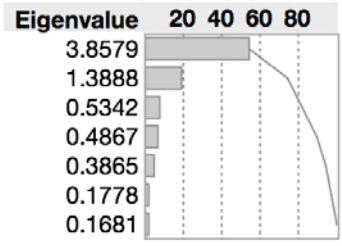

Outcome	PC1	PC2
Necropsy score (lung)	0.87342	0.16727
# of CFU+ LN	0.85715	-0.33478
Total CFU (lung)	0.77216	0.47619
Necropsy score (LN)	0.77137	-0.36220
Total CFU (LN)	0.75194	-0.13892
Necropsy score (EP)	0.74722	-0.31938
% CFU+ lung granulomas	0.21287	0.87723

Figure 19: Partitioning the macaques in the study based on outcome. Using the outcomes in previous figures, the macaques were partitioned into three major groups using *k*-means clustering [3]. The top plot contains the three clusters generated by this tool, colored according to outcome: worse (red), middle (blue), and better (green). Each dot represents one animal. The bottom left panel contains eigenvalues for each principal component (PC). The bottom right table contains loading values for each significant PC. These PCs are indicated in the top graph, i.e. PC1 as "worse outcome" and PC2 as "LN" versus "lung".

outcome? We used principal components analysis (PCA) to explore how each of the outcome measures contributed to the generation of these three groups. *K*-means clustering creates a space known as the cluster centroid subspace on to which the clusters are mapped, which has been

shown to be identical to the subspace spanned by principal components in PCA [359]. The centroid subspace here was then mapped to a PCA subspace to identify the relationships between outcome measures (i.e. pathology and CFU) that are separating the animals into three groups. Using the Kaiser rule, which dictates that only components with eigenvalue greater than one significantly impact variability [4], two principal components (PC) were identified as significant (Fig. 19, bottom left). PC1 represents the x-axis of the clustering subspace. The loading values indicate how strongly each outcome impacts the variability due to that component (Fig. 19, bottom right) [360]. Since PC1 contains loading values that are mostly all strongly positive, this likely indicates that PC1 represents outcome holistically ("worse outcome"). Thus, the more positive along the x-axis the macaque is, the worse all the outcome measures are, and vice versa. PC2 represents the y-axis of the clustering subspace, and has positive loading values for outcomes associated the lung, and negative loading values for outcomes associated with LN and other extrapulmonary sites, suggesting that when disease is more severe in one of those compartments it is less severe in the other ("LN" versus "lung"). The clusters are arranged left to right, or along the x-axis (PC1; overall outcome), suggesting that red represents macaques with worse outcomes (n=15), blue macaques in the middle of the spectrum (n=24), and green macaques with better outcomes (n=23). Thus, *k*-means clustering was used to partition the macaques into three groups based on quantifiable outcome measures at necropsy, and PCA was used to demonstrate that overall outcome drives the differences *between* the clusters and balance of TB in the lungs or in the LN and extrapulmonary sites drives the differences *within* the clusters. *K*-means clustering and PCA are tools that can therefore be used in vaccine studies with lots of variability in outcome to tease out the factors that drive the variability and separate subjects by outcome, regardless of treatment cohort.

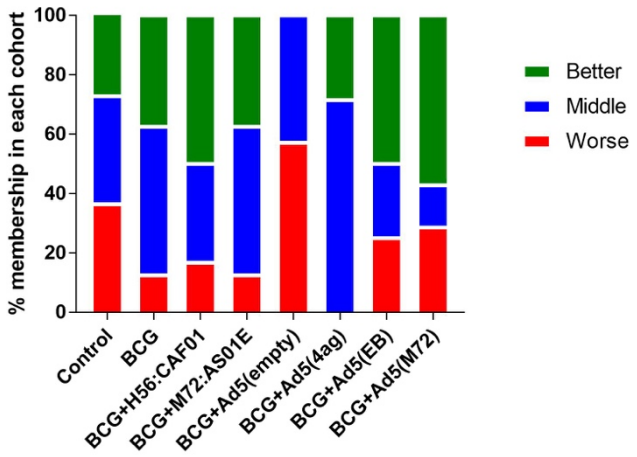

Figure 20: These graphs display the percentage of each study group (i.e. vaccine regimen) that belong to each outcome.

Control animals belong to each of these three groups in relatively similar numbers (Fig. 20). Vaccinated animals, with the exception of BCG boosted by empty Ad5, have relatively fewer animals with worse outcomes. However, boosting with empty Ad5 resulted in no animals with "better" outcomes, and nearly 60% of this group was in the worse outcome category. An interesting trend emerged in this analysis of outcome in the prime-boost cohorts, where boosting BCG either increased the number of macaques having a middle outcome (BCG+Ad5(4ag)) or increased the number of macaques both having better and worse outcomes (BCG+Ad5(EB)). Thus, vaccination in general reduces the incidence of the worst TB disease outcomes.

3.3.7 Early control of host inflammation correlates with improved outcome

We have demonstrated that we can sort the animals from this study into categories by worse, middle, or better outcomes (Fig. 20). Using the IFN-γ ELISPOT data (Fig. 7, 10, 14) before and

after Mtb challenge after stimulation with CFP (pan-mycobacterial), ESAT-6, and CFP-10 (both Mtb specific), we sought for differences at these early time points in recall response of macaques with better and worse outcomes. There was no significant difference in IFN-γ prior to challenge between the two groups of outcomes (Fig. 21, top panels). Six weeks post-Mtb challenge, the macaques that would later have better outcomes had significantly fewer T cells in blood that produced IFN-γ in response to mycobacterial stimulations (Fig. 21, bottom panels). These data indicate that increased peripheral responses to Mtb antigens after infection correlate with poor outcome. This is likely due to Mtb proliferation early in monkeys that are not controlling infection, resulting in stimulation of T cell responses.

We also utilized PET-CT markers similar to above (Fig. 8, 11, 15, 17) to see whether we

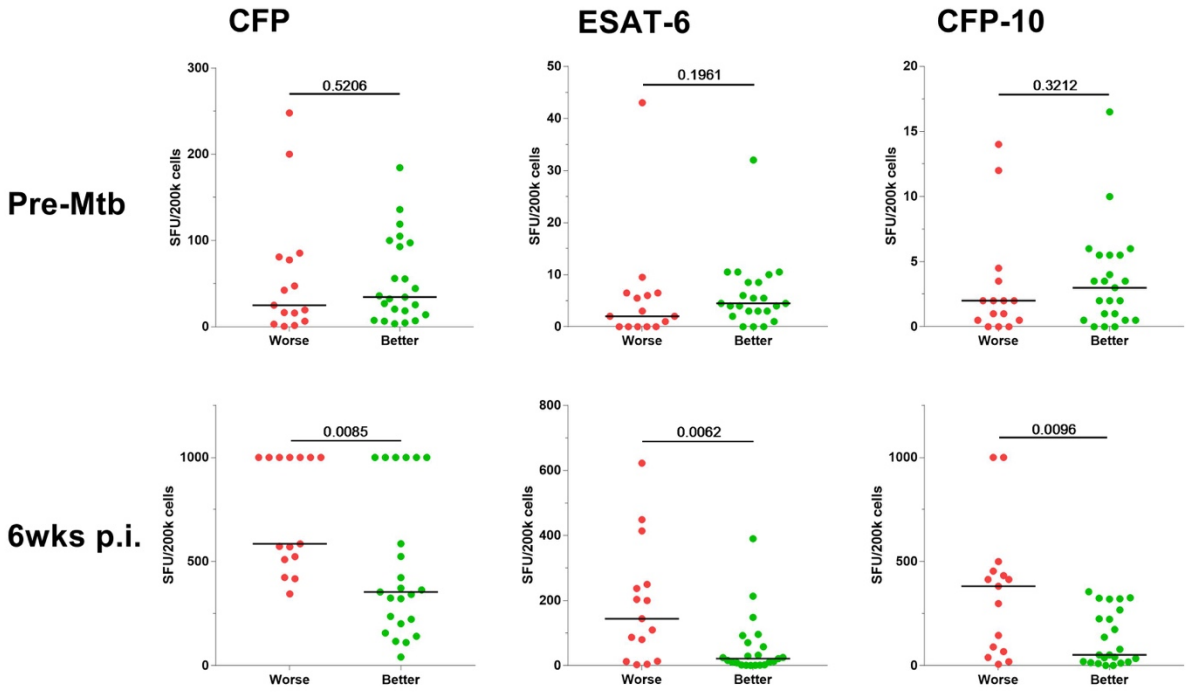

Figure 21: Early suppression of peripheral IFN-g response associated with improved outcome. The top panels are IFN-g ELISPOT responses from PMBCs two weeks before Mtb challenge, and the bottom panels are responses six weeks post-Mtb challenge. Each dot represents one animal, and bars represent medians. Comparisons were done using the Mann-Whitney test with p values directly reported. SFU=spot forming units.

could distinguish between better and worse outcomes early post-infection. Total lung inflammation as determined by PET at 8 and 12 weeks p.i. was significantly higher in the animals with worse outcomes (Fig. 22). Macaques with worse outcomes also exhibited more FDG-avid LNs at 8 weeks p.i., and formed more granulomas between 4-12 weeks p.i., indicating dissemination of infection (Fig. 22). These data suggest that modulation of lung inflammation early is related to control of TB disease. Early reduced IFN-γ responses and PET-assessed inflammation could be useful as indicators of vaccine effectiveness, and this is explored further in chapter 5.

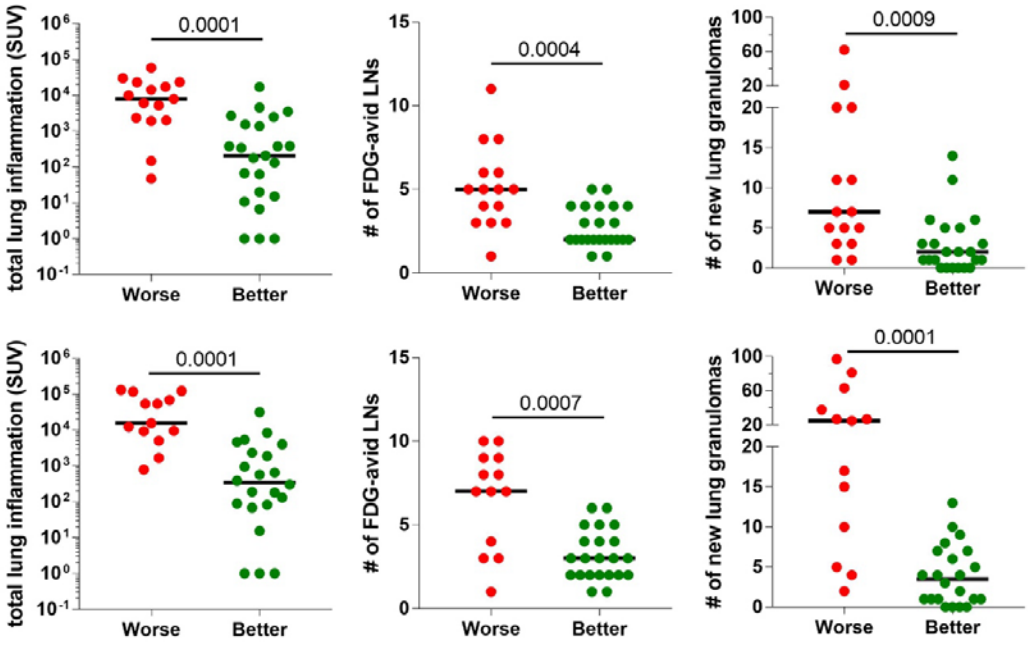

Figure 22: Less inflammation in the lung and LNs early corresponds to better outcomes. The top panels are PET-CT markers at 8 weeks post-Mtb infection and the bottom panels are PET-CT markers at 12 weeks post-Mtb infection. Each dot represents one animal, and bars represent medians. Comparisons were done using the Mann-Whitney test with p values directly reported.

3.3.8 Modulation of T cell activity in the LN, but not lung granulomas, associated with improved outcome

At necropsy, we assessed T cell function in individual lung granulomas and lung-draining LNs. There was no difference in CD3+ T cell function in cells from lung granulomas from animals with better outcomes versus worse outcomes (Fig. 23). T cells from lung-draining LNs either received no exogenous stimulation (Fig. 24A; i.e. were only stimulated by Mtb antigens already present in the LN at necropsy) or were stimulated with PDBU and ionomycin (P&I) to assess capabilities of cytokine production (Fig. 24B). There were lower frequencies of cytokine-

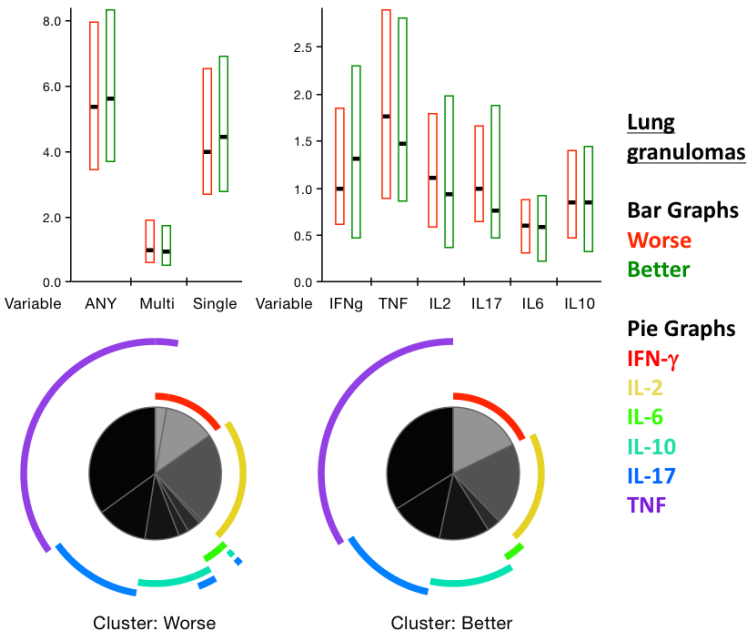

Figure 23: Immunologic differences in cytokine-producing T cell frequencies from lung granulomas between animals with better and worse outcomes. For the bar graphs, the bars represent interquartile ranges and the thick line represents the median. Comparisons were done using the Mann-Whitney test. For the pie graphs, the dark portion of the central pie represents single cytokine-producing T cells and the white portion represents multifunctional T cells. Comparisons of pie graphs was done using a permutation test as previously described [6]. None of the comparisons (Mann-Whitey or permutation) were statistically significant.

producing T cells that were multifunctional, single functional, or producing any cytokine at all in LNs from macaques with better outcomes (Fig. 24A). These LNs also had lower frequencies of T cells producing IFN-γ, interleukin-2 (IL-2), and tumor necrosis factor (TNF) (Fig. 24A). LNs from macaques with better outcomes contained relatively lower frequencies of T cells producing

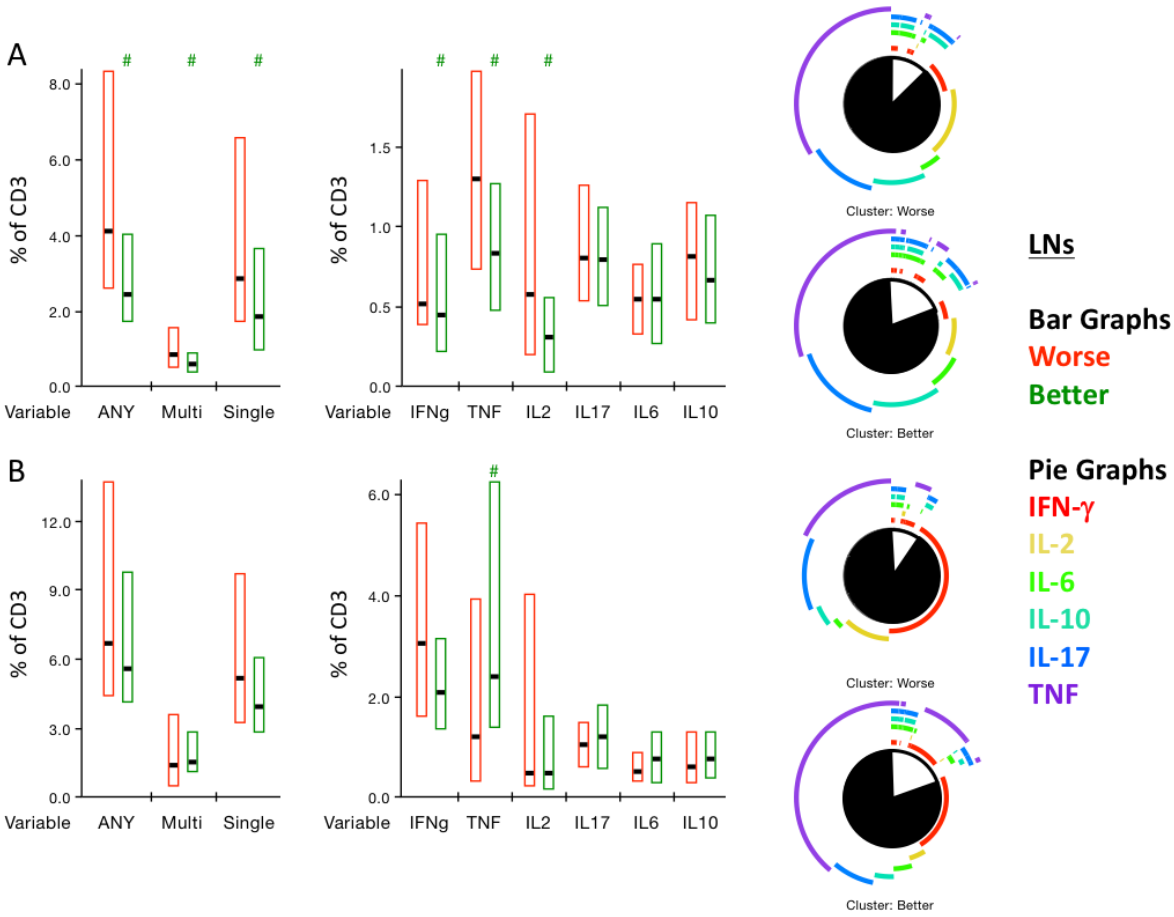

Figure 24: Immunologic differences in cytokine-producing T cell frequencies from LNs between animals with better and worse outcomes. For the bar graphs, the bars represent interquartile ranges and the thick line represents the median. The pound sign indicates a significant difference between the outcomes using the Mann-Whitney test. For the pie graphs, the dark portion of the central pie represents single cytokine-producing T cells and the white portion represents multifunctional T cells. Comparisons of pie graphs was done using a permutation test as previously described [6]. A These T cells were not exogenously stimulated with Mtb antigens. B These T cells were stimulated with phorbol 12, 13-dibutyrate and ionomycin.

IL-2 and higher frequencies of T cells producing interleukin-6 (IL-6) (Fig. 24A). These LNs also contained relatively more multifunctional T cells than LNs from animals with worse outcomes (Fig. 24A). While on their own LNs from animals with better outcomes have lower frequencies overall of cytokine-producing T cells (Fig. 24A), LNs from both groups of macaques were equally capable of making the same frequencies of cytokine-producing T cells (Fig. 24B). LNs from both groups were also equally capable of producing most cytokines in this study, with the exception of TNF, of which the LNs from macaques that fared better were capable of making higher frequencies of TNF-producing T cells (Fig. 24B). LNs from macaques with better outcomes contained relatively lower frequencies of T cells capable of making IFN-γ and relatively higher frequencies of T cells capable of making TNF (Fig. 24B). These LNs also contained relatively higher frequencies of T cells capable of being multifunctional (Fig. 24B). These data highlight the overall immune responses that are associated with control of Mtb in this model system.

3.4 DISCUSSION

The goal of this study was to assess whether boosting BCG by a variety of strategies was capable of conferring additional protection against Mtb challenge in a nonhuman primate (rhesus) model of TB. Rhesus were chosen due to their increased susceptibility to developing TB, and we reasoned that this model would provide a good option for identifying protective regimens. We demonstrated that with the selection of therapeutics utilized in this study that boosting BCG with subunit protein vaccines in adjuvant or with antigens encoded in an Ad5 viral vector did not provide any additional protection on top of BCG. BCG on its own did provide appreciable

protection to Mtb challenge. We then partitioned the macaques in this study by outcome, demonstrated the powerful ability of PET-CT to distinguish between good and bad outcomes early post-infection, and identified immune signatures in lung-draining LNs associated with relative protection against TB.

When comparing the different types of vaccines in this study, BCG gave the best protection against Mtb challenge in our model, although many of these animals still presented with disease. None of the vaccine regimens prevented infection. BCG so far is the only TB vaccine with demonstrated efficacy against any manifestation of tuberculous disease in humans, albeit not against pulmonary TB [132]. In this study, boosting BCG did not provide additional protection from disease. These data are mirrored in human studies, where a BCG antigen (Ag85B) delivered in modified vaccinia Ankara (MVA) failed to provide additional protection from BCG [38]. Another goal of this study was to determine whether lung-targeted vaccination was efficacious in boosting BCG, and more efficacious than vaccination administered only by i.m. While both of these questions resulted in generating moot answers, interestingly a control group (BCG boosted by empty Ad5) provided a strong, albeit negative, signal. Ad5 has been shown to elicit strong T cells responses, especially type I interferon responses via its shaft protein [331], which are detrimental to successful immunity to TB infection [42, 252, 361]. Indeed, the monkeys in this study had strong T cell responses in the lungs following Ad5-antigen vaccination. This could explain the increase in susceptibility in this study, but also suggests that immune polarization in the lung could either break, or potentially make, protection to TB. Vaccine systems that promote type I interferon should therefore not be utilized for tuberculosis, and systems that instead promote immunity shown to be efficacious against Mtb, e.g. Th1 and Th17 [169], should be investigated within the context of the lung. Once an ideal delivery system

is chosen, the antigens or attenuated organism delivered should then be picked. BCG's efficacy in this study would suggest that live vaccines should be of particular interest [362], including BCG delivered to the lungs or intravenously, which has been mildly investigated [108, 109, 363].

One of the major gaps in vaccine development for TB is the desperate need for new outcome measures. Current clinical trials for efficacy typically use two endpoints: isolating Mtb from a study subject or a clinical diagnosis of TB [295]. These endpoints can take months to years to appear, or never at all, and the diagnostic methods are not the most sensitive and are in need of improvement [364]. In this study we demonstrate the use of statistical methods to partition animals by outcome [3], allowing one to explore factors associated with variability in outcome. BCG in this study reduced the number of rhesus macaques having the worst TB outcomes, a phenotype that is mirrored in the efficacy of BCG preventing the worst outcomes (e.g. Pott's disease and meningitis) in human infants [132]. While boosting BCG does not appear to provide additional protection in this study, an interesting phenotype was observed when looking at how many macaques belonged to each outcome for each vaccine. Boosting BCG appeared to have one of two effects: either more animals had a middle outcome, with fewer having a better or worse outcome, e.g. BCG+Ad5(ESAT-6/Rv1733/Rv2626/RpfD); or more animals had better *and* worse outcomes, e.g. BCG+Ad5(M72). Since these vaccines were delivered the same way using the same vehicle, this suggests that the difference in phenotype is linked to the antigens delivered. This argues for potentially combining antigens from multiple vaccines into one boost, or for utilizing live attenuated mycobacterial vaccines that contain these and potentially more antigens.

We have previously illustrated the potency of PET-CT as a cutting-edge tool to assess TB disease at serial time points to predict disease outcome [345], to evaluate chemotherapeutic

efficacy [2, 350], and to determine risk of reactivation disease [5]. Here we show that early mitigation of lung and LN associated inflammation by PET is associated with improved outcomes in the rhesus macaques. Further work will continue to develop PET-CT as a predictive tool and novel outcome measure for pre-clinical vaccine efficacy studies for TB vaccines. In T cells from primary tissues at necropsy, differences immunologically between better and worse outcomes were observed not in lung lesions but in lung-draining LNs. The two strongest loading factors for the "overall outcome" component in our *k*-means clustering were gross pathology in the lung and number of LN with viable bacteria. These outcomes are both highly suggestive of dissemination, since lung pathology captures number and spread of lesions and number of involved LNs is evidence of trafficking of Mtb. Thus, the difference in dissemination in these animals is associated with divergent T cell phenotypes in the lung-draining LNs, not in T cells from lung lesions. These data generate two potential hypotheses: the difference in T cell phenotype could be responsible for control of dissemination of TB disease; or control of disease could be exerted through other means, leading to more of a memory phenotype rather than effector phenotype in the LN as a result. Further work in our laboratory will seek to test these hypotheses for improvement of TB vaccines moving forward.

3.5 MATERIAL AND METHODS

3.5.1 Animals

The Institutional Animal Care and Use Committee of the University of Pittsburgh approved all experiments. The animals were housed and maintained in accordance with standards established in the Animal Welfare Act and the Guide for the Care and Use of Laboratory Animals.

Vaccination. Rhesus macaques (*Macaca mulatta*) imported from China and in the United States for at least a year were used for these studies (N=64). Before study start, animals were screened for cross-reactivity to mycobacterial antigens by ELISPOT and for neutralizing antibodies to Ad5 in their serum. Animals with a neutralizing titer of 16 or lower were considered negative. Animals were pair housed during immunization at Bioqual (Rockville, MD) and randomized into study groups (Table 3). Group 1 (control) was not vaccinated. Groups 2-8 were vaccinated at week 0 with BCG Danish (2-8*10^5 CFU in 0.1 mL) from Statens Serum Institut (Copenhagen, Denmark) by the intradermal route (i.d.). Group 3 was boosted at weeks 16 and 20 with M72 (Mtb32A/Rv0125/PepA and Mtb39A/Rv1196/PPE18) in adjuvant AS01E by the intramuscular route (i.m.) [272, 330]. Group 4 was boosted at week 20 by M72 in replication-deficient recombinant human adenovirus 5 (Ad5) (1*10^{10} viral particles per route) by both i.m. and aerosol using the eFlow rapid nebulizer (4 μm drop size; PARI, Starnberg, Germany). Group 5 was boosted at week 20 by ESAT-6 and Ag85B in Ad5 by both i.m. and aerosol. Group 6 was boosted at week 25 with empty (i.e. no Mtb antigens) Ad5 by both i.m. and aerosol. Group 7 was boosted at week 25 with ESAT-6, Rv1733, Rv2626, and RpfD in Ad5 by both i.m. and aerosol. Group 8 was boosted at weeks 20 and 25 with H56 (ESAT-6/Ag85B/Rv2660c) in adjuvant

CAF01 by i.m. [276, 318]. Animals were transferred to the University of Pittsburgh at week 24, quarantined for 6 weeks, and transferred to an ABSL-3.

Challenge. Animals were challenged with 8-16 CFU in 2 mL volume per animal of Erdman strain *Mycobacterium tuberculosis* (Mtb) via bronchoscope. Animals were clinically monitored and examined daily, including: appetite, weight, erythrocyte sedimentation rate (ESR), activity, gastric aspirate, and coughing. These signs were utilized as criteria in determining if an animal qualified as meeting human endpoint before the conclusion of the study.

Necropsy. The macaques in this study were euthanized approximately 6 months (24-28 weeks) after Mtb challenge. All animals were euthanized with an intravenous overdose of sodium pentobarbital (Beuthanasia) and maximally bled. At necropsy each animal was examined grossly for pathology. Using our published scoring system [65], the total amount of pathology was recorded from each lung lobe (number and size of lesions), LN (size and extent of necrosis), and extrapulmonary compartments (number and size of lesions). A pre-necropsy PET-CT scan was used as a "map" for identifying and finding each lesions in the lungs. Each individual lesion in the lung and all thoracic LNs identified were excised and mechanically homogenized to create a single cell suspension. Portions of the suspensions were spread on 7H11 agar (Difco) and incubated at 37°C with 5% CO_2 for 3 weeks. CFU were then counted from these plates and used to both quantify individual lesion bacterial burden and—when summed together—the total bacterial burden for the animal [239, 365]. Portions of these suspensions were also used for multiparameter flow cytometry (see below), and the remained was stored at -80°C.

3.5.2 PET-CT scans and analysis

PET-CT scans were performed using a microPET Focus 220 preclinical PET scanner (Siemens Medical Solutions) and a clinical eight-slice helical CT scanner (Neurological Corp.) as previously described [2, 350]. ^{18}F-fluorodeoxyglucose (FDG), a non-specific marker of inflammation, was utilized as the probe for PET. Serial PET-CT scans were performed between 2 and 24 weeks post-Mtb infection, and before necropsy. OsiriX viewer, an open-source PACS (Picture Archiving and Communication System) workstation and DICOM (Digital Imaging and Communications in Medicine) image viewer, was used for scan analyses as previously described [350]. Briefly, a region of interest (ROI) was segmented which encompassed all lung tissue on CT and was then transferred to the co-registered PET scan. On the PET scan, all image voxels of FDG-avid pathology (SUV_{max} > 2.3) were selected and summated resulting in a total SUV_{max} value. To account for basal metabolic FDG uptake in the animal, the total SUV_{max} was normalized to resting muscle resulting in a total lung inflammation value. Individual granulomas as seen on CT were counted in each scan to enumerate them longitudinally. Number of FDG-avid LN is a full count of any LN visible by PET with SUV > 5 normalized to resting muscle.

3.5.3 ELISPOT

Heparinized blood was drawn from study macaques at time points pre-Mtb challenge (two weeks prior to Mtb challenge) and post-Mtb challenge (six weeks after). Peripheral blood mononuclear cells (PBMCs) were isolated using the standard Percoll gradient isolation (GE Healthcare) and washed with sterile PBS. ELISPOT for IFN-γ was performed as previously described [115]. Briefly, 96-well opaque multiscreen immunoprecipitation filtration plates (Merck

Millipore) were hydrated, washed, and coated with 7.5 μg/mL of anti-human/nonhuman primate IFN-γ (GZ-4: Mabtech) for 2 hours at 37°C with 5% CO_2. Plates were then blocked with complete RPMI containing 10% human AB serum for 2 hours at 37°C with 5% CO_2. Each stimulation condition was performed in duplicate. Medium only was used as a negative control, and phorbol dibutyrate/ionomycin (P&I) and anti-CD3 were used as positive controls. CFP and peptide pools of H56 vaccine antigens (ESAT-6, Ag85B, Rv2660c) were used at 10 μg/mL. PBMCs were then added, and the plate was incubated for 48 hours at 37°C with 5% CO_2. The plate was then washed and detection antibody (7-B6: Mabtech) was added at 2.5 μg/mL and incubated for 2 hours at 37°C with 5% CO_2. The plate was washed and streptavidin-conjugated horseradish peroxidase was added at a 1:100 dilution and incubated for 45 minutes at 37°C with 5% CO_2. The plate was washed and then developed using AEC substrate. The plate was dried overnight and read using an ImmunoSpot analyzer (Cellular Technologies Limited).

3.5.4 Flow cytometry on primary tissue samples

Data collection. Single cell suspensions of individual lung granulomas obtained at necropsy were incubated in brefeldin A (GolgiStop, BD Biosciences) for 2 hours at 37°C with 5% CO_2. Single cell suspensions of individual lung-draining LNs obtained at necropsy were either incubated in brefeldin A for 2 hours at 37°C with 5% CO_2, or incubated with phorbol 12,13-dibutyrate (PDBU) and ionomycin for 3.5 hours in the presence of brefeldin A at 37°C with 5% CO_2. The cell suspensions were then stained for viability (Invitrogen), surface, and intracellular markers. Surface markers included: CD3 (SP34-2: BD Biosciences); CD11b (ICRF44: BD Biosciences); and CD20 (2H7: eBiosciences). Intracellular markers included: IFNγ (B27: BD

Biosciences); TNF (MAB11: BD Biosciences); IL-2 (MQ1-17H12: BD Biosciences); IL-17 (eBio64CAP17: eBiosciences); IL-10 (JES3-9D7: eBiosciences); and IL-6 (MQ2-6A3: BD Biosciences). Data acquisition was performed using a LSR II (BD Biosciences) and the resulting data were gated and quantified using FlowJo (Version 9.9.3; Treestar Inc.).

Gating. Singlet cell populations were separated first using forward scatter area and height. Live cells were then gated, followed by the lymphocyte population based upon size. CD11b+ and CD20+ cells were then removed from this population, and remaining CD3+ cells were selected. Gates for each of the six cytokines were used to quantify individual production. The Boolean gating tool was then utilized to determine the combinations in which the six cytokines were produced.

3.5.5 Statistics

Graphics and statistics in all figures except 18-19 and 23-24 were created using Prism (Graphpad). In these figures where indicated: comparisons of time to human endpoint were done using the Mantel-Cox test; comparisons of two groups were performed using the Mann-Whitney test; and comparisons of three groups were done using Dunn's multiple comparisons. Graphics and statistics in the other part of figure 19 were generated using JMP (SAS). *K*-means clustering was utilized to partition the animals by outcome (k=3). Analysis and presentation of flow cytometric data in figures 23-24 was performed using SPICE (Ver. 5.23; https://exon.niaid.nih.gov/spice/) [6]. Comparisons of frequency of cytokine-producing CD3 T cells between outcomes were performed using the Mann-Whitney test. Comparisons between profiles of relative Boolean cytokine expression (pie graphs) were done using a permutation test as previously described [6].

4.0 BCG+H56:CAF01 LIMITS HOST INFLAMMATION AND BACTERIAL DISSEMINATION IN A NONHUMAN PRIMATE MODEL OF TUBERCULOSIS

This chapter is adapted from the manuscript in submission: DiFazio RM, Maiello P, Myers AJ, Rodgers MA, O'Malley M, Tomko J, Frye LJ, Fillmore D, Agger EM, Andersen P, Lin PL, and Flynn JL. BCG+H56:CAF01 limits host inflammation and bacterial dissemination in a nonhuman primate model of tuberculosis.

4.1 ABSTRACT

The experimental tuberculosis (TB) subunit vaccine H56 was previously shown to boost the effects of the currently licensed vaccine (BCG) to protect non-human primates (NHPs) infected with *Mycobacterium tuberculosis* (Mtb) from reactivation disease. The goal of this study was to determine which aspects of Mtb infection are influenced by this vaccine. Cynomolgus macaques received no vaccine, BCG only, or BCG boosted by H56 in CAF01, an experimental liposomal adjuvant. A combination of BCG with H56:CAF01 prevented early dissemination of lung granulomas after low dose Mtb challenge, substantially reduced lung inflammation, as measured by PET-CT, and limited infection of mediastinal lymph nodes (LNs). We then repeated the experiment and necropsied animals at 5-6 weeks post infection to examine the early local responses that confer protection. NHPs vaccinated with BCG+H56:CAF01 had significantly less

disease early in LNs than unvaccinated controls. T cells from the LNs of the vaccinated animals also had differential cytokine expression compared to controls. This study provides new insights into which aspects of Mtb infection are modulated by BCG+H56:CAF01 vaccination and is the first described use of PET-CT to evaluate vaccine efficacy in the macaque model of TB.

4.2 INTRODUCTION

Tuberculosis (TB) was responsible for 10.4 million new cases and 1.8 million deaths worldwide in 2015. Over 95% of TB deaths occur in developing countries, disproportionately affecting those in poverty [23]. This highlights a critical need for new interventions. Approximately 43 million lives were saved between 2000 and 2014 through TB chemotherapy [23]. The drug regimen for TB, although lengthy and complex, can ablate infection, but studies suggest that previously infected and treated persons are actually at an increased risk for TB disease [366]. The introduction of a new effective vaccine, along with optimization of current tools and increased health coverage and social protection, would improve the 2% annual decline in TB incidence to 17% [367]. All of these factors highlight the need for a vaccine or other therapeutic measures to gain control over this disease.

Individuals with active TB disease spread the infection via aerosolized droplets containing *Mycobacterium tuberculosis* (Mtb), the causative agent [368]. About 30% of people exposed to these droplets become infected [369]. In the infected population, approximately 10% will develop active TB while the other 90% will have an asymptomatic infection, known as latent TB infection (LTBI) [35]. Those with LTBI have a 10% per lifetime risk of later developing active (reactivation) TB [325]. Since approximately 2.3 billion people have LTBI [7],

this represents a massive pool of potential cases of active TB. Preventing infection or reactivation with a vaccine would have a major effect on the disease spread. There are no validated immunological correlates of protection against TB. Despite this, most vaccines in development against TB are specifically selected for immunogenicity and tested in murine models [257]. The MVA85A vaccine, the first new vaccine for TB tested in humans, was developed along these guidelines and was shown to have no efficacy against prevention of infection or disease [38, 295], highlighting the need for new endpoints of TB protection. These new endpoints should be tied to TB outcomes that are expected to be important for pathogenesis of TB. This could include bacterial burden in lungs, inflammation, dissemination of Mtb within a host, and involvement of mediastinal lymph nodes. Inflammation is responsible for most of the host-directed damage caused by Mtb [169, 370], and its limitation by a vaccine will likely limit disease and could limit transmission. Dissemination within a host, both within the lung and outside of the lung to other tissues, represents a lack of control and can lead to the most severe forms of TB disease [12]. Mediastinal lymphadenitis is among the most common forms of extrapulmonary TB and represents a niche for bacterial replication and growth [12, 371, 372]. Evaluating bacterial burden and immune function in these pathologies in humans is impractical.

While the murine model is the most commonly used animal model of TB, it fails to replicate the most essential aspects of the disease, namely human-like pathology and disease progression or latent infection [106]. Our lab has pioneered the use of the cynomolgus macaque non-human primate (NHP) model, which faithfully replicates all aspects of *M. tuberculosis* infection, pathology and disease [107, 373]. We can accurately assess bacterial burden and pathology in our model at necropsy [65, 239, 365], and use serial PET-CT imaging to track infection trajectory and inflammation [107, 374]. This technology matches similar data from

humans [347, 350], highlighting its translational capabilities. However, it has not been previously used to assess TB vaccines in a quantitative fashion.

H56, a protein subunit vaccine, was designed to boost and broaden the immune response to BCG [274]. BCG is the only licensed vaccine for TB, which protects infants from severe TB disease but has variable efficacy in adolescents and adults [132, 375]. H56 is composed of three proteins: Ag85B, which is expressed in BCG; ESAT-6, which is expressed in Mtb but deleted in BCG; and Rv2660c, which is highly expressed by Mtb under various nutritional and oxidative stress conditions in vitro [274]. Thus, H56 was designed as a multistage vaccine for pre- and post-exposure administration to prevent both acute disease after infection and reactivation of LTBI, as described in the murine model system [274, 320]. We previously published that cynomolgus macaques vaccinated with BCG + H56:IC31® are protected from reactivation TB induced by anti-TNF antibodies [275]. NHPs protected from reactivation had very little to no Mtb in their thoracic LNs, a striking finding as most unvaccinated animals, as well as those vaccinated with BCG alone, had several LNs with viable bacteria [5]. In the current study, we vaccinated and challenged NHPs to characterize the protection conferred by BCG and H56. We sought to use our PET-CT technology to investigate differences between vaccinated and control animals. We then performed early necropsies post-challenge in vaccinated animals to identify immunological and physiological mechanisms of protection.

4.3 RESULTS

4.3.1 Immune responses pre- and post-challenge

Twenty cynomolgus macaques were either unvaccinated (N=6), vaccinated with BCG Danish only (N=4), or received BCG Danish followed by two injections of H56 in CAF01 (N=10) (Fig. 25, top), a liposomal adjuvant designed to elicit Th1 and Th17 cellular immune responses [318, 328]. These animals were then challenged with low dose Erdman strain Mtb and necropsied 5-6 months post-infection. During challenge, PET-CT was used to assess extent of infection, inflammation, and disease severity.

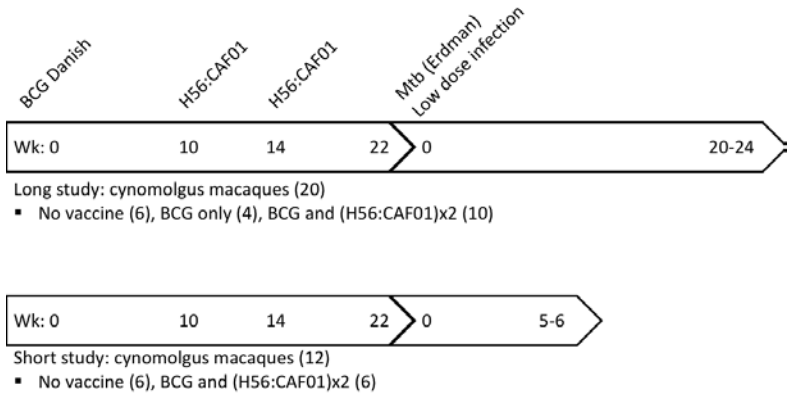

Figure 25: Chapter 4 study design. The top figure represents the six-month study. Of the 20 macaques used for this portion of the study, 6 were unvaccinated controls, 4 received BCG only, and 10 received BCG and H56:CAF01. The bottom figure represents the six-week study. Of the 12 macaques used for this portion of the study, 6 were unvaccinated and 6 were vaccinated with BCG and H56:CAF01.

Throughout the study, immunogenicity was assessed by IFN-γ ELISPOT and multicolor flow cytometry. Significantly more IFN-γ producing PBMCs responding to CFP, a pool of secreted proteins that elicit pan-mycobacterial responses, were observed in BCG/H56

vaccinated macaques compared to BCG only at two weeks pre-Mtb challenge (p=0.0118; Fig. 26), and in BCG/H56 vaccinated macaques compared to controls one and two weeks post-Mtb challenge (p=0.0381, p=0.0195 respectively). No significant differences by ESAT-6 specific ELISPOT responses between the groups were observed. A significant increase in Ag85B specific responses was observed in BCG/H56-vaccinated animals compared to those vaccinated with BCG only one week after the first H56 boost (p=0.0131). Stimulation with Rv2660c produced a significant, albeit small, difference between BCG/H56 and BCG only at

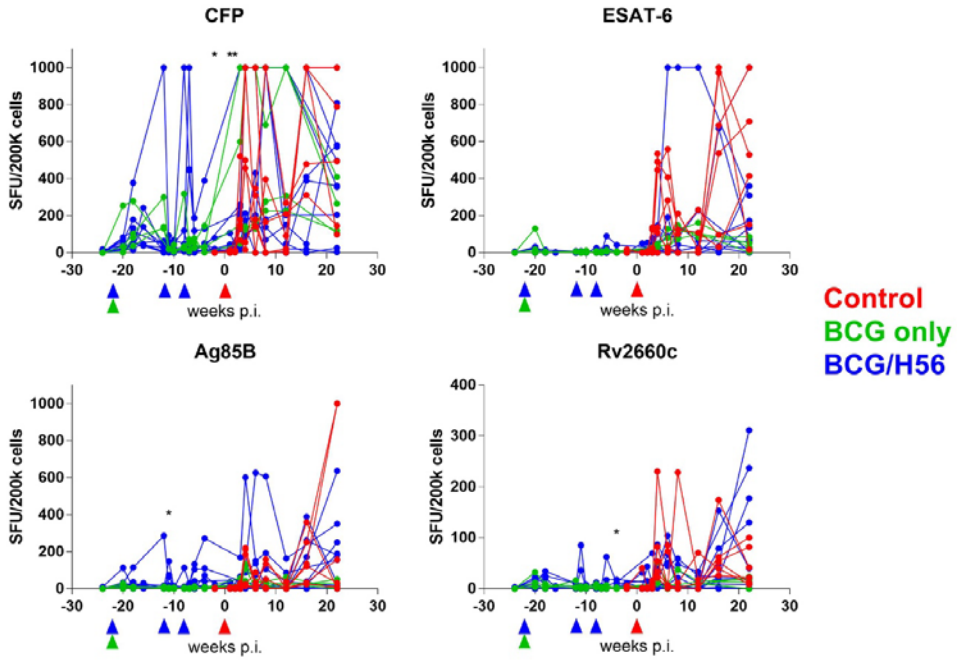

Figure 26: Antigen-specific IFN-γ responses to CFP (pan-mycobacterial stimulation) and peptide pools from H56 antigens in unvaccinated (control), BCG only, and BCG/H56 vaccinated macaques were determined by ELISPOT (depicted as spot-forming units (SFU) per 200,000 cells). Each line represents one animal. Green (BCG only) and blue (BCG/H56) wedges denote vaccinations, while the red wedge denotes Mtb challenge. Asterisks denotes significant difference between either two groups by Mann-Whitney (pre-challenge) or three groups by Dunn's multiple comparisons (post-challenge) with p values in the text. Medium background responses were subtracted from each antigen-specific result.

four weeks pre-Mtb challenge (p=0.0325).

When examining pre-challenge responses by flow cytometry, we observed that H56 significantly boosted the macaques' ability to produce cytokines (IFN-γ, TNF, IL-2, or IL-17) in non-naïve CD4 T cells one week after each boost compared to BCG only (p=0.0412, p=0.0338 respectively), determined using potent non-specific stimulation (phorbol dibutyrate and ionomycin (P&I); Fig. 27). A higher frequency of non-naïve T cells from BCG/H56 vaccinated macaques produce cytokines after ESAT-6 stimulation one week after the first H56 boost (p=0.0104). A significantly higher frequency of non-naïve T cells in

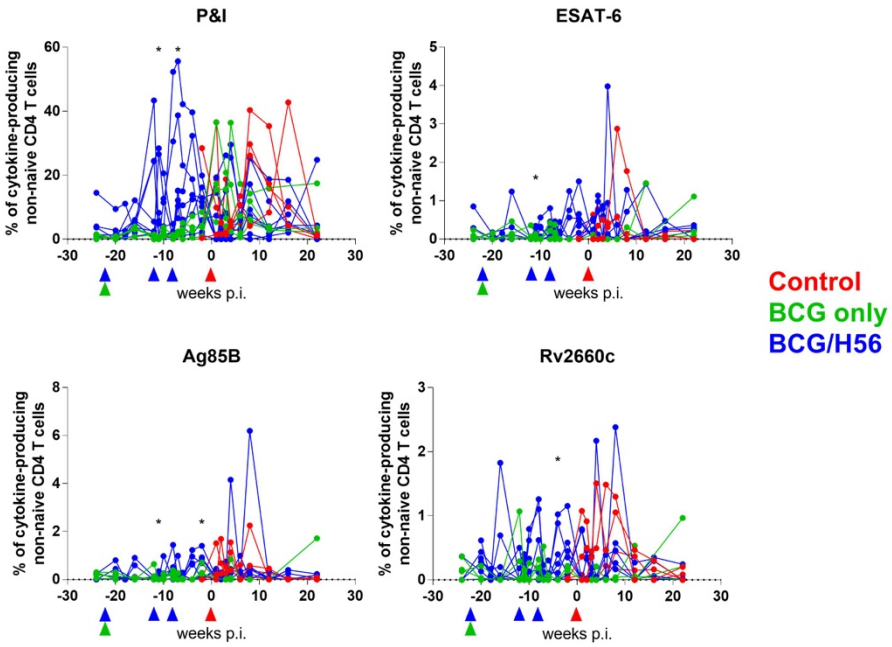

Figure 27: Frequencies of memory CD4 T cells producing IFN-γ, TNF, IL-2, or IL-17 in response to phorbol dibutyrate and ionomycin (P&I) or peptide pools of H56 vaccine antigens were determined using multicolor flow cytometry. Each line represents one animal. Green (BCG only) and blue (BCG/H56) wedges denote vaccinations, while the red wedge denotes Mtb challenge. Asterisks denotes significant difference between either two groups by Mann-Whitney (pre-challenge) or three groups by Dunn's multiple comparisons (post-challenge) with p values in the text. Medium background responses were subtracted from each antigen-specific result.

these animals also respond to Ag85B one week after the first H56 boost (p=0.0277) and two weeks pre-Mtb challenge (p=0.0411). Responses to Rv2660c were significantly higher in BCG/H56 vaccinated macaques four weeks pre-Mtb challenge (p=0.0371). Upon further dissection of responses just before Mtb challenge, non-naïve CD4 T cells from control animals were mostly only capable of being terminally differentiated IFN-γ+ effector cells (Fig. 28), while CD4 T cells from BCG/H56 vaccinated macaques were more capable of being multifunctional and displaying memory phenotypes (IL-2+ alone or with other

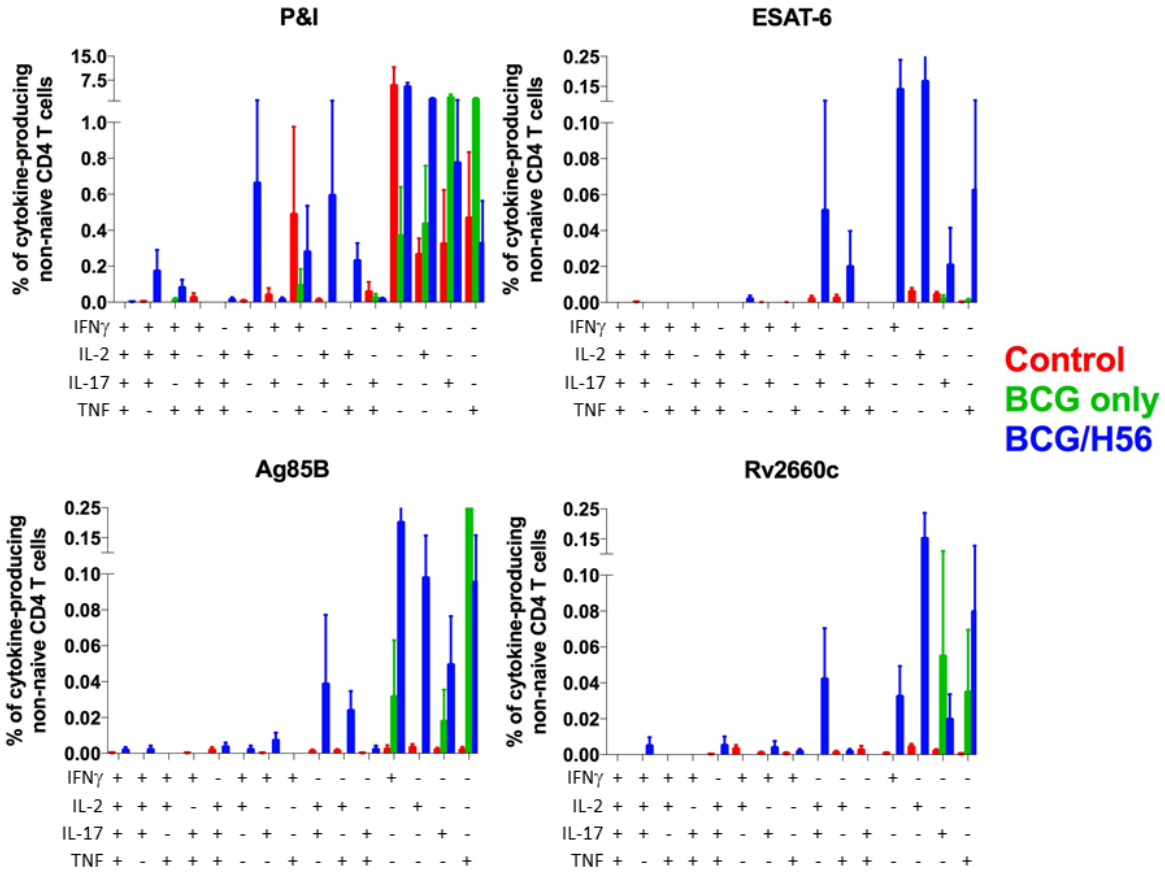

Figure 28: Boolean combinations of frequencies of memory CD4 T cells pre-Mtb challenge producing IFN-γ, TNF, IL-2, or IL-17 in response to P&I or peptide pools of H56 vaccine antigens were determined using multicolor flow cytometry. Each bar displays the mean response, and error bars represent SEM. Medium background responses were subtracted from each antigen-specific result.

cytokines). Non-naïve CD4 T cells from BCG only macaques produced only single cytokines in response to vaccine antigens (Fig. 28), and none to ESAT-6, which is not in BCG. Responders to vaccine antigens in BCG/H56 vaccinated animals exhibited multifunctionality and more robust memory phenotypes, including ones previously associated with protection in this family of vaccines (IL-2+, IL-2+TNF+; Fig. 4, top right) [136, 315]. We also observed a vaccine antigen-responsive population of IL-2+IL-17+ CD4 T cells that are likely memory CD4 T cells generated by CAF01, which was designed to elicit Th1 and Th17 type responses [328].

4.3.2 Vaccination prevents dissemination of granulomas in the lung

We reported previously that cynomolgus macaques with LTBI have fewer granulomas than those with active disease [65], and that the formation of new granulomas in the early phase of infection (3-6 weeks) is associated with development of active disease months later [345].

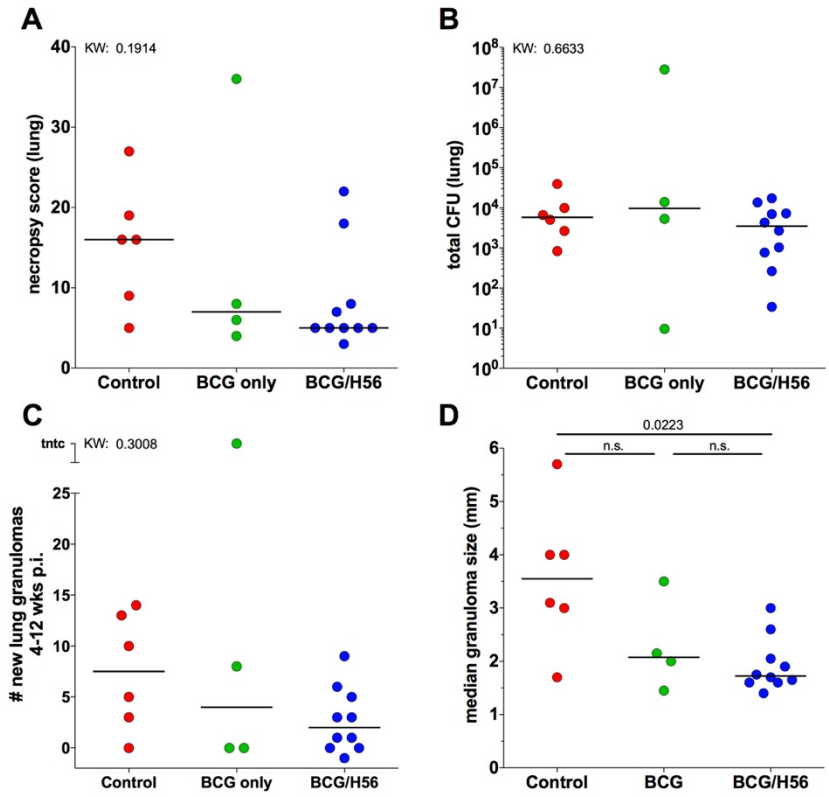

Figure 29: Vaccination prevents dissemination of granulomas in the lung. For all graphs, each dot represents one animal and bars represent medians. Comparisons were done using Kruskal-Wallis (KW), and if KW<0.05, Dunn's multiple comparions with p values directly reported. **A** Total amount of gross pathology in the lung observed at necropsy. **B** The total bacterial burden from lung granulomas in each animal enumerated from plates spread at necropsy. C Number of additional new granulomas in the lung of each animal that formed between 4 and 12 weeks p.i. D Median size of lung granulomas at 4 weeks p.i.

Mtb infection of cynomolgus macaques results in the full spectrum of infection outcomes, as can be seen in the variability in lung pathology of unvaccinated controls at necropsy (Fig. 29A), with two of the six control animals exhibiting minimal disease. In contrast, most of the vaccinated animals had minimal lung pathology at necropsy (Fig. 29A). As in our previously published study [275], BCG/H56 did not protect all macaques, since 2 of the 10 vaccinated animals had lung pathology similar to unvaccinated controls. Discordant with the

pathology scores, the median total bacterial burden in the lung among the three groups was similar, although one BCG vaccinated and several of the BCG/H56 vaccinated animals had relatively low lung bacterial burdens (Fig. 29B). Serial PET-CT scans showed that animals vaccinated with BCG/H56 formed fewer new lung granulomas than control animals after 4 weeks post-infection (although not statistically significant) (Fig. 29C), indicating a reduction in dissemination in most BCG/H56 monkeys, a phenotype associated with control of disease [345]. The majority of BCG/H56 vaccinated animals have a median lung granuloma size of less than 2 mm (median=1.725 mm), while the median size of lung granulomas from control animals is about twice as large (median=3.55 mm; Fig. 29D). Thus, vaccination seems to limit lung pathology through prevention of dissemination and spread in that compartment, not necessarily by reducing lung bacterial burden.

4.3.3 H56 in CAF01 limits pathology and bacterial burden in the mediastinal lymph nodes

In our previous study, BCG/H56 vaccinated animals with asymptomatic infection were protected from anti-TNF-induced reactivation disease and had completely sterile LNs, except for one animal with one LN that contained viable bacteria [5, 275]. This phenotype is strikingly different than what is typically seen in our NHP model, suggesting that control of Mtb in the mediastinal LNs is important for protection against reactivation. We sought to further explore this compartment in our current study. The median necropsy score (summary of gross pathology) in LNs for the animals vaccinated with BCG/H56 was half that of control animals (Fig. 30A), an indication of substantially less grossly visible involvement. The median of total CFU in the LN compartment was 20-fold lower in BCG/H56 vaccinated animals (820 CFU) compared to

unvaccinated animals (16960 CFU; Fig. 30B). The median number of thoracic LN with culturable Mtb per animal was 4 for unvaccinated animals, and 3.5 for BCG only vaccinated

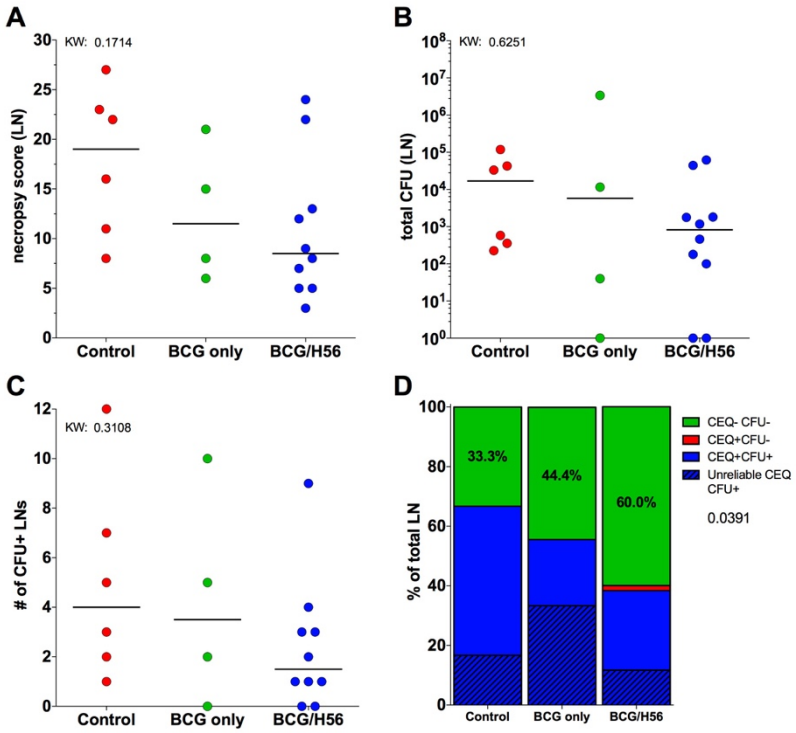

Figure 30: H56 in CAF01 limits pathology and bacterial burden in the mediastinal lymph nodes. For A-C, each dot represents one animal and each bar represents a median, and comparisons were done using the Kruskal-Wallis test (KW). **A** The amount of pathology (necropsy score) observed at necropsy in the LN compartment. **B** The total bacterial burden in the LNs determined by summing the plated CFU of all LN in each animal. **C** Number of LNs at necropsy with viable bacteria, i.e. CFU+. Historical data show that 4-5 LN are typically CFU+ at necropsy. **D** Stacked graphs representing the proportions of LNs containing total bacteria (CEQ; live and dead) and/or live bacteria (CFU). LN that lack both CEQ and CFU likely never had Mtb or Mtb was quickly killed upon arrival (CEQ-CFU-, green). Having CEQ but not CFU suggests that Mtb grew in the LN but were killed (CEQ+CFU-, red). The limit of detection for CEQ is about 1000, so LN without CEQ but with CFU usually means that the CEQ was below this limit (Unreliable CEQ, CFU+, hashed). In support of this, the CFU in these LN are usually below 1000 as well. LNs with both CEQ and CFU have viable bacteria and a total count of organisms (CEQ+CFU+, blue). A comparison of CEQ-CFU- proportions of LNs was done using Fisher's exact test.

animals, but only 1.5 in BCG/H56 vaccinated animals (Fig. 30C). This suggested that either H56:CAF01 prevents Mtb from reaching the LN compartment in most monkeys, or provides an immunologic environment that can kill Mtb that establish and are growing in the LN. To assess these possibilities, we compared the chromosomal equivalents (CEQ) of Mtb in all thoracic LN from the monkeys in each group. We previously showed that CEQ represents a total bacterial count in granulomas or lymph nodes that includes live and dead Mtb, since Mtb DNA persists in granulomas for many months [5, 86]. Having neither CEQ nor CFU (CEQ-CFU-) in a LN suggests that Mtb bacilli never reached that tissue, or are rapidly killed. The percentage of CEQ-CFU- LNs was significantly different among the study groups ($p=0.0391$), with 27.5% more LNs with no sign of current or previous Mtb infection in BCG/H56 animals compared to controls (Fig. 30D). CEQ-CFU- LNs also display no microscopic pathology or inflammation. These data together suggest that BCG/H56 is substantially limiting productive dissemination to the LN compartment.

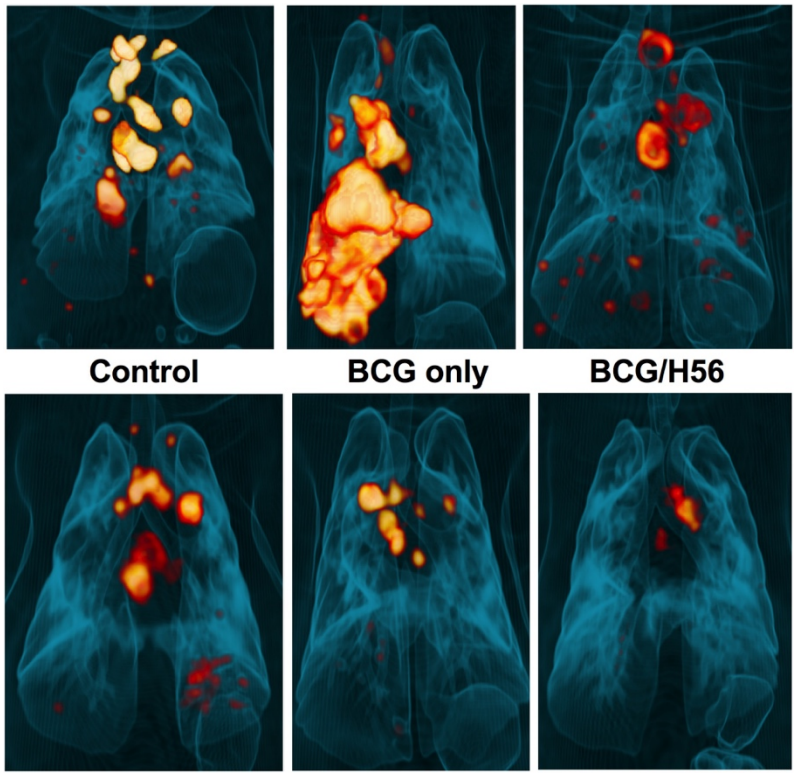

Figure 31: Qualitative comparisons of 3D PET-CT renderings at the conclusion of the study. 3D scan renderings were generated for two animals from each group to illustrate the impact of each vaccine on overall inflammation, or FDG avidity. Panels in the top row showcase the worst animal in each study cohort. Panels in the bottom row include the middle animal in each group. Worst and middle here are determined by total lung inflammation, quantified and graphed in Figure 32A.

4.3.4 H56 in CAF01 reduces lung inflammation and apparent risk of reactivation determined by PET-CT

Serial PET-CT imaging was pioneered by our laboratory in the nonhuman primate (NHP) model of TB as a quantitative and translational means of assessing the extent of disease during Mtb challenge [350, 374]. Using this tool, we observed striking differences in both spread of TB and

host inflammation (FDG avidity) in these macaques by the conclusion of this study (Fig. 31). BCG/H56 limits both the most severe cases of TB compared to BCG alone and controls (Fig. 31, top), and well as limiting the median amount of total lung inflammation (Fig. 31, bottom). The total lung inflammation (in standard uptake values; SUV) was quantified to visualize these differences between groups (Fig. 32A). BCG alone (median=1611) conferred about a 6.5-fold decrease in lung inflammation compared to controls (median=10482) by the end of the study. Boosting with H56:CAF01 (median=265) decreased lung inflammation by another 6 fold, a decrease in inflammation of 40 fold compared to controls.

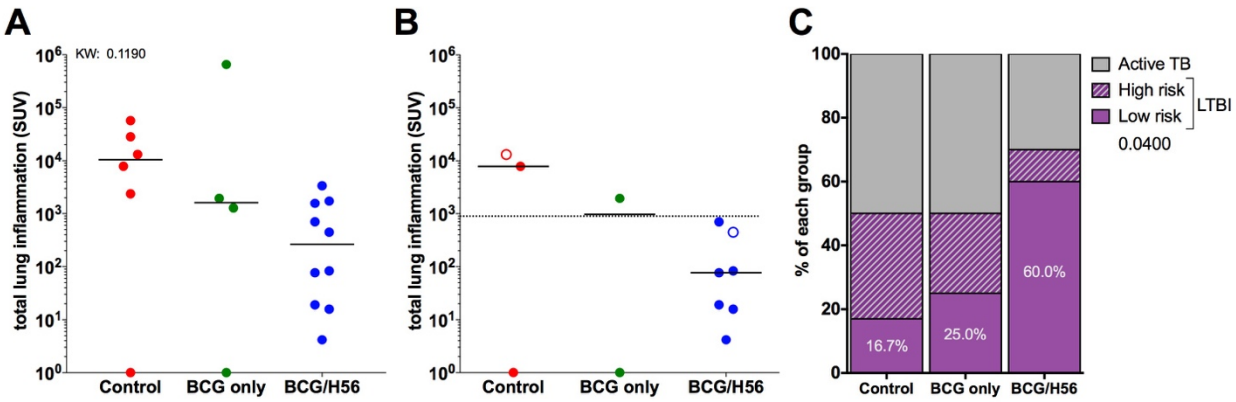

Figure 32: H56 in CAF01 reduces risk of reactivation disease determined by PET-CT. We have previously published that two PET-CT endpoints, low total lung inflammation and lack of sites of extrapulmonary involvement, predict low to no risk of reactivation disease [5]. **A** Total lung inflammation (standard uptake values; SUV) was plotted for all macaques at the conclusion of the study (6 months p.i.). Each dot represents one animal and bars represent medians. Comparisons between the groups was done using the Kruskal-Wallis test (KW). **B** Total lung inflammation was plotted for *only* the animals with LTBI in each group. Each dot represents one animal and bars represent medians. Open circles represent animals that have sites of extrapulmonary involvement by PET-CT. The dashed line represents the cutoff for high or low total lung inflammation. **C** The percentage of macaques in each group that either had clinically-determined active TB (grey) or LTBI (purple). Animals with LTBI were then further subdivided by risk as determined in Fig. 4B. Comparisons of percentage of low risk LTBI animals between groups was done using Fisher's exact test with the p value reported directly.

We recently published that PET-CT imaging parameters can be used to predict risk of reactivation disease induced by TNF neutralization in NHPs with LTBI six months or more after challenge [5]. Specifically, low total lung inflammation and lack of extrapulmonary sites of infection predict low to no risk of reactivation disease with 92% sensitivity and specificity. In that study, 50% of cynomolgus macaques classified as LTBI were at low risk of reactivation following anti-TNF antibody treatment. Using clinical measures as previously described [65], 50% of the unvaccinated and BCG only animals in this study would be classified as LTBI six months p.i. (n=3 and n=2, respectively), while 70% of BCG/H56 vaccinated animals had LTBI (n=7), similar to our previous study [275]. Using our published criteria for risk of reactivation on only the macaques with LTBI (Fig. 32B), one animal from the unvaccinated and one from the BCG only groups were at low risk, while 6 of the 7 (87.5%) BCG/H56 vaccinated animals with LTBI were classified as low risk for reactivation TB, a significant difference (p=0.04; Fig. 32C). These data are supported by our earlier findings that BCG boosted with H56 prevented reactivation induced by anti-TNF treatment [275], in which 0 of 4 LTBI BCG+H56:IC31® monkeys reactivated, while 3 of 4 BCG-only vaccinated animals reactivated. Together these data suggest that H56:CAF01 works to stabilize inflammation in the granulomas and lungs, and that maintenance of this low level of inflammation is important for long-term control of disease and prevention of immune-compromise induced reactivation.

4.3.5 Vaccination mitigates lung inflammation early post-infection

We then used serial PET-CT to investigate early differences in inflammation post-challenge that could be associated with the protection conferred by BCG/H56. Most of the unvaccinated animals experimentally infected with Mtb in this experiment had elevated total levels of FDG

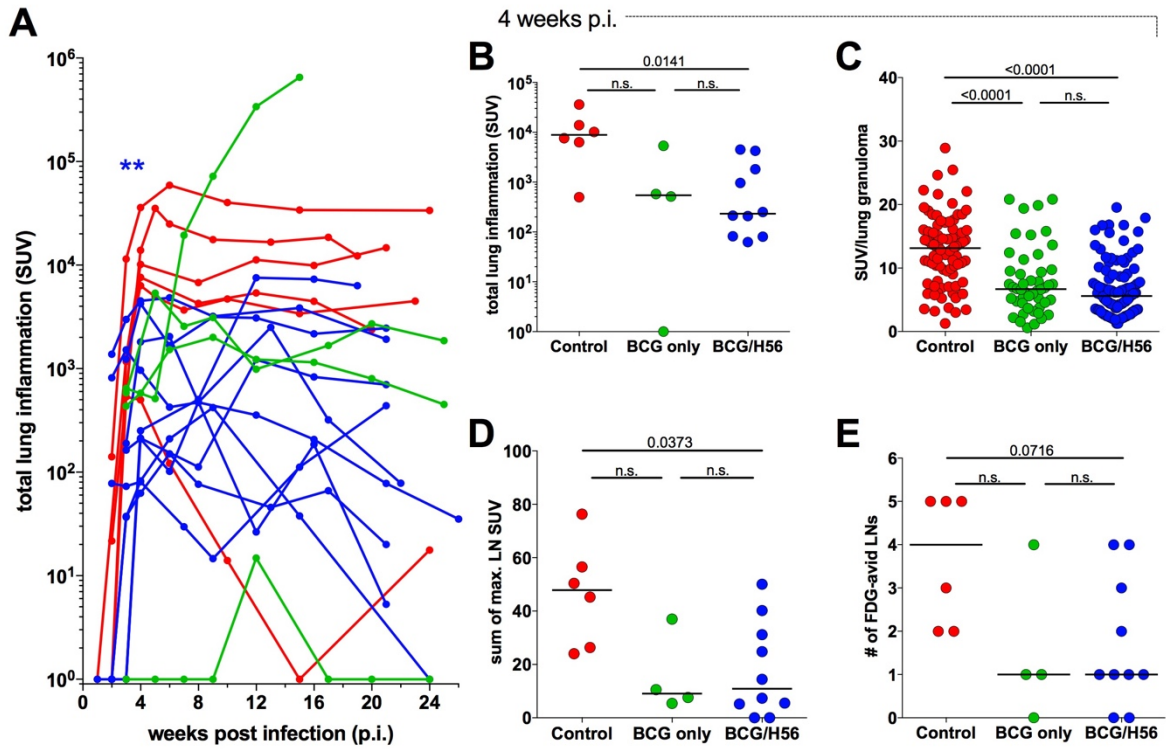

Figure 33: H56 in CAF01 mitigates lung inflammation early post-infection**. A** Total lung SUV of FDG was divided by the resting muscle SUV and plotted over time for controls (red), BCG only (green), and BCG/H56 (blue). Each dot represents a time point. Asterisks represent time points (3 and 4 weeks) post-infection where the BCG/H56 vaccinated animals are significantly different than the controls by Dunn's multiple comparisons. P values are reported in the manuscript. For B-E, all data are from 4 weeks p.i. and comparisons between groups were done using Dunn's multiple comparisons. **B** Total lung inflammation at 4 weeks p.i. Each dot represents one animal and bars represent medians. **C** FDG SUV per lung granuloma at 4 weeks p.i. Each dot represents one granuloma and bars represent medians. **D** The sum of the maximum LN SUV at 4 weeks p.i. Each dot represents one LN and bars represent medians. **E** The number of FDG-avid LNs (SUV>2.3) at 4 weeks p.i. Each dot represents one animal and bars represent medians.

avidity in lungs early, peaking around 4-6 weeks post-infection (p.i.) and maintaining high levels for the duration of challenge (Fig. 33A). Animals vaccinated with BCG only showed a wide range of lung inflammation, with one animal having very low FDG avidity in the lungs (Fig.

33A). The cohort vaccinated with BCG/H56 had significantly reduced FDG avidity compared to the unvaccinated controls at 4 weeks p.i. ($p = 0.0141$; Fig. 33A-B). We then investigated this early time point (4 weeks p.i.) further. The reduction in lung FDG avidity occurs early at the level of individual granulomas (Fig. 33C). Lung granulomas from control animals are more FDG avid than those from vaccinated animals at 4 weeks post-infection (Fig. 33C). The total inflammation of thoracic LN (sum of maximum LN SUV) (Fig. 33D) and the number of FDG avid LNs are significantly less in BCG/H56 vaccinated animals compared to controls (Fig. 33E).

4.3.6 H56 in CAF01 prevents mediastinal lymph node pathology early post-infection

The evidence presented thus far suggests that BCG/H56 provides long-term protection, as evidenced by reduced lung inflammation, minimal dissemination, and limited thoracic LN involvement. However, to assess the early events that contribute to this protection is difficult since these necropsies were performed 5-6 months after infection. Our previous data and the literature support that early events are crucial to infection outcome in natural infection [115, 345, 376]. In this current study, the mitigation of lung inflammation and reduction of dissemination in vaccinated animals was observed as early as four to six weeks (Fig. 29; Fig. 33). To address these early events, including LN involvement, we repeated the study but performed the necropsies earlier, at 5-6 weeks post-infection, focusing on unvaccinated and BCG/H56 vaccinated animals (n=6 per group; Fig. 25, bottom).

Grossly visible lung pathology and total lung bacterial burden were similar between the two groups (Fig. 34), suggesting that later control of inflammation is not associated with early bacterial control in the lungs. Early total lung inflammation (FDG avidity) was lower in BCG/H56 vaccinated animals than controls, along with the sum of maximum LN SUV and number of FDG-avid LNs (Fig. 35), similar to the first cohort of animals. There was pronounced early infection control in the LN of BCG/H56 vaccinated animals. The necropsy score of LNs

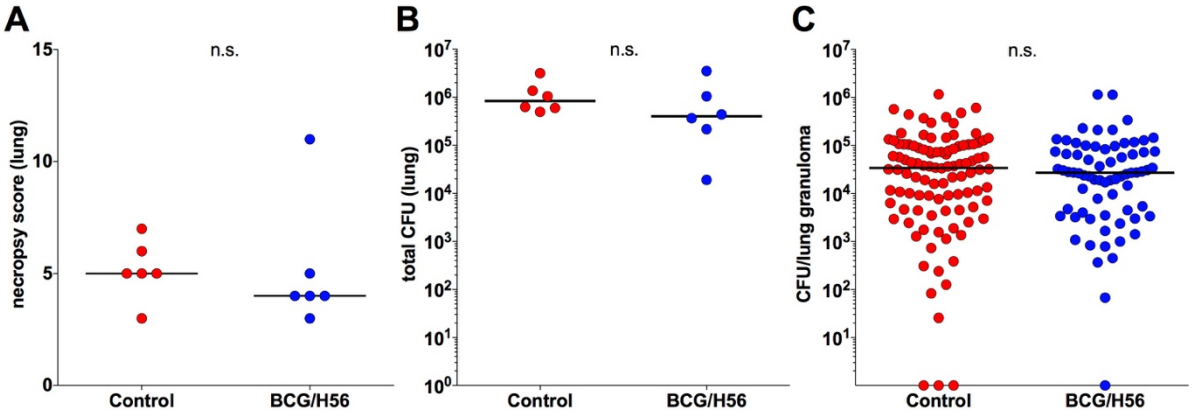

Figure 34: Bacterial burden in the lung early post-infection does not correspond to vaccination. Comparisons were done using the Wilcoxon rank-sum test. **A** The total amount of gross pathology observed in the lung compartment at necropsy in the early animals. Each dot represents one animal and bars represent medians. **B** The total bacterial burden from all lung granulomas plated at necropsy. Each dot represents one animal and bars represent medians. **C** The CFU from all granulomas excised at necropsy. Each dot represents one granuloma and bars represent medians.

was significantly reduced in the vaccinated macaques (Fig. 36A), and the median total CFU in LNs (870 CFU) was almost 300-fold lower than LNs from control animals (250550 CFU; Fig. 36B). The LN with the highest number of Mtb bacilli in each vaccinated macaque (median=310 CFU), with one exception, had 600-fold fewer bacteria than the LN with the highest Mtb burden from control animals (median=188000 CFU; Fig. 36C). LNs with neither CEQ nor CFU (CEQ-CFU-) were more prevalent from BCG/H56 vaccinated versus control animals (Fig. 36D),

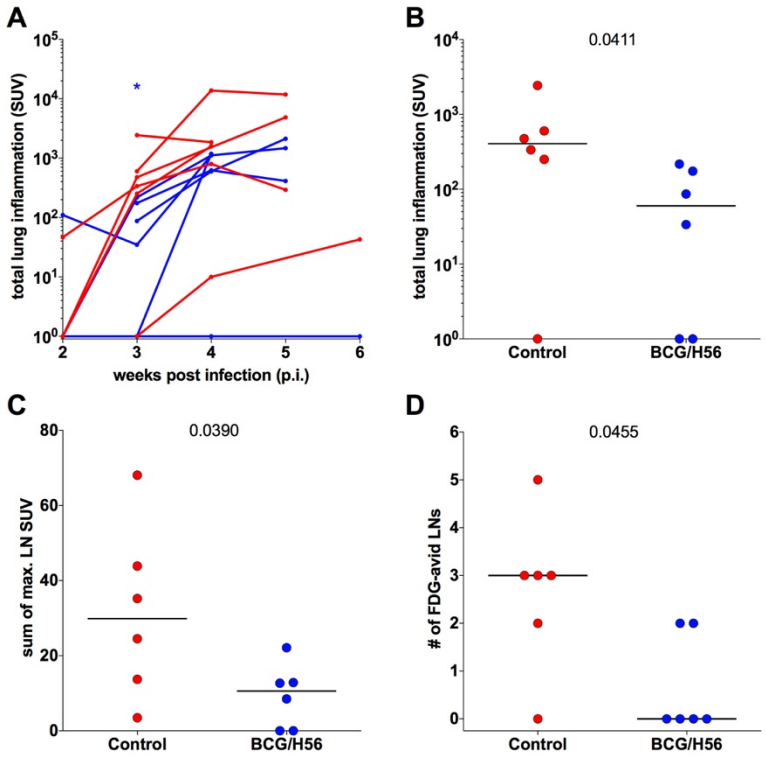

Figure 35: Radiological data from the second set of animals. These graphs demonstrate that the limited PET-CT data from the short course of animals (Fig. 25, bottom) match the radiological data from the long course (Fig. 33). These data include total lung inflammation graphed over the limited time points with an asterisk representing significant difference (**A**), total lung inflammation at 3 weeks p.i. (**B**), the sum of the maximum LN SUV (**C**), and the number of FDG-avid LN (SUV>2.3). **D.** Each line/dot represents one animal and bars represent medians. Comparisons were performed using Wilcoxon rank-sum tests.

confirming that BCG with H56 prevents early Mtb dissemination to or growth within the LN compartment. These early infection data support the longer-term studies, both showing a reduction in inflammation early and protection from LN infection by BCG/H56.

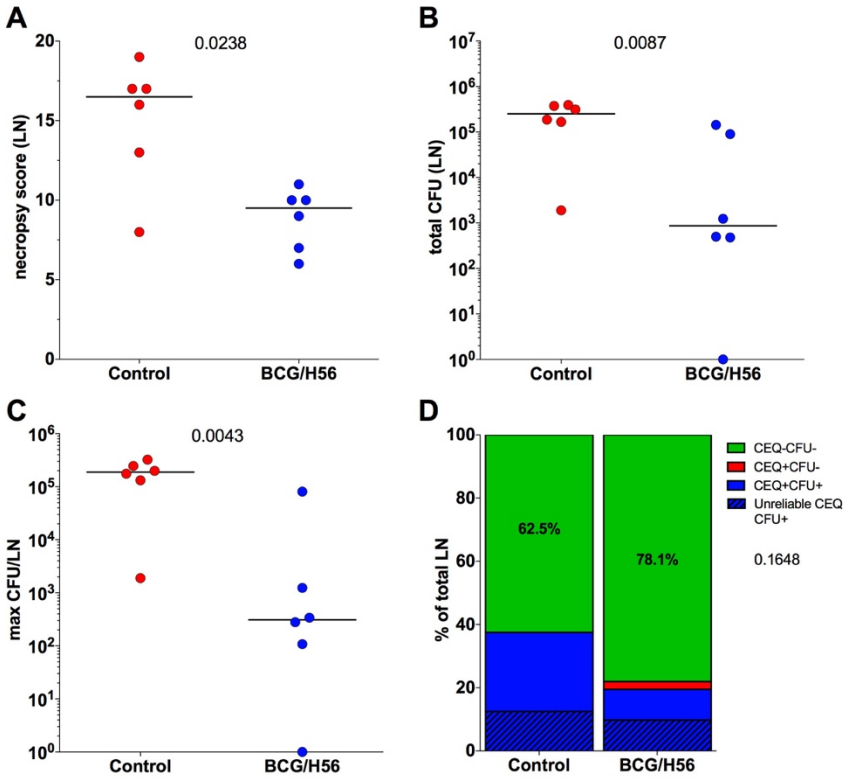

Figure 36: H56 in CAF01 prevents mediastinal lymph node pathology early post-infection. For A-C, each dot represents one animal and bars represent medians, and comparisons were performed using the Wilcoxon rank-sum test. **A** The amount of pathology observed at necropsy specifically in the LN compartment. **B** The total bacterial burden in all LN excised at necropsy. **C** The highest value for CFU in a LN for all animals in each cohort. **D** Stacked graphs representing the proportions of LNs containing total bacteria (CEQ; live and dead) and/or live bacteria (CFU). Group comparisons of CEQ-CFU- LNs were done using Fisher's exact test. See legend of Figure 30D for interpretations of each LN phenotype.

4.3.7 Mediastinal lymph nodes exhibit differential cytokine production in BCG/H56-vaccinated animals but not in lung granulomas

In our previous work, multicolor flow cytometry on excised and homogenized individual granulomas at necropsy identified T cell cytokine profiles associated with sterilized granulomas [239]. We used this same technology to identify *early* immune responses associated with vaccine-induced protection seen six months post-infection. All mediastinal LNs, both involved and uninvolved, were excised at necropsy, homogenized to create single cell suspensions, and then assayed by flow cytometry to elucidate immune function. There was a trend of lower frequencies of cytokine producing T cells in the vaccinated animals, most prominently observed in the percentage of any cell producing cytokines and in single functional T cell cytokine production (Fig. 37A). Lower frequencies of T cells from LNs of vaccinated animals produce interferon gamma (IFN-γ; $p=0.047$) and significantly higher frequencies of T cells produce tumor necrosis factor (TNF; $p=0.018$; Fig. 37B). When using a permutation test to compare the profiles of cytokine production from LNs, significant differences were observed between the unvaccinated and vaccinated groups of macaques.

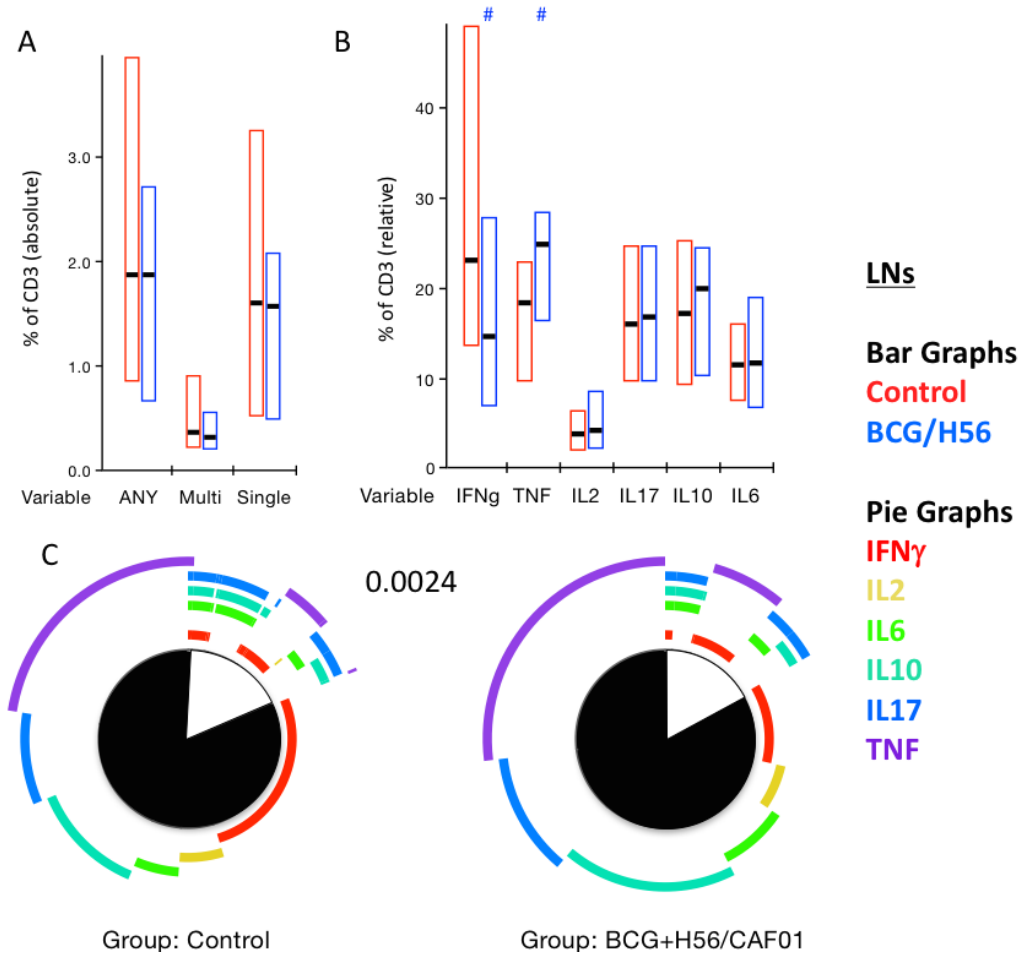

Figure 37: Mediastinal lymph nodes exhibit differential cytokine production in BCG/H56-vaccinated animals. These graphs represent flow cytometric data on primary tissue from early (5-6 weeks p.i.) necropsies from LNs. **A** Total cytokine production was measured in absolute numbers (% of CD3) for the production of any of the six cytokines (ANY), production of two or more cytokines (Multi), and production of only one cytokine (Single). Bars represent medians and boxes represent interquartile ranges. **B** Individual cytokine production was measured in relative numbers (percent of total production). Bars represent medians and boxes represent interquartile ranges. Pound signs indicate a significant difference between the two groups by Wilcoxon rank-sum test. **C** Profile of cytokine expression visualized from Boolean gating data into pie charts with arcs. Each wedge of the pie represents a single or multiple cytokine producing T cell population, and each arc represents a cytokine being produced alone or with other cytokines. Comparisons were performed using a permutation test as previously described [6].

Both cohorts had similar relative frequencies of multifunctional (center pie, white) to single functional (center pie, black) T cells (Fig. 37C). Within the multifunctional populations, however, BCG/H56 vaccinated animals had a higher relative frequency of IFN-γ+TNF+ T cells,

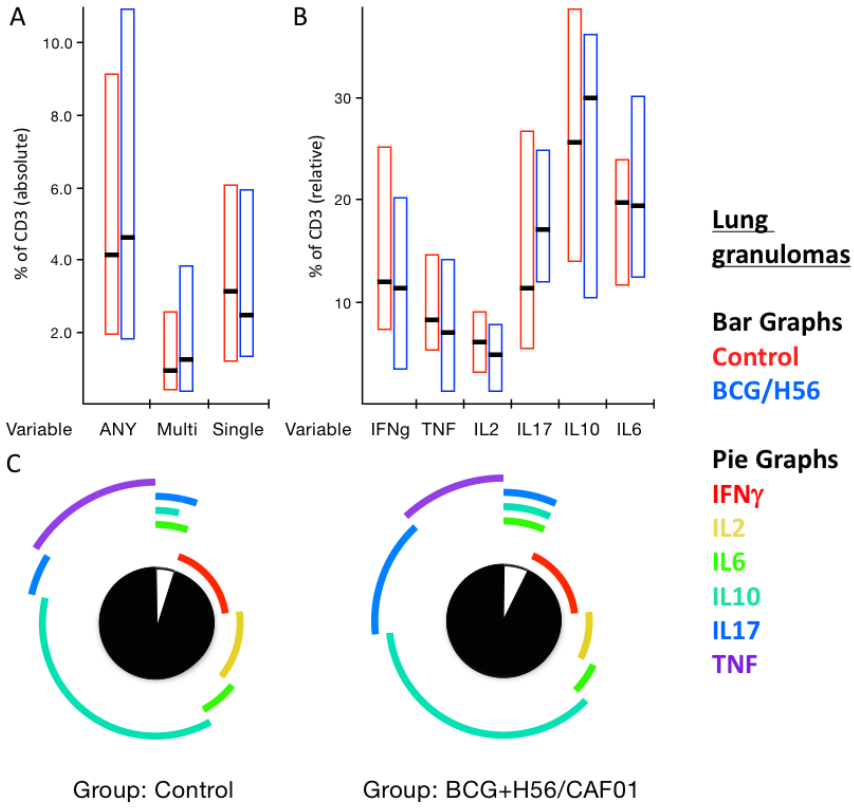

Figure 38: These graphs represent flow cytometric data on primary tissue from early necropsies from lung granulomas. **A** Total cytokine production was measured in absolute numbers (% of CD3) for the production of any of the six cytokines (ANY), production of two or more cytokines (Multi), and production of only one cytokine (Single). Bars represent medians and boxes represent interquartile ranges. **B** Individual cytokine production was measured in relative numbers (percent of total production). Bars represent medians and boxes represent interquartile ranges. Pound signs indicate a significant difference between the two groups by Wilcoxon rank-sum test. **C** Profile of cytokine expression visualized from Boolean gating data into pie charts with arcs. Each wedge of the pie represents a single or multiple cytokine producing T cell population, and each arc represents a cytokine being produced alone or with other cytokines. Comparisons were performed using a permutation test as previously described [6].

while control animals had a higher relative frequency of IL-6+IL-10+IL-17+ T cells (Fig. 37C). Within the single functional populations, control animals had a higher relative frequency of terminally differentiated IFN-γ+ T cells, while BCG/H56 vaccinees had higher relative frequencies of IL-6+, IL-10+, IL-17+, and TNF+ T cells in their LNs (Fig. 37C). In lung granulomas from early necropsies, there was no difference in total frequencies of T cells producing cytokines (in any combination) between vaccinated and control macaques (Fig. 38A). Similarly, there was no difference in relative production of any of the individual six cytokines examined (Fig. 38B). We applied a permutation test to compare the profiles of cytokine production between the cohorts, and again there was no difference (Fig. 38C). This corresponds to the fact that bacterial burden in the lung granulomas is similar between the cohorts (Fig. 34C).

4.4 DISCUSSION

The goal of this study was to identify correlates and mechanisms of protection in macaques vaccinated with BCG and H56, an experimental fusion protein boost. We showed previously in our NHP model, which faithfully replicates TB in humans [107], that BCG boosted by H56 protects against reactivation TB [275]. The estimated 2.3 billion people with LTBI [7] represent an enormous reservoir of potential reactivation TB. Active disease is the transmissible form, so by blocking active or reactivation TB, one can prevent transmission of Mtb and stop the spread of TB. Therefore, a vaccine that may not prevent infection but blocks disease, like BCG with H56, is crucial to the fight against TB. This study sought to identify which aspects of *M. tuberculosis* infection are influenced most strongly by BCG/H56.

In this study, animals vaccinated with both BCG and H56:CAF01 had significantly less total lung inflammation than animals vaccinated with BCG only or no vaccine as measured by PET-CT and reflected in the lung pathology score. The reduced inflammation was apparent at the individual granuloma level early; in addition, the granulomas from BCG/H56 vaccinated animals were smaller than those from control animals. Many of the clinical signs and symptoms of TB are caused by excessive host inflammation, so that lower total lung inflammation is associated with better control of disease [169, 370]. In other work performed by our laboratory [5], we established that PET-CT could be used to determine risk of reactivation disease using our model with TNF neutralization as an inducer of reactivation. Using this technology, we confirmed that most (87.5%) of the BCG/H56 vaccinated animals with LTBI are at low risk of reactivation, which corroborates our earlier data on H56 preventing anti-TNF induced reactivation [275]. In comparison, 17% of the unvaccinated and 25% of the BCG-only vaccinated animals with LTBI in the current study would be categorized as low risk of reactivation. Vaccination with BCG and H56:CAF01 could reduce total lung inflammation by either reducing the bacterial burden or modulating the host response to Mtb. We show here that, surprisingly, this decrease in lung inflammation was not associated with a change in lung bacterial burden, suggesting that this vaccine regimen is modulating the host immune response against Mtb. However, in our recent study [5], risk of reactivation determined by total lung inflammation was associated with lower bacterial burden in the lung. None of the animals in that study were vaccinated, suggesting that natural protection against reactivation disease is associated with control and reduction of Mtb, while BCG/H56 induced protection is associated with modulation of the host immune response. Host inflammation therefore is an important correlate of protection against reactivation disease, and modulating host immunity to Mtb either

through vaccination or host-directed therapy delivered specifically to the lungs or LN might be a tractable new therapeutic for eliminating reactivation disease in TB.

In this model of TB, BCG does confer some protection against Mtb challenge [275], as it does in humans [127, 132]. However, BCG alone does not protect against anti-TNF induced reactivation, while boosting with H56 does [275]. Where does H56 work to protect macaques from reactivation disease? How is the protection engendered by BCG/H56 different than BCG alone? Vaccination with BCG prevents pathology in the lung and restricts the size of granulomas early p.i. Surprisingly, this protection does not correspond to a decrease in bacterial burden in the lung. Boosting with H56 does not improve these specific outcomes, suggesting that the protection seen in the lung is generated by BCG. Dissemination within the lung, i.e. formation of new granulomas within the first few weeks after establishment of infection, is associated with eventual development of active TB [12]. While a few macaques in the control and BCG only groups naturally resisted dissemination of lung lesions, most BGC/H56 vaccinated animals were protected from dissemination, with the number of new granulomas after establishment being 0-1 for the majority of animals. Additionally, the median score for lung pathology in BCG/H56 vaccinated animals is nearly the same for macaques necropsied at both six weeks and six months, while the median score for lung pathology at six months in controls is three times higher than at six weeks p.i., indicating further dissemination in the absence of vaccination. In the mouse model, vaccination with H56:CAF01 generates vaccine specific T cells that efficiently and preferentially home to the lung parenchyma from the LNs [277], suggesting that these cells are responsible for the protection observed against dissemination of Mtb in the lung.

Host inflammation is a major driving factor of poor disease outcome in TB [169, 370]. We and our colleagues have shown that a decrease in lung inflammation, as determined by total

FDG avidity in the lung, correlates with successful TB chemotherapy in active TB in macaques and humans [2, 350, 351] and low risk of reactivation disease in monkeys with LTBI [5]. In our previous study with BCG/H56 vaccination [275], we observed that LNs from vaccinated animals that did not reactivate when treated with anti-TNF therapy were all completely sterile, except for one animal with one CFU+ LN [5]. This suggested that LNs were an important compartment for BCG/H56 induced protection against reactivation disease. The more detailed analysis in the current study showed that 80% of BCG/H56 vaccinated animals have less pathology and lower bacterial burden in the LN than the median of the control or BCG only groups. The control and BCG only groups have a median of four LNs with viable bacteria, while a majority of BCG/H56 vaccinated animals have two or fewer involved LNs, with quantitative PCR data suggesting that mycobacteria never productively disseminated to these LNs in the first place. These data together demonstrate that, while BCG confers some protection in the lungs, H56 works to boost protection specifically in the LN compartment.

Since early events post-infection are thought to be the most critical in determining TB outcome [115, 345, 376], we investigated vaccine induced protection at 5-6 weeks post-infection, to see whether control of Mtb in the LN compartment was still a phenotype strongly associated with BCG/H56 vaccination. Indeed, at early time points animals vaccinated with BCG/H56 had significantly less involvement of LNs as compared to controls. There are two possibilities for the reduction in CFU+ LN in vaccinated animals: prevention of dissemination to the LN or improved killing of bacteria that establish and grow in the LN. Our CEQ analysis supports the former possibility—that the vaccine not only limits dissemination within the lung, but also to the thoracic LNs, as CEQ were not detected in most of the LN in the BCG/H56 vaccinated animals. There was no difference in control of Mtb in the lungs of vaccinated and unvaccinated animals at

either time point, further corroborating the hypothesis that early control of Mtb in the LN generates vaccine-induced protection from reactivation TB later on. However, the CEQ data are also consistent with the possibility that Mtb do disseminate to the LNs but are immediately killed, resulting in CEQ that are below detectable limits. While the reduction in lung granuloma dissemination would support that dissemination to LN is also impaired, there isn't an appreciable difference in the *early* immune responses of the lung granulomas. In contrast, there were differences in *early* immune responses between the LNs from control and vaccinated animals, which may support immediate killing in the LNs. This would indicate that vaccination results in T cells that reside in thoracic LNs and are capable of preventing bacterial growth in that compartment. In any event, BCG/H56 clearly has a strong protective effect on the thoracic LNs. LNs are the most common site of extrapulmonary TB in both humans and non-human primates [371], and are known to be an important niche for disease and potentially a reservoir for infection and disease persistence [372]. New adjuvants are being developed to deliver antigen to the LN and stimulate immune responses in that compartment [377, 378]. A vaccine that specifically targets the LN, perhaps using new technology, would represent an important new therapeutic for TB.

The ability to investigate the immune responses in individual lesions is incredibly powerful and unique to our model system. In this study, we have utilized these techniques to identify immune responses that are associated with protection from reactivation. Just as there is a striking difference in bacterial burden early in the LN, there is a difference in cytokine profiles early post-infection in the LN of BCG/H56 vaccinated animals compared to controls. This cytokine profile is most likely a consequence of TB control and diminished bacterial replication in vaccinated animals. That this immunological difference is seen early is significant because

early events are likely influential in outcome of TB [376]. IFN-γ, while important for control of Mtb via macrophages [379], is detrimental in excess and may be responsible for TB-induced pathology [201]. We have shown that having a small pool of IFN-γ-producing T cells, not a lack nor excess, is associated with bacterial clearance in lung granulomas [239]. Single producing IFN-γ T cells are short-lived, terminally differentiated effector cells [380], and are associated with a lack of control of TB in murine models [176, 201]. T cells that produce TNF, IL-2, or both are central memory cells [380]. TB-specific central memory cells are associated with protection against Mtb challenge in mice [136], and are observed in mice vaccinated with H56:CAF01 [274, 277, 320]. Control animals have a greater relative frequency of IL-6+IL-10+IL-17+ triple producing T cells, while BCG/H56 vaccinated animals have greater relative frequencies of those three cytokines being singly produced and IFN-γ+TNF+ double producing T cells. IFN-γ+TNF+ T cells are uniquely poised to home from LNs to non-lymphoid organs [381], and both cytokines are more efficient at killing Mtb in macrophages than either alone [88]. IL-6+, IL-10+, and IL-17+ single producing T cells could be more efficient at migration from the LNs to the lung parenchyma as well. Indeed, one of the main phenotypes of this vaccine is generation of a potent lung-homing T cell population [277]. Thus, LNs from BCG/H56 have a greater relative frequency of central memory cells and smaller relative frequency of terminally differentiated cells than control animals early p.i. In general, frequencies of T cells producing IL-6, IL-10, and IL-17 are similar to frequencies of T cells producing IFN-γ and TNF. Mtb-specific T cells can control infection in a IFN-γ/T-bet independent manner [203], and there is mounting evidence for the importance of these other cytokines in TB disease [169, 361]. Taken together, these immune responses correlate with the reduction in bacterial burden in the LN at early time

points and may be contributing to the protection from reactivation disease that is seen later in the course of infection. This warrants further investigation into this phenotype of protection to further demonstrate mechanistically that this leads to protection. These data can thus be utilized to inform future vaccine design to aid in the development of a successful therapeutic to combat TB.

4.5 MATERIALS AND METHODS

4.5.1 Animals

The Institutional Animal Care and Use Committee of the University of Pittsburgh approved all experiments. The animals were housed and maintained in accordance with standards established in the Animal Welfare Act and the Guide for the Care and Use of Laboratory Animals.

Vaccination and challenge. Cynomolgus macaques (*Macaca fascicularis*) imported from China and in the United States for at least a year (Valley Biosystems) were used for these studies (n=32). For the six-month study (Fig. 25): control animals received no vaccination (n=6); BCG only animals were vaccinated with 0.1 mL BCG Danish (SSI) intramuscularly (n=4); BCG and H56:CAF01 animals were primed with 0.1 mL BCG Danish intramuscularly followed by two doses of the vaccine H56 (Ag85B-ESAT6-Rv2660c; 50 μg) formulated with CAF01 (625 μg dimethyldioctadecyl-ammonium (DDA) and 125 μg trehalose-6,6-dibehenate (TDB)) at weeks 10 and 14 after BCG priming (n=10). Originally, even groups (n=10) were planned for just control and BCG+H56:CAF01. The unequal group resulted from the need to capture PET-CT and outcome data from animals vaccinated with BCG alone, data that we lacked at the outset of

the study. Thus, we decided to split the control group to include this important and relevant control. For the six-week study: control animals received no vaccination (n=6); BCG and H56:CAF01 animals were primed with 0.1 mL BCG Danish intramuscularly followed by two doses of the vaccine H56 (50 μg) formulated with CAF01 (625 μg DDA and 125 μg TDB) at weeks 10 and 14 after BCG priming (n=6). All animals in the study were then challenged at 22 weeks post-BCG priming with 8-24 CFU in 2 mL volume per animal with virulent Erdman strain Mtb via bronchoscope. For the six-month study, macaques were determined to have active or latent TB by necropsy using clinical and microbiologic signs [65].

Necropsy. For the six-month study, macaques were euthanized approximately 22-24 weeks post-Mtb challenge, except for an early necropsy warranted by clinical condition (n=1, BCG only group). For the six-week study, macaques were euthanized 5-6 weeks post-Mtb challenge. All animals were euthanized with an intravenous overdose of sodium pentobarbital (Beuthanasia) and maximally bled. At necropsy each animal was examined grossly for pathology. Using our published scoring system [65], the total amount of pathology was recorded from each lung lobe (number and size of lesions), LN (size and extent of necrosis), and extrapulmonary compartments (number and size of lesions). A pre-necropsy PET-CT scan was used as a "map" for identifying and finding each lesion in the lungs. Each individual lesion in the lung and all thoracic LNs identified were excised and mechanically homogenized to create a single cell suspension. Portions of these samples were spread on 7H11 agar (Difco) and incubated at 37°C with 5% CO_2 for 3 weeks. CFU were then counted from these plates and used to both quantify individual lesion bacterial burden and—when summed together—the total bacterial burden for the animal [239, 365]. Portions of these samples were also used for

multiparameter flow cytometry (see below), and the remainder was stored at -80°C for other assays, including assessing chromosomal equivalents (CEQ; see below).

4.5.2 Peripheral blood immune response assays

Heparinized blood was drawn from study macaques at time points pre-Mtb challenge (weeks 0, 2, 4, 6, 10, 11, 12, 14, 15, 16, 18, and 22 weeks post-BCG) and post-Mtb challenge (weeks 1, 2, 3, 4, 6, 8, 12, 16, and 22). Peripheral blood mononuclear cells (PBMCs) were isolated using the standard Percoll gradient isolation (GE Healthcare) and washed with sterile PBS [115].

ELISPOT. ELISPOT for IFN-γ was performed as previously described [115]. Briefly, 96-well opaque multiscreen immunoprecipitation filtration plates (Merck Millipore) were hydrated, washed, and coated with 7.5 μg/mL of anti-human/nonhuman primate IFN-γ (GZ-4: Mabtech) for 2 hours at 37°C with 5% CO_2. Plates were then blocked with complete RPMI containing 10% human AB serum for 2 hours at 37°C with 5% CO_2. Each stimulation condition was performed in duplicate. Medium only was used as a negative control, and phorbol dibutyrate/ionomycin (P&I) and anti-CD3 were used as positive controls. CFP and peptide pools of H56 vaccine antigens (ESAT-6, Ag85B, Rv2660c) were used at 10 μg/mL. PBMCs were then added, and the plate was incubated for 48 hours at 37°C with 5% CO_2. The plate was then washed and detection antibody (7-B6: Mabtech) was added at 2.5 μg/mL and incubated for 2 hours at 37°C with 5% CO_2. The plate was washed and streptavidin-conjugated horseradish peroxidase was added at a 1:100 dilution and incubated for 45 minutes at 37°C with 5% CO_2. The plate was washed and then developed using AEC substrate. The plate was dried overnight and read using an ImmunoSpot analyzer (Cellular Technologies Limited).

Flow cytometry. PBMCs were stimulated with peptide pools of H56 vaccine antigens used at 10 μg/mL for 1 hour at 37°C with 5% CO_2, and then 5 hours in the presence of brefeldin A (Golgistop, BD Biosciences). Medium only was used as a negative control, and P&I was used as a positive control. The cells were then stained for surface and intracellular markers. Surface markers included: CD3 (SP34-2: BD Biosciences); CD4 (L200: BD Biosciences); CD45RA (5H9: BD Biosciences); and CD27 (0323: eBiosciences). Intracellular markers included: IFN-γ (B27: BD Biosciences); TNF (MAB11: BD Biosciences); IL-2 (MQ1-17H12: BD Biosciences); and IL-17 (eBio64CAP17: eBiosciences). Data acquisition was performed using a LSR II (BD Biosciences) and the resulting data were gated and quantified using FlowJo (Version 9.9.3; Treestar Inc.).

Gating. Singlet cell populations were separated first using forward scatter area and height. The lymphocyte population was then gated based upon size. CD3+ cells were selected, and CD45RA and CD27 were then used to remove naïve T cells. Gates for each of the four cytokines were used to quantify individual production. The Boolean gating tool was then utilized to determine the combinations in which the six cytokines were produced.

4.5.3 PET-CT scan analysis

PET-CT scans were performed using a microPET Focus 220 preclinical PET scanner (Siemens Medical Solutions) and clinical eight-slice helical CT scanner (Neurological Corp.) as previously described [2, 350]. ^{18}F-fluorodeoxyglucose (FDG), a non-specific marker of inflammation, was utilized as the probe for PET. Serial PET-CT scans were performed at 2, 3, 4, 6, 8, 12, and 16 weeks post-Mtb infection, and before necropsy. OsiriX viewer, an open-source PACS (Picture

Archiving and Communication System) workstation and DICOM (Digital Imaging and Communications in Medicine) image viewer, was used for scan analyses as previously described [350]. Briefly, a region of interest (ROI) was segmented which encompassed all lung tissue on CT and was then transferred to the co-registered PET scan. On the PET scan, all image voxels of FDG-avid pathology (SUV_{max} > 2.3) were selected and summated resulting in a total SUV_{max} value. In order to account for basal metabolic FDG uptake in the animal, the total SUV_{max} was normalized to resting muscle resulting in a total lung inflammation value [5]. Individual granulomas as seen on CT were counted in each scan to enumerate them longitudinally. SUV per lung granuloma was calculated as previously described [345]. The maximum SUV per LN was ascertained from the PET scan and was normalized to resting muscle. These values (one for each lymph node per monkey) were then summed to create the outcome measure. Number of FDG-avid LN is a full count of any LN visible by PET with SUV > 5 normalized to resting muscle.

4.5.4 Flow cytometry on primary tissue samples

Data collection. Single cell suspensions of individual lung granulomas and LNs obtained at necropsy were incubated in brefeldin A (GolgiStop, BD Biosciences) for 2 hours at 37°C with 5% CO_2. The cell suspensions were then stained for viability (Invitrogen), surface, and intracellular markers. Surface markers included: CD3 (SP34-2: BD Biosciences); CD11b (ICRF44: BD Biosciences); and CD20 (2H7: eBiosciences). Intracellular markers included: IFN-γ (B27: BD Biosciences); TNF (MAB11: BD Biosciences); IL-2 (MQ1-17H12: BD Biosciences); IL-17 (eBio64CAP17: eBiosciences); IL-10 (JES3-9D7: eBiosciences); and IL-6 (MQ2-6A3: BD Biosciences). Data acquisition was performed using a LSR II (BD

Biosciences) and the resulting data were gated and quantified using FlowJo (Version 9.9.3; Treestar Inc.).

Gating. Singlet cell populations were separated first using forward scatter area and height. Live cells were then gated, followed by the lymphocyte population based upon size. CD11b+ and CD20+ cells were then removed from this population, and remaining CD3+ cells were selected. Gates for each of the six cytokines were used to quantify individual production. The Boolean gating tool was then utilized to determine the combinations in which the six cytokines were produced.

4.5.5 Chromosomal equivalents (CEQ)

Following necropsy, tissue homogenates were re-suspended in 1xPBS and stored at -80C. *M. tuberculosis* genomes were extracted from thoracic lymph node and lung samples as previously described [5, 86]. Following DNA extraction and concentrations measurement, quantification of chromosomal equivalents (CEQ) of *M. tuberculosis* was performed using real-time PCR as previously described [5, 86].

4.5.6 Statistics

For the six-month study, comparisons between groups were performed using the Kruskal-Wallis test with Dunn's multiple comparisons test. For the six-week study, comparisons between groups were performed using the Mann-Whitney (Wilcoxon rank-sum) test for non-parametric values. Comparison of CEQ and CFU phenotypes between groups was performed using Fisher's exact test. With the exception of the flow cytometric data, all graphics and statistics were created using

Prism (Graphpad). Analysis and presentation of flow cytometric data was performed using SPICE (Ver. 5.23; https://exon.niaid.nih.gov/spice/) [6]. Comparisons between absolute and relative cytokine expression were performed using the Wilcoxon rank-sum test. Comparisons between profiles of Boolean cytokine expression (pie graphs) was done using a permutation test as previously described [6].

5.0 PET-CT IMAGING PREDICTS VACCINE EFFICACY IN NONHUMAN PRIMATE MODELS OF TUBERCULOSIS

Data from this chapter will subsequently be published in a first author manuscript.

5.1 ABSTRACT

Tuberculosis (TB) is a major global health concern, disproportionately affecting the world's poorest nations. Many new vaccines for TB are in development, but clinical and pre-clinical trials are lengthy and expensive. New outcome measures are needed accurately reflect disease status, and markers need to be identified that can quickly predict these outcomes. The goal of this study was to develop a holistic, single measure in a non-human model of TB and identify surrogates that accurately predict this measure. Quantifiable outcome measures were used to create a factor-weighted score, resulting in one comprehensive number that reflects outcome. PET-CT markers by two months after challenge can be used to accurately predict outcome months later at necropsy. Putative blood signatures collected pre-challenge were identified that predict outcome. These tools should be further developed for use in modern vaccine evaluation to expedite the deployment of a novel TB therapeutic.

5.2 INTRODUCTION

There are two main challenges in vaccine deployment: development and testing. Many novel vaccines have been developed for TB and are in various stages of pre-clinical and clinical trials [356, 382, 383]. This begs the question: how does one down-select a putative candidate? Thus far, only one new large-scale efficacy trial has been performed for a novel TB vaccine [295], using either isolation of *Mycobacterium tuberculosis* (Mtb; the causative agent) or clinical diagnosis of TB as the main outcome [38]. Unfortunately, there are some significant pitfalls to using these outcomes. A clinical diagnosis of TB may take years or decades after the initial phase of infection [23]. In addition, TB cases can be culture negative, and such studies can be particularly difficult in infants. These outcomes also produce a binary outcome—active disease and latent TB infection—which has been shown to poorly reflect the true nature of tuberculosis, which is a spectrum of disease featuring everything from well-controlled latency, to subclinical disease, mild disease, and fulminant TB [55, 56]. This highlights a critical need for new outcome measures that reflect this spectrum and capture all aspects of TB disease.

Blood correlates of TB outcome have been investigated in humans in attempts to develop a useful biomarker. Some studies show specific cellular immune responses that correlate with an outcome in the context of BCG vaccination [131, 268, 384], while some demonstrate that responses of hypothesized importance, e.g. production of IFN-γ, do not correlate with TB outcome [264]. Studies like these have led some in the field to question the reliance on a handful of immune effector molecules for an especially complex disease like TB [257]. Other studies have identified profiles of gene expression and/or cellular responses that correlate with outcome in adolescents and adults, years after BCG vaccination [42, 268, 269]. However, for a real correlate of protection, an effective vaccine for tuberculosis is

needed [256], creating a catch-22 in the process of trying to develop such a vaccine. All the studies performed to date sought to correlate a host response to binary TB outcome [385], which will not capture the heterogeneity in TB disease, highlighting the need for novel, modern outcome measures. Our lab has pioneered the use of live positron emission tomography (PET)-computed tomography (CT) imaging to accurately describe and model outcomes for TB chemotherapy studies [2, 350]. PET-CT is highly translatable, with data from non-human primates (NHPs) matching data from humans in a variety of applications [350, 386, 387]. PET-CT can also be utilized as a tool for predicting clinical outcome [345] and risk of reactivation disease in latency [5]. However, since clinical outcome is binary, PET-CT for vaccine efficacy is merely a correlate of risk. It is unknown if PET-CT correlates to a continuous outcome of disease, which would mechanistically demonstrate inflammation measured by PET-CT as a correlate of protection. Certainly, PET-CT would not be used as a routine determinant of disease, but could lead to more tractable biomarkers that could be used in humans.

The goals of this study were two-fold: to create a composite score that weights quantifiable outcome criteria to properly reflect their contribution to the overall outcome of each animal; and to identify markers, using PET-CT and flow cytometry, that are predictive of the composite score. Composite standardized scores have been used to great success in education and psychology [388]. Briefly, variables such as outcome measures are normalized to fit a Gaussian distribution then standardized, e.g. transformed into a *z*-score. Principal components analysis (PCA) can be utilized to assess relative contributions of each measure to overall variability [389], determining whether weighting of the measures is necessary. This technique has been used to create overall scores for diseases like chronic obstructive pulmonary disease

[390] and reduced 149 questions in a health questionnaire to the widely used and verified SF 36 [391]. Many types of models exist to use variables to forecast an outcome. The simplest is standard least squares (SLS), more commonly referred to as multiple regression, in which coefficients of the regression model can be used to infer importance to variability in outcome [392]. Danger arises when many parameters are used to construct models, as overfitting may occur, which means that the model is highly predictive of its own data but responds poorly to novel data. Cross validation techniques have been developed to overcome overfitting [393]. In this study, we used SLS models to construct predictive models of outcome score based upon PET-CT data early after Mtb, and peripheral immune data before challenge. These responses will be further vetted and developed in future studies.

5.3 RESULTS

The goal of this study was to create a score that would combine the quantifiable outcome data from macaques at necropsy into a single number that represents the spectrum of outcomes, and then to build models that use PET-CT and peripheral blood data to predict before and early after Mtb challenge outcomes 20-24 weeks later. In this dissertation, 96 macaques were utilized to study various aspects of TB vaccinology. The 64 rhesus macaques from chapter 3 and the 32 cynomolgus macaques from the long study in chapter 4 were combined with 28 control cynomolgus macaques from other studies (Table 4) [5, 345, 350, 365].

Table 4: List of macaques utilized in the modeling study.

n	Species	Use in this study	Refs
12	Rhesus	Control animals to standardize score	Chapter 3
52	Rhesus	Vaccinated animals for comparison	Chapter 3
6	Cynomolgus	Control animals to standardize score	Chapter 4
28	Cynomolgus	Additional controls from other studies	[5, 345, 350, 365]
14	Cynomolgus	Vaccinated animals for comparison	Chapter 4
12	Cynomolgus	Short-course animals to test PET-CT model	Chapter 4

5.3.1 Standardized score summarizes outcomes in one continuous metric

The first step was to develop a continuous score that neatly incorporated outcomes at necropsy into a single metric that reflected the spectrum observed in TB outcomes [55, 56]. Rather than having to build multiple predictive models for each outcome, e.g. a model for bacterial burden in the lung, a model for pathology in LN, etc., predictive models will only have to forecast this one metric that captures all outcome measures. How best to build a holistic outcome score? A standardized score, or *z*-score, is used frequently in many different scientific fields, especially in psychology and the social sciences, to combine different quantitative outcomes of various scales and units [388]. A *z*-score essentially takes a distribution of data and centers it using a mean and standard deviation, so that a value of zero represents the mean and each integer on the scale represents values a standard deviation higher (positive) or lower (negative) than the mean. Our scoring systems for gross pathology and bacterial burden have wildly different scales, and using a standardized score would facilitate the combination of these data. All of the macaques selected for this study could be used to create the score, but their score values would not be very

informative since this combines control and treatment group animals. For example, by standardizing each measure (e.g. lung bacterial burden) to all macaques, an animal at zero would represent the mean of all animals included, and an animal at -1 would have an outcome one standard deviation better than the mean of all animals, which is not very informative. On the other hand, by standardizing each measure to the control macaques, an animal at zero would

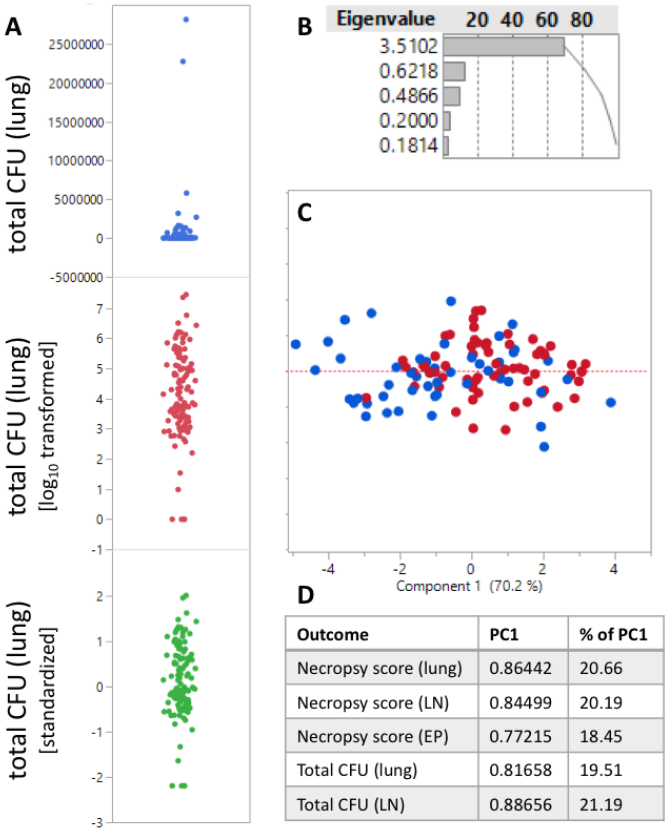

Outcome	PC1	% of PC1
Necropsy score (lung)	0.86442	20.66
Necropsy score (LN)	0.84499	20.19
Necropsy score (EP)	0.77215	18.45
Total CFU (lung)	0.81658	19.51
Total CFU (LN)	0.88656	21.19

Figure 39: Construction of a holistic, continuous outcome score. **A** Example of transformation and standardization of one outcome measure. Raw total CFU data for the lung (blue) are first $\log_{10}$ transformed (red) to fit those data to a normal, or Gaussian, distribution. The transformed data are then standardized to a *z*-score (green), so that the mean is zero and each integer is a standard deviation. **B** Eigenvalues for the principal components of the five necropsy outcome measures. **C** The macaques utilized for this study on a principal component space. Only one component was significant as determined by the Kaiser rule, i.e. eigenvalue>1 [4]. Each dot represents either one rhesus macaque (red) or one cynomolgus macaque (blue). **D** The loading values for the main principal component, and the percent of the total component each outcome represents.

represent the mean of the controls only, and an animal at -1 would have an outcome one standard deviation better than controls, thus displaying the impact of a treatment over controls.

We therefore planned to use the mean and standard deviation of only the control animals to standardize each necropsy outcome, allowing the score values to be more informative by depicting the magnitude of difference between treatment and control macaques. Gross pathology in the lungs, in the lymph nodes (LN), and in other extrapulmonary sites (EP) and total bacterial burden in the lung and LN were chosen as the five main quantifiable and objective outcome measures as these summarized the data collected at necropsy. The raw values for these five outcomes were first transformed to a normal distribution to aid in modeling (Fig. 39A). The data were then standardized to the 46 control macaques (12 rhesus and 34 cynomolgus) to create unitless measures all on the same scale that could then be combined into one holistic metric.

The next question was whether to weight each of the five main standard scores before combining them. If each standardized outcome contributes to the variability in overall outcome equally (i.e. has equal weight), then the five standard outcomes should be weighted by 0.2 since each contributes 20% to total outcome. However, if some outcomes contribute to the variability in overall outcome more, they should be weighted more to reflect that, e.g. if lung bacterial burden contributes to 50% of the variability it should be weighted by 0.5. To address this question, we utilized principal component analysis (PCA) to determine the extent to which each outcome measure contributed to the overall variability. The Kaiser rule dictates that only principal components (PC) that have an eigenvalue greater than one significantly contribute to variability [4]. Of the PC eigenvalues (Fig. 39B), only the first PC (PC1) was above one, suggesting that only PC1 significantly explained variability in macaque outcomes. PC1 explained 70.2% of the variability in outcome (Fig. 39C), and most of the rhesus (red) and

cynomolgus (blue) macaques overlap in this vector subspace. The loading values for each PC indicate how strongly each outcome impacts the variability due to that component [360]. The loading values for all five outcomes are very similar and each contributes approximately 20% to the principal component (Fig. 39D), suggesting that the outcomes do not need to be weighted since they contribute almost equally.

5.3.2 Using the outcome score to compare controls to vaccinated macaques

The five control-standardized outcomes were then averaged to create the overall outcome score (Fig. 40), where zero represents the mean of the controls and each integer represents a standard deviation better (negative) or worse (positive) than control macaques. To provide an example of the output, macaques were grouped by the chapter of this dissertation in which they were studied. There was no statistical difference between any of the vaccinated macaques and

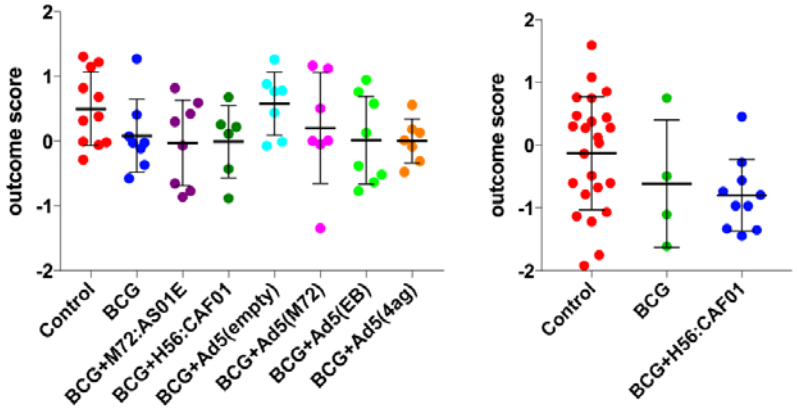

Figure 40: Comparisons of outcome scores between cohorts from the other studies in this dissertation. Each dot represents one animal and bars represent means and standard deviation. *Left,* Outcome scores from the rhesus macaques in chapter 3. Dunn's multiple comparisons were used to compare each vaccine regimen to controls specifically, and to compare each BCG boost regimen to BCG. None of the comparisons were statistically different. *Right,* Outcome scores from the cynomolgus macaques in chapter 4. Dunn's multiple comparisons were used to compare the groups, and no statistical difference was found.

controls, nor between any of the prime-boost cohorts and BCG, in the animals from chapter 3 (Fig. 40, left). These scores fit well with the what was demonstrated in that study, which is that none of the vaccines significantly protect rhesus macaques from TB. Most of the treatment groups, with the exception of BCG+Ad5(empty), have a difference in outcome score of about 0.5 from the rhesus controls, which based upon the *z*-score means about a 20% improvement. There was no difference in the cynomolgus macaques from chapter 4 by comparing all three cohorts (Fig. 40, right). However, BCG was severely underpowered in this comparison. Excluding BCG and using Welch's t test to compare control and BCG+H56:CAF01 only yields a p value of 0.0153. The mean outcome score of the BCG+H56:CAF01 vaccinees was about -0.8, which indicates that these animals on average had outcomes better than 78.8% of all control macaques. Thus, this outcome score represents a single metric that captures the spectrum of outcomes in the macaques and facilitates overall comparisons between cohorts.

5.3.3 Early PET-CT markers robustly predict outcomes

The second step of this study was to build models that integrate early serial PET-CT markers (4-12 weeks p.i.) to predict later outcomes (24+ weeks p.i.). There were four quantifiable PET-CT outcome measures in this study using the PET probe ^{18}F-fluorodeoxyglucose (FDG), a nonspecific marker for inflammation [374]. The first is the number of FDG-avid thoracic lymph nodes (LNs), which are inflamed LNs visible by PET. The second is the total amount of FDG uptake in the lungs, interpreted as total lung inflammation. The third is the number of new lung granulomas visible by CT that appear after 4 weeks p.i. Four weeks p.i. is the earliest reliable count of granulomas in the lungs following infection. The fourth is the number of sites of extrapulmonary (EP) involvement apparent by PET or CT. We first correlated each PET-CT

marker at each time point to the outcome to elucidate the individual influences of the radiological markers (Fig. 41, top panel). The number of FDG-avid LN was the most robust predictive PET-CT marker, followed by total lung inflammation. The ability of each of these markers to predict outcome score increased as the macaques progressed in their respective studies. At each of the early time points p.i. investigated, backwards stepwise parameter selection was used to pick one or more of the four PET-CT markers to create the most predictive regression model of outcome with the lowest amount of residual error compared to other models (Fig. 41, bottom panel, dotted line). To capture the dynamics of these markers over time, each

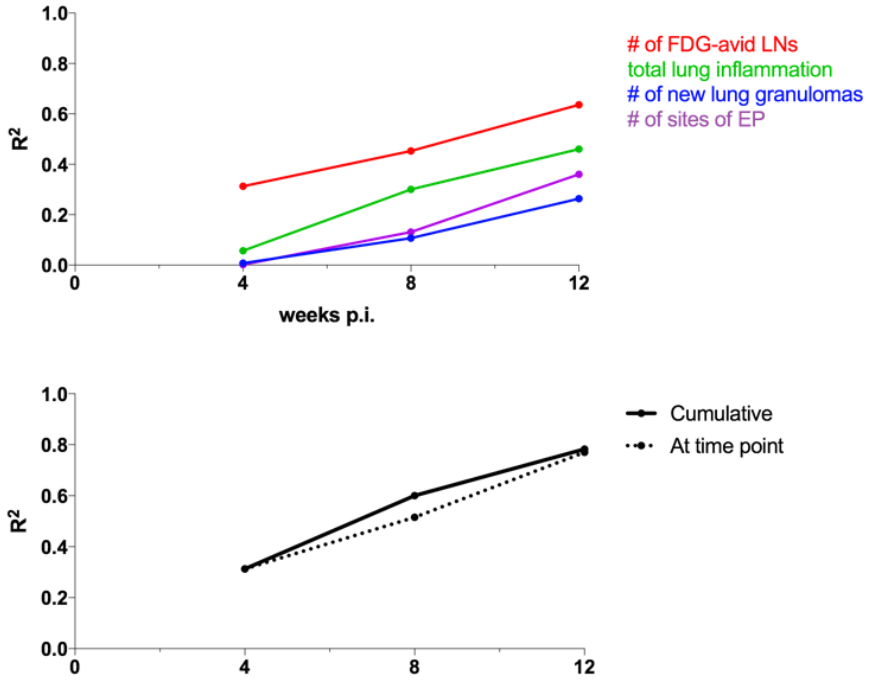

Figure 41: Predictive models of efficacy using serial PET-CT markers. The top panel represents models at each of three time points. The models on the dotted line only use PET-CT data from that particular time point. The models on the solid line use PET-CT data from that time point and potentially the time points prior. The bottom panel depicts each PET-CT marker directly correlated to the outcome score at each time point.

marker at 8 and 12 weeks p.i. had its 4 week value subtracted to determine the change over time. These new markers were then added to the original ones at each time point to create a cumulative model at each time point (solid line). The most predictive time point was determined to be 12 weeks p.i., which robustly predicted the outcome score at 20-24 weeks p.i. (R^2=0.7828; Fig. 42).

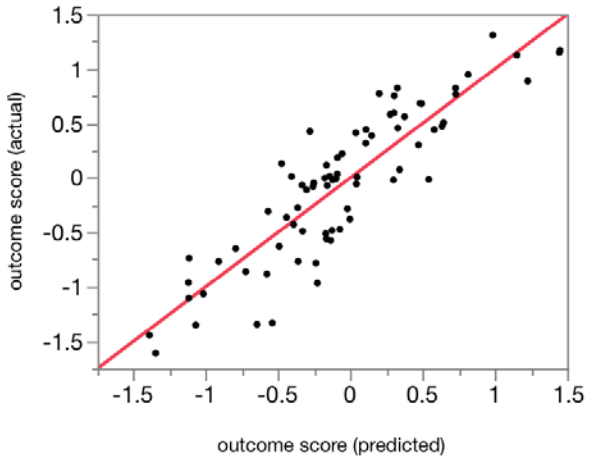

Figure 42: The most robust PET-CT predictive model, at 12 weeks p.i. The actual outcome scores (y-axis) fit to the outcome scores predicted by the PET-CT model (x-axis). Each dot represents one animal and the line is of best fit.

5.3.4 PET-CT model predicts likely long-term outcomes of short-term studies

Data from cynomolgus macaques in chapter 4 offered an opportunity to test the robustness of PET-CT's predictive ability. The twenty macaques in that study used to build the model were challenged and necropsied 24 weeks later (Fig. 43, left). However, to investigate early events associated with protection from reactivation TB, twelve macaques (unvaccinated or BCG/H56 vaccinated, see chapter 4) were challenged and necropsied 5-6 weeks later. To test the PET-CT model, we took PET-CT data from those macaques necropsied early and entered them into the

model to predict the outcomes of those macaques had they gone to 20-24 weeks p.i. (Fig. 43, right). The predicted outcome scores fell well within the range observed in the long-term vaccine study, and there were no significant differences between the actual and predicted distributions of scores using an equivalency test. These data suggest that early PET-CT markers robustly predict subsequent TB outcomes.

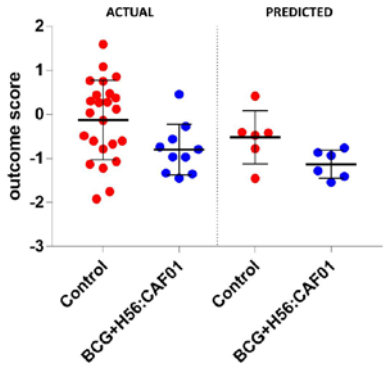

Figure 43: PET-CT model predicts outcome for a separate cohort of animals. Each dot represents the outcome score for one macaque, and bars represent means and standard deviation. The two cohorts of macaques on the left (ACTUAL) were necropsied at six months post-Mtb challenge, and the scores are from the data collected at necropsy. The two cohorts of macaques on the right (PREDICTED) were necropsied at six weeks post-Mtb challenge, and the scores were generated from the predictive models in Fig. 41.

5.3.5 Peripheral blood markers correlate with outcome score

The final step in this study was to build models that used flow cytometric data from peripheral blood mononuclear cells (PBMC) before challenge to predict outcomes months after challenge. While immunologic data was not available from all of the macaques used to build this model, flow cytometric data on PBMCs were available from 40 of the rhesus macaques in chapter 3 and all of the cynomolgus macaques from chapter 4. Since the goal of this final step was to identify vaccination-specific immune signatures, all control macaques were first excluded. A signature

independent of any particular TB vaccine is more useful than signatures for each individual vaccine, so rather than using PBMC responses to non-vaccine antigens (e.g. responses to H56 in M72 vaccinees), only vaccine-specific response were used (e.g. response to M72 in M72 vaccinees) and were compared equally across groups. Vaccine antigen-specific responses from PBMCs were then subset by lineage (CD4 or CD8) and by cytokine expression (producing any or all interferon-γ (G), IL-2 (2), or tumor necrosis factor (T)). Five time points before Mtb challenge were chosen, using immune responses from before BCG, two time points after BCG, and a time point after each boost (if boosted at that time point). Thus, these predictive models were built using cytokine production by T cells from vaccinated animals in response to antigen stimulation to whichever vaccine regiment they received at relevant time points before challenge.

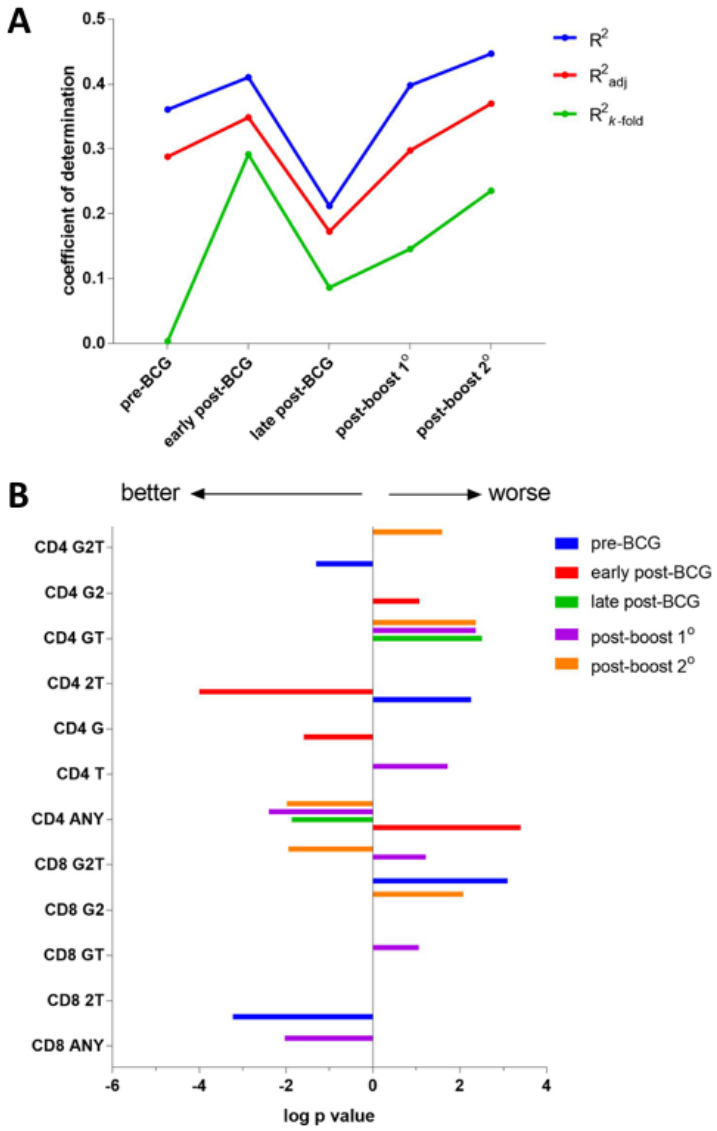

Figure 44: Predictive models of efficacy using peripheral T cell markers**. A** Backwards stepwise selection was used to build models of vaccine antigen-specific peripheral immune responses that predict outcome score. The blue line represents the overall R^2 (coefficient of determination) at each time point. The red line represents the R^2 adjusted for the number of parameters included by using the degrees of freedom (number of terms). The green line represents the R^2 for *k*-fold validation models. **B** Breakdown of the T cell markers that contribute to the predictive models at each time point. The subsets of T cells are on the y axis, with lineage (CD4 or CD8) and cytokine production (G=IFN-γ; 2=IL-2; T=TNF; ANY=any combination of those three cytokines) denoted. The length of each bar represents the strength of the contribution of that marker to the model, measured by $\log_{10}$ of the p value. Markers whose bars are on the left are associated with improved (lower) outcome score while markers whose bars are on the right are associated with worsened (higher) outcome scores.

Backwards stepwise selection of these T cell responses was used to build predictive regression models at each pre-challenge time point (Fig. 44A). Any or all the T cell markers were used at each time point and the robustness of the model (coefficient of determination, or R^2) was plotted (blue line). One major problem with regression models is overfitting, which means that a model is created that fits predictive markers to an outcome very well but poorly predicts new data entered into the model [392]. Overfitting usually occurs when too many irrelevant parameters (predictive markers) are entered into a model. To avoid overfitting in this study, two means of validation were used: the R^2 adjusted for degrees of freedom (R^2_{adj}, red), or the number of parameters used in each model; and *k*-fold cross validation ($R^2_{k\text{-fold}}$, green), which randomly subsets the data into *k* partitions and in turn builds a model using *k*-1 partitions and tests it against the remaining one [393]. The adjusted R^2 combats overfitting by penalizing the model every time a new parameter is added, i.e. the more T cell signatures used the more the R^2 is penalized (decreased). Cross-validation is even more stringent by repeatedly constructing models and fitting data set aside against the model, thus continually testing the ability of the model to react to new data.

Essentially, the closer the three R^2 values are to one another, the more robust the model, and validation R^2 values (red and green) that are much lower than the main one (blue) hint at overfitting or inaccurate models. The models early post-BCG and after the second boost have the highest main R^2 (blue) and relatively similar validation R^2 values (red and green). This suggests that vaccine antigen-specific responses are most reliably predictive of outcome score early post-BCG vaccination and after secondary boosting of BCG (Fig. 44A).

We then sought to elucidate the specific cytokine responses at each time point that significantly contribute to the models. We determined the p value of each immune marker in its

relationship to the model and $\log_{10}$ transformed the data, keeping it negative if it contributed to a lower (better) outcome score and making it positive if it contributed to a higher (worse) outcome score (Fig. 44B). Thus we have demonstrated the ability of peripheral T cell responses to predict outcome before Mtb challenge, and have identified putative markers that will be vetted and further developed in subsequent studies.

5.4 DISCUSSION

The goal of this study was to create a holistic outcome score and to construct models that can accurately forecast the score before or early post-Mtb challenge. The development of a broad score would allow for macaques between many different studies to be compared to one another, and would be the first step in pursuit of predictive markers (Fig. 45). Between Mtb challenge and necropsy, radiological data are collected that robustly predict outcome and can abbreviate the length of a pre-clinical study. Before challenge, during vaccination, blood markers can be identified that can more easily be translated to clinical studies. This study has presented a metric that combines five different outcome measures into one score. This score is based upon a z-score, which is unitless and allows different continuous measures to be combined. In this study, instead of using the mean and standard deviation of all the macaques, the outcomes were standardized to the controls. This allows for more meaningful statements to be made about the different study cohorts. Thus, the control animals should have a mean of zero and standard deviation from -1 to 1. If a vaccination group has a mean of -1, that means the group overall did one standard deviation better than controls, or better than about 84% of controls. This score may be standardized to any control, so that comparisons could be made directly to BCG only vaccinated

macaques instead, for example in a study examining prime-boost efficacy. This score is also continuous, and while providing more power and less type I error, also reflects the natural spectrum of outcomes in TB [55, 56].

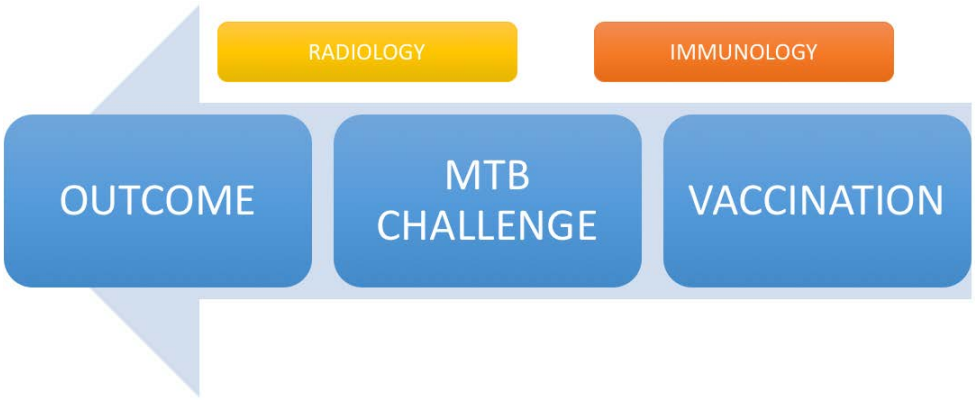

Figure 45: Approach for building predictive models of vaccine efficacy. The blue arrow represents the temporal direction of the study, which begins with vaccination and ends with outcome determined at necropsy. The step was to build an outcome score (OUTCOME) which encapsulates the various outcome measures into a single continuous score. The next step was to build a model that utilized PET-CT markers (RADIOLOGY) after Mtb challenge to predict outcome. The final step was to build a model that incorporated various CD4 and CD8 T cell cytokine profiles (IMMUNOLOGY) to predict outcome.

This study features predictive models that utilize early PET-CT data to robustly predict outcome much later. These models were used to predict outcomes in separate cohorts of macaques for which there were PET-CT data but not outcome data. The predicted values not only fit well with actual outcome scores six months p.i. but are not statistically different from one another. This provides more evidence to the robustness of PET-CT as a predictive tool. PET-CT thus should be further developed as a pre-clinical instrument to abbreviate the process of down-selecting vaccine candidates to move into human trials. The most protected macaques included in this study were at a low risk of reactivation disease, which had been previously shown using that vaccine [275] and shown using a PET-CT metric [5] in Chapter 4. This

protection was apparent both in total lung inflammation and in the LN. The best PET-CT associated predictors were related to both of those markers. However, the best vaccine would be one that prevents initial establishment of Mtb, as evidenced by prevention of granuloma formation. A vaccine that accomplishes this does not yet exist, but we have provided evidence that a vaccine with this protective phenotype could be identified very quickly using PET-CT, most likely by 4 weeks post-Mtb challenge, thus greatly expediting pre-clinical trials.

At the end of the study we used peripheral blood markers collected before Mtb challenge to build predictive models of outcome score. These models were not as robust as the models using PET-CT markers, but are more translatable to human clinical trials since they are linked to immune responses following vaccination and not radiological responses following Mtb infection. The most robust of these pre-infection models were early after BCG vaccination and after the secondary boosting of BCG immunity. We then identified the immune markers in each model that contributed to its robustness the most. These T cell responses were all vaccine antigen-specific, and thus were technically recalled by a variety of different antigens. However, the goal was to identify signatures that were vaccine-independent and correlative of protection against TB. Thus, these markers could theoretically be applied to any novel TB vaccine trial. Most of these cytokine markers were present in CD4 T cells, which makes sense since most TB vaccines are designed to elicit immunity in those cells [356]. Most of these markers only appear at one time point, while others are significantly associated with outcome at multiple time points. Production of IFN-γ and TNF by CD4 T cells is mostly associated with poor outcome scores. IL-2 and TNF production, associated with central memory T cells [380], is very strongly associated with improved outcome scores early after BCG vaccination. The production of all three cytokines together by CD8 is associated with poor outcome scores early during vaccination, but

slowly becomes associated with improved outcome over the course of vaccination. CD4 T cells that make any cytokine (ANY) exhibit similar associations with outcome scores, suggesting dynamic associations peripherally with protection. More macaques are needed to vet these observations and further develop peripheral blood markers as a signature of vaccine-engendered protection.

5.5 MATERIALS AND METHODS

5.5.1 Animals

The Institutional Animal Care and Use Committee of the University of Pittsburgh approved all experiments. The animals were housed and maintained in accordance with standards established in the Animal Welfare Act and the Guide for the Care and Use of Laboratory Animals.

The animals utilized for this study were primarily studied in chapters 3 and 4 of this dissertation, and extensive descriptions of vaccinations, Mtb challenge, and necropsy procedures can be found in this section of those chapters, as can data on PET-CT data and peripheral blood responses using flow cytometry. Data on additional controls have been published [5, 345, 350, 365].

5.5.2 Outcome score

Raw data on gross pathology from the lung, LN, and EP and total bacterial burden from the lung and LN were imported from those earlier studies into JMP (SAS). Discrete count data (necropsy

score) were transformed using a square root transformation to a Gaussian (normal) distribution, and continuous data (CFU) were transformed using a $\log_{10}$ transformation. These five outcomes were then standardized using the prototypical *z*-score:

$$z = \frac{x-\mu}{\sigma}$$

where x is an outcome value for a macaque, μ is the mean of the population, and σ is the standard deviation. For this study, the mean and standard deviation utilized for each outcome measures were of only the control animals to compare the treatment groups to them. These five *z*-scores were then averaged together without weight, since they equally impact the variability on outcome (see results).

5.5.3 PET-CT models

PET-CT data from the macaques at 4, 8, and 12 weeks p.i. was imported and transformed to Gaussian distributions using a square root transformation for count data (FDG-avid LN, # of new granulomas, # of sites of EP) and a $\log_{10}$ transformation for continuous data (total lung inflammation). Backwards stepwise parameter selection was used to pick one or more of these measures at each time point. The model with the highest R^2 and lowest residual error (AICc) was selected as the best for each time point. For the components, each PET-CT marker was correlated to outcome score and R^2 was then reported. These models were saved as formulae for subsequent prediction of outcome scores. PET-CT data from the twelve short-course macaques in Ch. 4 was imported and transformed as above. These data were then entered into the appropriate formulae to calculate predicted outcome score.

5.5.4 Immunology models

Rhesus and cynomolgus macaque peripheral blood data were matched, and five shared time points and sixteen shared T cell markers emerged. Vaccine antigen-specific responses were used for the model, e.g. response to peptide pools of H56 antigens for H56 vaccinees, responses to M72 antigens for M72 vaccinees, etc. Thus, there were sixteen potential markers at each time point. Backwards stepwise parameter selection was to pick one or more of each marker at each time point. The model with the highest R^2 from the *k*-fold cross validation models was selected as the best model for each time point (k=4). For each model, p values were reported to measure the significance of the association between the selected markers (one or more of the sixteen) and the outcome scores. These p values were then $\log_{10}$ transformed and reported. Transformed p values were all negative, but those with an association to poor outcome were made positive for clarity in presentation.

5.5.5 Statistics

All statistics and data presentation were done in JMP (SAS) and Prism (Graphpad). Comparisons were done using Welch's t test and the Holm-Šídák test in Prism to compare the outcome scores. JMP was used to build SLS or multiple regression models, to create the outcome score, to test the actual and predicted outcome scores using an equivalency test, and to perform correlations where described in this study.

6.0 IMPLICATIONS OF THIS DISSERTATION

6.1 PROTECTION ENGENDERED BY BCG AND BCG/H56

In all the studies performed in the course of this dissertation, a wide spectrum of outcomes was observed. These data add to the growing body of evidence that tuberculosis (TB) is not merely two distinct binary outcomes, but rather a spectrum from well-contained latency to fulminant disease [55, 56]. In the rhesus macaque model of TB, BCG arguably provided the best protection against low dose *Mycobacterium tuberculosis* (Mtb) challenge. BCG vaccinated rhesus macaques exhibited a lower bacterial burden in the lung, reduced extrapulmonary pathology visible at necropsy, and less total lung inflammation by PET. This cohort of animals also had reduced evidence of TB disease using PET-CT markers at early time points. BCG here appears to work at the level of some sterilizing immunity in the lung and prevention of dissemination to extrapulmonary sites. However, the LN compartment seems to be neglected by this vaccination, as there was no difference in bacterial burden in the LN between control macaques and those vaccinated with BCG. These data are similar to data from BCG in cynomolgus macaques from this dissertation. BCG vaccinated cynomolgus macaques exhibited less gross pathology in the lungs at necropsy than control macaques, albeit without reducing bacterial burden in the lung. This BCG vaccinated cohort also had animals with smaller median lung granuloma sizes, lower FDG SUV per lung granuloma, and lower total lung FDG avidity at

early time points post Mtb challenge. Interestingly, some LN protection is also seen early by PET-CT in this cohort, as macaques in it had fewer FDG-avid LN and lower summations of maximal LN SUV than control macaques. That being said, by necropsy later in the study, no protection in the LN compartment was observed for BCG vaccinated animals. These data together with the rhesus data suggest that BCG confers some protection from TB by working early in the lung and LN, but not maintaining protection within the LN compartment. This lack of long-lasting effect in the LN compartment could be one explanation for the incomplete protection conferred by BCG, as the data in this dissertation strongly demonstrate that LN are critical for protection against TB disease. Although BCG does not protect against pulmonary infection in humans later in life, BCG does protect infants from severe manifestations of TB disease which are typically extrapulmonary in nature [132]. This dissertation has provided some evidence that BCG is protective in rhesus macaques against extrapulmonary TB, which is thus supported by these observations in humans.

The fact that BCG is a live vaccine might explain why it does confer such potent initial immunity to TB, as live vaccines typically engender more robust immunity [394]. None of the vaccines used to boost BCG conferred protection beyond BCG, and none of them were live. There are live vaccine candidates in clinical trials [356]. These were developed to replace BCG, but their ability to boost BCG has yet to be investigated. That being said, revaccination with BCG has already been explored and shown to instill no additional protection against TB [138]. The fact that none of the experimental vaccines could increase protection against TB beyond BCG additionally suggests that either they are inadequate or that they should be investigate using alternative routes of vaccination. Boosting BCG with empty Ad5 not only removed the protection conferred by BCG but made the macaques more susceptible to Mtb challenge than

completely unvaccinated controls. Ad5 induces type I interferon (IFN) responses which have been demonstrated to be detrimental to anti-TB immunity [150, 255]. The Ad5 vector was replication deficient, though, and thus was not replicating when the macaques were challenged. It is possible that the vector polarized the cells in the lung and thus reacted later to Mtb challenge differently. Immunization of mice with poly(I:C), which also induces type I IFN, leads to worse TB outcomes after Mtb challenge [251]. These data suggest that viral vectors, or any adjuvant that stimulates type I IFN, should not be used in vaccination against TB. Though these were the macaques vaccinated via aerosol and i.m., the aerosol route of vaccination should not be ignored. Other adjuvants and delivery systems that are more successful through other routes could be investigated by aerosol. A similar sentiment should be applied towards the strategy of prime-boost vaccination. It still represents a highly tractable approach to TB vaccination, as there is evidence for its efficacy in cynomolgus macaques, and should continue to be investigated and developed in that nonhuman primate model.

Although the evidence in the rhesus macaque model does not paint prime-boost in a favorable color, boosting BCG with H56 in CAF01 reduces the risk of reactivation disease in cynomolgus macaques, like our previous data utilizing IC31® [275]. The protection conferred by H56 appears to be orchestrated in the lymph nodes (LN). This compartment has emerged as pivotal to TB outcome, and will be discussed in depth in the next section. The protection against disease observed in BCG vaccinated rhesus macaques appeared to be mostly in the lungs, by both bacterial burden and total lung inflammation. This implies that different vaccines might work through different routes, and confer different types of protection. Perhaps, to achieve optimal protection against TB, multiple types of vaccine need to combined to stimulate immunity in all relevant physiological compartments. After these studies, a “home-run” vaccine has yet to

emerge. None of the vaccines in this dissertation prevented infection or fully prevented active TB disease. The data contained within highlight a major gap that continues to exist in TB vaccinology, which is not knowing the best route of vaccination. Too much of the efforts of the field have been expended on identifying antigens that could be utilized in a vaccine without completely understanding where and how these antigens should be administered to a host to protect it from TB. We have a vaccine that demonstrates some quantity of efficacy against TB (BCG), and this represents a powerful tool to probe the various routes and vehicles for vaccine administration. Once the best route is identified, the could be systematically tested to determine which construct engenders the best protection from TB. These studies therefore highlight the need for both investigation of novel vaccines and delivery of promising candidates through alternative routes.

6.2 LYMPH NODES ARE A CRITICAL SITE OF MTB INFECTION

In both nonhuman primate models, the LN compartment played an extremely critical role in determining the ability of a macaque to resist TB disease. Rhesus macaques that completed the study in this dissertation with better outcomes had LN with T cell cytokine profiles that were significantly different that those from LN of rhesus macaques with worse outcomes. This difference in immune profile was not observed in lung granulomas from these two different groups of animals. Since outcome in that study was determined independently of treatment group, this suggests that having a beneficial T cell signature in the LN is broadly important for protection against TB disease, and further suggests that the LN exert considerable influence over eventual outcome. Protection against reactivation TB with BCG/H56 in cynomolgus macaques

was elucidated further by demonstrating that early post-Mtb infection there is a reduction in bacterial burden and more CEQ-CFU- LN, or LN where Mtb did not establish infection. These data all highlight the critical role that LN play in determining TB outcome.

This dissertation thus adds to the theory that LN could be the epicenter of TB, not the lung. Even before Mtb was identified as the causative agent of TB [17], it was observed that primary lung infection is not a prerequisite for the development of pulmonary TB [395]. The clear majority of bacterial burden is in the LN, not the lung. This was observed in most of the nonhuman primates in this dissertation, apart from those animals with especially severe lung disease, e.g. TB pneumonia. In humans, it has also been noted that there is "a difference in tissue susceptibility…provided by the freer multiplication of the bacillus in the lymph nodes draining a site of primary infection than in the infected site itself." [396]. Only after systemic immunity against TB is mounted are pathological responses recorded in the lung [75]. In all routes of Mtb or *M. bovis* infection observed, the LN eventually become a stronghold for mycobacteria. In the classic route, pulmonary exposure to Mtb in humans and nonhuman primates leads to infection of the lung-draining LN [12, 111], as does pulmonary exposure to *M. bovis* in cattle [397]. Ingestion of *M. bovis* by cattle leads to lymphatic spread from a primary gut infection to mediastinal or tracheobronchial LN, with or without pulmonary disease [398, 399]. Intratonsilar inoculation of M. bovis in cattle leads to initial colonization of the tonsils or medial retropharyngeal LN with subsequent spread to the lung-draining LN [400]. Lymphatic endothelial cells have been demonstrated to be a replicative niche, in which autophagy either promotes or restricts the growth of Mtb based on the activation profile of the cell [401]. In addition to the role of the LN as a preferred replicative niche, we have demonstrated the clear role of the LN as a key player in reactivation TB. In experimental reactivation with anti-TNF, the

first signs of reactivation appeared in the LN which exhibited satellite lesions forming from established granulomas, which were not apparent in the macaques that did not reactivate [57]. CD4 depletion of LTBI macaques induces reactivation that is associated with lower CD4 counts in the LN [58]. Both this dissertation and a previous study also highlight the LN as a protected site in macaques with a low risk of reactivation TB engendered by BCG/H56 vaccination [275]. This body of evidence thus suggests that not only are the LN a critical site of Mtb infection, but that they should be targeted by therapeutics, especially those that seek to block TB disease specifically.

6.3 A NEW FRAMEWORK FOR PRE-CLINICAL MODELS

The rhesus macaque model exhibits pathology like that of human infants, while we have clearly demonstrated that the cynomolgus macaque model is incredibly similar TB of adolescents and adults [107]. Interesting, this dissertation has provided evidence that BCG confers a decent amount of protection to rhesus macaques against disease and no protection against clinical TB in cynomolgus macaques. These data are like the data in humans that suggest that BCG protects infants, but not adolescents or adults [132]. Therefore, this dissertation could begin to provide a framework for future pre-clinical models. Rhesus macaques could be used for pre-exposure vaccines, in which prevention of infection is the endpoint, and cynomolgus macaques used for post-exposure vaccines, in which prevention of clinical disease is the endpoint. H56 vaccination data in this dissertation provides a neat example for this framework. H56 was developed as a multistage vaccine useful for both pre- and post-exposure TB [274]. That being said, there is a lack of strong evidence that this vaccine prevents infection. In this dissertation, BCG/H56

vaccination does not prevent initial granuloma formation in cynomolgus macaques and has no efficacy beyond BCG in rhesus macaques. There is evidence, though, in this dissertation and published that BCG/H56 reduces the risk of reactivation TB [275], and is thus efficacious as a post-exposure vaccine. This was observed not in the rhesus macaque model but the cynomolgus macaque model.

A new outcome score was developed in this dissertation that is holistic and captures all the outcomes at necropsy into a single number. This score is relatively easy to build from a set of controls, and since it is standardized to a normal curve, it is relatively easy to interpret. This score can be standardized based on any control. For example, if the study's aim is to compare boosting BCG prime to prime alone, the BCG group can serve as the base for the outcome score. This score also is the most amenable way to build predictive models. Few models can predict multiple outcome variables simultaneously, and models that predict continuous variables are decidedly more powerful than those that predict binary outcomes. Thus, this continuous outcome score serves both needs. One of the major limitations of this score, however, is the masking of the various individual outcomes of TB infection and disease, such as compartmental outcomes (lung or LN or EP). This dissertation has demonstrated a very clear role for the LN in association with the eventual outcome of TB disease. The better outcomes of rhesus macaques in the prime-boost study had a differential T cell signature in the LN but not in lung granulomas. BCG/H56 vaccinated cynomolgus macaques had a reduced apparent risk of reactivation TB by PET-CT which was associated with protection in the LN, as these macaques had similar bacterial burden in the lung as control macaques. This distinction between protection in these divergent sites is essentially lost in a holistic outcome score as all of the different outcomes are merged into a single number. If the question is simply modeling the *overall* outcome of a macaque, this is of no

consequence. However, if the LN are a critical compartment of special interest for a study, then the outcome score may not be the best tool to build models or answer other questions. However, this challenge is easily overcome as models can be built directly to bacterial burden or pathology in the LN. These two outcomes could even be combined in a "LN outcome score" using the methodology laid out in this dissertation, and predictive models using immunological markers or PET-CT based markers could be built to this instead. Instead of a "one size fits all" mentality, the tools developed in this dissertation should be applied flexibly to suit the appropriate research question. If the goal of a therapeutic is to prevent disease, LN are the likely target and outcome scores and predictive markers can be adjusted accordingly. However, if a novel vaccine that prevents initial infection is under scrutiny, the lung is the likely site for this protection to occur, and again, the outcome score and predictive markers can be manipulated to accommodate this alternative (and preferred) research objective.

This dissertation demonstrates a clear role for PET-CT imaging in predicting vaccine efficacy. This technology has displayed a clear role in assessing efficacy of TB chemotherapy [2, 350, 351]. We now have evidence that this technology may be applied successfully to pre-clinical vaccine studies to shorten them and increase their power. The immediate implication of the research in this dissertation around this cause is the ability to drastically condense pre-clincal vaccine trials in cynomolgus macaques. This represents an immediate savings in research dollars that can be spent to procure additional macaques to increase power, new reagents or additional procedures to investigate cellular and molecular responses, among many other things. This powerful tool using the framework provided by this dissertation should hopefully hasten successful pre-clinical candidates from the nonhuman primate model into clinical trials for humans. However, a nasty problem still awaits any new (or old) therapeutic candidate that dare

arrive at this stage. The endpoints currently used in human trials are sadly antiquated and greatly contribute to the cost and length of these trials. PET-CT may be a robust means of predicting vaccine efficacy in nonhuman primates, but its use in humans for clinical trials is dubious. PET-CT is expensive at the large scale and exposes individuals to potentially high doses of radiation. Additionally, this technique is powerful as a tool *after* Mtb challenge, which means that within the context of human trials, cohorts of patients would need to be vaccinated and then *wait* to become infected with Mtb, their infection status would need to be precisely known temporally which is currently extremely difficult to determine, and then the predictive model would be applied. Thus, for clinical trials, PET-CT is neither the most practical nor feasible means of assessing vaccine efficacy. One of the goals of this dissertation was to identify peripheral immune markers that were predictive of vaccine efficacy as well. This additional tool would represent a much more attractive means of measuring vaccine efficacy in human cohorts as blood is easily sampled, they are not exposed to many other risks by this means of sampling, and this occurs after vaccination but *before* Mtb challenge, thus reducing the length and ultimate cost of a clinical trial. This dissertation contains predictive models of TB outcome that utilize vaccine antigen specific T cell cytokine responses. These models are not nearly as robust as the PET-CT predictive models, but bring two extremely important concepts to the table. The first is simply the idea that peripheral blood signatures *can* be used to predict TB outcomes. The second concerns the fact that the signatures were identified across all vaccines. This is significant because a signature should not be vaccine specific but rather vaccination specific, meaning that the goal of research in this field should be to identify *one* set of blood markers that would predict success or failure against any novel TB vaccine, as having to develop separate sets of markers for each vaccine going into trials would be pointless. This would represent a significant advance

in other ways. If such markers could be identified, markers that predict protection conferred by *any* vaccination regardless of target disease could potentially be identified. These data would also suggest a common immune "theme" to TB protection, which would shed light on the basic immunology of protective immunity to TB. Thus, the continued development of a blood signature that is predictive of vaccine efficacy and TB outcome should be of the utmost importance in the field of TB vaccinology.

6.4 FUTURE DIRECTIONS FOR THESE FINDINGS

One of the things this dissertation highlighted was the importance of model selection. Earlier it was posited that rhesus macaques are more appropriate as a pre-exposure model, and cynomolgus macaques should be used for post-exposure studies. Thus, future pre-clinical trials using nonhuman primates should be designed with this framework in mind. This dissertation also demonstrated the need to focus on route of vaccination. The best route of vaccination necessary to protect against TB should be identified first, with the actual antigens or vaccine chosen after. BCG demonstrated efficacy in the rhesus macaques suggesting that it would be worthwhile to test alternative routes of vaccination with this vaccine. Intravenous and aerosol BCG have been shown to provide superior protection to Mtb challenge in rhesus macaques versus intradermal BCG [108, 109]. These routes have not been investigated in the model that more closely resembles the target demographic for novel TB vaccination (cynomolgus macaque), and thus future studies should investigate intravenous and aerosol BCG in the cynomolgus macaque model. Of special interest should be an intravenous prime that utilizes repeated aerosol boosts to attract memory T cells to the site of initial infection of Mtb to act as a pre-exposure vaccination

regimen. Any post-exposure vaccination should be designed to target the LN as this compartment has been shown to be critical for protection against reactivation TB. As previously mentioned, the most susceptible rhesus macaque cohort was the one receiving empty Ad5, suggesting that adjuvants or vectors that induce type I IFN should not be utilized in subsequent studies. The LN compartment should continue to be investigated to both understand how it might be functioning as the epicenter of TB disease and its role in reactivation TB. PET-CT should continue to be developed for pre-clinical vaccine trials. This dissertation and other published research demonstrate the ability of PET to assess risk of reactivation TB, which will be useful for evaluating post-exposure vaccines. CT can identify granulomas as the form, and thus could very rapidly identify cohorts of macaques in which early granuloma formation is suppressed by a vaccine candidate. Future work will also seek to validate the peripheral immune biomarkers identified in this dissertation. Data from more vaccines should be collected for this, as a universal signature of vaccine-induced protection would be the most useful tool in quickly evaluating efficacy in humans during clinical trials. Finally, although it is a bit outside the scope of this dissertation, I wish to express the continued hope for additional TB work in the form of ending poverty in developing nations. TB is mainly a social disease, and poverty-associated factors increase the likelihood of infection and progression to active disease [8]. The associated expenses and lost income due to illness can impede TB care, deepen impoverishment, and increase the risk of adverse outcomes and recurrence. Social protection interventions in the future can be TB specific [402]. In countries that are now developed, it has been shown that increased spending on social protection decreases the prevalence, incidence, and mortality of TB [353]. I sincerely hope that these tools, in combination with new therapeutics, will receive the funding and attention they deserve, and remain optimistic that TB may one day be eradicated.

APPENDIX A

ACTIVE TRANSFORMING GROWTH FACTOR-β IS ASSOCIATED WITH PHENOTYPIC CHANGES IN GRANULOMAS AFTER DRUG TREATMENT IN PULMONARY TUBERCULOSIS

This chapter is adapted from the original publication: DiFazio RM, Mattila JT, Klein EC, Cirrincione LR, Howard M, Wong EA, Flynn JL. Active transforming growth factor-β is associated with phenotypic changes in granulomas after drug treatment in pulmonary tuberculosis. Fibrogenesis and Tissue Repair. 2016. 9(6).

A.1 ABSTRACT

Tuberculosis (TB) chemotherapy clears bacterial burden in the lungs of patients and allows the tuberculous lesions to heal through a fibrotic process. The healing process leaves pulmonary scar tissue that can impair lung function. The goal of this study was to identify fibrotic mediators as a stepping-stone to begin exploring mechanisms of tissue repair in TB. Hemotoxylin and eosin staining and Masson's trichrome stain were utilized to determine levels of collagenization in tuberculous granulomas from non-human primates. Immunohistochemistry was then employed

to further interrogate these granulomas for markers associated with fibrogenesis, including transforming growth factor β (TGFβ), α-smooth muscle actin (αSMA), phosphorylated SMAD-2/3, and CD163. These markers were compared across states of drug treatment using one-way ANOVA, and Pearson's test was used to determine the association of these markers with one another. Active transforming growth factor β (TGFβ) and α-smooth muscle actin (αSMA) were present in granulomas from primates with active TB disease. These molecules were reduced in abundance after TB chemotherapy. Phosphorylated SMAD-2/3, a signaling intermediate of TGFβ, was observed in greater amounts after one month of drug treatment than in active disease, suggesting that this particular pathway is blocked in active disease. Collagen production during tissue repair is strongly associated with TGFβ in this model, but not with CD163+ macrophages. Tissue repair and fibrosis in TB that occurs during drug treatment is associated with active TGFβ that is produced during active disease. Further work will identify mechanisms of fibrosis, and work towards mitigating lung impairment with treatments that target those mechanisms.

A.2 BACKGROUND

With 10.4 million new cases and 1.8 million deaths annually worldwide, tuberculosis (TB) is one of humanity's greatest health threats [7]. Granulomas, the pathologic hallmark of TB, are well-circumscribed organized collections of host immune cells that form in response to the inhalation of aerosols containing Mycobacterium tuberculosis (Mtb)—the causative agent of TB. Although granulomas can function to kill or contain Mtb, they can also serve as a niche for growth and persistence of the organism [59, 60, 403]. Granulomas often feature a necrotic center and are

thus dubbed as necrotizing or caseous, while granulomas lacking this necrosis are said to be non-necrotizing. Granulomas feature epithelioid macrophages, elongated cells with larger nuclei, surrounded by other macrophages and lymphocytes [69]. Bacteria can be found in epithelioid macrophages and in caseum [69]. Uncontrolled replication leads to dissemination of the bacteria and formation of new granulomas. However, some granulomas can restrain bacterial dissemination or even develop locally sterilizing immunity. As a result, these granulomas are often fibrotic and can contain a calcified core (referred to as fibrocalcific lesions) [404]. A mixture of necrotizing and collagenous lesions is typical of secondary pulmonary tuberculosis and is referred to as fibrocaseous disease [404, 405]. Although the host factors that lead to control or dissemination of a single granuloma are unclear, we have demonstrated that various types of granulomas and outcomes exist within a single non-human primate, similar to humans [86, 404].

Tissue fibrosis can result from a wound healing response that includes fibroblast activation and recruitment, production of extracellular matrix materials, and distortion of the normal tissue architecture. The most common extracellular matrix component is collagen I, which is the most fibrous form of collagen and represents about 84% of the collagen produced by fibroblasts [406]. Fibrosis can be caused by a local inflammatory response and fibrosis-related pathogenesis is associated with dysfunction of many organs, including lungs, liver, and kidneys [407-409]. Transforming growth factor-β (TGFβ) is the main cytokine implicated in fibrogenesis, although other cytokines are implicated, including TNF, IL-6, IL-10, IL-13, and IL-17 [410-415]. TGFβ is produced in a latent form (L-TGFβ) and can be activated through the plasmin protease pathway, CD36 and thrombospondin (TSP), reactive oxygen and nitrogen species, hypoxia, low pH, and matrix metalloproteases [416]. Active TGFβ utilizes type 1 and 2

TGFβ receptors, signaling through a variety of intermediaries, including phosphorylated SMAD-2/3 [417]. Through these intermediaries, TGFβ stimulates differentiation of fibroblasts into myofibroblasts that then produce alpha-smooth muscle actin (αSMA), a key indicator of and contributor to fibrotic pathogenesis [418]. TGFβ has been observed and measured in pulmonary fibrosis and, in the lung, is produced by alveolar macrophages, fibrocytes, and lung epithelial cells [419-422]. Alveolar macrophages from humans with pulmonary fibrosis display an alternatively activated (M2) phenotype, and induction and maintenance of M2 macrophages is critical to pathology in pulmonary fibrosis [423]. M2 macrophages are also major producers and activators of TGFβ [421].

Although several types of pulmonary fibrosis have been characterized and studied, fibrosis in tuberculosis is not well understood. Significant pulmonary impairment was observed in 59% of patients with TB disease [424], half of whom had less than 50% of their original forced vital capacity [424]. This loss of pulmonary function resulted in 177 subjects losing 1189 disability adjusted-life years [425]. Lung function does not improve over the course of chemotherapy [426], and this chronic impairment increases incrementally with the number of TB episodes experienced in a progressive manner [426]. The main course of treatment for post-tuberculosis lung damage is pulmonary rehabilitation, which has mixed results [427], highlighting the need for more targeted therapies to resolve TB-induced fibrosis and scarring. Since macrophages produce TGFβ in pulmonary fibrosis, and are a major cellular component of granulomas [421], macrophages may be important contributors to fibrosis in TB lesions [428]. The environment of the granuloma may contain almost all of the conditions that activate TGFβ, including hypoxia [83], nitrogen radicals [69] and metalloproteases [429], so it is likely that the disease process activates TGFβ locally at the site of infection. Cutaneous TB lesions in humans

have been noted as centers of fibrosis, with lesions containing active TGFβ [430]. Patients with TB have peripheral blood monocytes and alveolar macrophages that produce and active more TGFβ than cells from healthy controls [243, 245]. TGFβ has also been observed directly in granulomas from human TB patients by immunohistochemistry[242].

Drug treatment for *M. tuberculosis* infection [23, 431] is a lengthy process that slowly clears bacterial burden in the lung and induces tissue repair in TB-affected lung. The factors that promote fibrotic resolution of tuberculous granulomas are poorly understood. This has been a challenging topic to address because of difficulties associated with studying human TB and a lack of appropriate mouse models demonstrating the granuloma structures seen in humans. Our laboratory previously published that drug-treated macaques with TB had fibrotic granulomas, and the fibrotic granulomas were most often sterile [432], representing a successful outcome of drug treatment. Since macaques recapitulate the spectrum of granuloma types and infection outcomes seen in humans, they represent a useful system for studying the process of drug-associated fibrosis. Understanding the fibrotic processes that occur in TB may provide insights into treatments to safely resolve residual lung fibrosis during or after drug therapy. The objective of this study was to determine how the cell types and molecules associated with pulmonary fibrosis differ between granulomas associated with active TB and fibrotic changes after chemotherapy. This study will open up further exploration of the fibrogenic mechanisms, with the aim of developing treatments to minimalize or reverse scarring after drug treatment.

A.3 RESULTS

A.3.1 Macrophages experience spindloid transformation in tuberculous granulomas.

After the original uptake of mycobacterial organisms by macrophages, a chemokine and cytokine cascade leads to monocyte recruitment, differentiation of macrophages, and epithelioid transformation. The latter is characterized by a large, plumper, more eosinophilic staining cell

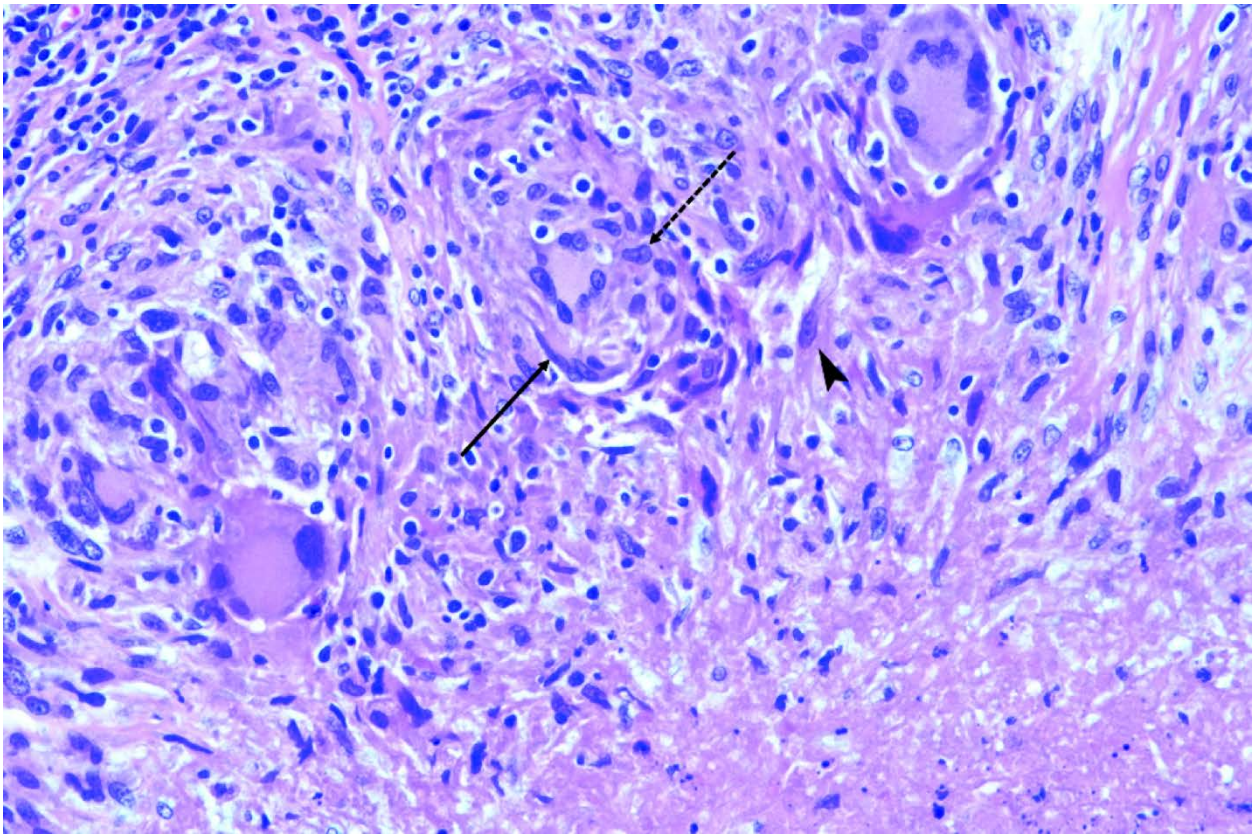

Figure 46: Macrophages experience spindloid transformation in tuberculous granulomas. H&E stained granuloma that demonstrates spindloid transformation of histiocytes. This figures provides microhistological examples of: epithelioid transformation of macrophages with elongated nuclei, dashed arrow, top; tapered, spindled macrophages further transformed, solid arrow, left; and collagen deposition, arrowhead, right. Magnification at 200x.

with somewhat elongated, sole-shaped nuclei (Fig. 46, dashed arrow). In contained tuberculous lesions, especially non-necrotizing ones that do not expand or infiltrate into adjacent bronchial or alveolar airspaces, further change then occurs globally in the appearance of these cells. Cell bodies become less plump and more streaming in shape, with nuclei progressing to a more tapered, spindled appearance (Fig. 46, solid arrow). A similarity between other aspects of nuclear (e.g. chromatin pattern) and cytoplasmic morphology remains between cells in different stages of this continuum. Fibroblasts and associated collagen fiber formation (Fig. 46, arrowhead) is seen in both necrotizing and non-necrotizing lesions, followed by the development of dense bands and sheets of fibrous connective tissue. Eosinophils have been linked to promotion of fibrogenesis [433], but are rarely abundant in lung granulomas in nonhuman primates (unpublished observations).

A.3.2 Granulomas exhibit a range of collagen deposition before and after drug treatment.

Our laboratory has previously provided histologic evidence for the resolution of TB pathology after two months of chemotherapy in cynomolgus macaques [432]. We used Masson's trichrome staining, a histologic technique for specifically identifying collagen, on pooled granulomas from two previously published drug studies [2, 432] to confirm our hemotoxylin and eosin (H&E)-based findings on the same set of animals. We examined if representative lesions have more (Figs. 47A, C, E) or less (Figs. 47B, D, F) collagen present by both histological stains. The more collagenous granuloma from an animal with active disease exhibits a faint ring of peripheral collagen deposition (Fig. 47A), which is not uncommon in tuberculous lesions, while less collagen-rich non-fibrotic granulomas lack this peripheral cuff of collagen (Fig. 47B). After one month of drug treatment, some granulomas exhibit a "healing" phenotype [1], as evidenced by a

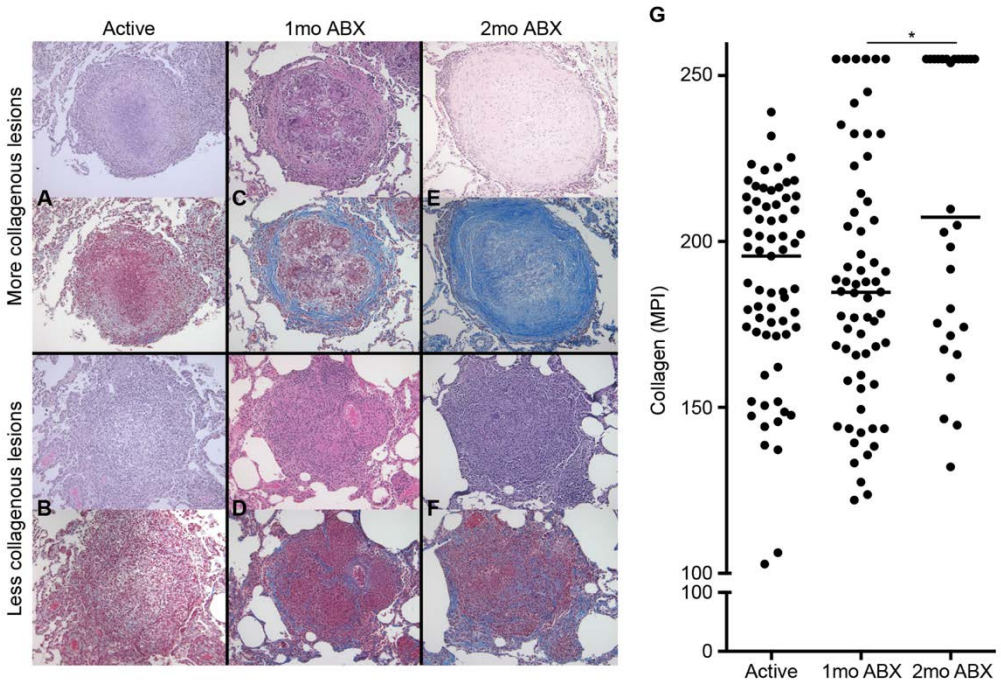

Figure 47: Granulomas exhibit range of collagen deposition before and after drug treatment. Representative sections of histology from granulomas pooled from two TB chemotherapy studies [1, 2], each with H&E staining (top panel) and Masson's trichrome staining (bottom panel) for the same lesion. **a** Granuloma from active disease with some peripheral fibrogenesis. **b** Granuloma from active disease with no apparent collagenization. **c** Granuloma from one month drug treated animal with robust peripheral fibrotic cuffing. **d** Granuloma from one month drug treated animal with some central fibrous organization**. e** Fibrotic granuloma from two month drug treated animal. **f** Granuloma from two month drug treated animal with pervasive central fibrous organization. **g** Quantification of all Masson's trichrome sections. Median pixel intensity was calculated from the blue channel of each micrograph and plotted by stage of drug therapy. Bars in each column represent medians. Kruskal-Wallis test: $p=0.0285$. *$p<0.05$.

thickening of the peripheral fibrotic cuff and central fibrous organization (Fig. 47C). Other granulomas lack this degree of collagenization, but still exhibit some central fibrous organization (Fig. 47D). By two months of chemotherapy, there are many lesions whose phenotype is solidly collagenous (Fig. 47E). There are still lesions though that are not completely resolved, and these

granulomas are characterized as having some central fibrous development without a robust peripheral cuff (Fig. 47F). These data suggest potentially different cellular mechanisms of tissue repair in tuberculosis, with various degrees of collagenization. We then quantified the photomicrographs for aniline blue-stained collagen to determine how drug treatment modifies collagen deposition (Fig. 47G). We found that granulomas from animals with active disease and one month of chemotherapy exhibit a wide range of collagen deposition (Fig. 47G). After two

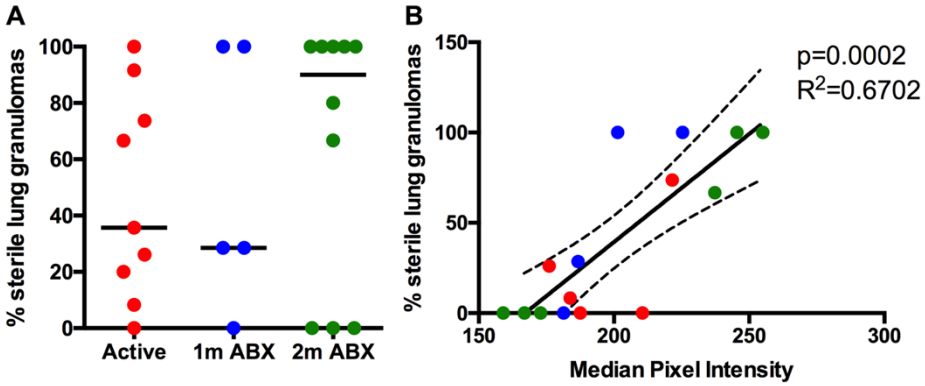

Figure 48: Antibacterial chemotherapy promotes collagen-associated bacterial clearance**. a** The number of lung granulomas with viable bacterial growth were divided by the total number of lung granulomas and plotted for each animal in the three groups. Each dot represents one animal. Bars represent medians. **b** The median of the median pixel intensity of the aniline blue staining was determined. This was then plotted against the percent of lung granulomas with viable bacteria. Significance of the interaction between percent of Mtb+ lung granulomas and collagen staining (p) and strength of interaction (R^2) are shown. Each dot represents one animal, and colors match the colors of the treatment groups in part A of this figure. Dotted lines represent 95% confidence intervals.

months of drug therapy, half of the granulomas are highly collagenous, but the other half displayed lesser degrees of collagenization (Fig. 47G). To put these data within the context of bacterial burden and sterilization, we divided the number of sterile lung granulomas by the total number of lung granulomas to get percentages of sterile lung granulomas for all of the animals in

the study (Fig. 48). We found that that the frequency of sterile granulomas increases as drug therapy progresses (Fig. 48A), and that this rise is concurrent with a significant increase the presence of collagen-rich granulomas (p=0.0002; Fig. 48B).

A.3.3 Tuberculous granulomas bear signs of TGFβ-driven fibrosis.

We next wanted to determine whether M2 macrophages and TGFβ were associated with tissue repair. Granulomas from animals with active disease, one month of antibiotic therapy (ABX),

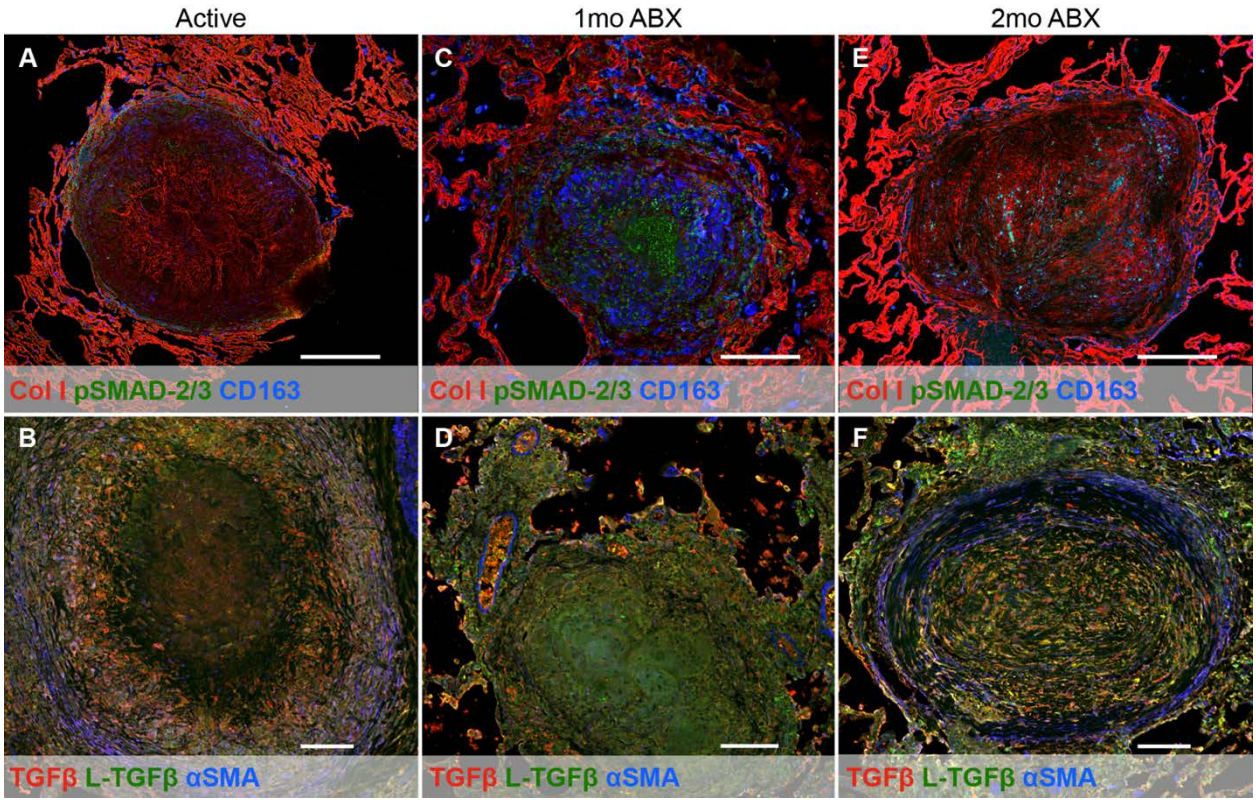

Figure 49: Tuberculous granulomas bear signs of TGFβ-driven fibrosis. Top panels feature granulomas stained for collagen I (red), phosphorylated SMAD-2/3 (green), and CD163 (blue). Bottom panels feature granulomas stained for TGFβ (red), L- TGFβ (green), and αSMA (blue). Magnification x 200. Scale bar represents 500 um. **a,b** Granulomas from animals with active disease. **c,d** Granulomas from animals after one month of TB chemotherapy. **e,f** Granulomas from animals after two months of TB chemotherapy.

and two months of ABX were analyzed by multiparameter immunohistochemistry for collagen I, phosphorylated (p) SMAD-2/3 (an intermediary of TGFβ signaling), and CD163 (a marker of M2-polarized macrophages in primates[69]) or TGFβ, L- TGFβ, and αSMA. This approach provides information on the location and quantity of factors upstream of TGFβ induction and TGFβ activation. We found that caseous granulomas from animals with active, untreated disease contained strongly-staining fibrils of collagen I that could be visualized in the central region of the lesion while pSMAD-2/3+ and CD163+ cells were present along the periphery of the structure (Fig. 49A). In similar granulomas from untreated animals, active TGFβ was present around the necrotic portion of the lesion (Fig. 49B), an area populated by epithelioid macrophages [69, 111]. Latent TGFβ was observed throughout this granuloma, and αSMA was strongly present in a region of robust peripheral fibrosis. After one month of drug treatment, collagen I was detected around the edge of the structure, suggesting mild peripheral fibrotic development (Fig. 49C). Strong pSMAD-2/3 staining was interspersed among the CD163+ cells that were localized towards the center of the structure, a position in which they are not normally found during active disease. Another granuloma from an animal with one month of drug therapy exhibited very little αSMA or active TGFβ, except minor staining in the exterior and in an adjacent blood vessel (Fig. 49D). Granulomas from animals two months post chemotherapy displayed plentiful collagen I staining, with both peripheral fibrosis and central fibrotic organization (Fig. 49E). In this particular lesion, pSMAD-2/3 and CD163 appear to co-localize in the fibrosis. We found that αSMA is present in a ring around the periphery of the structure (Fig. 49F). The active and latent forms of TGFβ appear to be intermixed within the lesion. These data overall indicate that active TGFβ is present in these granulomas and drives expression of TGFβ-regulated products including αSMA.

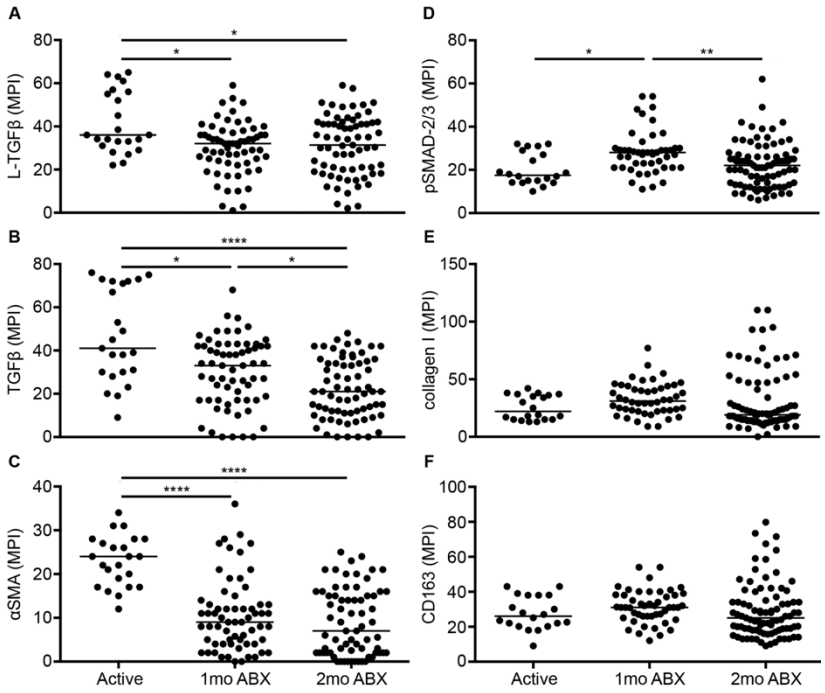

Figure 50: Active Mtb infection and disease activates TGFβ and suppresses SMAD-2/3 signaling. a-f Quantification of IHC. Median pixel intensity (MPI) was calculated from red, green, and blue color channels of each micrograph and plotted by stage of drug therapy. Bars in each column represent medians. Kruskal-Wallis test had p values of less than 0.0001 for TGFβ and αSMA, pSMAD-2/3 (0.0006), L-TGFβ (0.0148), and collagen I and CD163 (not significant). *p<0.05. **p<0.01. ***p<0.001. ****p<0.0001.

A.3.4 Active Mtb infection and disease activates TGFβ and suppresses SMAD-2/3 signaling.

We quantified median pixel intensity (MPI) from a collection of granulomas to elucidate how latent and active TGFβ, αSMA, pSMAD2/3, collagen and CD163 expression change over the three time points we are examining. We found an initial decrease in latent TGFβ levels at the initiation of drug treatment, but unchanged levels between one and two months of drug therapy (Fig. 50A). In contrast, active TGFβ appeared to decline in animals over the full two-month course of drug therapy (Fig. 50B), while the trend in αSMA expression was

consistent with trend observed for latent TGFβ (Fig. 50C). Interestingly, levels of phosphorylated SMAD-2/3 were higher after one month of chemotherapy, but then decreased by two months of antibiotics (Fig. 50D). Relative amounts of collagen I and CD163 do not change between following antibiotic treatment (Fig. 50E-F). These data further demonstrate the role that active TGFβ is playing in drug-promoted tissue repair.

We used immunologic and biochemical assays to confirm our immunohistochemical analysis of TGFβ and collagen. Consistent with our immunohistochemical data, ELISAs for active TGFβ demonstrated greater quantities of TGFβ in granulomas from animals during active disease and lesser in animals after two months of drug treatment (Fig. 51A). Collagen levels were measured by hydroxyproline assay (Fig. 51B), and were unchanged between treated and untreated animals, coinciding with our microscopic data (Fig. 50F).

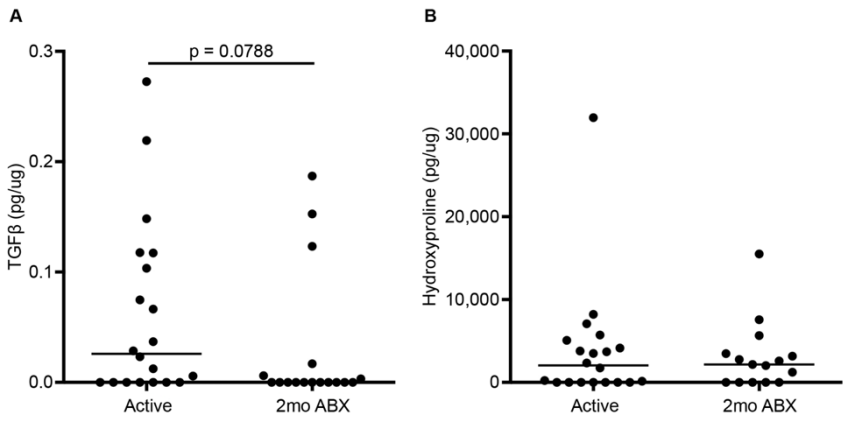

Figure 51: Biochemical evidence of TGFβ and collagen. a ELISA for active TGFβ. TGFβ in granulomas was converted into pg and then normalized by the total amount of protein in each granuloma as determined by BCA assay. Wilcoxon signed rank test was used to compare granulomas from active disease to granulomas from two months of drug treatment. **b** Hydroxyproline assay. Collagen present in granulomas was determined using the hydroxyproline assay. Values were converted into pg and then normalized by the total amount of protein in each granuloma as determined by BCA assay.

A.3.5 TGFβ is strongly associated with collagen I expression.

We used our quantitative immunohistochemical data (Fig. 50) to perform pairwise correlations to identify the relationships between these factors. At all study time points, collagen I and pSMAD-2/3 exhibit a robust positive association (Fig. 52), especially during active disease and one month of drug therapy. In these time points, we found that over 50% of the variability in collagen I levels was explained by pSMAD-2/3 (Pearson's $r>0.7$). In granulomas from animals with active disease, or two months of drug treatment, there is a weak but significant association between pSMAD-2/3 and CD163 (Fig. 52). However, CD163 and collagen I are not statistically associated at any time point of the study (Fig. 52). This is in contrast to active TGFβ, latent TGFβ, and αSMA, which are all strongly and positively associated with one another at all time points (Fig. 53).

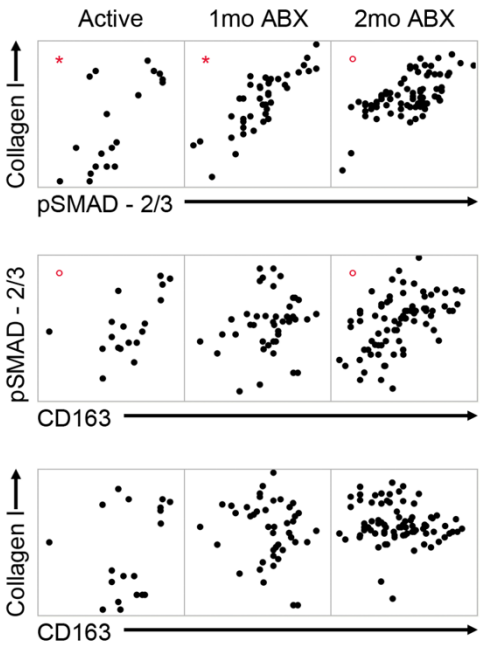

Figure 52: TGFβ is strongly associated with the presence of collagen I. IHC values for each granuloma were plotted against one another to assess association between collagen I, TGFβ signaling, and M2 macrophages. Values were transformed, and Pearson's test for parametric correlation was used to determine significance. Significant correlations are denoted by red symbols. Open circles are significant but $r<0.7$, while asterisks indicate that $r>0.7$.

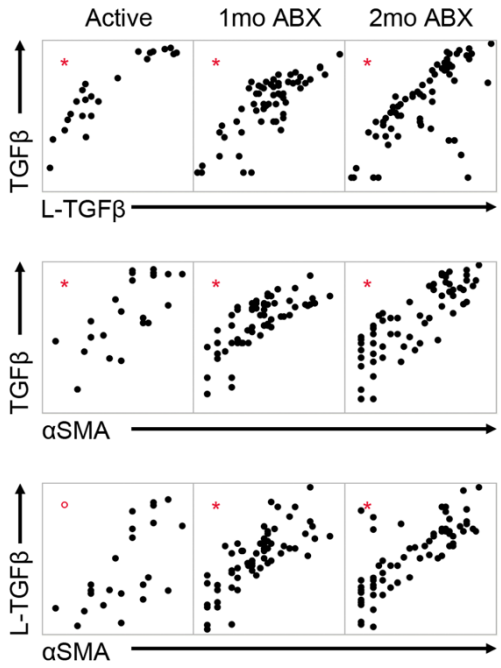

Figure 53: Active TGFβ is highly associated with its latent form and αSMA. IHC values for each granuloma were plotted against one another to assess association between TGFβ, L- TGFβ, and αSMA—which is produced by cells activated by TGFβ. Values were transformed, and Pearson's test for parametric correlation was used to determine significance. Significant correlations are denoted by red symbols. Open circles are significant but $r<0.7$, while asterisks indicate that $r>0.7$.

A.4 DISCUSSION

The goal of this study was to identify molecular and cellular markers associated with fibrotic resolution in experimental tuberculosis infection. Tuberculosis produces a wide range of pulmonary pathologies through infection and disease, which typically result in chronic fibrocaseous disease [404, 405]. Drug treatment reduces bacterial burden and allows for tissue repair, although this does not quickly alter the pathology remaining in the lung as demonstrated by computed tomography in both human and non-human primates [350]. Chemotherapy additionally leaves individuals vulnerable to relapse; more than half of smear positive TB cases have been previously treated for TB [366]. Relapse was originally thought to be cause by endogenous sources of Mtb remaining after drug treatment, but 75% of relapse cases in a high TB burden cohort were exogenously re-infected [434]. Why is this population prone to reinfection after successful chemotherapy? The risk of developing active TB is about 4.5 times higher in patients with chronic interstitial lung disease and idiopathic pulmonary fibrosis [435, 436]. This could be due to the specific pathology of fibrotic lung tissue as it may promote colonization and establishment of infection [437]. The residual scar tissue left after drug therapy and loss of normal lung architecture could play roles in increasing the risk of relapse. Therefore, understanding the mechanism of fibrogenesis in TB and ameliorating tissue damage after drug treatment could reduce the risk of reinfection and help shrink the pool of infected individuals.

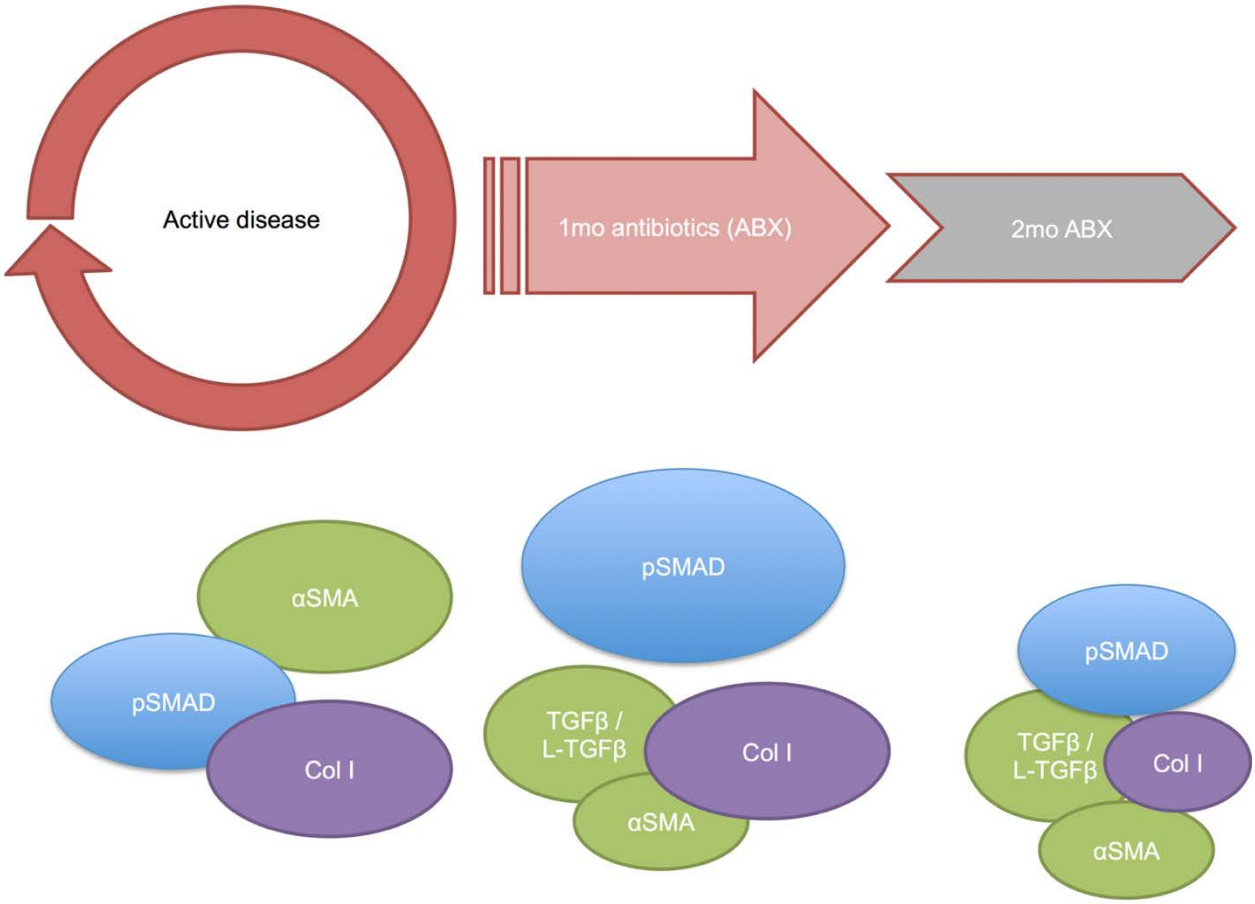

Figure 54: Model that demonstrates the TGFβ-associated processes explores in this study. The red arrow around active disease represents processes that activate fibrotic cytokines, which then diminish during the early course of drug therapy (smaller arrows that are less red). αSMA and TGFβ drop, represented in green, while pSMAD-2/3 appears to rise and fall, in blue. Levels of collagen I do not change, shown in purple.

Several cell types are likely to play significant roles in driving fibrotic processes in granulomas, but it has been difficult to identify the specific cells that are the most important drivers of fibrosis. Histologic assessment can be used to evaluate the cellular responses to infection from a morphological perspective and can provide insights into lesion development and resolution. Identifying the cellular origin of some spindle-type cells in granulomas is not always possible, but histologic examination can provide important inferences as to whether these cells arose from epithelioid macrophages or collagen-producing fibroblasts. Based on our histologic

observations and immunohistochemical analyses, we hypothesize that collagen-producing fibroblast-like cells may originate from several sources, and in some cases not from fibroblasts recruited from nearby tissues, but from non-fibroblast-like cells that have undergone a process similar to endothelial–mesenchymal progression. Additionally, circulating monocyte-derived cells (fibrocytes) can have phenotypes reminiscent of the phenotypes we have identified [438, 439]. Given the ability of some circulating monocytes to differentiate into fibroblast-like cells instead of macrophages, the question of whether subsequent differentiation between macrophages and fibroblasts can occur should be considered. The wide range in collagen presence, plus the appearance of various collagenous phenotypes suggest that different mechanisms for fibrotic resolution occur in tuberculous granulomas. Some granulomas manifest both peripheral and central fibrous organization, while others demonstrate only central collagenization, or none at all. Future studies should seek to correlate these divergent repair mechanisms to lesion specific Mtb burden to determine efficacy of clearance and elucidate the immunologic processes of each.

Our observations that latent TGFβ changes only slightly between granulomas from animals with active disease and drug-treated animals suggest that a pool of latent TGFβ remains in the lung even after Mtb is cleared. Latent TGFβ is maintained in the lung epithelium by latent TGFβ binding proteins where it can remain until activated [440]. Our data indicate that conditions within granulomas activate TGFβ, an anti-inflammatory cytokine associated with fibrosis. This molecule exerts biological action in the granuloma, as is supported by the presence of αSMA in direct proportion to TGFβ. The lower levels of TGFβ and αSMA in granulomas of animals on drug therapy suggests that therapy itself does not activate more TGFβ, and that the amount activated during active TB is utilized for

tissue repair. Interestingly, phosphorylated SMAD-2/3 is lower during active disease, even though active TGFβ levels are high. Since SMAD-2/3 is phosphorylated when cells come into contact with active TGFβ [417], this suggests that live Mtb somehow block SMAD-2/3 activation even in the presence of active TGFβ. The presence of αSMA, also an indicator of the cellular effects of TGFβ, could be explained by the utilization of alternative TGFβ-stimulated pathways [441, 442]. The alternative TGFβ signaling pathways may be prominent in disease, and since the SMAD-2/3 pathway only becomes used in tissue repair once Mtb is cleared, the SMAD-2/3 pathway may be preferential for healing and clearance and the alternative pathways preferential for TB pathogenesis. Collagen I levels are similar between granulomas with active disease and drug treatment, suggesting that treatment only promotes and does not exacerbate fibrosis. Collagen I is strongly associated with active TGFβ; over 50% of the variability in levels of collagen I is explained by TGFβ signaling through SMAD-2/3, indicating that active TGFβ is likely the main molecular driver of fibrosis and tissue repair in tuberculous lesions. CD163 and collagen I are not associated in this model, implying that the CD163+ macrophages are not major producers of collagen I. Macrophages in granulomas are not a uniform population of cells [69], and other CD163- macrophage subsets could be responsible for collagen production in the granuloma. Unfortunately, there are no pan-macrophage markers for primates, and our efforts to identify the specific population of cells responsible for collagen expression are ongoing [69]. Collagen appears to stream from the epithelioid macrophages into the caseous necrotic center. Interestingly, this population of cells is not comprised of the M2-polarized CD163+ macrophages we expected would correlate with fibrosis, but instead appear to be M1-polarized cells [69], suggesting the capacity of these cells may be more

diverse than previously known. Active TGFβ was mostly localized in the epithelioid macrophage region of the granulomas as well. Alternatively, macrophage-expressed products could support collagen production by neighboring fibroblasts. These cells could potentially be contributors to collagenization, as well as surrounding lung epithelial cells transformed by active TGFβ. Further work will include markers for these types of cells and determine their association with collagen production in the granuloma.

A.5 CONCLUSIONS

Fibrosis occurs in TB lesions during and after drug treatment. The goal of this project was to determine the cell types and molecules associated with fibrosis in non-human primates with TB. We provide additional evidence of activated TGFβ being present in lesions from *M. tuberculosis*-infected lung tissue. Collagen production in active disease and TB chemotherapy is strongly associated with TGFβ, suggesting its role as the chief cytokine driving tissue repair. Future studies will seek to further explore these results mechanistically with hopes of developing adjunct treatment to minimize, or possibly reverse, scar formation after TB chemotherapy.

A.6 METHODS

A.6.1 Animals

The Institutional Animal Care and Use Committee of University of Pittsburgh approved all experiments. The animals were housed and maintained in accordance with standards established in the Animal Welfare Act and the Guide for the Care and Use of Laboratory Animals.

Infections. Cynomolgus macaques (4-9 years of age) imported from China (Valley Biosystems, Sacramento, CA) were used for these studies (n=21). Monkeys were infected via bronchoscope with 25 CFU of *M. tuberculosis* Erdman strain. Using published criteria, monkeys were determined to have active or latent TB by 6-8 months post-infection, and were randomized to treatment or non-treatment groups; treatment was initiated when monkeys developed active TB, as determined by clinical and microbiologic signs [65, 111].

Drug therapy. The samples described in the current study were obtained from macaques in a previously published study from our laboratory [1, 2]. Monkeys with active disease were: untreated (n=9, 110 granulomas), treated with isoniazid (INH) and rifampin (RIF) for 1 month (n=2, 22 granulomas) or 2 months (n=5, 91 granulomas), or treated with INH, RIF, and metronidazole (MTZ) for 1 month (n=3, 154 granulomas) or 2 months (n=5, 93 granulomas).

Necropsies were performed as previously described (35 52). Individual granuloma and lung samples were taken from each monkey from sites of infection and surrounding tissue. Portions of these samples were homogenized into single cell suspension before storing at -80°C for ELISA and hydroxyproline assays, while another portion was formalin-fixed paraffin-embedded for histology.

A.6.2 Hematoxylin and eosin (H&E) staining

Formalin-fixed paraffin-embedded tissue sections were cut and stained with Harris hemotoxylin modified (Sigma-Aldrich, St. Louis, MO) and eosin Y solution (Sigma-Aldrich, St. Louis, MO). Slides were deparaffinized in deionized water. Slides were then stained with hemotoxylin for three minutes. Slides were rinsed under running tap water, rinsed with 70% ethanol, and then stained with eosin for three minutes. Slides were rinsed and dehydrated in ethanol, cleared in xylene, and then mounted. Criteria for characterizing granulomas were based on size and shape, type of granuloma, and cellular composition. A veterinary pathologist who is an expert in macaque tuberculosis (ECK) performed all histologic analyses.

A.6.3 Masson's trichrome

Formalin-fixed paraffin-embedded tissue sections were stained with Masson's trichrome to identify connective tissue, muscle and collagen fibers (Sigma-Aldrich, St. Louis, MO). Slides were deparaffinized to deionized water. Slides were then immersed in Bouin's solution overnight at room temperature to intensify the subsequent staining. Slides were washed with tap water then stained with Harris hematoxylin solution (Sigma-Aldrich, St. Louis, MO) for five minutes. Slides were washed again in running tap water for five minutes, rinsed in deionized water, and stained in Biebrich Scarlet-Acid Fucshin for five minutes. Slides were rinsed in deionized water and placed in phosphotungstic and phosphomolybdic acid solution for five minutes. Slides were moved to Aniline Blue solution for five minutes, and then placed in 1% acetic acid solution for two minutes. Slides were rinsed in deionized water, dehydrated through alcohol, cleared in xylene, and then mounted.

A.6.4 Immunohistochemistry

Tissue sections were stained for collagen I (rabbit polyclonal, Abcam, Cambridge, MA, 1:50 dilution), pSMAD-2/3 (goat polyclonal, Santa Cruz Biotechnology, Dallas, TX, 1:10 dilution), CD163 (mouse clone 10D6, Neomarkers, Fremont, CA, 1:30 dilution), L-TGFβ (goat polyclonal, R&D Systems, Minneapolis, MN, 1:10 dilution), TGFβ (chicken polyclonal, R&D Systems, Minneapolis, MN, 1:10 dilution), and αSMA (mouse clone 1A4, Thermo Fisher, Pittsburgh, PA, 1:100 dilution). Antigen retrieval and staining were done as previously described [69]. Briefly, formalin fixed paraffin embedded tissues samples were deparaffinized in xylene and rehydrated in ethanol. Samples were then placed into a pressure cooker with boiling antigen retrieval buffer (Tris-HCl, EDTA, Tween-20) for seven minutes. After allowing for the slides to cool, the sections were blocked with 2% fetal bovine serum in phosphate buffered saline for 30 minutes. Antibodies and fluorescent tags were incubated on each sample for one hour with washes in between with phosphate buffered saline with 0.2% Tween-20. Prolong Gold Mounting Medium with DAPI (Invitrogen) was then applied to the slides, which were then cured in the dark overnight before being imaged.

A.6.5 Quantification of histology

Trichrome- and H&E-stained sections were imaged using Provis fluorescent microscope (Olympus America, Center Valley, PA) and fluorescently stained slides visualized with a FluoView 1000 confocal microscopes (Olympus). For images used for quantitative imaging, care was taken to keep the camera settings constant between granulomas and animals. These images were then saved as 24-bit TIFF files and read into the language R via the package “EBImage”

from Bioconductor (http://www.bioconductor.org/packages/release/bioc/html/EBImage.html). For the trichrome slides, the blue channel only was isolated. Red, green, and blue channels were pulled from the IHC slides. The median pixel intensity for each channel was then saved and exported to Microsoft Excel (Microsoft, Redmond, WA).

A.6.6 Enzyme-linked immunosorbent assays (ELISAs)

Active TGFβ-1 in granuloma homogenates was measured by using a commercial ELISA (eBioscience, San Diego, CA) according to manufacturer's instructions. Briefly, a high affinity protein binding plate was coated with a capture antibody overnight and blocked with assay diluent for an hour before adding standards and undiluted granuloma homogenates for overnight incubation. TGFβ was detected the next day using a biotinylated detection antibody and streptavidin-HRP, and the absorbance was immediately measured at 450nm. Total protein of the same samples was quantified by Pierce BCA Protein Assay (Thermo Scientific, Pittsburgh, PA), where granuloma homogenates were added to BCA Working Reagent, and the absorbance measured at 562 nm after 30 minutes at 37°C. Levels of TGFβ were normalized to total protein in granuloma homogenates.

A.6.7 Hydroxyproline assay

Collagen was detected in homogenized granulomas by using a commercial hydroxyproline kit (Sigma Aldrich, St. Louis, MO). Briefly, samples were mixed with hydrochloric acid and hydrolyzed at 120°C for 3 hours. These samples and standards were then transferred to a 96-well plate and dried. Chloramine T/oxidation buffer was added to wells and incubated at room

temperature for five minutes. To this, diluted DMAB reagent was added and incubated at 60°C for 90 minutes. Absorbance at 560 nm was then measured. Levels of collagen were normalized to total protein in granuloma homogenates.

A.6.8 Statistics

Quantitative data from Masson's trichrome staining and immunohistochemical staining were visualized using Prism (Graphpad, La Jolla, CA). Analysis of these data was done using the tests indicated, typically a one-way ANOVA and a multiple comparison test for either parametric or non-parametric data. P values were significant if less than 0.05. Further analysis of the immunohistochemical staining was performed with JMP (SAS, Cary, NC). Correlations between markers in histological stains were performed using the multivariate function and scatterplots were generated. Significance was determined using pairwise correlations with the strength of the relationship given as Pearson's r.

APPENDIX B

PUBLICATION RECORD

Green AM, **DiFazio RM,** Flynn JL. (2013). "IFN-γ from CD4 T cells is essential for host survival and enhances CD8 T cell function during *Mycobacterium tuberculosis* infection." J Immunol **190(1):** 270-7. PMID: 23233724

DiFazio RM, Mattila JT, Klein EC, Cirrincione LR, Howard M, Wong EA, Flynn JL. (2016). "Active transforming growth factor-ß is associated with phenotypic changes in granulomas after drug treatment in pulmonary tuberculosis." Fibrogenesis Tissue Repair **9(6).** PMID: 27148404.

Lin PL, Maiello P, Gideon HP, Coleman MT, Cadena AM, Gregg RW, O'Malley M, Tomko J, Fillmore D, Frye LJ, Kane T, **DiFazio RM**, Janssen C, Klein EC, Andersen PL, Fortune S, Flynn JL. (2016). "PET CT identifies reactivation risk in cynomolgus macaques with latent *M. tuberculosis*." PLoS Path **12(7).** PMID: 27379816.

APPENDIX C

MANUSCRIPTS TO BE PUBLISHED

Chapter 3: Data from this chapter will be incorporated with addition data from collaborators at the NIAID Vaccine Research Center and subsequently published as a co-first author manuscript.

Chapter 4: DiFazio RM, Maiello P, Myers AJ, Rodgers MA, O'Malley M, Tomko J, Frye LJ, Fillmore D, Agger EM, Andersen P, Lin PL, and Flynn JL. BCG+H56:CAF01 limits host inflammation and bacterial dissemination in a nonhuman primate model of tuberculosis. Soon to be submitted and likely published in 2017.

Chapter 5: Data from this chapter will subsequently be published in a first author manuscript.

BIBLIOGRAPHY

1. Lin, P.L., et al., *Metronidazole prevents reactivation of latent Mycobacterium tuberculosis infection in macaques.* Proc Natl Acad Sci U S A, 2012. **109**(35): p. 14188-14193.

2. Lin, P.L., et al., *Radiologic responses in cynomolgus macaques for assessing tuberculosis chemotherapy regimens.* Antimicrob Agents Chemother, 2013. **57**(9): p. 4237.

3. MacQueen, J.B., *Some methods for classification and analysis of multivariate observations*, in *Proceedings of 5th Berkeley Symposium on Mathematical Statistics and Probability*. 1967, University of California Press. p. 281-97.

4. Kaiser, H.F., *The application of electronic computers to factor analysis.* Ed Psych Measurement, 1960. **20**: p. 141-51.

5. Lin, P.L., et al., *PET CT Identifies Reactivation Risk in Cynomolgus Macaques with Latent M. tuberculosis.* PLOS Pathogens, 2016. **12**(7): p. e1005739.

6. Roederer, M., J.L. Nozzi, and M.C. Nason, *SPICE: exploration and analysis of post-cytometric complex multivariate datasets.* Cytometry A, 2011. **79**(2): p. 167-74.

7. WHO, *Global tuberculosis report.* 2016.

8. Rocha, C., et al., *The Innovative Socio-economic Interventions Against Tuberculosis (ISIAT) project: an operational assessment.* Int J Tuberc Lung Dis, 2011. **15 Suppl 2**: p. S50-7.

9. Herzog, H., *History of tuberculosis.* Respiration, 1998. **65**: p. 5-15.

10. Hippocrates, *Of the epidemics*. Vol. 3. 400 BCE, Athens.

11. Fracastoro, G., *De contagione et contagiosis morbis*. 1546, Verona.

12. Milburn, H.J., *Primary tuberculosis.* Curr Opin Pul Med, 2001. **7**: p. 133-41.

13. Sylvius, F., *Opera medica*. 1680, Amsterdam: Elsevirus and Wolfgang. 934.

14. Radloff, W., *Nachtraege zum Chuastuanit, dem Bussgebete der Manichaer.* Bull de l'Acad Imp des Sci de St. Petersburg, 1911. **5**(12): p. 867-96.

15. Sledzik, P.S. and N. Bellantoni, *Brief communication: bioarcheological and biocultural evidence for the New England vampire folk belief.* Am J Phys Anthropol, 1994. **94**(2): p. 269-74.

16. Villemin, J.A., *Cause et nature de la tuberculose*, in *Bulletin de l'Academie nationale de medecine*. 1865, Masson: Paris. p. 211-16.

17. Koch, R., *Die Atiologie der Tuberkulose.* Berliner Klinische Wochenschrift, 1882. **15**: p. 428-45.

18. Riley, R.L., et al., *Air hygiene in tuberculosis: quantitative studies of infectivity and control in a pilot ward.* Am Rev Tuberc Pulmonary Diseases, 1957. **75**: p. 420-31.

19. Riley, R.L., et al., *Aerial dissemination of pulmonary tuberculosis, a two-year study of contagion in a tuberculosis ward.* Am J Hyg, 1959. **70**: p. 185-96.

20. Mangara, B.T., et al., *Mycobacterium tuberculosis Miniepidemic in a Church Gospel Choir.* Chest, 1998. **113**(1): p. 234-237.

21. Marks, G.B., et al., *Incidence of tuberculosis among a cohort of tuberculin-positive refugees in Australia.* Am J Respir Crit Care Med, 2000. **162**: p. 1851-4.

22. Jereb, J., et al., *Tuberculosis contact investigations: outcomes in selected areas of the United States, 1999.* Int J Tuberc Lung Dis, 2003. **7**(12): p. S384-90.

23. Dheda, K., C.E. Barry, and G. Maartens, *Tuberculosis.* The Lancet, 2015.

24. Pindell, M.L., *Roentgen diagnosis of tracheo-bronchial and pulmonary tuberculosis - its value.* Cal West Med, 1932. **36**(2): p. 81.

25. Aggerbeck, H., et al., *Randomised clinical trial investigating the specificity of a novel skin test (C-Tb) for diagnosis of M. tuberculosis infection.* PLoS One, 2013. **8**(5): p. e64215.

26. Borgstrom, E., et al., *Immune responses to ESAT-6 and CFP-10 by FASCIA and multiplex technology for diagnosis of M. tuberculosis infection; IP-10 is a promising marker.* PLoS One, 2012. **7**(11): p. e43438.

27. Mgode, G.F., et al., *Ability of Cricetomys rats to detect Mycobacterium tuberculosis and discriminate it from other microorganisms.* Tuberculosis (Edinb), 2012. **92**(2): p. 182-6.

28. Houk, V.H., et al., *The Byrd study. In-depth analysis of a micro-outbreak of tuberculosis in a closed environment.* Arch Environ Health, 1968. **16**(1): p. 4-6.

29. Morrison, J., M. Pai, and P.C. Hopewell, *Tuberculosis and latent tuberculosis infection in close contacts of people with pulmonary tuberculosis in low-income and middle-income countries: a systematic review and meta-analysis.* The Lancet Infectious Diseases, 2008. **8**(6): p. 359-368.

30. Cobat, A., et al., *Two loci control tuberculin skin test reactivity in an area hyperendemic for tuberculosis.* J Exp Med, 2009. **206**(12): p. 2583-91.

31. Jones-Lopez, E.C., et al., *Cough aerosols of Mycobacterium tuberculosis predict new infection: a household contact study.* Am J Respir Crit Care Med, 2013. **187**(9): p. 1007-15.

32. Poulsen, A., *Some clinical features of tuberculosis. 1.* Acta tuberculosea Scandinavica, 1950. **24**(3-4): p. 311-46.

33. Poulsen, A., *Some clinical features of tuberculosis. 2-7.* Acta tuberculosea Scandinavica, 1957. **33**(1-2): p. 37-92.

34. Chiba, Y., *Significance of endogenous reactivation. 30 years' observation of subjects whose tuberculin test reaction has changed.* Bull Int Union Tuberc, 1974. **49**(1): p. 347-50.

35. Vynnycky, E. and P.E.M. Fine, *The natural history of tuberculosis: the implications of age-dependent risks of disease and the role of reinfection.* Epidemiol. Infect., 1997. **119**: p. 183-201.

36. Steingart, K.R., et al., *Sputum processing methods to improve the sensitivity of smear microscopy for tuberculosis: a systematic review.* The Lancet Infectious Diseases, 2006. **6**(10): p. 664-674.

37. Pfyffer, G.E., et al., *Rapid detection of mycobacteria in clinical specimens by using the automated BACTEC 9000 MB system and comparison with radiometric and solid-culture systems.* J Clin Microbiol, 1997. **35**(9): p. 2229-34.

38. Tameris, M., et al., *Lessons learnt from the first efficacy trial of a new infant tuberculosis vaccine since BCG.* Tuberculosis (Edinb), 2013. **93**(2): p. 143-9.

39. Agranoff, D., et al., *Identification of diagnostic markers for tuberculosis by proteomic fingerprinting of serum.* The Lancet, 2006. **368**(9540): p. 1012-1021.

40. Djoba Siawaya, J.F., et al., *Differential cytokine/chemokines and KL-6 profiles in patients with different forms of tuberculosis.* Cytokine, 2009. **47**(2): p. 132-6.

41. Steingart, K.R., et al., *Performance of purified antigens for serodiagnosis of pulmonary tuberculosis: a meta-analysis.* Clin Vaccine Immunol, 2009. **16**(2): p. 260-76.

42. Berry, M.P., et al., *An interferon-inducible neutrophil-driven blood transcriptional signature in human tuberculosis.* Nature, 2010. **466**(7309): p. 973-7.

43. Maertzdorf, J., et al., *Functional correlations of pathogenesis-driven gene expression signatures in tuberculosis.* PLoS One, 2011. **6**(10): p. e26938.

44. Ottenhoff, T.H., et al., *Genome-wide expression profiling identifies type 1 interferon response pathways in active tuberculosis.* PLoS One, 2012. **7**(9): p. e45839.

45. Mihret, A., et al., *Combination of gene expression patterns in whole blood discriminate between tuberculosis infection states.* BMC Inf Dis, 2014. **14**(257).

46. Sweeney, T.E., et al., *Genome-wide expression for diagnosis of pulmonary tuberculosis: a multicohort analysis.* The Lancet Respiratory Medicine, 2016. **4**(3): p. 213-224.

47. Biselli, R., et al., *Detection of interleukin-2 in addition to interferon-gamma discriminates active tuberculosis patients, latently infected individuals, and controls.* Clin Microbiol Infect, 2010. **16**(8): p. 1282-4.

48. Marin, N.D., et al., *Reduced frequency of memory T cells and increased Th17 responses in patients with active tuberculosis.* Clin Vaccine Immunol, 2012. **19**(10): p. 1667-76.

49. Rozot, V., et al., *Mycobacterium tuberculosis-specific CD8+ T cells are functionally and phenotypically different between latent infection and active disease.* Eur J Immunol, 2013. **43**(6): p. 1568-77.

50. Silva, B.D., et al., *Different phenotypes of CD8+ T cells associated with bacterial load in active tuberculosis.* Immunol Lett, 2014. **160**(1): p. 23-32.

51. Arlehamn, C.L., et al., *Transcriptional profile of tuberculosis antigen-specific T cells reveals novel multifunctional features.* J Immunol, 2014. **193**(6): p. 2931-40.

52. Sandhu, G., et al., *Discriminating active from latent tuberculosis in patients presenting to community clinics.* PLoS One, 2012. **7**(5): p. e38080.

53. Weiner, J., 3rd, et al., *Biomarkers of inflammation, immunosuppression and stress with active disease are revealed by metabolomic profiling of tuberculosis patients.* PLoS One, 2012. **7**(7): p. e40221.

54. Horsburgh, C., *Priorities for the treatment of latent tuberculosis infection in the United States.* N Engl J Med, 2004. **350**: p. 2060-7.

55. Barry, C.E., 3rd, et al., *The spectrum of latent tuberculosis: rethinking the biology and intervention strategies.* Nat Rev Microbiol, 2009. **7**(12): p. 845-55.

56. Lin, P.L. and J.L. Flynn, *Understanding latent tuberculosis: a moving target.* J Immunol, 2010. **185**(1): p. 15-22.

57. Lin, P.L., et al., *Tumor necrosis factor neutralization results in disseminated disease in acute and latent Mycobacterium tuberculosis infection with normal granuloma structure in a cynomolgus macaque model.* Arthritis Rheum, 2010. **62**(2): p. 340-50.

58. Lin, P.L., et al., *CD4 T cell depletion exacerbates acute Mycobacterium tuberculosis while reactivation of latent infection is dependent on severity of tissue depletion in cynomolgus macaques.* AIDS Res Hum Retroviruses, 2012. **28**(12): p. 1693-702.

59. Russell, D.G., *Who puts the tubercle in tuberculosis?* Nat Rev Microbiol, 2007. **5**(1): p. 39-47.

60. Ramakrishnan, L., *Revisiting the role of the granuloma in tuberculosis.* Nat Rev Immunol, 2012. **12**(5): p. 352-66.

61. Ghon, A., *The Primary Lung Focus of Tuberculosis in Children*. 1916, New York: Paul B. Hober. 1001.

62. Ranke, K.E., *Primäraffekt, sekundäre und tertiäre Stadien der Lungentuberkulose, auf Grund von histologischen Untersuchungen der Lymphdrüsen der Lungenpforte.* Ausgewählte Schriften zur Tuberkulosepathologie, 1928. **6**: p. 37-40.

63. Barnes, P.F., et al., *Chest roentgenogram in pulmonary tuberculosis.* Chest, 1988. **94**(2): p. 316-20.

64. Medlar, E.M., *The pathogenesis of minimal pulmonary tuberculosis; a study of 1,225 necropsies in cases of sudden and unexpected death.* Am Rev Tuberc, 1948. **58**(6): p. 583-611.

65. Lin, P.L., et al., *Quantitative comparison of active and latent tuberculosis in the cynomolgus macaque model.* Infect Immun, 2009. **77**(10): p. 4631-42.

66. Wolf, A.J., et al., *Mycobacterium tuberculosis Infects Dendritic Cells with High Frequency and Impairs Their Function In Vivo.* The Journal of Immunology, 2007. **179**(4): p. 2509-2519.

67. Lukacs, N.W., et al., *Inflammatory granuloma formation is mediated by TNF-alpha-inducible intercellular adhesion molecule-1.* J Immunol, 1994. **152**: p. 5883.

68. Rhoades, E., et al., *Identification and macrophage-activating activity of glycolipids released from intracellular Mycobacterium bovis BCG.* Mol Microbiol, 2003. **48**(4): p. 875-88.

69. Mattila, J.T., et al., *Microenvironments in tuberculous granulomas are delineated by distinct populations of macrophage subsets and expression of nitric oxide synthase and arginase isoforms.* J Immunol, 2013. **191**(2): p. 773-84.

70. Wolf, A.J., et al., *Initiation of the adaptive immune response to Mycobacterium tuberculosis depends on antigen production in the local lymph node, not the lungs.* J Exp Med, 2008. **205**(1): p. 105-15.

71. Appelmelk, B.J., et al., *Cutting Edge: Carbohydrate Profiling Identifies New Pathogens That Interact with Dendritic Cell-Specific ICAM-3-Grabbing Nonintegrin on Dendritic Cells.* The Journal of Immunology, 2003. **170**(4): p. 1635-1639.

72. Shafiani, S., et al., *Pathogen-specific regulatory T cells delay the arrival of effector T cells in the lung during early tuberculosis.* J Exp Med, 2010. **207**(7): p. 1409-20.

73. Hanekom, W., et al., *Mycobacterium tuberculosis inhibits maturation of human monocyte-derived dendritic cells in vitro.* J Infect Dis, 2003. **188**: p. 257-66.

74. Satchidanandam, V., et al., *The glycosylated Rv1860 protein of mycobacterium tuberculosis inhibits dendritic cell mediated TH1 and TH17 polarization of T cells and abrogates protective immunity conferred by BCG.* PLoS Pathog, 2014. **10**(6): p. e1004176.

75. Chackerian, A.A., et al., *Dissemination of Mycobacterium tuberculosis Is Influenced by Host Factors and Precedes the Initiation of T-Cell Immunity.* Infection and Immunity, 2002. **70**(8): p. 4501-4509.

76. Reiley, W.W., et al., *ESAT-6-specific CD4 T cell responses to aerosol Mycobacterium tuberculosis infection are initiated in the mediastinal lymph nodes.* Proc Natl Acad Sci U S A, 2008. **105**(31): p. 10961-6.

77. Ulrichs, T., et al., *Human tuberculous granulomas induce peripheral lymphoid follicle-like structures to orchestrate local host defence in the lung.* J Pathol, 2004. **204**(2): p. 217-28.

78. Phuah, J.Y., et al., *Activated B cells in the granulomas of nonhuman primates infected with Mycobacterium tuberculosis.* Am J Pathol, 2012. **181**(2): p. 508-14.

79. Kahnert, A., et al., *Mycobacterium tuberculosis triggers formation of lymphoid structure in murine lungs.* J Infect Dis, 2007. **195**: p. 46-54.

80. Mattila, J.T., et al., *Granzyme B-expressing neutrophils correlate with bacterial load in granulomas from Mycobacterium tuberculosis-infected cynomolgus macaques.* Cell Microbiol, 2015. **17**(8): p. 1085-97.

81. Eum, S.Y., et al., *Neutrophils are the predominant infected phagocytic cells in the airways of patients with active pulmonary TB.* Chest, 2010. **137**(1): p. 122-8.

82. Marakalala, M.J., et al., *Inflammatory signaling in human tuberculosis granulomas is spatially organized.* Nat Med, 2016.

83. Via, L.E., et al., *Tuberculous granulomas are hypoxic in guinea pigs, rabbits, and nonhuman primates.* Infect Immun, 2008. **76**(6): p. 2333-40.

84. Galagan, J.E., et al., *The Mycobacterium tuberculosis regulatory network and hypoxia.* Nature, 2013. **499**(7457): p. 178-83.

85. Munoz-Elias, E.J., et al., *Replication dynamics of Mycobacterium tuberculosis in chronically infected mice.* Infect Immun, 2005. **73**(1): p. 546-51.

86. Lin, P.L., et al., *Sterilization of granulomas is common in active and latent tuberculosis despite within-host variability in bacterial killing.* Nat Med, 2014. **20**(1): p. 75-9.

87. Barrios-Payan, J., et al., *Extrapulmonary locations of mycobacterium tuberculosis DNA during latent infection.* J Infect Dis, 2012. **206**(8): p. 1194-205.

88. Chan, J., et al., *Killing of virulent Mycobacterium tuberculosis by reactive nitrogen intermediates produced by activated murine macrophages.* J Exp Med, 1992. **175**: p. 1111.

89. Caron, E. and A. Hall, *Identification of two distinct mechanisms of phagocytosis controlled by different rho GTPases.* Science, 1998. **282**: p. 1717.

90. Behar, S.M., et al., *Apoptosis is an innate defense function of macrophages against Mycobacterium tuberculosis.* Mucosal Immunol, 2011. **4**(3): p. 279-87.

91. Divangahi, M., et al., *Eicosanoid pathways regulate adaptive immunity to Mycobacterium tuberculosis.* Nat Immunol, 2010. **11**(8): p. 751-8.

92. Fabri, M., et al., *Vitamin D is required for IFN-g-mediated antimicrobial activity of human macrophages.* Sci Transl Med, 2011. **3**(104).

93. Kimmey, J.M., et al., *Unique role for ATG5 in neutrophil-mediated immunopathology during M. tuberculosis infection.* Nature, 2015. **528**(7583): p. 565-9.

94. Gatfield, J. and J. Pieters, *Essential role for cholesterol in entry of mycobacteria into macrophages.* Science, 2000. **288**: p. 1647.

95. Harding, C.V. and W.H. Boom, *Regulation of antigen presentation by Mycobacterium tuberculosis: a role for Toll-like receptors.* Nat Rev Microbiol, 2010. **8**(4): p. 296-307.

96. Cambier, C.J., et al., *Mycobacteria manipulate macrophage recruitment through coordinated use of membrane lipids.* Nature, 2014. **505**(7482): p. 218-22.

97. Mehra, A., et al., *Mycobacterium tuberculosis type VII secreted effector EsxH targets host ESCRT to impair trafficking.* PLoS Pathog, 2013. **9**(10): p. e1003734.

98. Keane, J., H.G. Remold, and H. Kornfeld, *Virulent Mycobacterium tuberculosis Strains Evade Apoptosis of Infected Alveolar Macrophages.* The Journal of Immunology, 2000. **164**(4): p. 2016-2020.

99. Velmurugan, K., et al., *Mycobacterium tuberculosis nuoG is a virulence gene that inhibits apoptosis of infected host cells.* PLoS Pathog, 2007. **3**(7): p. e110.

100. Patel, N.R., et al., *HIV Impairs TNF- Mediated Macrophage Apoptotic Response to Mycobacterium tuberculosis.* The Journal of Immunology, 2007. **179**(10): p. 6973-6980.

101. Gan, H., et al., *Mycobacterium tuberculosis blocks crosslinking of annexin-1 and apoptotic envelope formation on infected macrophages to maintain virulence.* Nat Immunol, 2008. **9**(10): p. 1189-97.

102. Wong, K.W. and W.R. Jacobs, Jr., *Critical role for NLRP3 in necrotic death triggered by Mycobacterium tuberculosis.* Cell Microbiol, 2011. **13**(9): p. 1371-84.

103. Srinivasan, L., et al., *Identification of a Transcription Factor That Regulates Host Cell Exit and Virulence of Mycobacterium tuberculosis.* PLoS Pathog, 2016. **12**(5): p. e1005652.

104. Srivastava, S., P.S. Grace, and J.D. Ernst, *Antigen Export Reduces Antigen Presentation and Limits T Cell Control of M. tuberculosis.* Cell Host Microbe, 2016. **19**(1): p. 44-54.

105. Flynn, J., et al., *Experimental animal models of tuberculosis*, in *Handbook of Tuberculosis: immunology and Cell Biology*, S.H. Kaufmann and W.J. Britton, Editors. 2008, Wiley-VCH. p. 389-417.

106. McShane, H. and A. Williams, *A review of preclinical animal models utilised for TB vaccine evaluation in the context of recent human efficacy data.* Tuberculosis (Edinb), 2014. **94**(2): p. 105-10.

107. Scanga, C.A. and J.L. Flynn, *Modeling tuberculosis in nonhuman primates.* Cold Spring Harb Perspect Med, 2014. **4**(12): p. a018564.

108. Barclay, W.R., et al., *Aerosol-induced tuberculosis in subhuman primates and the course of the disease after intravenous BCG vacination.* Infect Immun, 1970. **2**(5): p. 574-82.

109. Barclay, W.R., et al., *Protection of monkeys against airborne tuberculosis by aerosol vaccination with bacillus Calmette-Guerin.* Am Rev Respir Dis, 1973. **107**: p. 351.

110. Walsh, G.P., et al., *The Philippine cynomolgus monkeys (Macaca fasicularis) provides a new nonhuman primate model of tuberculosis that resembles human disease.* Nat Med, 1996. **2**(4): p. 430.

111. Capuano, S.V., 3rd, et al., *Experimental Mycobacterium tuberculosis infection of cynomolgus macaques closely resembles the various manifestations of human M. tuberculosis infection.* Infect Immun, 2003. **71**(10): p. 5831-44.

112. Rizvi, N., N.A. Rao, and M. Hussain, *Yield of gastric lavage and bronchial wash in pulmonary tuberculosis.* Int J Tuberc Lung Dis, 2000. **4**(2): p. 147-51.

113. Al-Marri, M. and M.B. Kirkpatrick, *Erythrocyte sedimentation rate in childhood tuberculosis: is it stil worthwhile?* Int J Tuberc Lung Dis, 2000. **4**(3): p. 237-9.

114. Gormus, B.J., et al., *Evidence for a rhesus monkey model of aymptomatic tuberculosis.* J Med Primatol, 2004. **33**: p. 134-45.

115. Lin, P.L., et al., *Early events in Mycobacterium tuberculosis infection in cynomolgus macaques.* Infect Immun, 2006. **74**(7): p. 3790-803.

116. Sibley, L., et al., *Route of delivery to the airway influences the distribution of pulmonary disease but not the outcome of Mycobacterium tuberculosis infection in rhesus macaques.* Tuberculosis (Edinb), 2015.

117. Lewinsohn, D.M., et al., *High resolution radiographic and fine immunologic definition of TB disease progression in the rhesus macaque.* Microbes Infect, 2006. **8**(11): p. 2587-98.

118. Sharpe, S.A., et al., *Determination of lesion volume by MRI and stereology in a macaque model of tuberculosis.* Tuberculosis (Edinb), 2009. **89**(6): p. 405-16.

119. Yan, G., et al., *Genome sequencing and comparison of two nonhuman primate animal models, the cynomolgus and Chinese rhesus macaques.* Nat Biotechnol, 2011. **29**(11): p. 1019-23.

120. Mothe, B.R., et al., *The TB-specific CD4(+) T cell immune repertoire in both cynomolgus and rhesus macaques largely overlap with humans.* Tuberculosis (Edinb), 2015. **95**(6): p. 722-35.

121. Weill-Halle, B. and R. Turpin, *Premiers essais de vaccination antituberculeuse de l'enfant par le Bacille Calmette-Guerin (BCG).* Bull Mem Soc Med l'Hosp de Paris, 1925. **49**: p. 1589-601.

122. Calmette, A., *Preventive vaccination against tuberculosis with BCG.* Proc R Soc Med, 1931. **24**(11): p. 1481-90.

123. *The Lübeck catastrophe.* Brit Med J, 1931: p. 986.

124. Comstock, G.W. and C.E. Palmer, *Long-term results of BCG vaccination in the southern United States.* Am Rev Respir Dis, 1966. **93**(2): p. 171.

125. Hart, P.D. and I. Sutherland, *BCG and vole bacillus vaccines in the prevention of tuberculosis in adolescence and early adult life.* Brit Med J, 1977. **2**: p. 293-5.

126. Aronson, N.E., et al., *Long-term efficacy of BCG vaccine in American Indians and Alaska natives.* JAMA, 2004. **291**(17): p. 2086.

127. Nguipdop-Djomo, P., et al., *Duration of BCG protection against tuberculosis and change in effectiveness with time since vaccination in Norway: a retrospective population-based cohort study.* The Lancet Infectious Diseases, 2016. **16**(2): p. 219-226.

128. (ICMR), T.R.C., *Fifteen year follow up of trial of BCG vaccinees in south India for tuberculosis prevention.* Indian J Med Res, 1999. **110**: p. 56-69.

129. Packe, G. and J. Innes, *Protective effect of BCG vaccination in infant Asians: a case-control study.* Arch Dis Child, 1988. **63**: p. 277-81.

130. Brandt, L., et al., *Failure of the Mycobacterium bovis BCG Vaccine: Some Species of Environmental Mycobacteria Block Multiplication of BCG and Induction of Protective Immunity to Tuberculosis.* Infect Immun, 2002. **70**(2): p. 672-678.

131. Black, G.F., et al., *BCG-induced increase in interferon-gamma response to mycobacterial antigens and efficacy of BCG vaccination in Malawi and the UK: two randomised controlled studies.* The Lancet, 2002. **359**(9315): p. 1393-1401.

132. Colditz, G., et al., *Efficacy of BCG Vaccine in the Prevention of Tuberculosis.* JAMA, 1994. **271**(9): p. 698-704.

133. Behr, M.A., et al., *Comparative genomics of BCG vaccines by whole-genome DNA microarray.* Science, 1999. **284**: p. 1520.

134. Murray, R.A., et al., *Bacillus Calmette-Guerin vaccination of human newborns induces a specific, functional CD8+ T cell response.* J Immunol, 2006. **177**: p. 5647-51.

135. Soares, A., et al., *Bacillus Calmette-Guerin vaccination of human newborns induces T cells with complex cytokine and phenotypic profiles.* J Immunol, 2008. **180**: p. 3569-77.

136. Lindenstrom, T., et al., *Control of chronic mycobacterium tuberculosis infection by CD4 KLRG1- IL-2-secreting central memory cells.* J Immunol, 2013. **190**(12): p. 6311-9.

137. Soares, A.P., et al., *Longitudinal changes in CD4(+) T-cell memory responses induced by BCG vaccination of newborns.* J Infect Dis, 2013. **207**(7): p. 1084-94.

138. Barreto, M.L., et al., *Evidence of an effect of BCG revaccination on incidence of tuberculosis in school-aged children in Brazil: second report of the BCG-REVAC cluster-randomised trial.* Vaccine, 2011. **29**(31): p. 4875-7.

139. Belisle, J.T., et al., *Role of the major antigen of Mycobacterium tuberculosis in cell wall biogenesis.* Science, 1997. **276**: p. 1420.

140. Prendergast, K.A., et al., *The Ag85B protein of the BCG vaccine facilitates macrophage uptake but is dispensable for protection against aerosol Mycobacterium tuberculosis infection.* Vaccine, 2016. **34**(23): p. 2608-15.

141. Horwitz, M.A. and G. Harth, *A New Vaccine against Tuberculosis Affords Greater Survival after Challenge than the Current Vaccine in the Guinea Pig Model of Pulmonary Tuberculosis.* Infection and Immunity, 2003. **71**(4): p. 1672-1679.

142. Sørensen, A.L., et al., *Purification and characterization of a low-molecular-mass T-cell antigen secreted by Mycobacterium tuberculosis.* Infect Immun, 1995. **63**(5): p. 1710-17.

143. Vordermeier, H.M., *Correlation of ESAT-6-Specific Gamma Interferon Production with Pathology in Cattle following Mycobacterium bovis BCG Vaccination against Experimental Bovine Tuberculosis.* Infection and Immunity, 2002. **70**(6): p. 3026-3032.

144. Kanaujia, G.V., et al., *Recognition of ESAT-6 Sequences by Antibodies in Sera of Tuberculous Nonhuman Primates.* Clinical and Vaccine Immunology, 2004. **11**(1): p. 222-226.

145. Pathak, S.K., et al., *Direct extracellular interaction between the early secreted antigen ESAT-6 of Mycobacterium tuberculosis and TLR2 inhibits TLR signaling in macrophages.* Nat Immunol, 2007. **8**(6): p. 610-8.

146. Smith, J., et al., *Evidence for pore formation in host cell membranes by ESX-1-secreted ESAT-6 and its role in Mycobacterium marinum escape from the vacuole.* Infect Immun, 2008. **76**(12): p. 5478-87.

147. Samten, B., X. Wang, and P.F. Barnes, *Mycobacterium tuberculosis ESX-1 system-secreted protein ESAT-6 but not CFP10 inhibits human T-cell immune responses.* Tuberculosis, 2009. **89**: p. S74-6.

148. Kinhikar, A.G., et al., *Potential role for ESAT6 in dissemination of M. tuberculosis via human lung epithelial cells.* Mol Microbiol, 2010. **75**(1): p. 92-106.

149. Simeone, R., et al., *Phagosomal rupture by Mycobacterium tuberculosis results in toxicity and host cell death.* PLoS Pathog, 2012. **8**(2): p. e1002507.

150. Mayer-Barber, K.D., et al., *Innate and adaptive interferons suppress IL-1alpha and IL-1beta production by distinct pulmonary myeloid subsets during Mycobacterium tuberculosis infection.* Immunity, 2011. **35**(6): p. 1023-34.

151. Houben, D., et al., *ESX-1-mediated translocation to the cytosol controls virulence of mycobacteria.* Cell Microbiol, 2012. **14**(8): p. 1287-98.

152. Pym, A.S., et al., *Recombinant BCG exporting ESAT-6 confers enhanced protection against tuberculosis.* Nat Med, 2003. **9**(5): p. 533-9.

153. Berthet, F., et al., *A Mycobacterium tuberculosis operon encoding ESAT-6 and a novel low-molecular-mass culture filtrate protein (CFP-10).* Microbiol, 1998. **144**: p. 3195-203.

154. Pym, A.S., et al., *Loss of RD1 contributed to the attenuation of the live tuberculosis vaccines Mycobacterium bovis BCG and Mycobacterium microti.* Mol Microbiol, 2002. **46**(3): p. 709-717.

155. Renshaw, P.S., et al., *Conclusive evidence that the major T-cell antigens of the Mycobacterium tuberculosis complex ESAT-6 and CFP-10 form a tight, 1:1 complex and characterization of the structural properties of ESAT-6, CFP-10, and the ESAT-6*CFP-*

10 complex. Implications for pathogenesis and virulence. J Biol Chem, 2002. **277**(24): p. 21598-603.

156. Guinn, K.M., et al., *Individual RD1-region genes are required for export of ESAT-6/CFP-10 and for virulence of Mycobacterium tuberculosis.* Mol Microbiol, 2004. **51**(2): p. 359-70.

157. Volkman, H.E., et al., *Tuberculous granuloma formation is enhanced by a mycobacterium virulence determinant.* PLoS Biol, 2004. **2**(11): p. e367.

158. Langermans, J.A., et al., *Divergent effect of bacillus Calmette-Guerin (BCG) vaccination on Mycobacterium tuberculosis infection in highly related macaque species: implications for primate models in tuberculosis vaccine research.* Proc Natl Acad Sci U S A, 2001. **98**(20): p. 11497-502.

159. Hervas-Stubbs, S., et al., *High frequency of CD4+ T cells specific for the TB10.4 protein correlates with protection against Mycobacterium tuberculosis infection.* Infect Immun, 2006. **74**(6): p. 3396-407.

160. Dillon, D.C., et al., *Molecular characterization and human T-cell responses to a member of a novel Mycobacterium tuberculosis mtb39 gene family.* Infect Immun, 1999. **67**(6): p. 2941-50.

161. Lindestam Arlehamn, C.S., et al., *Memory T cells in latent Mycobacterium tuberculosis infection are directed against three antigenic islands and largely contained in a CXCR3+CCR6+ Th1 subset.* PLoS Pathog, 2013. **9**(1): p. e1003130.

162. Comas, I., et al., *Human T cell epitopes of Mycobacterium tuberculosis are evolutionarily hyperconserved.* Nat Genet, 2010. **42**(6): p. 498-503.

163. Woodworth, J.S., et al., *Protective CD4 T cells targeting cryptic epitopes of Mycobacterium tuberculosis resist infection-driven terminal differentiation.* J Immunol, 2014. **192**(7): p. 3247-58.

164. Betts, J.C., et al., *Evaluation of a nutrient starvation model of Mycobacterium tuberculosis persistance by gene and protein expression profiling.* Mol Microbiol, 2002. **43**(3): p. 717-31.

165. Govender, L., et al., *Higher human CD4 T cell response to novel Mycobacterium tuberculosis latency associated antigens Rv2660 and Rv2659 in latent infection compared with tuberculosis disease.* Vaccine, 2010. **29**(1): p. 51-7.

166. Houghton, J., et al., *A small RNA encoded in the Rv2660c locus of Mycobacterium tuberculosis is induced during starvation and infection.* PLoS One, 2013. **8**(12): p. e80047.

167. Jiang, X., et al., *Skin infection generates non-migratory memory CD8+ T(RM) cells providing global skin immunity.* Nature, 2012. **483**(7388): p. 227-31.

168. Flynn, J.L. and J. Chan, *Immunology of tuberculosis.* Annu Rev Immunol, 2001. **19**: p. 93-129.

169. O'Garra, A., et al., *The immune response in tuberculosis.* Annu Rev Immunol, 2013. **31**: p. 475-527.

170. Havlir, D.V. and P.F. Barnes, *Tuberculosis in patients with human immunodeficiency virus infection.* N Engl J Med, 1999. **340**(5): p. 367.

171. Lawn, S.D., et al., *Short-term and long-term risk of tuberculosis associated with CD4 cell recovery during antiretroviral therapy in South Africa.* AIDS, 2009. **23**(13): p. 1717-25.

172. Diedrich, C.R., et al., *Reactivation of latent tuberculosis in cynomolgus macaques infected with SIV is associated with early peripheral T cell depletion and not virus load.* PLoS One, 2010. **5**(3): p. e9611.

173. Gallegos, A.M., E.G. Pamer, and M.S. Glickman, *Delayed protection by ESAT-6-specific effector CD4+ T cells after airborne M. tuberculosis infection.* J Exp Med, 2008. **205**(10): p. 2359-68.

174. Connor, L.M., et al., *A key role for lung-resident memory lymphocytes in protective immune responses after BCG vaccination.* Eur J Immunol, 2010. **40**(9): p. 2482-92.

175. Srivastava, S. and J.D. Ernst, *Cutting edge: Direct recognition of infected cells by CD4 T cells is required for control of intracellular Mycobacterium tuberculosis in vivo.* J Immunol, 2013. **191**(3): p. 1016-20.

176. Sakai, S., et al., *Cutting edge: control of Mycobacterium tuberculosis infection by a subset of lung parenchyma-homing CD4 T cells.* J Immunol, 2014. **192**(7): p. 2965-9.

177. Zhang, M., et al., *T-cell cytokine responses in human infection with Mycobacterium tuberculosis.* Infect Immun, 1995. **63**(8): p. 3231.

178. Wangoo, A., et al., *Contribution of Th1 and Th2 cells to protection and pathology in experimental models of granulomatous lung disease.* J Immunol, 2001. **166**: p. 3432-9.

179. Rook, G.A., et al., *IL-4 in tuberculosis: implications for vaccine design.* Trends Immunol, 2004. **25**(9): p. 483-8.

180. Lin, Y., et al., *Absence of a prominent Th2 cytokine response in human tuberculosis.* Infect Immun, 1996. **64**(4): p. 1351-6.

181. Chatterjee, S., et al., *Filarial infection modulates the immune response to Mycobacterium tuberculosis through expansion of CD4+ IL-4 memory T cells.* J Immunol, 2015. **194**(6): p. 2706-14.

182. Flynn, J.L., et al., *An essential role for interferon gamma in resistance to Mycobacterium tuberculosis infection.* J Exp Med, 1993. **178**: p. 2249-54.

183. Cooper, A., et al., *Disseminated tuberculosis in interferon gamma gene-disrupted mice.* J Exp Med, 1993. **178**: p. 2243-7.

184. Seder, R., et al., *Interleukin 12 acts directly on CD4+ T cells to enhance priming for interferon gamma production and minishes interleukin 4 inhibition of such priming.* Proc Natl Acad Sci U S A, 1993. **90**: p. 10188-92.

185. Cooper, A., et al., *The role of interleukin-12 in acquired immunity to Mycobacterium tuberculosis infection.* Immunology, 1995. **84**: p. 423-32.

186. Flynn, J.L., et al., *IL-12 increases resistance of BALB/c mice to Mycobacterium tuberculosis infection.* J Immunol, 1995. **155**: p. 2515-24.

187. Jouanguy, E., et al., *Interferon-gamma-receptor deficiency in an infant with fatal bacille Calmette-Guérin infection.* N Engl J Med, 1996. **335**(26): p. 1956.

188. de Jong, R., *Severe Mycobacterial and Salmonella Infections in Interleukin-12 Receptor-Deficient Patients.* Science, 1998. **280**(5368): p. 1435-1438.

189. Jouanguy, E., et al., *A human IFNGR1 small deletion hotspot assocaited with dominant susceptibility to mycobacterial infection.* Nat Genet, 1999. **21**: p. 370.

190. Green, A.M., R. DiFazio, and J.L. Flynn, *IFN-gamma from CD4 T cells is essential for host survival and enhances CD8 T cell function during Mycobacterium tuberculosis infection.* J Immunol, 2013. **190**(1): p. 270-7.

191. Jacobs, M., et al., *Fatal Mycobacterium bovis BCG infection in TNF-LT-alpha-deficient mice.* Clin Immunol, 2000. **94**(3): p. 192-9.

192. Flynn, J.L., et al., *Tumor necrosis factor-a is required in the protective immune response against Mycobacterium tuberculosis in mice.* Immunity, 1995. **2**: p. 561-72.

193. Keane, J., et al., *Tuberculosis associated with infliximab, a tumor necrosis factor a-neutralizing agent.* N Engl J Med, 2001. **345**(15): p. 1098-104.

194. Harris, J., J.C. Hope, and J. Keane, *Tumor necrosis factor blockers influence macrophage responses to Mycobacterium tuberculosis.* J Infect Dis, 2008. **198**(12): p. 1842-50.

195. Ray, J.C., J.L. Flynn, and D.E. Kirschner, *Synergy between individual TNF-dependent functions determines granuloma performance for controlling Mycobacterium tuberculosis infection.* J Immunol, 2009. **182**(6): p. 3706-17.

196. Algood, H.M.S., et al., *TNF Influences Chemokine Expression of Macrophages In Vitro and That of CD11b+ Cells In Vivo during Mycobacterium tuberculosis Infection.* The Journal of Immunology, 2004. **172**(11): p. 6846-6857.

197. Bruns, H., et al., *Anti-TNF immunotherapy reduces CD8+ T cell-mediated antimicrobial activity against Mycobacterium tuberculosis in humans.* J Clin Invest, 2009. **119**(5): p. 1167-77.

198. Giardina, A.R., et al., *Blocking TNF in vitro with infliximab determines the inhibition of expansion and interferon gamma production of Vgamma9/Vdelta2 T lymphocytes from patients with active rheumatoid arthritis.* Reumatismo, 2009. **61**(1): p. 21-6.

199. Verbon, A., et al., *Serum concentrations of cytokines in patients with active tuberculosis (TB) and after treatment.* Clin Exp Immunol, 1999. **115**: p. 110-3.

200. Tsao, T., et al., *Levels of interferon-gamma and interleukin-2 receptor-a for bronchoalveolar lavage fluid and serum were correlated with clinical grade and treatment of pulmonary tuberculosis.* Int J Tuberc Lung Dis, 2002. **6**(8): p. 720-7.

201. Sakai, S., et al., *CD4 T Cell-Derived IFN-gamma Plays a Minimal Role in Control of Pulmonary Mycobacterium tuberculosis Infection and Must Be Actively Repressed by PD-1 to Prevent Lethal Disease.* PLoS Pathog, 2016. **12**(5): p. e1005667.

202. Cowley, S.C. and K.L. Elkins, *CD4+ T Cells Mediate IFN- -Independent Control of Mycobacterium tuberculosis Infection Both In Vitro and In Vivo.* The Journal of Immunology, 2003. **171**(9): p. 4689-4699.

203. Gallegos, A.M., et al., *A gamma interferon independent mechanism of CD4 T cell mediated control of M. tuberculosis infection in vivo.* PLoS Pathog, 2011. **7**(5): p. e1002052.

204. Orr, M.T., et al., *Interferon gamma and Tumor Necrosis Factor Are Not Essential Parameters of CD4+ T-Cell Responses for Vaccine Control of Tuberculosis.* J Infect Dis, 2015. **212**(3): p. 495-504.

205. Derrick, S.C., et al., *Immunization with a DNA Vaccine Cocktail Protects Mice Lacking CD4 Cells against an Aerogenic Infection with Mycobacterium tuberculosis.* Infection and Immunity, 2004. **72**(3): p. 1685-1692.

206. Flynn, J.L., et al., *Major histocompatibility complex class I-restricted T cells are required for resistance to Mycobacterium tuberculosis infection.* Proc Natl Acad Sci U S A, 1992. **89**: p. 12013-7.

207. Stenger, S., et al., *An antimicrobial activity of cytolytic T cells mediated by granulysin.* Science, 1998. **282**: p. 121.

208. van Pinxteren, L.A., et al., *Control of latent Mycobacterium tuberculosis infection is dependent on CD8 T cells.* Eur J Immunol, 2000. **30**(12): p. 3689-98.

209. Chen, C.Y., et al., *A critical role for CD8 T cells in a nonhuman primate model of tuberculosis.* PLoS Pathog, 2009. **5**(4): p. e1000392.

210. Lindenstrom, T., et al., *High-frequency vaccine-induced CD8(+) T cells specific for an epitope naturally processed during infection with Mycobacterium tuberculosis do not confer protection.* Eur J Immunol, 2014. **44**(6): p. 1699-709.

211. Baldwin, S.L., et al., *Protection against tuberculosis with homologous or heterologous protein/vector vaccine approaches is not dependent on CD8+ T cells.* J Immunol, 2013. **191**(5): p. 2514-25.

212. Scott-Browne, J.P., et al., *Expansion and function of Foxp3-expressing T regulatory cells during tuberculosis.* J Exp Med, 2007. **204**(9): p. 2159-69.

213. Windish, H.P., et al., *Aberrant TGF-beta signaling reduces T regulatory cells in ICAM-1-deficient mice, increasing the inflammatory response to Mycobacterium tuberculosis.* J Leukoc Biol, 2009. **86**(3): p. 713-25.

214. Green, A.M., et al., *CD4(+) regulatory T cells in a cynomolgus macaque model of Mycobacterium tuberculosis infection.* J Infect Dis, 2010. **202**(4): p. 533-41.

215. Dieli, F., et al., *Vgamma9/Vdelta2 T lymphocytes reduce the viability of intracellular Mycobacterium tuberculosis.* Eur J Immunol, 2000. **30**(5): p. 1512-9.

216. Lockhart, E., A.M. Green, and J.L. Flynn, *IL-17 Production Is Dominated by T Cells rather than CD4 T Cells during Mycobacterium tuberculosis Infection.* The Journal of Immunology, 2006. **177**(7): p. 4662-4669.

217. Umemura, M., et al., *IL-17-mediated regulation of innate and acquired immune response against pulmonary Mycobacterium bovis bacille Calmette-Guérin infection.* J Immunol, 2007. **178**: p. 3786-96.

218. Montoya, C.J., et al., *Invariant NKT cells from HIV-1 or Mycobacterium tuberculosis-infected patients express an activated phenotype.* Clin Immunol, 2008. **127**(1): p. 1-6.

219. Venkataswamy, M.M., et al., *Incorporation of NKT cell-activating glycolipids enhances immunogenicity and vaccine efficacy of Mycobacterium bovis bacillus Calmette-Guerin.* J Immunol, 2009. **183**(3): p. 1644-56.

220. Gold, M.C., et al., *Human mucosal associated invariant T cells detect bacterially infected cells.* PLoS Biol, 2010. **8**(6): p. e1000407.

221. Kasmar, A.G., et al., *CD1b tetramers bind alphabeta T cell receptors to identify a mycobacterial glycolipid-reactive T cell repertoire in humans.* J Exp Med, 2011. **208**(9): p. 1741-7.

222. Tameris, M., et al., *A double-blind, randomised, placebo-controlled, dose-finding trial of the novel tuberculosis vaccine AERAS-402, an adenovirus-vectored fusion protein, in healthy, BCG-vaccinated infants.* Vaccine, 2015. **33**(25): p. 2944-54.

223. Greene, J.M., et al., *MR1-restricted mucosal-associated invariant T (MAIT) cells respond to mycobacterial vaccination and infection in nonhuman primates.* Mucosal Immunol, 2016.

224. Teitelbaum, R., et al., *A mAb recognizing a surface antigen of Mycobacterium tuberculosis enhances host survival.* Proc Natl Acad Sci U S A, 1998. **95**: p. 15688-93.

225. Brusasca, P.N., et al., *Antigen recognition by serum antibodies in non-human primates experimentally infected with Mycobacterium tuberculosis.* Comp Med, 2003. **53**(2): p. 165-72.

226. Kunnath-Velayudhan, S., et al., *Proteome-scale antibody responses and outcome of Mycobacterium tuberculosis infection in nonhuman primates and in tuberculosis patients.* J Infect Dis, 2012. **206**(5): p. 697-705.

227. Kozakiewicz, L., et al., *B cells regulate neutrophilia during Mycobacterium tuberculosis infection and BCG vaccination by modulating the interleukin-17 response.* PLoS Pathog, 2013. **9**(7): p. e1003472.

228. du Plessis, W.J., et al., *The Functional Response of B Cells to Antigenic Stimulation: A Preliminary Report of Latent Tuberculosis.* PLoS One, 2016. **11**(4): p. e0152710.

229. Lu, L.L., et al., *A Functional Role for Antibodies in Tuberculosis.* Cell, 2016. **167**(2): p. 433-443 e14.

230. Khader, S.A., et al., *IL-23 Compensates for the Absence of IL-12p70 and Is Essential for the IL-17 Response during Tuberculosis but Is Dispensable for Protection and Antigen-Specific IFN- Responses if IL-12p70 Is Available.* The Journal of Immunology, 2005. **175**(2): p. 788-795.

231. Khader, S.A., et al., *IL-23 and IL-17 in the establishment of protective pulmonary CD4+ T cell responses after vaccination and during Mycobacterium tuberculosis challenge.* Nat Immunol, 2007. **8**(4): p. 369-77.

232. Vordermeier, H.M., et al., *Viral booster vaccines improve Mycobacterium bovis BCG-induced protection against bovine tuberculosis.* Infect Immun, 2009. **77**(8): p. 3364-73.

233. Gopal, R., et al., *Interleukin-17-dependent CXCL13 mediates mucosal vaccine-induced immunity against tuberculosis.* Mucosal Immunol, 2013. **6**(5): p. 972-84.

234. Redford, P.S., et al., *Enhanced protection to Mycobacterium tuberculosis infection in IL-10-deficient mice is accompanied by early and enhanced Th1 responses in the lung.* Eur J Immunol, 2010. **40**(8): p. 2200-10.

235. Balcewicz-Sablinska, M.K., et al., *Pathogenic Mycobacterium tuberculosis evades apoptosis of host macrophages by release of TNF-R2, resulting in inactivation of TNF-a.* J Immunol, 1998. **161**: p. 2636-41.

236. Othieno, C., et al., *Interaction of Mycobacterium tuberculosis-induced transforming growth factor beta1 and interleukin-10.* Infect Immun, 1999. **67**(11): p. 5730-5735.

237. Schreiber, T., et al., *Autocrine IL-10 induces hallmarks of alternative activation in macrophages and suppresses antituberculosis effector mechanisms without compromising T cell immunity.* J Immunol, 2009. **183**(2): p. 1301-12.

238. Higgins, D.M., et al., *Lack of IL-10 alters inflammatory and immune responses during pulmonary Mycobacterium tuberculosis infection.* 2009.

239. Gideon, H.P., et al., *Variability in tuberculosis granuloma T cell responses exists, but a balance of pro- and anti-inflammatory cytokines is associated with sterilization.* PLoS Pathog, 2015. **11**(1): p. e1004603.

240. Cilfone, N.A., et al., *Computational modeling predicts IL-10 control of lesion sterilization by balancing early host immunity-mediated antimicrobial responses with caseation during mycobacterium tuberculosis infection.* J Immunol, 2015. **194**(2): p. 664-77.

241. Toossi, Z., et al., *Enhanced production of TGF-beta by blood monocytes from patients with active tuberculosis and presence of TGF-beta in tuberculous granulomatous lung lesions.* J Immunol, 1995. **154**(1): p. 465-73.

242. Aung, H., et al., *Expression of transforming growth factor-β but not tumor necrosis factor-α, interferon-γ, and interleukin-4 in granulomatous lung lesions in tuberculosis.* Tubercle and Lung Disease, 2000. **80**(2): p. 61-67.

243. Toossi, Z., et al., *Induction of transforming growth factor beta 1 by purified protein derivative of Mycobacterium tuberculosis.* Infect Immun, 1995. **63**(1): p. 224-8.

244. Marshall, B.G., et al., *Enhanced antimycobacterial response to recombinant Mycobacterium bovis BCG expressing latency-associated peptide.* Infect Immun, 2001. **69**(11): p. 6676-82.

245. Aung, H., et al., *Bioactivation of latent transforming growth factor beta1 by Mycobacterium tuberculosis in human mononuclear phagocytes.* Scand J Immunol, 2005. **61**(6): p. 558-65.

246. Rosas-Taraco, A.G., et al., *Local pulmonary immunotherapy with siRNA targeting TGFbeta1 enhances antimicrobial capacity in Mycobacterium tuberculosis infected mice.* Tuberculosis (Edinb), 2011. **91**(1): p. 98-106.

247. Obieglo, K., et al., *Chronic Gastrointestinal Nematode Infection Mutes Immune Responses to Mycobacterial Infection Distal to the Gut.* J Immunol, 2016. **196**(5): p. 2262-71.

248. Barber, D.L., et al., *CD4 T cells promote rather than control tuberculosis in the absence of PD-1-mediated inhibition.* J Immunol, 2011. **186**(3): p. 1598-607.

249. Manca, C., et al., *Virulence of a Mycobacterium tuberculosis clinical isolate in mice is determined by failure to induce Th1 type immunity and is associated with induction of IFN-alpha /beta.* Proc Natl Acad Sci U S A, 2001. **98**(10): p. 5752-7.

250. Stanley, S.A., et al., *The Type I IFN Response to Infection with Mycobacterium tuberculosis Requires ESX-1-Mediated Secretion and Contributes to Pathogenesis.* The Journal of Immunology, 2007. **178**(5): p. 3143-3152.

251. Antonelli, L.R., et al., *Intranasal Poly-IC treatment exacerbates tuberculosis in mice through the pulmonary recruitment of a pathogen-permissive monocyte/macrophage population.* J Clin Invest, 2010. **120**(5): p. 1674-82.

252. Teles, R.M., et al., *Type I interferon suppresses type II interferon-triggered human anti-mycobacterial responses.* Science, 2013. **339**(6126): p. 1448-53.

253. Divangahi, M., et al., *Mycobacterium tuberculosis evades macrophage defenses by inhibiting plasma membrane repair.* Nat Immunol, 2009. **10**(8): p. 899-906.

254. Mayer-Barber, K.D., et al., *Caspase-1 independent IL-1beta production is critical for host resistance to mycobacterium tuberculosis and does not require TLR signaling in vivo.* J Immunol, 2010. **184**(7): p. 3326-30.

255. Mayer-Barber, K.D., et al., *Host-directed therapy of tuberculosis based on interleukin-1 and type I interferon crosstalk.* Nature, 2014. **511**(7507): p. 99-103.

256. Qin, L., et al., *A framework for assessing immunological correlates of protection in vaccine trials.* J Infect Dis, 2007. **196**(9): p. 1304-12.

257. Abebe, F., *Is interferon-gamma the right marker for bacille Calmette-Guerin-induced immune protection? The missing link in our understanding of tuberculosis immunology.* Clin Exp Immunol, 2012. **169**(3): p. 213-9.

258. Nunes-Alves, C., et al., *In search of a new paradigm for protective immunity to TB.* Nat Rev Microbiol, 2014. **12**(4): p. 289-99.

259. Badell, E., et al., *Protection against tuberculosis induced by oral prime with Mycobacterium bovis BCG and intranasal subunit boost based on the vaccine candidate Ag85B-ESAT-6 does not correlate with circulating IFN-gamma producing T-cells.* Vaccine, 2009. **27**(1): p. 28-37.

260. Darrah, P.A., et al., *Multifunctional TH1 cells define a correlate of vaccine-mediated protection against Leishmania major.* Nat Med, 2007. **13**(7): p. 843-50.

261. Mueller, H., et al., *Mycobacterium tuberculosis-specific CD4+, IFNgamma+, and TNFalpha+ multifunctional memory T cells coexpress GM-CSF.* Cytokine, 2008. **43**(2): p. 143-8.

262. Caccamo, N., et al., *Multifunctional CD4(+) T cells correlate with active Mycobacterium tuberculosis infection.* Eur J Immunol, 2010. **40**(8): p. 2211-20.

263. Mattila, J.T., et al., *Simian immunodeficiency virus-induced changes in T cell cytokine responses in cynomolgus macaques with latent Mycobacterium tuberculosis infection are associated with timing of reactivation.* J Immunol, 2011. **186**(6): p. 3527-37.

264. Kagina, B.M., et al., *Specific T cell frequency and cytokine expression profile do not correlate with protection against tuberculosis after bacillus Calmette-Guerin vaccination of newborns.* Am J Respir Crit Care Med, 2010. **182**(8): p. 1073-9.

265. Darrah, P.A., et al., *Aerosol vaccination with AERAS-402 elicits robust cellular immune responses in the lungs of rhesus macaques but fails to protect against high-dose Mycobacterium tuberculosis challenge.* J Immunol, 2014. **193**(4): p. 1799-811.

266. Verhagen, L.M., et al., *A predictive signature gene set for discriminating active from latent tuberculosis in Warao Amerindian children.* BMC Genomics, 2013. **14**(74).

267. Kurtz, S.L. and K.L. Elkins, *Correlates of Vaccine-Induced Protection against Mycobacterium tuberculosis Revealed in Comparative Analyses of Lymphocyte Populations.* Clin Vaccine Immunol, 2015. **22**(10): p. 1096-108.

268. Fletcher, H.A., et al., *T-cell activation is an immune correlate of risk in BCG vaccinated infants.* Nat Commun, 2016. **7**: p. 11290.

269. Zak, D.E., et al., *A blood RNA signature for tuberculosis disease risk: a prospective cohort study.* The Lancet, 2016.

270. Romano, M. and K. Huygen, *An update on vaccines for tuberculosis - there is more to it than just waning of BCG efficacy with time.* Exp Opin Biol Ther, 2012. **12**(12): p. 1601-10.

271. Brandt, L., et al., *The protective effect of the Mycobacterium bovis BCG vaccine is increased by coadministration with the Mycobacterium tuberculosis 72-kilodalton fusion polyprotein Mtb72F in M. tuberculosis-infected guinea pigs.* Infect Immun, 2004. **72**(11): p. 6622-32.

272. Leroux-Roels, I., et al., *Improved CD4(+) T cell responses to Mycobacterium tuberculosis in PPD-negative adults by M72/AS01 as compared to the M72/AS02 and Mtb72F/AS02 tuberculosis candidate vaccine formulations: a randomized trial.* Vaccine, 2013. **31**(17): p. 2196-206.

273. Reed, S.G., et al., *Defined tuberculosis vaccine, Mtb72F/AS02A, evidence of protection in cynomolgus monkeys.* Proc Natl Acad Sci U S A, 2009. **106**(7): p. 2301-6.

274. Aagaard, C., et al., *A multistage tuberculosis vaccine that confers efficient protection before and after exposure.* Nat Med, 2011. **17**(2): p. 189-94.

275. Lin, P.L., et al., *The multistage vaccine H56 boosts the effects of BCG to protect cynomolgus macaques against active tuberculosis and reactivation of latent Mycobacterium tuberculosis infection.* J Clin Invest, 2012. **122**(1): p. 303-14.

276. Luabeya, A.K., et al., *First-in-human trial of the post-exposure tuberculosis vaccine H56:IC31 in Mycobacterium tuberculosis infected and non-infected healthy adults.* Vaccine, 2015. **33**(33): p. 4130-40.

277. Woodworth, J.S., et al., *Subunit vaccine H56/CAF01 induces a population of circulating CD4 T cells that traffic into the Mycobacterium tuberculosis-infected lung.* Mucosal Immunol, 2016.

278. Hoft, D.F., et al., *A new recombinant bacille Calmette-Guerin vaccine safely induces significantly enhanced tuberculosis-specific immunity in human volunteers.* J Infect Dis, 2008. **198**(10): p. 1491-501.

279. Grode, L., et al., *Increased vaccine efficacy against tuberculosis of recombinant Mycobacterium bovis bacille Calmette-Guerin mutants that secrete listeriolysin.* J Clin Invest, 2005. **115**(9): p. 2472-9.

280. Desel, C., et al., *Recombinant BCG DeltaureC hly+ induces superior protection over parental BCG by stimulating a balanced combination of type 1 and type 17 cytokine responses.* J Infect Dis, 2011. **204**(10): p. 1573-84.

281. Grode, L., et al., *Safety and immunogenicity of the recombinant BCG vaccine VPM1002 in a phase 1 open-label randomized clinical trial.* Vaccine, 2013. **31**(9): p. 1340-8.

282. Sun, R., et al., *Novel recombinant BCG expressing perfringolysin O and the over-expression of key immunodominant antigens; pre-clinical characterization, safety and protection against challenge with Mycobacterium tuberculosis.* Vaccine, 2009. **27**(33): p. 4412-23.

283. Hoft, D.F., et al., *Safety and Immunogenicity of the Recombinant BCG Vaccine AERAS-422 in Healthy BCG-naive Adults: A Randomized, Active-controlled, First-in-human Phase 1 Trial.* EBioMedicine, 2016. **7**: p. 278-86.

284. Kupferschmidt, K., *Taking a new shot at a TB vaccine.* Science, 2011. **334**: p. 1488-90.

285. Martin, C., *Tuberculosis vaccines: past, present and future.* Curr Opin Pul Med, 2006. **12**: p. 186-91.

286. Verreck, F.A., et al., *MVA.85A boosting of BCG and an attenuated, phoP deficient M. tuberculosis vaccine both show protective efficacy against tuberculosis in rhesus macaques.* PLoS One, 2009. **4**(4): p. e5264.

287. Arbues, A., et al., *Construction, characterization and preclinical evaluation of MTBVAC, the first live-attenuated M. tuberculosis-based vaccine to enter clinical trials.* Vaccine, 2013. **31**(42): p. 4867-73.

288. Spertini, F., et al., *Safety of human immunisation with a live-attenuated Mycobacterium tuberculosis vaccine: a randomised, double-blind, controlled phase I trial.* The Lancet Respiratory Medicine, 2015. **3**(12): p. 953-962.

289. Kaushal, D., et al., *Mucosal vaccination with attenuated Mycobacterium tuberculosis induces strong central memory responses and protects against tuberculosis.* Nat Commun, 2015. **6**: p. 8533.

290. Brennan, M.J., et al., *Preclinical evidence for implementing a prime-boost vaccine strategy for tuberculosis.* Vaccine, 2012. **30**(18): p. 2811-23.

291. Hawkridge, T., et al., *Safety and immunogenicity of a new tuberculosis vaccine, MVA85A, in healthy adults in South Africa.* J Infect Dis, 2008. **198**(4): p. 544-52.

292. Scriba, T.J., et al., *Modified vaccinia Ankara-expressing Ag85A, a novel tuberculosis vaccine, is safe in adolescents and children, and induces polyfunctional CD4+ T cells.* Eur J Immunol, 2010. **40**(1): p. 279-90.

293. Scriba, T.J., et al., *Dose-finding study of the novel tuberculosis vaccine, MVA85A, in healthy BCG-vaccinated infants.* J Infect Dis, 2011. **203**(12): p. 1832-43.

294. Scriba, T.J., et al., *A phase IIa trial of the new tuberculosis vaccine, MVA85A, in HIV- and/or Mycobacterium tuberculosis-infected adults.* Am J Respir Crit Care Med, 2012. **185**(7): p. 769-78.

295. Tameris, M.D., et al., *Safety and efficacy of MVA85A, a new tuberculosis vaccine, in infants previously vaccinated with BCG: a randomised, placebo-controlled phase 2b trial.* The Lancet, 2013. **381**(9871): p. 1021-1028.

296. Ndiaye, B.P., et al., *Safety, immunogenicity, and efficacy of the candidate tuberculosis vaccine MVA85A in healthy adults infected with HIV-1: a randomised, placebo-controlled, phase 2 trial.* The Lancet Respiratory Medicine, 2015. **3**(3): p. 190-200.

297. Beverley, P., *TB vaccine failure was predictable.* Nature, 2013. **503**: p. 469.

298. White, A.D., et al., *Evaluation of the safety and immunogenicity of a candidate tuberculosis vaccine, MVA85A, delivered by aerosol to the lungs of macaques.* Clin Vaccine Immunol, 2013. **20**(5): p. 663.

299. Satti, I., et al., *Safety and immunogenicity of a candidate tuberculosis vaccine MVA85A delivered by aerosol in BCG-vaccinated healthy adults: a phase 1, double-blind, randomised controlled trial.* The Lancet Infectious Diseases, 2014. **14**(10): p. 939-946.

300. Abel, B., et al., *The novel tuberculosis vaccine, AERAS-402, induces robust and polyfunctional CD4+ and CD8+ T cells in adults.* Am J Respir Crit Care Med, 2010. **181**(12): p. 1407-17.

301. Hokey, D.A., et al., *A nonhuman primate toxicology and immunogenicity study evaluating aerosol delivery of AERAS-402/Ad35 vaccine: Evidence for transient t cell responses in peripheral blood and robust sustained responses in the lungs.* Hum Vaccin Immunother, 2014. **10**(8): p. 2199-210.

302. Bertholet, S., et al., *A defined tuberculosis vaccine candidate boosts BCG and protects against multidrug-resistant Mycobacterium tuberculosis.* Sci Transl Med, 2010. **2**(53).

303. Coler, R.N., et al., *Therapeutic immunization against Mycobacterium tuberculosis is an effective adjunct to antibiotic treatment.* J Infect Dis, 2013. **207**(8): p. 1242-52.

304. Skeiky, Y.A., et al., *Differential immune responses and protective efficacy induced by components of a tuberculosis polyprotein vaccine, Mtb72F, delivered as naked DNA or recombinant protein.* J Immunol, 2004. **172**(12): p. 7618-28.

305. Irwin, S.M., et al., *Tracking antigen-specific CD8 T lymphocytes in the lungs of mice vaccinated with the Mtb72F polyprotein.* Infect Immun, 2005. **73**(9): p. 5809-16.

306. Tsenova, L., et al., *Evaluation of the Mtb72F polyprotein vaccine in a rabbit model of tuberculous meningitis.* Infect Immun, 2006. **74**(4): p. 2392-401.

307. Leroux-Roels, I., et al., *Evaluation of the safety and immunogenicity of two antigen concentrations of the Mtb72F/AS02(A) candidate tuberculosis vaccine in purified protein derivative-negative adults.* Clin Vaccine Immunol, 2010. **17**(11): p. 1763-71.

308. Day, C.L., et al., *Induction and regulation of T-cell immunity by the novel tuberculosis vaccine M72/AS01 in South African adults.* Am J Respir Crit Care Med, 2013. **188**(4): p. 492-502.

309. Montoya, J., et al., *A Randomized, Controlled Dose-Finding Phase II Study of the M72/AS01 Candidate Tuberculosis Vaccine in Healthy PPD-Positive Adults.* J Clin Immunol, 2013. **33**(8): p. 1360-75.

310. Spertini, F., et al., *The candidate tuberculosis vaccine Mtb72F/AS02 in PPD positive adults: a randomized controlled phase I/II study.* Tuberculosis (Edinb), 2013. **93**(2): p. 179-88.

311. Weinrich Olsen, A., et al., *Protection of mice with a tuberculosis subunit vaccine based on a fusion protein of antigen 85b and esat-6.* Infect Immun, 2001. **69**(5): p. 2773-8.

312. Langermans, J.A., et al., *Protection of macaques against Mycobacterium tuberculosis infection by a subunit vaccine based on a fusion protein of antigen 85B and ESAT-6.* Vaccine, 2005. **23**(21): p. 2740-50.

313. Agger, E.M., et al., *Protective immunity to tuberculosis with Ag85B-ESAT-6 in a synthetic cationic adjuvant system IC31.* Vaccine, 2006. **24**(26): p. 5452-60.

314. Kamath, A.T., et al., *Adult-like anti-mycobacterial T cell and in vivo dendritic cell responses following neonatal immunization with Ag85B-ESAT-6 in the IC31 adjuvant.* PLoS One, 2008. **3**(11): p. e3683.

315. Lindenstrom, T., et al., *Tuberculosis subunit vaccination provides long-term protective immunity characterized by multifunctional CD4 memory T cells.* J Immunol, 2009. **182**(12): p. 8047-55.

316. Lindenstrom, T., et al., *Vaccine-induced th17 cells are maintained long-term postvaccination as a distinct and phenotypically stable memory subset.* Infect Immun, 2012. **80**(10): p. 3533-44.

317. van Dissel, J.T., et al., *Ag85B-ESAT-6 adjuvanted with IC31 promotes strong and long-lived Mycobacterium tuberculosis specific T cell responses in naive human volunteers.* Vaccine, 2010. **28**(20): p. 3571-81.

318. van Dissel, J.T., et al., *A novel liposomal adjuvant system, CAF01, promotes long-lived Mycobacterium tuberculosis-specific T-cell responses in human.* Vaccine, 2014. **32**(52): p. 7098-107.

319. Geldenhuys, H., et al., *The tuberculosis vaccine H4:IC31 is safe and induces a persistent polyfunctional CD4 T cell response in South African adults: A randomized controlled trial.* Vaccine, 2015. **33**(30): p. 3592-9.

320. Hoang, T., et al., *ESAT-6 (EsxA) and TB10.4 (EsxH) based vaccines for pre- and post-exposure tuberculosis vaccination.* PLoS One, 2013. **8**(12): p. e80579.

321. Beverley, P.C., et al., *Harnessing local and systemic immunity for vaccines against tuberculosis.* Mucosal Immunol, 2014. **7**(1): p. 20-6.

322. Lai, X., et al., *Immune biology of macaque lymphocyte populations during mycobacterial infection.* Clin Exp Immunol, 2003. **133**: p. 182-92.

323. Walrath, J., et al., *Resident Th1-like effector memory cells in pulmonary recall responses to Mycobacterium tuberculosis.* Am J Respir Cell Mol Biol, 2005. **33**(1): p. 48-55.

324. Jung, Y.J., et al., *'Immunization' against airborne tuberculosis by an earlier primary response to a concurrent intravenous infection.* Immunology, 2008. **124**(4): p. 514-21.

325. Andrews, J.R., et al., *Risk of progression to active tuberculosis following reinfection with Mycobacterium tuberculosis.* Clin Infect Dis, 2012. **54**(6): p. 784-91.

326. Price, D.N., et al., *Oral Tolerance to Environmental Mycobacteria Interferes with Intradermal, but Not Pulmonary, Immunization against Tuberculosis.* PLoS Pathog, 2016. **12**(5): p. e1005614.

327. Olafsdottir, T.A., et al., *IC31, a two-component novel adjuvant mixed with a conjugate vaccine enhances protective immunity against pneumococcal disease in neonatal mice.* Scand J Immunol, 2009. **69**(3): p. 194-202.

328. Agger, E.M., et al., *Cationic liposomes formulated with synthetic mycobacterial cordfactor (CAF01): a versatile adjuvant for vaccines with different immunological requirements.* PLoS One, 2008. **3**(9): p. e3116.

329. Ingvarsson, P.T., et al., *Designing CAF-adjuvanted dry powder vaccines: spray drying preserves the adjuvant activity of CAF01.* J Control Release, 2013. **167**(3): p. 256-64.

330. Penn-Nicholson, A., et al., *Safety and immunogenicity of candidate vaccine M72/AS01E in adolescents in a TB endemic setting.* Vaccine, 2015. **33**(32): p. 4025-34.

331. Cheng, C., et al., *Mechanism of ad5 vaccine immunity and toxicity: fiber shaft targeting of dendritic cells.* PLoS Pathog, 2007. **3**(2): p. e25.

332. Rhee, E.G., et al., *Multiple innate immune pathways contribute to the immunogenicity of recombinant adenovirus vaccine vectors.* J Virol, 2011. **85**(1): p. 315-23.

333. Lindsay, R.W., et al., *CD8+ T cell responses following replication-defective adenovirus serotype 5 immunization are dependent on CD11c+ dendritic cells but show redundancy in their requirement of TLR and nucleotide-binding oligomerization domain-like receptor signaling.* J Immunol, 2010. **185**(3): p. 1513-21.

334. Tatsis, N., et al., *Multiple immunizations with adenovirus and MVA vectors improve CD8+ T cell functionality and mucosal homing.* Virology, 2007. **367**(1): p. 156-67.

335. Baldwin, S.L., et al., *The importance of adjuvant formulation in the development of a tuberculosis vaccine.* J Immunol, 2012. **188**(5): p. 2189-97.

336. Tchilian, E., et al., *Immunization with different formulations of Mycobacterium tuberculosis antigen 85A induces immune responses with different specificity and protective efficacy.* Vaccine, 2013. **31**(41): p. 4624-31.

337. Jeyanathan, M., et al., *Differentially imprinted innate immunity by mucosal boost vaccination determines antituberculosis immune protective outcomes, independent of T-cell immunity.* Mucosal Immunol, 2013. **6**(3): p. 612-25.

338. Orr, M.T., et al., *A dual TLR agonist adjuvant enhances the immunogenicity and protective efficacy of the tuberculosis vaccine antigen ID93.* PLoS One, 2014. **9**(1): p. e83884.

339. Raniga, S., et al., *Is HRCT reliable in determining disease activity in pulmonary tuberculosis?* Indian J Radiol Imaging, 2006. **16**(2): p. 221-8.

340. Jones, H.A., et al., *In vivo measurement of neutrophil activity in experimental lung inflammation.* Am J Respir Crit Care Med, 1994. **149**: p. 1635-9.

341. Soussan, M., et al., *Patterns of pulmonary tuberculosis on FDG-PET/CT.* Eur J Radiol, 2012. **81**(10): p. 2872-6.

342. Ghesani, N., et al., *Increased cellular activity in thoracic lymph nodes in early human latent tuberculosis infection.* Am J Respir Crit Care Med, 2014. **189**(6): p. 748.

343. Kim, I.J., et al., *Double-phase 18F-FDG PET-CT for determination of pulmonary tuberculoma activity.* Eur J Nucl Med Mol Imaging, 2008. **35**(4): p. 808-14.

344. Heysell, S.K., et al., *18-fluorodeoxyglucose positron emission tomography for tuberculosis diagnosis and management: a case series.* BMC Pulmonary Med, 2013. **13**(14).

345. Coleman, M.T., et al., *Early Changes by (18)Fluorodeoxyglucose positron emission tomography coregistered with computed tomography predict outcome after Mycobacterium tuberculosis infection in cynomolgus macaques.* Infect Immun, 2014. **82**(6): p. 2400-4.

346. Jeong, Y.J., et al., *(18)F-FDG positron-emission tomography/computed tomography findings of radiographic lesions suggesting old healed tuberculosis.* J Korean Med Sci, 2014. **29**(3): p. 386-91.

347. Esmail, H., et al., *18F-FDG PET/CT characterization of progresive HIV-associated tuberculosis.* Nat Med, 2016.

348. Sathekge, M., et al., *Use of 18F-FDG PET to predict response to first-line tuberculostatics in HIV-associated tuberculosis.* J Nucl Med, 2011. **52**(6): p. 880-5.

349. Sathekge, M., et al., *Tuberculous lymphadenitis: FDG PET and CT findings in responsive and nonresponsive disease.* Eur J Nucl Med Mol Imaging, 2012. **39**(7): p. 1184-90.

350. Coleman, M.T., et al., *PET/CT imaging reveals a therapeutic response to oxazolidinones in macaques and humans with tuberculosis.* Sci Transl Med, 2014. **6**(265): p. 265ra167.

351. Chen, R.Y., et al., *PET/CT imaging correlates with treatment outcome in patients with multidrug-resistant tuberculosis.* Sci Transl Med, 2014. **6**(265).

352. Calmette, A., *La vaccination préventive de la tuberculose par le BCG*. 1928, Paris: Libraires de l'Académie de Médecine. 66.

353. Siroka, A., N.A. Ponce, and K. Lönnroth, *Association between spending on social protection and tuberculosis burden: a global analysis.* The Lancet Infectious Diseases, 2016. **16**(4): p. 473-479.

354. Hawn, T.R., et al., *Tuberculosis vaccines and prevention of infection.* Microbiol Mol Biol Rev, 2014. **78**(4): p. 650-71.

355. Evans, T.G., L. Schrager, and J. Thole, *Status of vaccine research and development of vaccines for tuberculosis.* Vaccine, 2016. **34**(26): p. 2911-4.

356. Andersen, P. and S.H. Kaufmann, *Novel vaccination strategies against tuberculosis.* Cold Spring Harb Perspect Med, 2014. **4**(6).

357. Alving, C.R., et al., *Adjuvants for human vaccines.* Curr Opin Immunol, 2012. **24**(3): p. 310-5.

358. Mehra, S., et al., *Granuloma correlates of protection against tuberculosis and mechanisms of immune modulation by Mycobacterium tuberculosis.* J Infect Dis, 2013. **207**(7): p. 1115-27.

359. Ding, C. and X. He, *K-means clustering via principal component analysis.* Proc Int'l Conf Machine Learning, 2004. **21**: p. 225-32.

360. Wold, S., K. Esbensen, and P. Geladi, *Principal component analysis.* Chem Intel Lab Sys, 1987. **2**: p. 37-52.

361. Mayer-Barber, K.D. and A. Sher, *Cytokine and lipid mediator networks in tuberculosis.* Immunol Rev, 2015. **264**(1): p. 264-75.

362. Scriba, T.J., et al., *Vaccination Against Tuberculosis With Whole-Cell Mycobacterial Vaccines.* J Infect Dis, 2016. **214**(5): p. 659-64.

363. White, A.D., et al., *Evaluation of the Immunogenicity of Mycobacterium bovis BCG Delivered by Aerosol to the Lungs of Macaques.* Clin Vaccine Immunol, 2015. **22**(9): p. 992-1003.

364. Pai, M. and M. Schito, *Tuberculosis diagnostics in 2015: landscape, priorities, needs, and prospects.* J Infect Dis, 2015. **211 Suppl 2**: p. S21-8.

365. Phuah, J., et al., *Effects of B Cell Depletion on Early Mycobacterium tuberculosis Infection in Cynomolgus Macaques.* Infect Immun, 2016. **84**(5): p. 1301-11.

366. den Boon, S., et al., *High prevalence of tuberculosis in previously treated patients, Cape Town, South Africa.* EID, 2007. **13**(8): p. 1189-94.

367. Dye, C. and B.G. Williams, *Eliminating human tuberculosis in the twenty-first century.* J R Soc Interface, 2008. **5**(23): p. 653-62.

368. Yates, T.A., et al., *The transmission of Mycobacterium tuberculosis in high burden settings.* The Lancet Infectious Diseases, 2016. **16**(2): p. 227-238.

369. Verrall, A.J., et al., *Early clearance ofMycobacterium tuberculosis: a new frontier in prevention.* Immunology, 2014. **141**(4): p. 506-513.

370. Sasindran, S.J. and J.B. Torrelles, *Mycobacterium Tuberculosis Infection and Inflammation: what is Beneficial for the Host and for the Bacterium?* Front Microbiol, 2011. **2**: p. 2.

371. Loddenkemper, R., M. Lipman, and A. Zumla, *Clinical Aspects of Adult Tuberculosis.* Cold Spring Harb Perspect Med, 2016. **6**(1): p. a017848.

372. Behr, M.A. and W.R. Waters, *Is tuberculosis a lymphatic disease with a pulmonary portal?* The Lancet Infectious Diseases, 2014. **14**(3): p. 250-255.

373. Flynn, J., et al., *Immunology studies in non-human primate models of tuberculosis.* Immun Rev, 2015. **264**: p. 60-73.

374. Scanga, C.A., et al., *In vivo imaging in an ABSL-3 regional biocontainment laboratory.* Pathog Dis, 2014. **71**(2): p. 207-12.

375. Zumla, A., et al., *Tuberculosis.* N Engl J Med, 2013. **368**(8): p. 745-55.

376. Cadena, A.M., J.L. Flynn, and S.M. Fortune, *The Importance of First Impressions: Early Events in Mycobacterium tuberculosis Infection Influence Outcome.* MBio, 2016. **7**(2).

377. Reed, S.G., M.T. Orr, and C.B. Fox, *Key roles of adjuvants in modern vaccines.* Nat Med, 2013. **19**(12): p. 1597-608.

378. O'Hagan, D.T. and C.B. Fox, *New generation adjuvants - From empiricism to rational design.* Vaccine, 2015. **33 Suppl 2**: p. B14-B20.

379. Flynn, J.L., J. Chan, and P.L. Lin, *Macrophages and control of granulomatous inflammation in tuberculosis.* Mucosal Immunol, 2011. **4**(3): p. 271-8.

380. Seder, R., P.A. Darrah, and M. Roederer, *T-cell quality in memory and protection: implications for vaccine design.* Nat Rev Immunol, 2008. **8**(4): p. 247-58.

381. Lichterfeld, M., et al., *HIV-1-specific cytotoxicity is preferentially mediated by a subset of CD8(+) T cells producing both interferon-gamma and tumor necrosis factor-alpha.* Blood, 2004. **104**(2): p. 487-94.

382. Kaufmann, S.H.E., *Fact and fiction in tuberculosis vaccine research: 10 years later.* The Lancet Infectious Diseases, 2011. **11**(8): p. 633-640.

383. Kaufmann, S.H., *Tuberculosis vaccine development at a divide.* Curr Opin Pulm Med, 2014. **20**(3): p. 294-300.

384. Smith, S.G., et al., *Mycobacterium tuberculosis PPD-induced immune biomarkers measurable in vitro following BCG vaccination of UK adolescents by multiplex bead array and intracellular cytokine staining.* BMC Immunol, 2010. **11**(35).

385. Walzl, G., et al., *Immunological biomarkers of tuberculosis.* Nat Rev Immunol, 2011. **11**(5): p. 343-54.

386. Ankrah, A.O., et al., *PET/CT imaging of Mycobacterium tuberculosis infection.* Clin Transl Imaging, 2016. **4**: p. 131-144.

387. Esmail, H., et al., *Characterization of progressive HIV-associated tuberculosis using 2-deoxy-2-[18F]fluoro-D-glucose positron emission and computed tomography.* Nat Med, 2016. **22**(10): p. 1090-1093.

388. DiStefano, C., M. Zhu, and D. Mîndrila, *Understanding and using factor scores: considerations for the applied researcher.* Prac Assess Res Eval, 2009. **14**(20).

389. Pearson, K., *On lines and planes of closest fit to systems of points in space.* Philos Mag, 1901. **2**(11): p. 559-72.

390. Ries, A.L., R.M. Kaplan, and E. Blumberg, *Use of factor analysis to consolidate multiple outcome measures in chronic obstructive pulmonary disease.* J Clin Epidemiol, 1991. **44**(6): p. 497-503.

391. Garratt, A.M., et al., *The SF 36 health survey questionnaire: an outcome measures suitable for routine use within the NHS?* Brit Med J, 1993. **306**: p. 1440.

392. Alexopoulos, E.C., *Introduction to multivariate regression analysis.* Hippokratia, 2010. **14**: p. 23-8.

393. Picard, R.R. and R.D. Cook, *Cross-validation of regression models.* J Am Stat Assoc, 1983. **79**(387): p. 575-83.

394. Hajj Hussein, I., et al., *Vaccines Through Centuries: Major Cornerstones of Global Health.* Front Public Health, 2015. **3**: p. 269.

395. Sanderson, J.B., *On the communicability of tubercule by innoculation.* , in *Tenth report of the Medical Officer of the Privy Council*. 1867, George E Eyre and William Spottiswoode: London. p. 11-151.

396. RIch, A.R., *The pathogenesis of tuberculosis*. 1st ed. 1944, Springfield, IL: Charles C. Thomas.

397. Waters, W.R., et al., *Efficacy and immunogenicity of Mycobacterium bovis DeltaRD1 against aerosol M. bovis infection in neonatal calves.* Vaccine, 2009. **27**(8): p. 1201-9.

398. Calmette, A. and C. Guerin, *Origine intestinal de la tuberculose pulmonaire et mechanisme de l'infection tuberculeuse.* Ann Inst Pasteur, 1906. **20**: p. 609-24.

399. Palmer, M.V., W.R. Waters, and D.L. Whipple, *Milk containing Mycobacterium bovis as a source of infection for white-tailed deer fawns (Odocoileus virginianus).* Tuberculosis, 2002. **82**(4-5): p. 161-165.

400. Palmer, M.V., W.R. Waters, and T.C. Thacker, *Lesion development and immunohistochemical changes in granulomas from cattle experimentally infected with Mycobacterium bovis.* Vet Pathol, 2007. **44**: p. 863-74.

401. Lerner, T.R., et al., *Lymphatic endothelial cells are a replicative niche for Mycobacterium tuberculosis.* J Clin Invest, 2016. **126**(3): p. 1093-108.

402. Wingfield, T., et al., *Designing and implementing a socioeconomic intervention to enhance TB control: operational evidence from the CRESIPT project in Peru.* BMC Public Health, 2015. **15**: p. 810.

403. Russell, D.G., C.E. Barry, 3rd, and J.L. Flynn, *Tuberculosis: what we don't know can, and does, hurt us.* Science, 2010. **328**(5980): p. 852-6.

404. Hunter, R.L., *Pathology of post primary tuberculosis of the lung: an illustrated critical review.* Tuberculosis (Edinb), 2011. **91**(6): p. 497-509.

405. Canetti, G., *The Tubercle Bacillus in the Pulmonary Lesion of Man*. 1955, New York City, NY, USA: Springer. 230.

406. Cutroneo, K.R., *How is Type I procollagen synthesis regulated at the gene level during tissue fibrosis.* J Cell Biochem, 2003. **90**(1): p. 1-5.

407. Sime, P.J. and K.M. O'Reilly, *Fibrosis of the lung and other tissues: new concepts in pathogenesis and treatment.* Clin Immunol, 2001. **99**(3): p. 308-19.

408. Wynn, T.A., *Integrating mechanisms of pulmonary fibrosis.* J Exp Med, 2011. **208**(7): p. 1339-50.

409. Wynn, T.A. and T.R. Ramalingam, *Mechanisms of fibrosis: therapeutic translation for fibrotic disease.* Nat Med, 2012. **18**(7): p. 1028-40.

410. Mi, S., et al., *Blocking IL-17A promotes the resolution of pulmonary inflammation and fibrosis via TGF-beta1-dependent and -independent mechanisms.* J Immunol, 2011. **187**(6): p. 3003-14.

411. Sun, L., et al., *New concepts of IL-10-induced lung fibrosis: fibrocyte recruitment and M2 activation in a CCL2/CCR2 axis.* Am J Physiol Lung Cell Mol Physiol, 2011. **300**(3): p. L341-53.

412. Redente, E.F., et al., *Tumor necrosis factor-alpha accelerates the resolution of established pulmonary fibrosis in mice by targeting profibrotic lung macrophages.* Am J Respir Cell Mol Biol, 2014. **50**(4): p. 825-37.

413. Fielding, C.A., et al., *Interleukin-6 signaling drives fibrosis in unresolved inflammation.* Immunity, 2014. **40**(1): p. 40-50.

414. Gistera, A., et al., *Transforming growth factor-beta signaling in T cells promotes stabilization of atherosclerotic plaques through an interleukin-17-dependent pathway.* Sci Transl Med, 2013. **5**(196): p. 196ra100.

415. Lee, C.G., et al., *Interleukin-13 induces tissue fibrosis by selectively stimulating and activating transforming growth factor beta(1).* J Exp Med, 2001. **194**(6): p. 809-21.

416. Khalil, N., *TGF-beta: from latent to active.* Microbes Infect, 1999. **1**(15): p. 1255-63.

417. Massague, J., *TGF-beta signal transduction.* Annu Rev Biochem, 1998. **67**: p. 753-91.

418. Broekelmann, T.J., et al., *Transforming growth factor ß1 is present at sites of extracellular matrix gene expression in human pulmonary fibrosis.* Proc Natl Acad Sci U S A, 1991. **88**(15): p. 6642-6.

419. Khalil, N., et al., *Macrophage production of transforming growth factor beta and fibroblast collagen synthesis in chronic pulmonary inflammation.* J Exp Med, 1989. **170**(3): p. 727-37.

420. Limper, A.H., et al., *Immunohistochemical localization of transforming growth factor-beta 1 in the nonnecrotizing granulomas of pulmonary sarcoidosis.* Am J Respir Crit Care Med, 1994. **149**(1): p. 197-204.

421. Khalil, N., et al., *Regulation of the effects of TGF-beta1 by activation of latent TGF-beta1 and differential expression of TGF-beta receptors (TbetaR-I and TbetaR-II) in idiopathic pulmonary fibrosis.* Thorax, 2001. **56**: p. 907-915.

422. Lekkerkerker, A.N., et al., *Cellular players in lung fibrosis.* Curr Pharm Des, 2012. **18**: p. 4093-102.

423. Pechkovsky, D.V., et al., *Alternatively activated alveolar macrophages in pulmonary fibrosis-mediator production and intracellular signal transduction.* Clin Immunol, 2010. **137**(1): p. 89-101.

424. Pasipanodya, J.G., et al., *Pulmonary impairment after tuberculosis.* Chest, 2007. **131**(6): p. 1817-24.

425. Pasipanodya, J., et al., *Pulmonary impairment after tuberculosis and its contribution to TB burden.* BMC Pub Heal, 2010. **10**(259).

426. Hnizdo, E., T. Singh, and G. Churchyard, *Chronic pulmonary function impairment caused by initial and recurrent pulomary tuberculosis following treatment.* Thorax, 2000. **55**: p. 32-8.

427. Bansal, V. and R. Prasad, *Pulmonary rehabilitation in chronic respiratory diseases.* Indian J Chest Dis Allied Sci, 2014. **56**: p. 147-8.

428. Dheda, K., et al., *Lung remodeling in pulmonary tuberculosis.* J Infect Dis, 2005. **192**(7): p. 1201-9.

429. Ong, C.W., P.T. Elkington, and J.S. Friedland, *Tuberculosis, pulmonary cavitation, and matrix metalloproteinases.* Am J Respir Crit Care Med, 2014. **190**(1): p. 9-18.

430. Marshall, B.G., et al., *Increased inflammatory cytokines and new collagen formation in cutaneous tuberculosis and sarcoidosis.* Thorax, 1996. **51**: p. 1253-61.

431. Shin, H.J. and Y.S. Kwon, *Treatment of Drug Susceptible Pulmonary Tuberculosis.* Tuberc Respir Dis (Seoul), 2015. **78**(3): p. 161-7.

432. Lin, P.L., et al., *Metronidazole prevents reactivation of latent Mycobacterium tuberculosis infection in macaques.* Proc Natl Acad Sci U S A, 2012. **109**(35): p. 14188-93.

433. Van Linthout, S., K. Miteva, and C. Tschope, *Crosstalk between fibroblasts and inflammatory cells.* Cardiovasc Res, 2014. **102**(2): p. 258-69.

434. van Rie, A., et al., *Exogenous reinfection as a cause of recurrent tuberculosis after curative treatment.* N Engl J Med, 1999. **341**: p. 1174-9.

435. Shachor, Y., et al., *Increased incidence of pulmonary tuberculosis in chronic interstitial lung disease.* Thorax, 1989. **44**(2): p. 151-3.

436. Chung, M.J., J.M. Goo, and J.G. Im, *Pulmonary tuberculosis in patients with idiopathic pulmonary fibrosis.* Eur J Radiol, 2004. **52**(2): p. 175-9.

437. Ahn, C.H., D.R. Nash, and G.A. Hurst, *Ventilatory defects in atypical mycobacteriosis.* Am Rev Respir Dis, 1976. **113**(3): p. 273-9.

438. Bellini, A. and S. Mattoli, *The role of the fibrocyte, a bone marrow-derived mesenchymal progenitor, in reactive and reparative fibroses.* Lab Invest, 2007. **87**(9): p. 858-70.

439. Reilkoff, R.A., R. Bucala, and E.L. Herzog, *Fibrocytes: emerging effector cells in chronic inflammation.* Nat Rev Immunol, 2011. **11**(6): p. 427-35.

440. Camelo, A., et al., *The epithelium in idiopathic pulmonary fibrosis: breaking the barrier.* Front Pharmacol, 2014. **4**: p. 173.

441. Daniels, C.E., et al., *Imatinib mesylate inhibits the profibrogenic activity of TGF-beta and prevents bleomycin-mediated lung fibrosis.* J Clin Invest, 2004. **114**(9): p. 1308-16.

442. Hu, Y., et al., *Role of extracellular signal-regulated kinase, p38 kinase, and activator protein-1 in transforming growth factor-beta1-induced alpha smooth muscle actin expression in human fetal lung fibroblasts in vitro.* Lung, 2006. **184**(1): p. 33-42.